

ANNUAL REPORT 2019-20

Institute of Seismological Research
Department of Science and Technology
Government of Gujarat

CONTRIBUTORS

| Group & Principal Investigator | Scientist/ Researcher |
|---|---|
| Near Real Time Seismology PI: Dr. Santosh Kumar, Scientist-E | Dr. P Mahesh, Scientist-C Dr. A P Singh, Scientist-C Mr. Ketan Singha Roy, Scientist-B Ms. Vishwa Joshi, Scientist-B Ms. Vandana Patel, Sr Geophysicist Mr. Alla Sateesh, Sr Geophysicist Ms. Monika Bhatia, JRF |
| Seismic Hazard Assessment and Microzonation PI: Dr. Sumer Chopra, Scientist-G | Dr. Kapil Mohan, Scientist-D Dr. Pallabee Choudhury, Scientist-D Dr. B Sairam, Scientist-C Dr. Madan Mohan Rout, Scientist-C Dr. Vasu Pancholi, Scientist-B Dr. Archana Das, Scientist-B Ms. Vandana Patel, Sr Geophysicist Mr. Naveen Kumar, Sr Geophysicist Mr. Vinay Kr Dwivedi, Sr Geophysicist Mr. Tarun Solanki, Sr Geophysicist Mr. Peush Chaudhary, Geophysicist Mr. Pruthul Patel, Geophysicist Mr. Dilip Singh, Geophysicist Mr. Mehul Nagar, Geophysicist Ms. Charu Kamra, JRF |
| Solid Earth Geophysics PI: Dr. M.Ravi Kumar, Distinguished Scientist | Dr. A P Singh, Scientist-C Dr. Jyoti Sharma, Scientist-C Dr. G. Srijayanthi, Scientist-B Mr. Avinash Chauhan, Sr. Geophysicist Mr. Mayank Dikshit, Geophysicist Mr. Mehul Nagar, Geophysicist Mr. Dilip Singh, Geophysicist Mr. Virender Kumar Singh, JRF Ms. Indu Chaudhary, JRF Ms. Monika Bhatia, JRF Mr. Rakesh Nikam, PF |
| Earthquake Precursory Research PI: Dr. K.M. Rao, Scientist-E | Mr. M.S.B.S.Prasad, Scientist-B Mr. C.P.Simha , Geophysicist |

| | |
|--|---|
| | Mr. Sushant Sahoo, Geophysicist Mr. Shivam Joshi, JRF |
| Active Tectonics PI: Dr. Pallabee Choudhury, Scientist-D | Dr. Siddharth Prizomwala, Scientist-B Dr. Girish Kothiyari, Scientist-B Dr. Falguni Bhattacharya, Scientist-B Dr. Rakesh Dumka, Scientist-B Dr. Rajeev Kr. Yadav, Scientist-B Dr. Archana Das, Scientist-B Mr. Tarun Solanki, Sr.Geologist Mr. Nisarg Makwana, Geophysicist Mr. Durga Prasad, JRF Mr. Raj Sunil Kandergula, JRF Ms. Sneha Mishra, JRF Ms. Neha Joshi, JRF Mr. D. Suribabu, JRF Ms. Aashima Sodhi, JRF Mr. Chintan Vedpathak, PF |
| Commercial Research and Development PI: Dr. Kapil Mohan, Scientist-D | Dr. Siddharth Prizomwala, Scientist-B Dr. Vasu Pancholi, Scientist-B Mr. Naveen Kumar, Sr Geophysicist |

CONTENTS

| | | Page No. |
|---|---|-----------|
| HIGHLIGHTS | | 1 |
| RESEARCH CONTRIBUTIONS | | 5 |
| 1. NEAR REAL TIME SEISMOLOGY | | 5 |
| 1.1 | Earthquake Monitoring and Seismicity Patterns in Gujarat | 5 |
| 1.2 | Description of Earthquakes in Different Parts of Gujarat | 5 |
| 1.3 | Description of Recorded Earthquakes in different Parts of Gujarat since inception of the network till 2019 | 7 |
| 1.4 | Earthquake data processing and interpretation of MEQ data collected during Jan-Dec 2018 for the study of seismogenic sources around the Subansiri Lower Hydro Electric (H.E) Project, Arunachal Pradesh | 9 |
| 1.5 | Processing and interpretation of MEQ data collected during Jan-Jun 2019 for the study of Seismogenic sources around the Subansiri Lower H.E. Project | 10 |
| 1.6 | Analysis of earthquake swarm activity in Jamnagar District, Gujarat | 12 |
| 1.7 | Moment Release and Mechanical coupling between fault systems | 14 |
| 1.8 | Earthquake swarm activity in and around Navsari district, South Gujarat | 15 |
| 1.9 | Low Frequency Passive Seismic study in Ahmedabad and Ankaleswar | 16 |
| 1.10 | Low Frequency Passive Seismic study at Jotana and Mansa regions | 18 |
| 1.11 | New Insights from the Investigation of Remotely Triggered Earthquakes in Cambay and Narmada regions of Gujarat, India | 19 |
| 1.12 | Remote Dynamic Triggering in Hindukush Region following the Megaquakes ($M_w \geq 8.0$) | 21 |
| 1.13 | Estimation of Source Parameters | 22 |
| 2. SEISMIC HAZARD ASSESSMENT AND MICROZONATION | | 24 |
| 2.1 | Development of Site Specific Response Spectrum at Khavda windmill site, Kachchh | 24 |
| 2.2 | Multi-criteria study for Seismic Hazard Assessment of UNESCO world heritage Ahmedabad city, Gujarat, Western India | 25 |
| 2.3 | Geotechnical characteristics of soils to identify liquefaction potential of the coastal area of the Bhavnagar, Gujarat, Western India | 26 |
| 2.4 | Geotechnical Investigation for estimation of the Liquefaction hazard for the capital city of Gujarat state, Western India | 26 |
| 2.5 | Engineering Geological Mapping for Seismic Hazard Assessment of the Gandhinagar City, western India | 27 |
| 2.6 | Seismic Hazard assessment in northern Kachchh | 27 |
| 2.7 | Magnetotelluric investigation in the western part of Narmada Son lineament zone | 28 |
| 2.8 | 2D modeling of the magnetotelluric data acquired in and around Bhadbhut area | 29 |
| 2.9 | Electrical Resistivity Tomography (ERT) on the Ukai dam site (Dist. Tapi), Gujarat | 30 |

| | | Page No. |
|--|--|-----------|
| 2.10 | Magnetotelluric study in the Bhavnagar region of Saurashtra | 31 |
| 2.11 | Magnetotelluric Investigation in the Talala area of Saurashtra | 32 |
| 2.12 | Estimation of sedimentary thickness using 1D inversion of Magnetotelluric (MT) data | 34 |
| 2.13 | Electrical Resistivity Survey in Ahwa (Dist. Dang), Gujarat | 35 |
| 2.14 | Conductive and Vp/Vs anomalies across the Cambay and Kachchh basins | 36 |
| 2.15 | Estimation of near surface attenuation parameter Kappa (κ) in Northwest and Northeast Himalaya region | 37 |
| 2.16 | Site specific geological map of the Bhadbhut Barrage Site, Bharuch, Gujarat | 38 |
| 2.17 | Assessment of Relative Active Tectonics in Parts of Dadra and Nagar Haveli, Western India | 38 |
| 3. SOLID EARTH GEOPHYSICS | | 40 |
| 3.1 | Lowermost mantle (D'') anisotropy inferred from splitting of S, ScS and SK(K)S phases recorded by the Gujarat Seismic Network | 40 |
| 3.2 | Shear Wave Velocity Structure Beneath the Northwestern Deccan Volcanic Province from Joint and Separate Inversion of the Rayleigh and Love waves | 43 |
| 3.3 | Low Velocity Zones and Negative Radial Anisotropy Beneath the Northwestern Deccan Volcanic Province | 48 |
| 3.4 | Magnetotelluric (MT) investigations in the Great Rann of Kachchh to map the Allah Bund Fault | 49 |
| 3.5 | Shallow Imaging of the Himalayan Frontal Thrust | 49 |
| 3.6 | Lithospheric structure of Kaladgi rift basin and adjoining regions, southwestern India through Magnetotelluric perspective | 51 |
| 3.7 | Delineation of intertrappean layers beneath the Deccan Volcanic province of western India through Microtremor analysis | 52 |
| 3.8 | Shallow Subsurface Imaging of Anjar Taluka, Kachchh using Transient Electromagnetic Studies | 53 |
| 3.9 | Delineation of lineaments in the Cambay rift and surrounding regions of NW India utilizing satellite derived EIGEN6C4 gravity data | 55 |
| 3.10 | Lithospheric structure beneath the seismically active northwestern Deccan volcanic province, India: Insight from the gravity data | 55 |
| 3.11 | Structural fabric over the seismically active Kachchh rift basin, India: Insight from world gravity model 2012 | 56 |
| 3.12 | Upper crustal structure of the North Cambay rift, India deduced from integrated study of gravity, seismic and borehole data | 56 |
| 3.13 | Determination of the local earthquake locations and velocity model for the Arunachal Himalaya using Joint Hypocentral Determination technique | 56 |
| 4. EARTHQUAKE PRECURSORY RESEARCH | | 59 |
| 4.1 | Source Characteristics of observed low latitude magnetic pulsations Pc3-4s | 59 |
| 4.2 | Analysis of anomalous variations of Surface Latent Heat flux, Air temperature at 2m and Outgoing Long wave Radiation prior to the New Zealand earthquake | 60 |

| | | Page No. |
|----------------------------|--|-----------|
| 4.3 | Observation of Seismo-Geomagnetic Pulsations using LEMI 30 at Badargadh, Kutch | 63 |
| 4.4 | Local Trend Analysis of Irregular pulsations (Pi2:6-25 mHz) at low latitude station Desalpar, Kachchh | 66 |
| 4.5 | Classification of Geomagnetic Pulsations during a moderate Geomagnetic storm | 68 |
| 4.6 | Pi2 Pulsations during Quiet and Disturbed Geomagnetic Conditions: Low latitude Observations | 72 |
| 4.7 | Spatio-temporal variation of Total electron content prior to Jamaica earthquake (M=7.7) on 28 Jan 2020 | 76 |
| 4.8 | Deterministic Analysis of the soil radon along with all the other meteorological parameters | 80 |
| 4.9 | Scaling characteristics of the Earth's magnetic field data of Desalpar in association with local earthquakes | 81 |
| 4.10 | Soil Radon surveys along the Seismic array sites of Kachchh Gujarat | 84 |
| 4.11 | Installation of 10 Soil Radon monitors (Barasol BMC2) in Kachchh | 86 |
| 4.12 | Observation of the ULF Electromagnetic emissions prior to the New Zealand Earthquake of M 7.8 on 13th November 2016 | 88 |
| 5. ACTIVE TECTONICS | | 93 |
| 5.1 | Geodetic monitoring of Landslide movement at two sites in the Garhwal Himalaya | 93 |
| 5.2 | Active Tectonics of Himalaya, Rift Basins in Central India and those Related to Crustal Deformation at Different Time Scales | 94 |
| 5.3 | Crustal deformation study of Gujarat | 96 |
| 5.4 | Anomalous transients in GPS measurements due to induced changes in local site conditions | 96 |
| 5.5 | Reconstructing Late Quaternary Palaeo-environmental change from the dryland fluvial landscape of the Southern Kachchh Mainland, Western India: Insights from new OSL and sedimentological datasets | 97 |
| 5.6 | Did the seawater retreat play a key role in abandonment of the coastal Harappan settlement Lothal (Gujarat)? | 98 |
| 5.7 | Signatures of tectonic instability (?) along the North Cambay basin during the Late Holocene period, North Gujarat, India | 98 |
| 5.8 | Tectonic implications on controlled dimensions and fluid dynamics of Bedrock Gorge, Kachchh: Western India | 99 |
| 5.9 | Basin-wide aggradation-incision events and triggering processes: insights from the fluvial response of Shetrunji river (Western India) since the Last Glacial Maxima | 99 |
| 5.10 | Geomorphic response to neotectonic instability in the Deccan volcanic province, Shetrunji River, Gujarat, Western India: Insights from quantitative geomorphology | 100 |
| 5.11 | Testing the sensitivity of Relative Index of Active Tectonics from areas experiencing variable uplift: An example from the Himalayan Frontal Thrust in the NW and NE Himalayas | 101 |
| 5.12 | Morpho-structural approach in predicting the neotectonic attributes of Vigodi Fault, Kachchh, India | 102 |
| 5.13 | Structural Attributes and Paleostress Analysis of Vigodi Fault (VF) in Western Kachchh Region | 102 |

| | | Page No. |
|---|--|------------|
| 5.14 | Mudflats of little Rann of Kachchh: implication for palaeo climatic and palaeo environmental changes during Middle to Late Holocene period and understanding the role of such changes on the landscape and past human settlement | 102 |
| 5.15 | Palaeo climatic and paleo environmental reconstruction deduced from the higher Banni Plains, Kachchh (BKR trench site) during the last 5 Ka. | 104 |
| 5.16 | Response of Harappan coastal sites in Gujarat to middle-late Holocene Palaeo-environmental changes: a multiple proxy approach | 104 |
| 6. COMMERCIAL RESEARCH AND DEVELOPMENT | | 108 |
| 6.1 | Time Domain Electromagnetic (TDEM) survey at Regional Science Museum, Patan | 108 |
| 6.2 | Magnetotelluric (MT) Investigation to locate geothermal source zone at Lasundra area (Kheda), Gujarat (India) | 109 |
| 6.3 | Phase-III: Delineation of freshwater layer at the selected sites in the Lakhpata, Nakhatrana, Bhuj (Banni area), Mandvi and Abdasa Talukas of Kachchh (Gujarat) using Time Domain Electromagnetic Survey | 111 |
| PUBLICATIONS | | 114 |
| NOTABLE EVENTS | | 119 |
| SOCIETAL OUTREACH | | 125 |

HIGHLIGHTS

- ✦ 39 papers were published in reputed scientific journals with a cumulative impact factor of 68.2. A total 19 consultancy and GAP(GoI) projects were received with a total budget of 20.2 Cr.
- ✦ Dam Safety inspection was carried out at 7 major old dams (maintained by Water Resources Department) under the Dam Rehabilitation and Improvement Project. ISR proposed seismicity monitoring, development of a Strong Motion Seismic Network for Dams, reassessment of site specific seismic hazard in the context of revised guidelines of CWC and Geophysical Investigations to discern the zone and path of seepages in the dams.
- ✦ Epicentral parameters of 976 earthquakes, in the magnitude range of ML 0.6-4.4, which occurred in Gujarat in 2019, are estimated. Of these, 721 earthquakes are from Kachchh, 182 earthquakes are from Saurashtra and 73 earthquakes are from the Mainland.
- ✦ Earthquake swarm activity that occurred during the end of 2019 summer monsoon, from mid of September to November 2019, was reported. About 76 of these earthquakes are well recorded in near real time by the ISR network. The epicenters of these events are located near Khankotda region and the magnitudes range from ML 1.0 to ML 3.7 and the depths are mostly ≤ 10 km.
- ✦ Seismic Moment release in different faults in Kachchh is estimated.
- ✦ The study of the seismogenic sources around the Subansiri Lower Hydro Electric Project Arunachal Pradesh was carried out using waveform data recorded during Jan-Dec 2018.
- ✦ Source parameters of earthquakes in the magnitude range of 1.7 to 5.0 that occurred in Arunachal Pradesh, are estimated.
- ✦ Estimation of 1-D velocity model and precise earthquake locations in the Arunachal Himalaya were carried out using the joint hypocentral determination technique.
- ✦ Instances of dynamic triggering of micro-earthquakes in the Mainland region of Gujarat and Hindukush were reported following remote mega earthquakes ($M_w \geq 8.0$).
- ✦ A maiden scientific study was carried out for location of Primary Data Centre and Data Recovery Site for MCX India. SEBI modified the guidelines based on ISR's recommendations –minimum distance between them is reduced from 1000km to 500km.
- ✦ A peak ground acceleration amplification factor of 1.25 is computed (between Engineering Bed Layer and surface) at Khavda through deterministic seismic hazard assessment.
- ✦ A multi-criteria study was carried out for Seismic Hazard Assessment of UNESCO world heritage Ahmedabad city utilizing geotechnical, geological and geophysical inputs. An integrated seismic hazard map of Ahmedabad city was prepared using an analytical hierarchal process.
- ✦ Liquefaction potential of the coastal area of Bhavnagar city was estimated. The study shows that the coastal area has moderate to high probability of liquefaction during a major earthquake.
- ✦ An engineering geological map of the Gandhinagar city is prepared based on data of 14 boreholes drilled based on lithology, soil properties, standard penetration test (N Value) and shear wave velocity (V_s). The study shows that areas in the central and southwestern parts of the city are more prone to high ground shaking and related damage during a major earthquake in Gujarat.

- ✦ The spectral decay parameter, kappa (κ) for the North-West Himalaya and the North-East India regions was estimated from strong motion records. The average values (horizontal and vertical components) of κ for are $0.050\pm 0.009s$ and $0.048\pm 0.010s$ for the NW Himalaya and $0.0368\pm 0.0054s$ and $0.0334\pm 0.0091s$ for NE India.
- ✦ The intra-trappean layers beneath the Deccan Volcanic province of western India were delineated through Microtremor analysis.
- ✦ The shallow subsurface of the seismically active eastern part of the Kachchh district, comprising Bhachau, Anjar and Gandhidham talukas is imaged to delineate the groundwater aquifers and fresh water-saline water interface. The freshwater zone has been delineated at two locations in Bhachau Taluka at 300-400 m depth.
- ✦ Ground water table in the Dang district is delineated using the standard DC Resistivity technique.
- ✦ Time domain electromagnetic investigations are carried out in the Bhadbhut barrage site for salinity ingress assessment.
- ✦ A geothermal source zone has been inferred at Lasundra, Kheda district, Gujarat.
- ✦ Feasibility studies were carried out to characterize the Low Frequency Passive Seismic (LFPS) response that enables localization of sweet spots for hydrocarbon exploitation and field development, around the Dholka village, Ahmedabad and Digas village, Bharuch.
- ✦ Low Frequency Passive Seismic (LFPS) investigations were carried out at 320 sites in the Mansa and Jotana areas for localization of sweet spots for hydrocarbon exploitation.
- ✦ Characterization of the shallow subsurface of the Himalayan Frontal Thrust (HFT) was performed using Time-domain Electromagnetic (TDEM) Technique.
- ✦ Shallow subsurface investigations were carried out using Time Domain Electromagnetic (TDEM) technique, to characterize the Kachchh Mainland Fault (KMF).
- ✦ The Narmada Fault in the western part of Son-Narmada -Tapti zone (SONATA) and the Girnar fault in the Talala area of Saurashtra are characterized through Magnetotelluric investigations.
- ✦ The Allah Bund Fault (ABF) in the Great Rann of Kachchh was imaged using Magnetotelluric investigations.
- ✦ The teleseismic shear phases (S, SK(K)S, ScS) recorded by a network of seismic stations in Gujarat, northwestern India were utilized to understand the seismic character of the lowermost mantle. The results from both ScS-S and SKS-SKKS methods clearly indicate an anisotropic nature of the D'' region beneath NE & SE Asia.
- ✦ The radially anisotropic shear wave velocity structure was determined beneath the Northwestern Deccan Volcanic Province.
- ✦ The lineaments in Cambay rift basin were delineated using satellite-derived EIGEN6C4 gravity data. Majority of the lineaments trend in the NW-SE and NE-SW directions and their source depth ranges between 4.4 and 15 km. The NE-SW trending Diyodar and Tharad ridges in the Cambay rift basin are identified for the first time using gravity data.
- ✦ An insight into the Lithospheric structure beneath the seismically active northwestern Deccan volcanic province, India was obtained using gravity data.
- ✦ Upper crustal structure of the North Cambay rift, India was deduced from an integrated study of gravity, seismic and borehole data.
- ✦ Lithospheric structure beneath the Kaladgi basin and adjoining regions was determined using Magnetotelluric data.

- ✦ Pulsation Continuous (Pc) and Pulsation Irregular (Pi) signals were identified using magnetic data of ULF magnetometer at Desalpar, Kachchh, Gujarat. The relation between magnetic pulsations and solar parameters was investigated.
- ✦ Local trend analysis of irregular pulsations (Pi2:6-25 mHz) at low latitude station of Desalpar, Kachchh is carried out. The morphology of Pi2 pulsation bursts (6-25 mHz) and its local time variations during 2013 are reported.
- ✦ Scaling characteristics of the Earth's magnetic field data of Desalpar MPMGO in association with local earthquakes that occurred in 2012, are studied.
- ✦ Soil radon surveys are conducted at 49 locations in Kachchh to identify potential sites for radon monitoring. Installation of 10 soil radon monitoring stations in Kachchh area was completed.
- ✦ The anomalous variations of Surface Latent Heat flux (SLHF), Air temperature at 2m (AT2m) and Outgoing Long wave Radiation (OLR) prior to the New Zealand earthquake, that occurred on 13 November 2016 are analysed.
- ✦ Precursors to the M7.7 Jamaica earthquake that occurred on 28 Jan 2020 were identified using Total Electron Content of the ionosphere.
- ✦ The ULF Electromagnetic emissions before the New Zealand Earthquake of M 7.8 that occurred on 13 November, 2016 were documented.
- ✦ The transient deformation at two GPS sites PTNA and KUNR revealed that anomalous ground motion observed at the GPS site situated in Patna, Bihar, which continued for ~50-60 days after the 2015 Gorkha earthquake, is probably due to the slow and permanent deformation in the water-saturated alluvial plains caused by the moderate shaking due to the mainshock. Another anomalous biannual cyclic deformation is observed at site Kunair, near Tehri reservoir that represents altered local hydrological conditions due to the impoundment of the Tehri reservoir.
- ✦ Anomalous site motion is reported at three GPS sites situated in Raithal (RATH), Bhatwari (BHTW, Uttarkashi) and Phata (GUPT, Guptkashi) villages of the Garhwal region. The residual motion at sites RATH and BHTW, calculated after removal of plate motion from observed motion at the site, results in ~22 mm/yr of eastward motion and ~6 mm/yr of subsidence from 2012. The residual motion at site GUPT indicates a motion of ~15 mm/yr towards northeast. A detailed field investigation using RTK surveying suggests that the residual motion at these sites is towards the dip of the bedrock, implying that these sites are located on a slow-moving potential landslide zone in the Garhwal region.
- ✦ The study utilizing geodetic measurements in the past five years provided the current-day shortening rate and locking depth of the brittle part of Main Himalaya Thrust (MHT) in the Northwest and Northeast Himalaya. Strain-budget analysis indicates an overdue of at least 4 m of slip on the MHT in these regions which has the potential to produce a megathrust earthquake (Mw~8) in the near future.
- ✦ The fluvial to fluvio-marine records were integrated employing geomorphology, detailed sedimentology supported by geochemistry and optical dating, to evaluate the potential of dryland environments in archiving the palaeo-events. The climate reconstructions suggest that the fluvial systems have responded to the variations in monsoonal strength through widespread aggradation during 57 ka until 41 ka.
- ✦ A detailed geochemical, stable isotopic, mineralogical, and sedimentological proxy based record reveals evidences for a marginally higher sea stand between (~5000 yr BP to ~2000 yr BP), indicating a higher sea stand pushing the estuarine zone close to the Lothal site, facilitating ship-movements. Based on the results of the study, it was suggested that climatic changes possibly led to scarcity of water in the up as well as downstream Indus stretches, leading to a defunct dockyard for business and

consequently a decline in trade, that played a key role in the abandonment of the coastal Harappan settlement at Lothal.

- ✦ An investigation was carried out to infer the response of fluvial sequences to paleoenvironmental changes since the last glacial maximum (LGM) from the arid to semi-arid Saurashtra region. A composite lithostratigraphy with aggradational and incisional events since the LGM was presented.
- ✦ The sensitivity of RIAT in identifying areas undergoing variable uplift was assessed with an example from the Northwestern and Northeastern segments of the Himalayan Frontal Thrust (HFT).
- ✦ The geomorphic landform and drainage pattern within the NW-SE oriented Vigodi Fault (VF) was analysed to assess the neotectonic deformation. The results of geomorphic, geological and morphometric analyses together show that the area is neotectonically active.
- ✦ A drainage map was prepared for the Northeast Himalaya (Kameng to Dikrong) using toposheets (scale of 1:50000) and satellite imagery. This was further used to identify the drainage anomalies and locate sites for further detailed field investigations.
- ✦ Implications of palaeo climatic and palaeo environmental changes during Middle to Late Holocene period were studied to understand the role of such changes on the landscape and past human settlements in the little Rann.

RESEARCH CONTRIBUTIONS

1. NEAR REAL TIME SEISMOLOGY

1.1 Earthquake Monitoring and Seismicity Patterns in Gujarat

(Santosh Kumar, A P Singh, P Mahesh, Ketan Singha Roy, Vandna Patel)

The Gujarat State Seismic Network being maintained by the Institute of Seismological Research, Gandhinagar since July 2006 (Fig.1.1), functioned well with 60 Broadband Seismograph Stations (BBS) spread throughout the state and neighboring areas, total 45 of which are connected via VSAT to ISR. 54 Strong Motion Accelerographs (SMA) are also deployed. The network has a detectability of M2.0 in the Kachchh active area and M2.5 in the other areas of Gujarat.

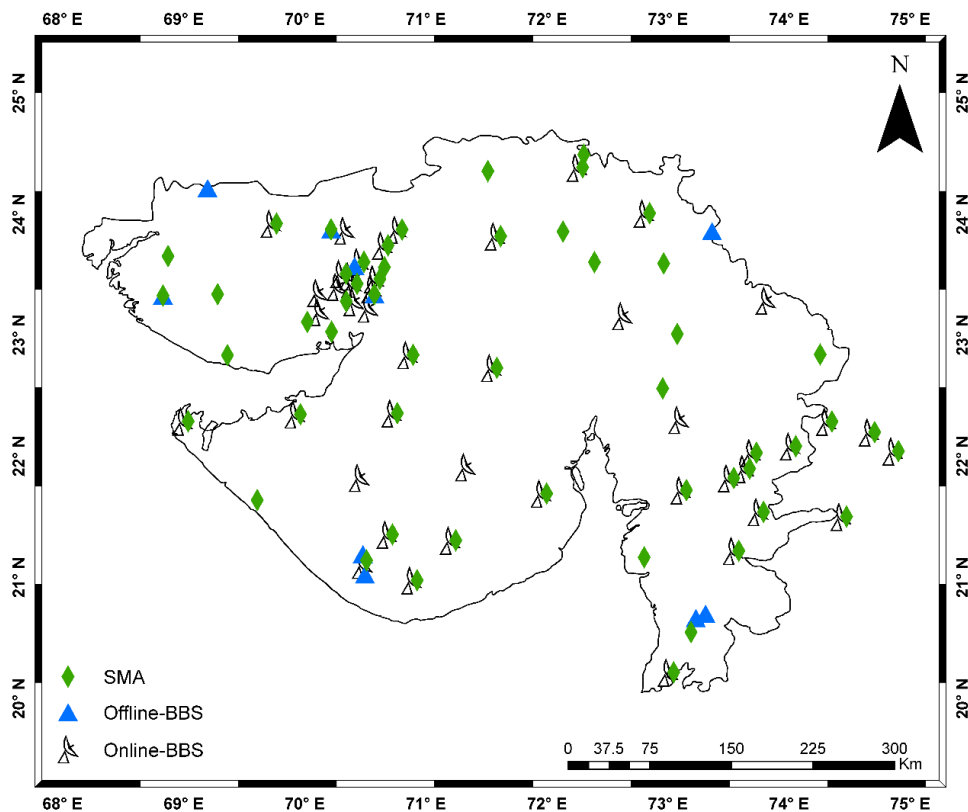


Fig. 1.1: Gujarat network of 60 Seismograph stations in Gujarat (45 online) and 54 Accelerographs

1.2 Description of Earthquakes in Different Parts of Gujarat

(Santosh Kumar, A P Singh, P Mahesh, Ketan Singha Roy, Vandna Patel)

Magnitude-wise distribution of earthquakes in the three regions of Gujarat during 2019 is given in Table 1.1. In the Kachchh region, 721 shocks of M0.6- 4.4 were located. In the Saurashtra and Mainland, 182 shocks of M0.5 - 3.8 and 73 shocks of M1.0 – 4.4 were located, respectively (Fig. 1.2).

Table 1.1: Regional Distribution of Earthquakes Located in Gujarat during 2019

| Region | 0.5 – 1.9 | 2.0 - 2.9 | 3.0 – 3.9 | 4.0 – 4.9 | Total |
|-------------------|-----------|-----------|-----------|-----------|-------|
| Kachchh | 465 | 209 | 43 | 4 | 721 |
| Saurashtra | 58 | 94 | 30 | 0 | 182 |
| Mainland | 45 | 20 | 7 | 1 | 73 |
| Total | 568 | 323 | 80 | 5 | 976 |

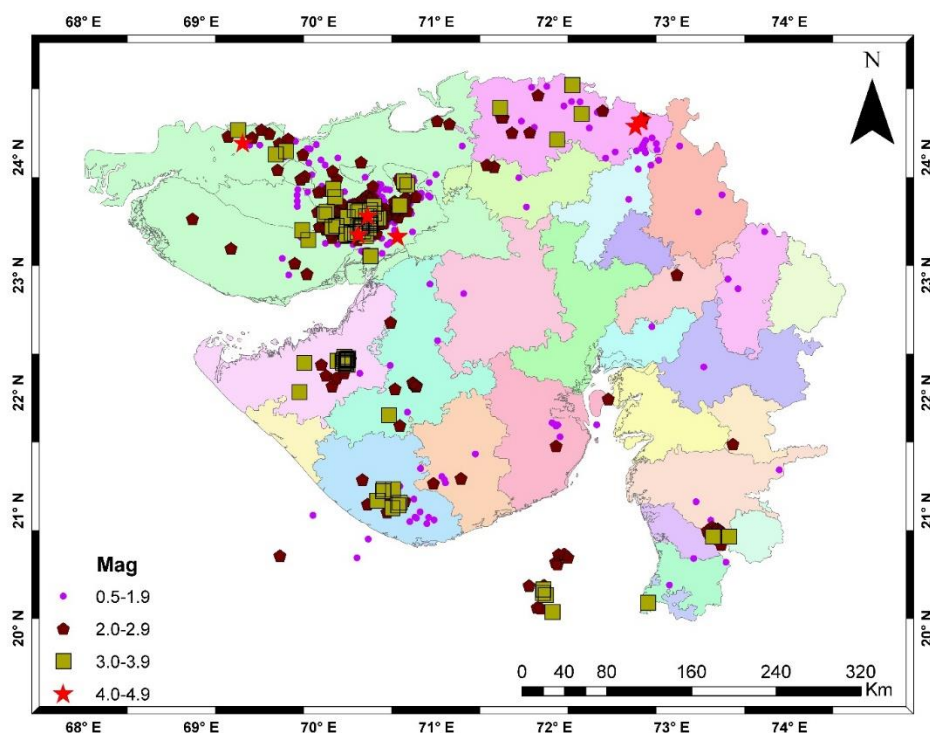


Fig. 1.2: Epicenters of earthquakes of M0.5-4.5 that occurred Gujarat in 2019

1.2.1 Seismicity in Kachchh

This year, in Kachchh, there were 724 shocks out of which 465 are of M0.6-1.9, 209 shocks are of M2.0-2.9, 43 shocks are of M3.0-3.9, and 4 shocks are of M \geq 4.0. Shock of the largest magnitude, i.e., M4.4 occurred on 18 Nov 2019, ~23 Km NNE from Bhachau, Kachchh.

1.2.2 Seismicity in Saurashtra

This year, in Saurashtra, there were 58 shocks of M<2.0, 94 shocks of 2.0-2.9, and 30 shocks of M3.0-3.9. Shock of the largest magnitude, i.e., Mmax.3.8 occurred 15 km ESE from Talala, Gir Somnath. Details of earthquakes of magnitude M \geq 3.0 in Saurashtra during 2019 are shown in Table 1.2

Table 1.2: List of earthquakes with magnitude M \geq 3.0 in the Saurashtra region during 2019

| Sr. No. | Year | MN | DD | HR | MN | LAT | LONG | M |
|---------|------|----|----|----|----|--------|--------|-----|
| 1 | 2019 | 1 | 20 | 6 | 53 | 21.044 | 70.672 | 3.8 |
| 2 | 2019 | 3 | 8 | 6 | 35 | 21.168 | 70.545 | 3.6 |
| 3 | 2019 | 3 | 8 | 9 | 7 | 21.184 | 70.63 | 3.5 |
| 4 | 2019 | 4 | 11 | 15 | 34 | 22.008 | 69.835 | 3 |
| 5 | 2019 | 4 | 12 | 18 | 37 | 21.068 | 70.685 | 3.5 |
| 6 | 2019 | 10 | 10 | 17 | 8 | 22.309 | 70.217 | 3.3 |
| 7 | 2019 | 10 | 13 | 2 | 3 | 22.284 | 70.212 | 3 |
| 8 | 2019 | 10 | 14 | 17 | 50 | 22.273 | 70.23 | 3.3 |
| 9 | 2019 | 10 | 17 | 17 | 52 | 22.274 | 70.201 | 3.2 |
| 10 | 2019 | 10 | 18 | 7 | 1 | 22.286 | 70.24 | 3.2 |
| 11 | 2019 | 10 | 18 | 16 | 5 | 22.282 | 70.239 | 3.6 |
| 12 | 2019 | 10 | 19 | 2 | 14 | 22.291 | 70.233 | 3.3 |
| 13 | 2019 | 10 | 21 | 22 | 50 | 22.254 | 69.876 | 3.4 |

| | | | | | | | | |
|----|------|----|----|----|----|--------|--------|-----|
| 14 | 2019 | 10 | 21 | 22 | 55 | 22.242 | 70.244 | 3 |
| 15 | 2019 | 10 | 22 | 21 | 1 | 22.276 | 70.155 | 3.4 |
| 16 | 2019 | 10 | 23 | 21 | 27 | 22.281 | 70.245 | 3.1 |
| 17 | 2019 | 10 | 28 | 8 | 17 | 21.812 | 70.595 | 3.1 |
| 18 | 2019 | 10 | 30 | 2 | 39 | 22.281 | 70.233 | 3 |
| 19 | 2019 | 11 | 4 | 14 | 21 | 22.286 | 70.237 | 3.7 |
| 20 | 2019 | 11 | 4 | 18 | 55 | 22.295 | 70.247 | 3.1 |
| 21 | 2019 | 11 | 4 | 20 | 10 | 22.28 | 70.245 | 3 |
| 22 | 2019 | 11 | 8 | 6 | 19 | 22.253 | 70.233 | 3 |
| 23 | 2019 | 11 | 15 | 4 | 20 | 22.263 | 70.228 | 3.2 |
| 24 | 2019 | 11 | 26 | 16 | 55 | 21.084 | 70.494 | 3.4 |
| 25 | 2019 | 12 | 2 | 11 | 5 | 21.02 | 70.621 | 3.4 |
| 26 | 2019 | 12 | 11 | 5 | 31 | 22.254 | 70.206 | 3 |
| 27 | 2019 | 10 | 25 | 17 | 41 | 20.333 | 71.908 | 3 |
| 28 | 2019 | 10 | 29 | 21 | 47 | 20.283 | 71.928 | 3.8 |
| 29 | 2019 | 10 | 31 | 5 | 42 | 20.139 | 71.985 | 3.3 |
| 30 | 2019 | 10 | 31 | 12 | 29 | 20.304 | 71.904 | 3 |

1.2.3 Earthquakes in Mainland Gujarat

In the Mainland, 73 shocks of M1.0 – 4.4 were located by the ISR network. Out of these, 8 shocks are of M3.0-4.4. The shock of the largest magnitude, i.e., Mmax.4.4 occurred on 5 June 2019, ~14 km NNW from Danta in North Gujarat.

Table 1.3: List of earthquakes with magnitude $M \geq 3.0$ in the Mainland region during 2019

| Sr. No | Year | MN | DD | HR | MN | LAT. | LONG | M |
|--------|------|----|----|----|----|--------|--------|-----|
| 1 | 2019 | 2 | 6 | 17 | 39 | 24.616 | 72.153 | 3.5 |
| 2 | 2019 | 2 | 13 | 5 | 14 | 20.218 | 72.797 | 3.6 |
| 3 | 2019 | 6 | 5 | 17 | 1 | 24.314 | 72.735 | 4.4 |
| 4 | 2019 | 10 | 20 | 3 | 25 | 24.371 | 72.232 | 3.2 |
| 5 | 2019 | 10 | 28 | 10 | 13 | 20.78 | 73.485 | 3.0 |
| 6 | 2019 | 11 | 15 | 8 | 6 | 20.779 | 73.347 | 3.3 |
| 7 | 2019 | 11 | 21 | 22 | 15 | 24.153 | 72.022 | 3.5 |
| 8 | 2019 | 12 | 9 | 2 | 57 | 24.421 | 71.541 | 3.1 |

1.3 Description of Earthquakes Recorded in different Parts of Gujarat since the inception of the network, till 2019

(Santosh Kumar, A P Singh, P Mahesh, Ketan Singha Roy, Vandna Patel)

Seismicity in Kachchh has consistently been lower since 2008 (Table 1.4) with about 60 shocks of $M \geq 3$ per year, in general. However, the seismicity in 2019 is slightly more than that in 2018, as there are 43 shocks of M3.0 – 3.9 in 2019. However, 30 shocks of M 3.0 – 3.9 occurred in 2018. There are 4 shocks of $M \geq 4.0$ in 2019, while in 2018 there were 3 shocks of $M \geq 4.0$ (Tables 1.4 & Figure 1.3).

Table 1.4: No. of earthquakes of $M \geq 3.0$ that occurred in Kachchh during 2008-19

| M | 2008 | 2009 | 2010 | 2011 | 2012 | 2013 | 2014 | 2015 | 2016 | 2017 | 2018 | 2019 |
|---|------|------|------|------|------|------|------|------|------|------|------|------|
| | | | | | | | | | | | | |

| | | | | | | | | | | | | |
|-----------|----|----|----|----|----|----|----|----|----|----|----|----|
| 3.0 - 3.9 | 66 | 73 | 52 | 62 | 56 | 59 | 45 | 70 | 49 | 47 | 31 | 43 |
| 4.0 - 4.9 | 5 | 4 | 1 | 3 | 2 | 3 | 1 | 1 | 2 | 5 | 3 | 4 |
| ≥5.0 | 0 | 0 | 0 | 0 | 1 | 0 | 0 | 0 | 0 | 0 | 0 | 0 |



Fig. 1.3: Annual no. of shocks in Kachchh during 2007-2019

Table 1.5: Shocks of $M \geq 3.0$ from 2007 to 2019 in the Saurashtra region

| M | No. of earthquakes |
|---------|--------------------|
| 3.0-3.9 | 136 |
| 4.0-4.9 | 8 |
| ≥5.0 | 2 |

Table 1.6: Annual number of earthquakes (M 3.0-5.1) in Saurashtra region during 2008-19

| M | 2008 | 2009 | 2010 | 2011 | 2012 | 2013 | 2014 | 2015 | 2016 | 2017 | 2018 | 2019 |
|-----------|------|------|------|------|------|------|------|------|------|------|------|------|
| 3.0 - 3.9 | 12 | 6 | 12 | 18 | 6 | 3 | 5 | 7 | 3 | 1 | 3 | 30 |
| 4.0 - 4.9 | 2 | 0 | 0 | 4 | 0 | 0 | 0 | 0 | 1 | 0 | 0 | 0 |
| 5.0 - 5.9 | 0 | 0 | 0 | 1 | 0 | 0 | 0 | 0 | 0 | 0 | 0 | 0 |
| Total | 14 | 6 | 12 | 23 | 6 | 3 | 5 | 7 | 4 | 1 | 3 | 31 |

During 2008-2019, 106 earthquakes $M3-3.9$, 7 earthquakes of $M4-4.9$, and 1 earthquake of $M5.1$ were recorded from Saurashtra. In 2019, the seismicity in Saurashtra was more than that in 2018, as there are 30 shocks of $M3.0 - 3.9$ in 2019. However, in 2018 only 3 shocks of $M 3.0 - 3.9$ were recorded (Tables 1.5, 1.6 & Fig. 1.4). This increase was due to the swarm type of activity observed near Jamnagar. The seismicity around Surendernagar has been categorized as blasts based on the analysis done previously and observation during the lockdown period and has been excluded.

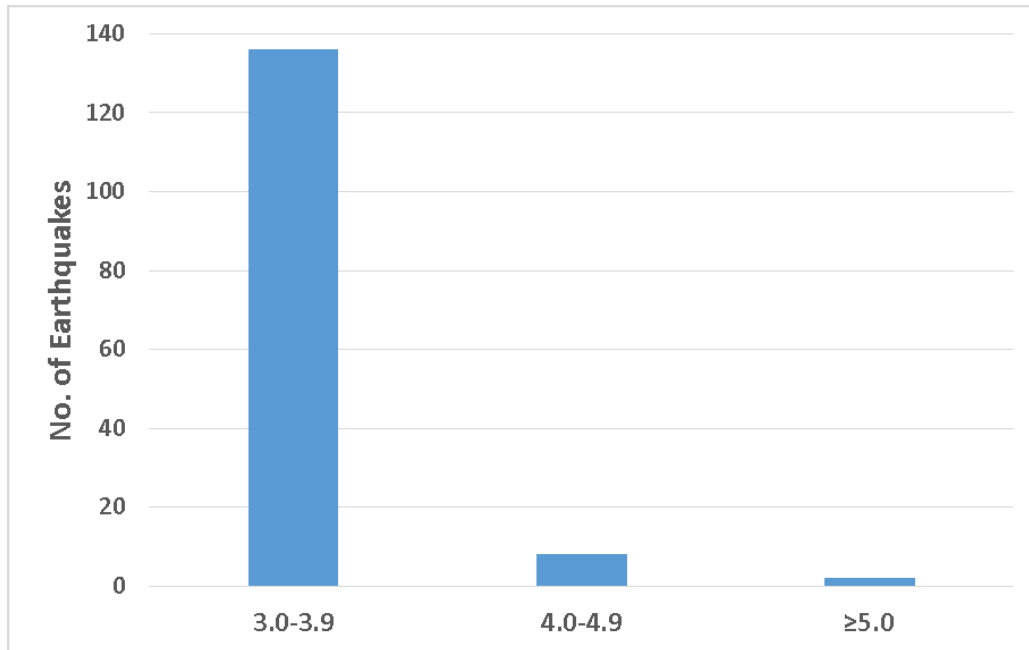


Fig. 1.4: Magnitude wise distribution of earthquakes in Saurashtra during 2007-2019

1.4 Earthquake data processing and interpretation of MEQ data collected during Jan-Dec 2018 for the study of seismogenic sources around the Subansiri Lower Hydro Electric (H.E) Project, Arunachal Pradesh

(P Mahesh, Kunjal Parmar, Santosh Kumar)

NHPC Limited is carrying out microearthquake (MEQ) studies in the Subansiri Lower HE Project, Arunachal Pradesh, since May 2006. The network consists of eight observatories in and around Subansiri Lower HE project that are acquiring local seismic data. While data acquisition is undertaken by NHPC, the work of analysis and interpretation of the data acquired is entrusted to ISR. The waveform data corresponding to micro earthquake occurrences has been acquired by NHPC at eight seismic observatories for 12 months period, from January to December 2018. In total, within the periphery of about 300 km from the Subansiri Lower project site, 766 earthquakes were located within a magnitude range of M_L 0.7-4.8 during 2018. There are 61 earthquakes in the magnitude range of 0.7 to 3.6 within 50 km radius of the dam site and most of these earthquakes are in the depth range of 10-30 km (Fig. 1.5). Within 50 km radius of the dam site, all the events are of small magnitude ($M < 4.0$) and among these the largest earthquake is of magnitude M_L 3.6 located around 24 km west of the dam site. Epicentres of earthquakes of $M \geq 4.0$ are at a distance of 136 km or more from the dam site and the pattern of seismicity is observed to be associated with the known tectonic features in the region. The obtained focal mechanism solution is in conformity with the thrust environment in the region.

The distribution of earthquakes within 50 km radius of the dam site, with depth error less than 5 km along the two profiles AA' and BB' is shown in Fig. 1.5. The depth distribution of earthquakes within 10 km on either side of these profiles is shown in Fig. 1.6. Most of the earthquakes within 50 km radius of the dam site are in the depth range of 10-30 km. From the depth sections, it can be observed that the depth distribution of earthquakes within the 50 km radius of the dam site are associated with the known seismogenic features in the region, namely, MFT, MBT and the Thrusts T1, T2 and T3 (running parallel / sub parallel to MBT in this region) to the northwest of the dam site.

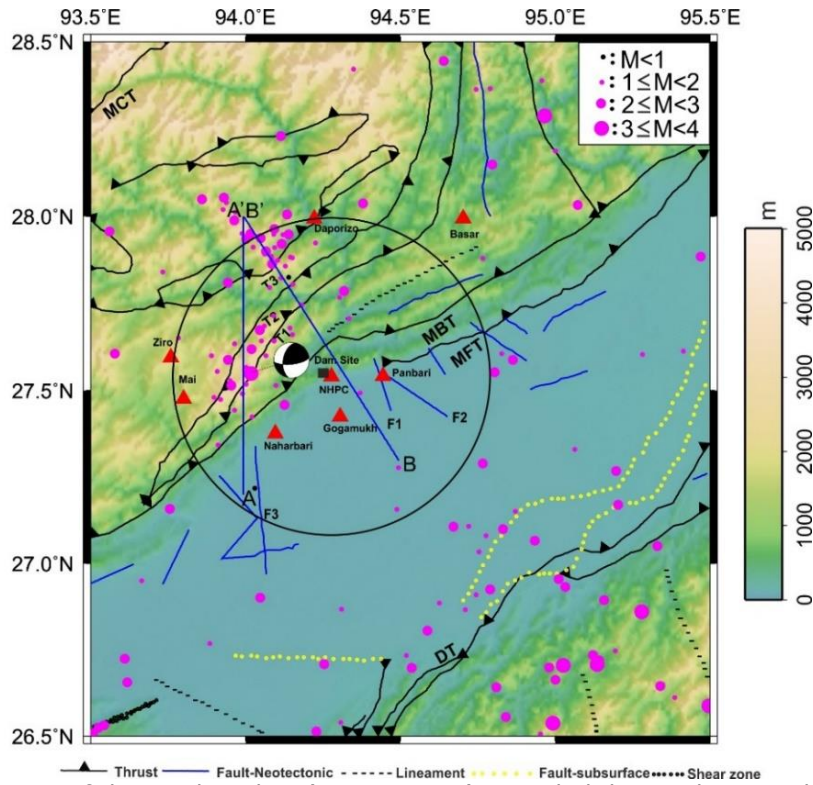


Fig. 1.5: Distribution of the earthquakes (S-P < 15 sec) recorded during the period Jan- Dec 2018. MCT: Main Central Thrust, MBT: Main Boundary Thrust, MFT: Main Frontal Thrust, DT: Disang Thrust. The small black rectangle represents the dam location and circle has a radius of 50 km from the dam site.

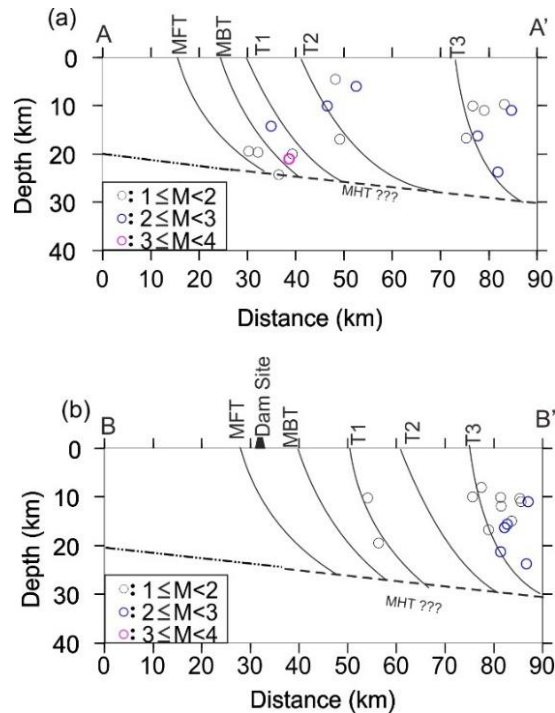


Fig. 1.6: Depth distribution of the earthquakes that occurred within 10 km width on either side of the two profiles (a) AA' and (b) BB' as shown in Fig. 1.5

1.5 Processing and interpretation of MEQ data collected during Jan-Jun 2019 for the study of Seismogenic sources around the Subansiri Lower H.E. Project
 (G. Srijayanthi, P. Mahesh, Santosh Kumar, Kunjal Parmar and Sumer Chopra)

This preliminary report provides information on data processing, analysis and interpretation of the digital earthquake data acquired by NHPC for a 6 month period from January to June 2019. The three-component raw seismic data from all the eight SLHEP (Subansiri Lower Hydro-electric Project) observatories are recorded continuously at 100 samples/s. Therefore, each station (observatory) has 24 files (one hour each) corresponding to 24 hours for each day. To check for the local seismic events, the data files recorded at different observatories were thoroughly analysed by systematic visual inspection of the recorded waveforms after applying different bandpass filters. The waveform data corresponding to each seismic event thus identified was fetched from all the observatories during the current period of study and were analysed to determine the local earthquake parameters like earthquake location and magnitude, by picking the arrival times of P-phase, S-phase and maximum amplitude of the S-wave. The earthquake waveforms for which the differential travel time between the S and P phases (i.e. S-P) is less than or equal to 40 s (epicentral distance < ~300 km at stations) were only considered for determining the earthquake locations.

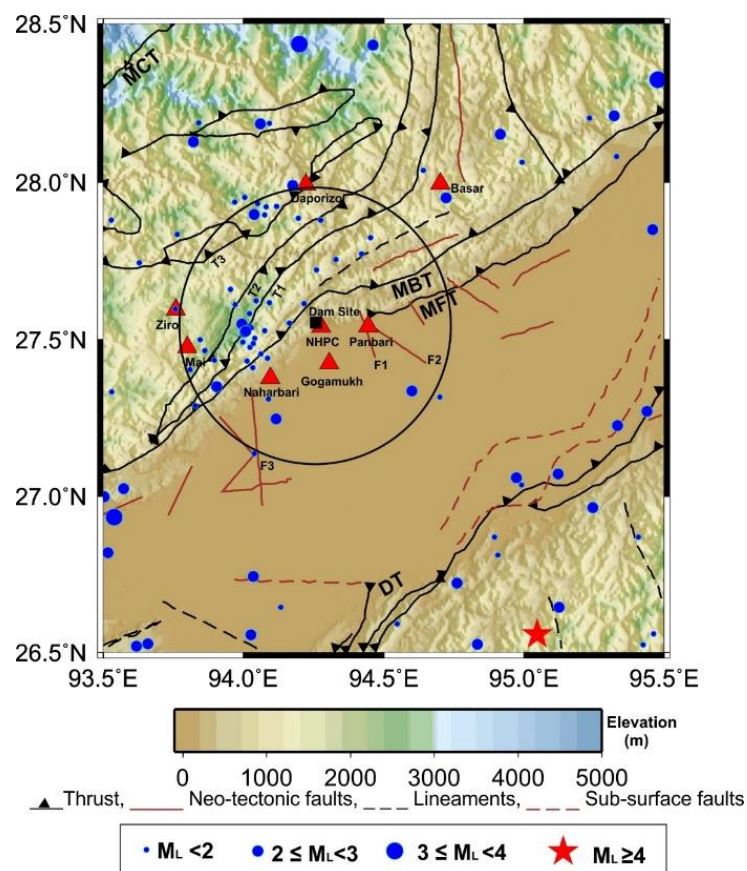


Fig. 1.7: Distribution of epicentres of earthquakes (with S-P < 15 sec) that occurred during Jan-Jun 2019, recorded by 3 or more SLHEP network observatories (red triangles). The black square indicates the dam site and the circle shows a radius of 50 km from the dam site. MFT: Main Frontal Thrust, MBT: Main Boundary Thrust, MCT: Main Central Thrust and DT: Dapsi Thrust.

There are 46 (Fig. 1.7) earthquakes in the magnitude range of M_L 0.8 and M_L 2.7 within 50 km radius from the dam site, with most of these earthquakes in the depth range of 10-30 km. In the 50 km vicinity of the dam site, only micro earthquakes ($M_L < 3.0$) are observed. Among these, the largest earthquake is of magnitude M_L 2.7 which is located around 35 km from the dam site. Majority of the earthquakes are either to the north or south of the dam site and trend NNE-SSW along the thrust faults T1, T2 & T3 dipping north-west. A few earthquakes are observed along DT and between DT and MFT. The seismicity pattern in general is associated with the known tectonic features of the region. During this study period, within the periphery of about 300 km from the Subansiri project

site, a total of 390 earthquakes (Fig. 1.8) were located in the magnitude range of M_L 0.8-5.6.

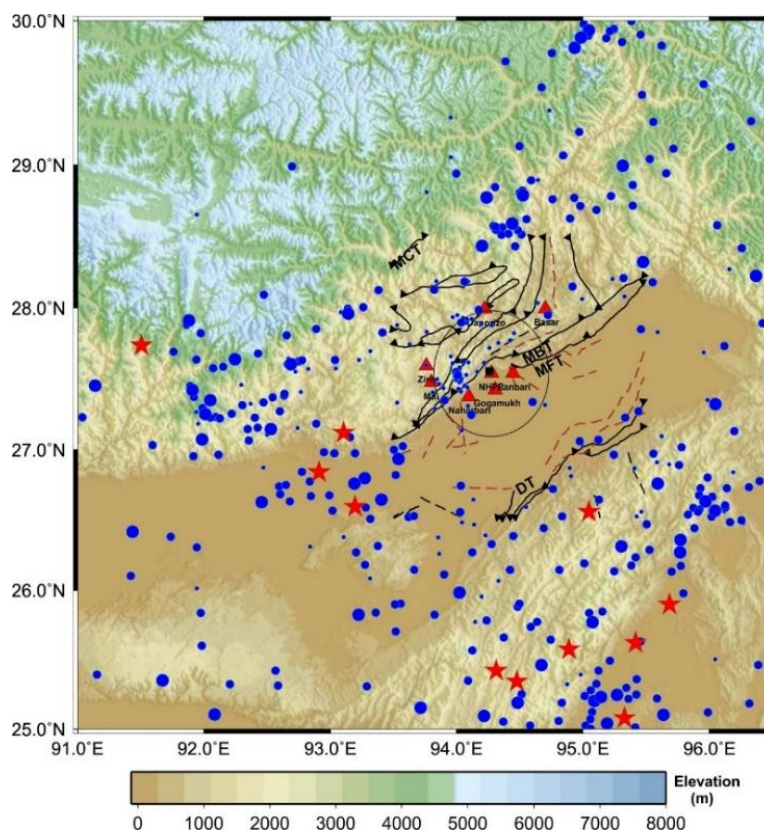


Fig. 1.8: Distribution of the earthquakes of different magnitudes (with $S-P < 40$ s) that occurred during Jan-Jun 2019, recorded by the SLHEP network. Tectonic features shown near the dam site are similar to those in figure 1.7. Circle shows a radius of 50 km from the dam site. The blue circles are earthquakes with $M_L < 4.0$ (with the legend same as in figure 1.7) and red stars are earthquakes with $M_L \geq 4.0$.

1.6 Analysis of earthquake swarm activity in Jamnagar District, Gujarat

(G. Srijayanthi, Sumer Chopra, Santosh Kumar and Harsh Limbachiya)

The clustering of earthquakes in both time and space with no prominent large magnitude earthquake is termed as an earthquake swarm. Numerous previous studies indicated that the swarm kind of earthquakes are either triggered due to large magnitude earthquakes or intrusion of fluids into weak/fracture zones associated with volcanic activity or rainfall (pore fluid pressure). Generally, swarm earthquakes are small in magnitude, of the order M 1.0 to M 5.0, and may not lead to large magnitude earthquakes. In such cases, the region, instead of being under stress for a long duration and prepare itself for a large magnitude earthquake, releases strain energy instantaneously through these small magnitude earthquakes. Previous studies by ISR researchers (Chopra et al., 2008) indicated that many regions in southern India are prone to short term earthquake swarm activity following the monsoons. Previously, a few regions in South Gujarat and Saurashtra (like the Talala, Navsari, Jamnagar, Haripur) hosted such swarm earthquakes (Chopra et al., 2008; Yadav et al., 2011, Singh, et al., 2017; Sateesh et al., 2019), which are attributed to triggering due to rainfall during monsoon. Further, they also observed that these earthquakes were associated with energy in the high frequency audible range (20-40 Hz), which was also confirmed by the locals, since these earthquakes were reported to produce subterranean sounds like those due to blasting.

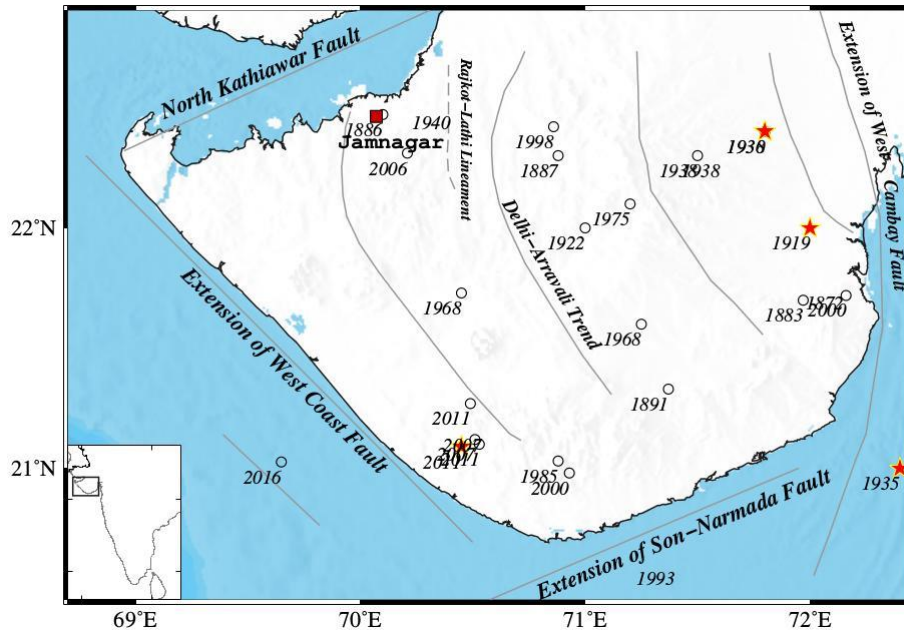


Fig. 1.9: The regional tectonic map of Saurashtra, Gujarat, north-western India, also showing the historical earthquakes with the year of occurrence mentioned below each event. The open circles and red stars indicate the magnitude of earthquakes $4.0 \leq M < 5.0$ and $M \geq 5.0$ respectively. The major tectonic features are shown with grey lines. Inset shows the location of Saurashtra (marked with rectangle) on the India map.

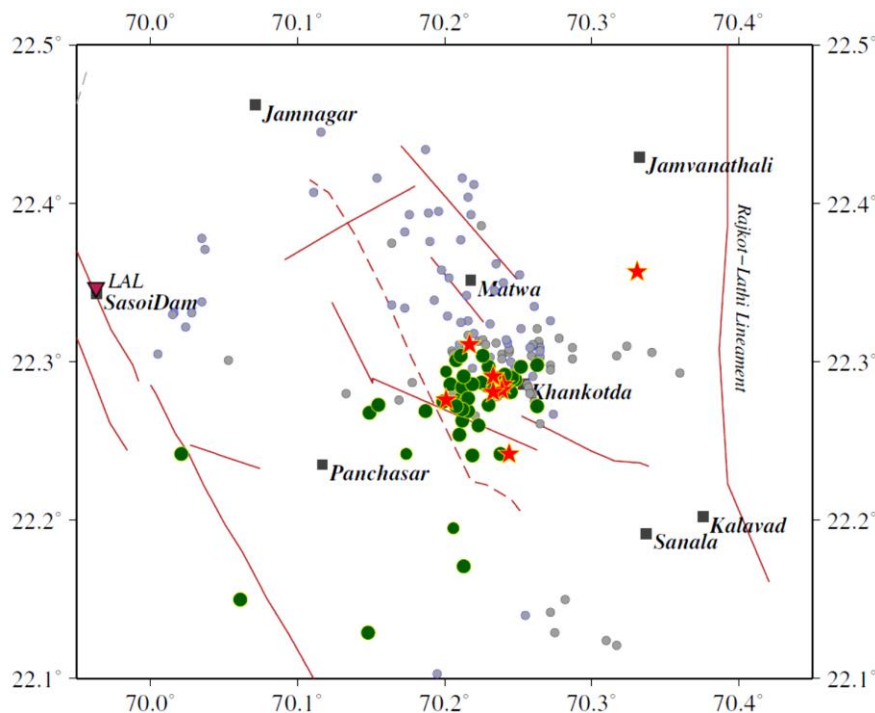


Fig. 1.10: The swarm activity observed from mid of September to November 2019 (green circles $M_L < 3$ and red stars $M_L \geq 3.0$). The maroon lines represent the local lineaments and the dotted line indicates a NW-SE trending dyke (a volcanic intrusive) (Mishra et al., 2001). Grey dots are the earthquake locations of the previous swarm activity in the region during 2006 and 2007.

The earthquake catalog of Saurashtra region compiled by ISR (source: https://isr.gujarat.gov.in/sites/default/files/eq_catalogue_saurashtra.pdf) validates that Jamnagar district is devoid of any major earthquakes of magnitude $M \geq 5$ (Fig. 1.9). However, even during the past, the region experienced earthquake swarm activity in confined regions during monsoons of August-September 2003, September-October 2006,

and August-September 2007. Detailed studies conducted by ISR established that these small (localised) regions temporarily become seismically active after heavy rainfall and the seismic activity decays in a month or two after monsoon.

During the end of 2019 summer monsoon, from mid of September to November 2019, we observed clustering of earthquakes in Jamnagar region, which we refer as the 2019 earthquake swarm. About 76 of these earthquakes are well recorded in near real time by the ISR network. The epicenters of these events are located near Khankotda region (Fig. 1.10). The seismic data is received from various recording stations through VSAT, which are analysed in near real time to estimate earthquake parameters like location, depth and magnitude. Further, the earthquake locations are updated/communicated immediately to the concerned control centres. The magnitudes range from M_L 1.0 to M_L 3.7 and the depths are mostly ≤ 10 km. We, also relocated the earthquakes with double difference algorithm (Waldhauser and Ellsworth, 2000), which drastically refined the relative earthquake location, depth and residual errors, thereby improving the location accuracies.

Two general trends were observed, one along NW-SE and another ENE-WSW. Out of these 76, 18 earthquakes have $M \geq 3.0$, with a maximum magnitude of 3.7 that occurred on November 4, 2019. Most of the earthquakes ($\sim 76\%$) have magnitudes less than 3. The activity in 2019 is SW of the swarm activity noticed during 2006-2007.

1.7 Moment Release and Mechanical coupling between fault systems

(Vishwa Joshi and Sumer Chopra)

The total moment release along different active sub regions of Kachchh is estimated for earthquakes of magnitude $M \geq 4$ and shown by different colours in Fig. 1.11 to understand the complex spatiotemporal patterns of the earthquakes in Kachchh. This will enable to understand if the earthquakes are simply random effects of long recurrence times on different faults or these migrating earthquakes reflect mechanical coupling between the fault systems.

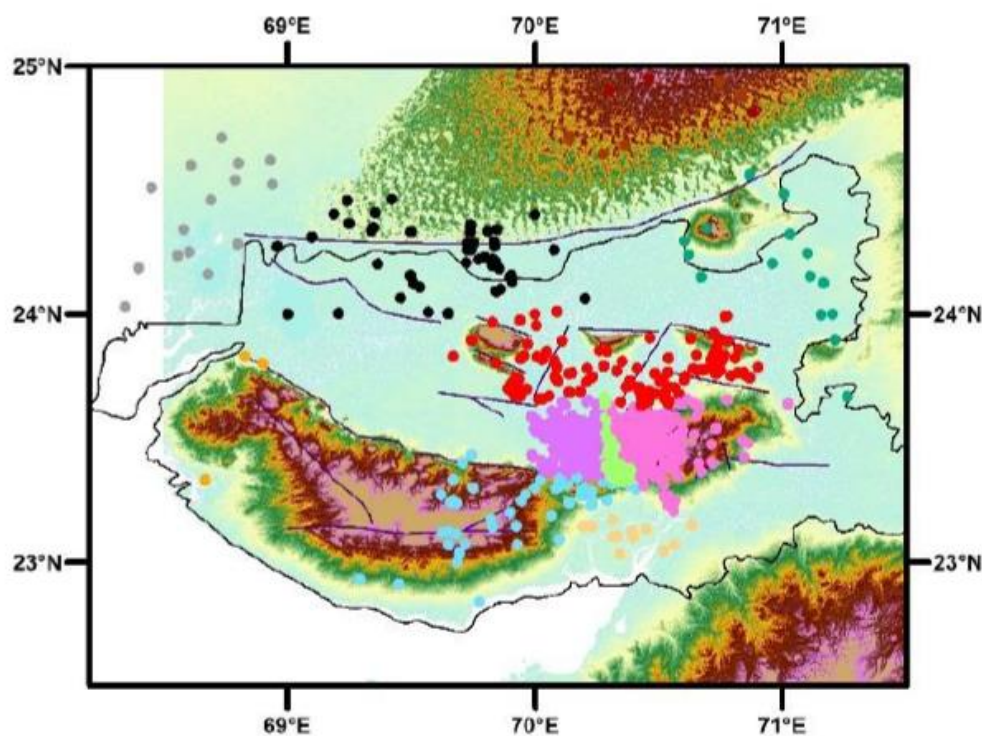


Fig. 1.11: Distribution of earthquakes in active regions shown by different colour

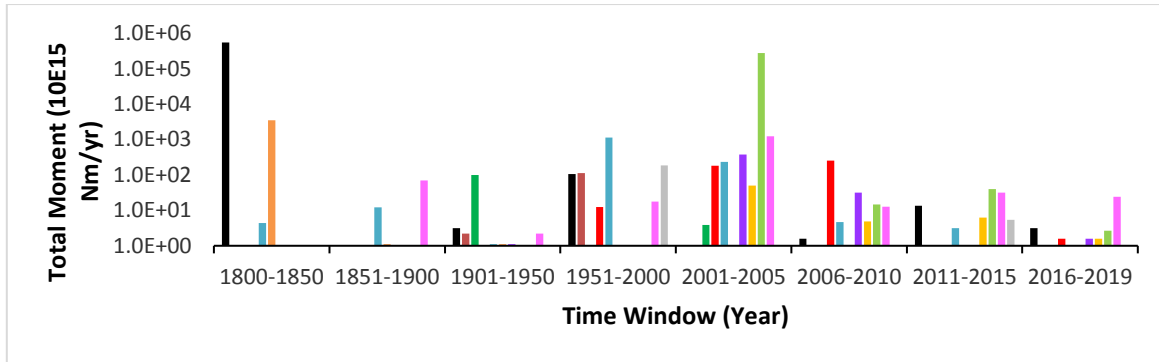


Fig. 1.12: Total moment release (colour of the bar represents the area shown in Fig. 1.1)

1.8 Earthquake swarm activity in and around Navsari district, South Gujarat

(A. Sateesh, S. Kumar, N. Makwana, S Chopra)

A swarm type of activity was being experienced in and around Vansda, Navsari and Dholvan talukas of Tapi district, since October 2019. These earthquake swarms were of low magnitude, accompanied by sound. A quick response team of three members from ISR was deputed to visit the seismically active areas and conduct an outreach program in order to create awareness among the people and ascertain the probable reason behind this. A similar activity was noticed in 2016, post monsoon. During Sep 2016 to Nov 2019, around 1246 earthquakes in the magnitude range of 0.7 to 3.1 have been located by ISR (Fig. 1.13). It is noted that the depth of these earthquake swarms is very shallow, in the range of 1-3 km.

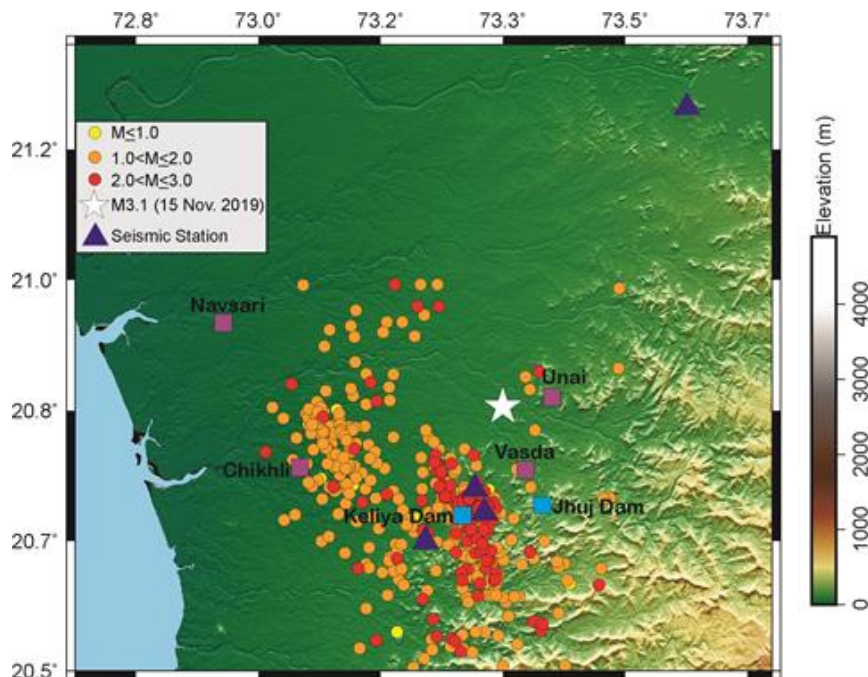


Fig. 1.13: Seismicity map for the Navsari region for the period Sep 2016-Nov 2019

The swarms were highly localized and became less intensive after 2-3 months. The swarm activity observed in Navsari region of South Gujarat appears to occur with some delay after the monsoon. Kaveru and Ambica are the two major river systems in this study region, and flow for only 2-4 months during and post monsoon season. The monsoon supplies water to these rivers which pass through the seismically active region. Since Kaveru and Ambica Rivers flow only during the monsoon period, they may be one of the causes for increase in the groundwater level. The water column weight on the underlying rocks may alter the pressure, making it easier for the existing fault to move, which is

apparently enough to trigger an event. Moreover, rain water percolates into the existing fractures and faults/lineaments, leading to pore pressure changes in the crust. Such incidents were reported from other parts of the globe also (Hanzl et al. 2006). The epicenter of the M 3.1 event on 15 Nov 2019 has been located near Unai, which lies between the Kaveru and Ambica rivers. Figure 1.4 is the histogram showing the month-wise number of earthquakes recorded by the network. It is observed that the earthquake activity is enhanced significantly from its normal value during Oct-Dec, immediately after the Indian summer monsoon. It is very difficult to assume that some tectonic activity is going on based on the geological filed investigation. However, the area needs extensive geological and geophysical investigations.

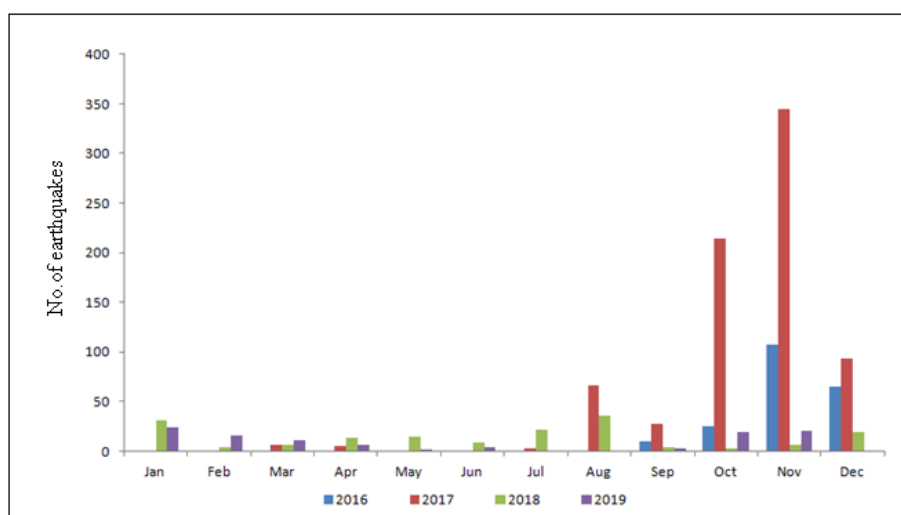
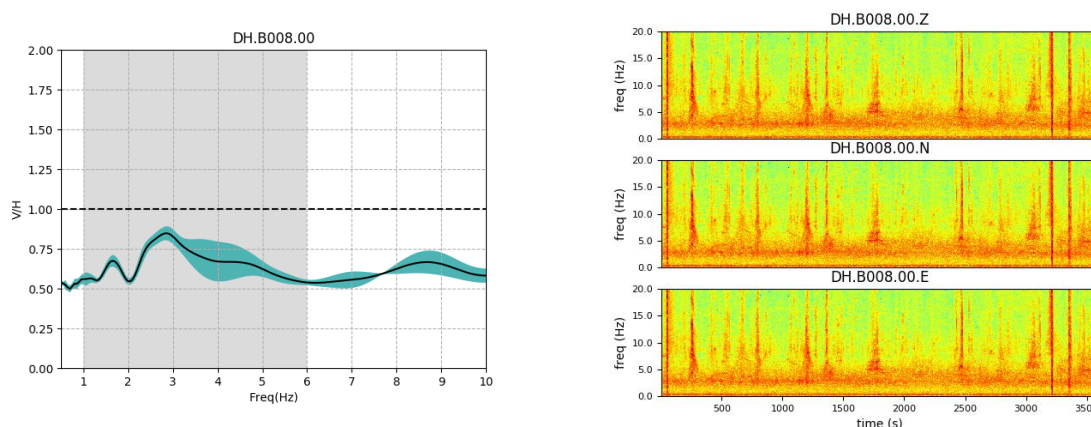


Fig. 1.14: Temporal distribution of seismicity in Navsari region during 2016 to November 2019

1.9 Low Frequency Passive Seismic study in Ahmedabad and Ankaleswar (Ketan Singha Roy and A P Singh)

Microtremor data recorded at potential hydrocarbon reservoirs display characteristic spectral anomalies at low frequencies between 1–6 Hz. This spectral anomaly is called Hydrocarbon Microtremor (HM) signal. Analysis of this characteristic spectral anomaly has been used as a technique to provide information about the presence of a hydrocarbon reservoir or Direct Hydrocarbon Indicator (DHI). V/H ratio can be an affirmative indicator for hydrocarbon reservoir when the vertical component of signal is greater than the horizontal component. The V/H spectral ratios have been calculated at 57 sites in Ahmedabad and 51 sites in Digas areas of Ankaleswar.



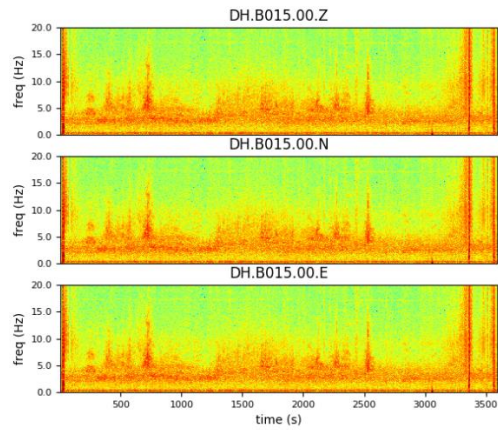
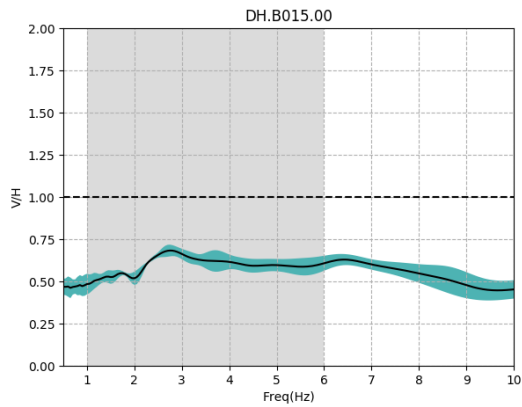
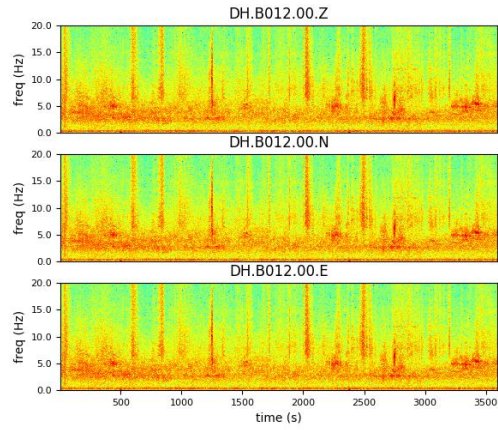
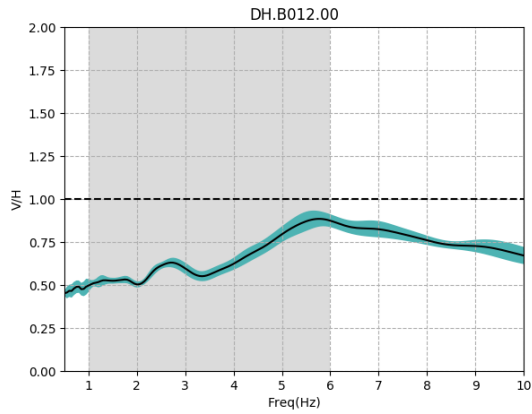
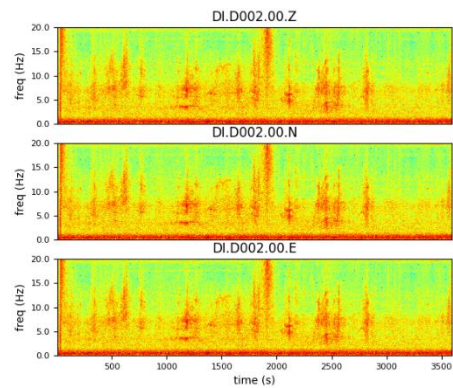
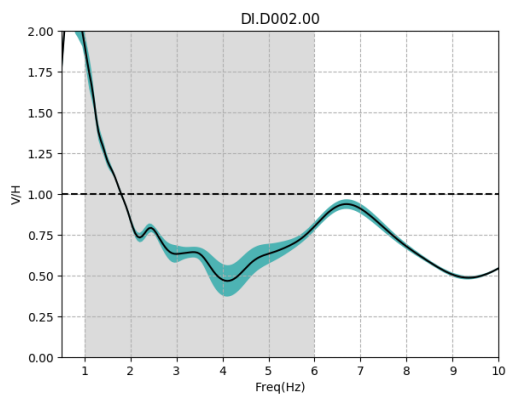
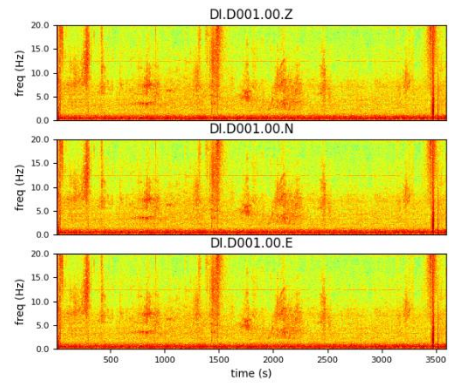
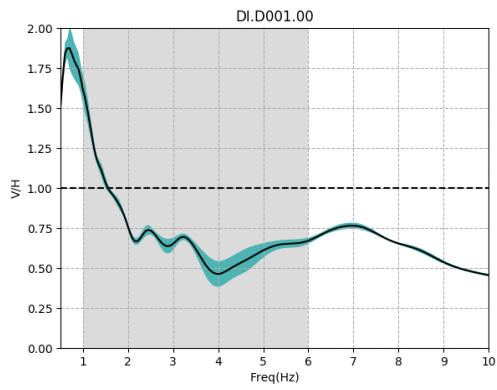


Fig. 1.15: V/H spectral ratio plots and spectrograms at some sites near Ahmedabad



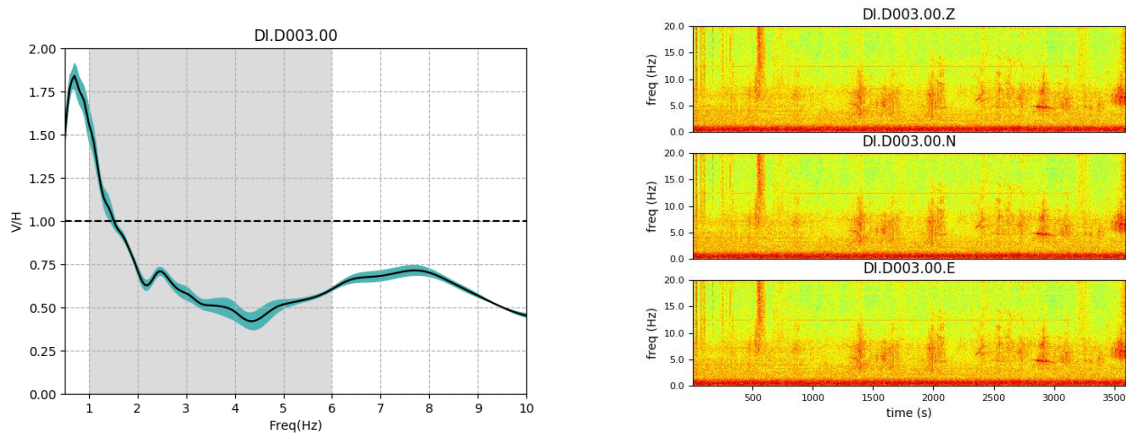


Fig. 1.16: V/H spectral ratio plots and spectrograms at some sites near Digas, Ankleswar

1.10 Low Frequency Passive Seismic study at Jotana and Mansa regions
(Ketan Singha Roy and A P Singh)

Microtremor data recorded at proven hydrocarbon reservoirs display characteristic spectral anomalies at low frequencies between 1 and 6 Hz. This spectral anomaly is called Hydrocarbon Microtremor (HM) signal. Analysis of this characteristic spectral anomaly has been used as a technique to provide information about the presence of hydrocarbon reservoirs or Direct Hydrocarbon Indicator (DHI). The V/H ratio can be a promising indicator for hydrocarbon reservoir when the vertical component of signal is greater than horizontal component signal (Lambert et al., 2009). Comparison of spectral V/H curves near different characteristic wells like Dry (or without oil) have been done for Jotana and Mansa regions (Figure 1.17 & 1.18).

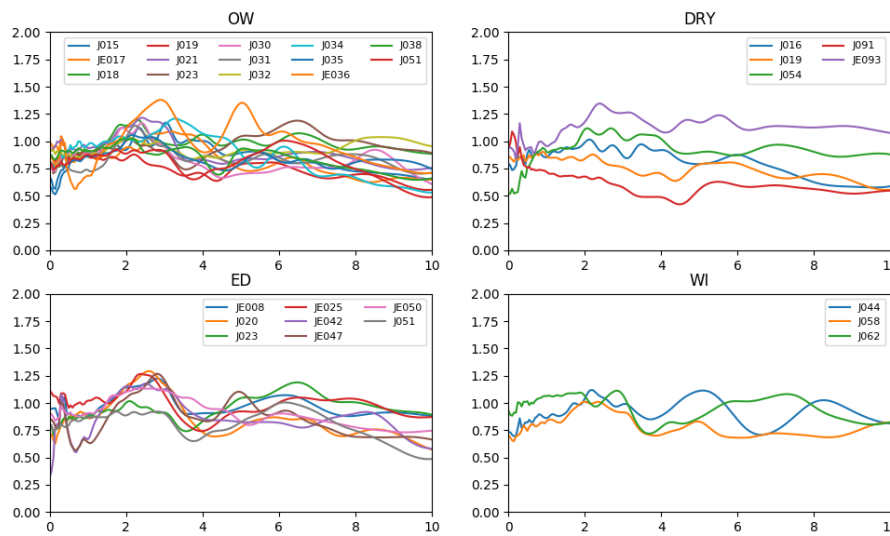


Fig. 1.17: Comparison of V/H plots for different types of wells for Jotana region

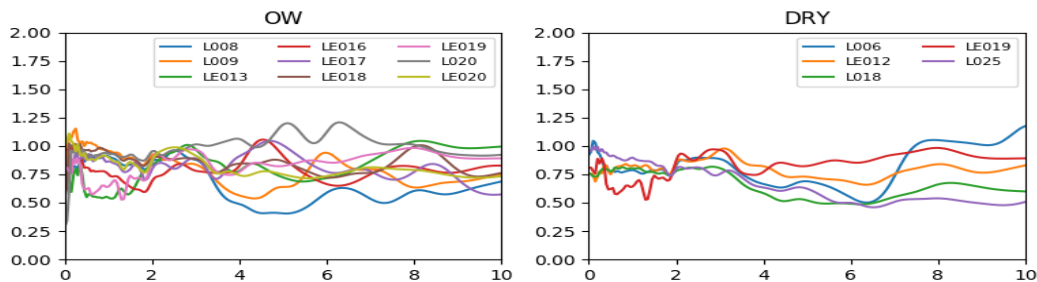


Fig. 1.18: Comparison of V/H plots for different types of wells for Linch region

1.11 New Insights from the Investigation of Remotely Triggered Earthquakes in Cambay and Narmada regions of Gujarat, India

(Mayank Dixit)

Recent studies suggest that seismic waves from significant earthquakes could trigger seismic events and deep tremors in tectonically active regions in the long-distance range. Dynamic stresses carried by teleseismic waves can promote failure on the critically stressed faults at depth and trigger local microseismicity. This phenomenon is also known as remote triggering. Since 2007, a new generation of broadband sensors has been deployed by ISR as permanent stations in different seismic zones of Gujarat. This, together with other permanent and temporary seismic stations, provides critical infrastructure to investigate the remote triggering phenomenon in Mainland region of Gujarat. In this study, we examine the remotely triggered seismicity following 14 mega distant mainshocks since 2007 through visual inspection of raw waveforms and spectrograms. The 2012 Indian Ocean mainshock was the only event that produced clear dynamic triggering in this region, although, some other events (e.g., the 2011 M9.1 Tohoku-Oki earthquake) also produced similar peak ground velocities. Our study suggests that the Mainland region is stress sensitive and susceptible for remote dynamic triggering, although the apparent triggering threshold appears to be slightly higher than other regions. It is noteworthy that the long period surface waves are primarily responsible for triggering. Additionally, we have found no correlation between the triggering events and back azimuth, due to limited observation of the positive triggering cases.

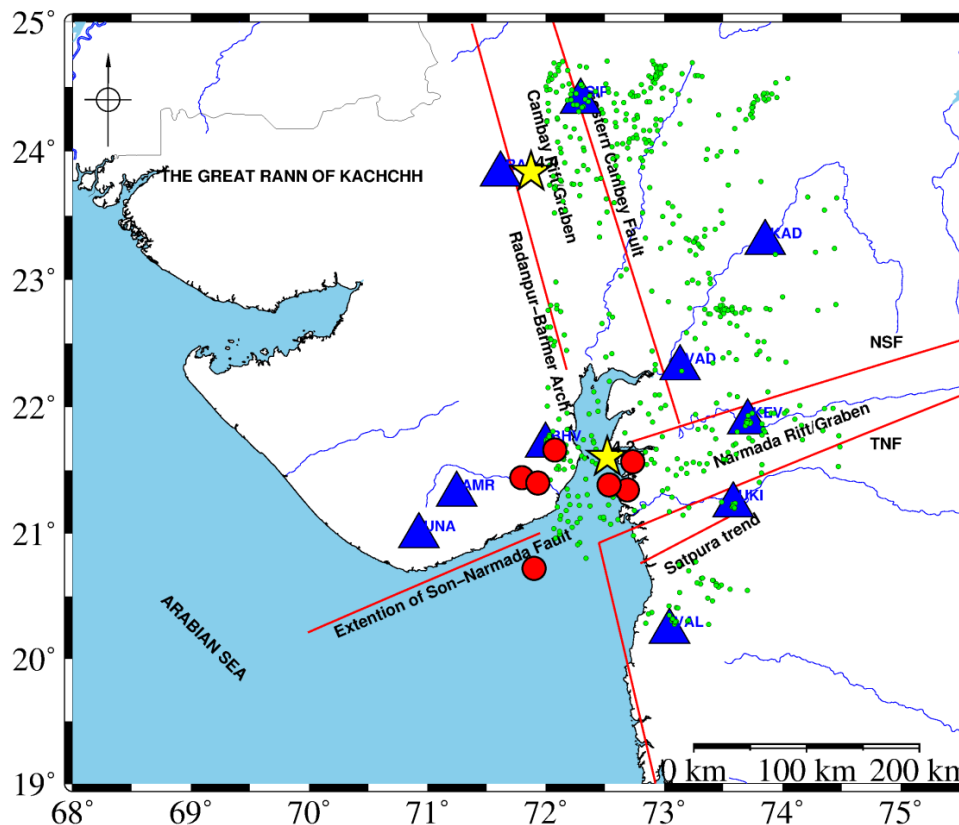


Fig. 1.19: Seismotectonic map of the Mainland Gujarat. The blue triangles are broad-band stations and red lines are active faults along with the background seismicity since 2007 (green dots). The red circles indicate triggered microearthquakes. Two yellow stars indicate earthquakes of magnitude ≥ 4.0 .

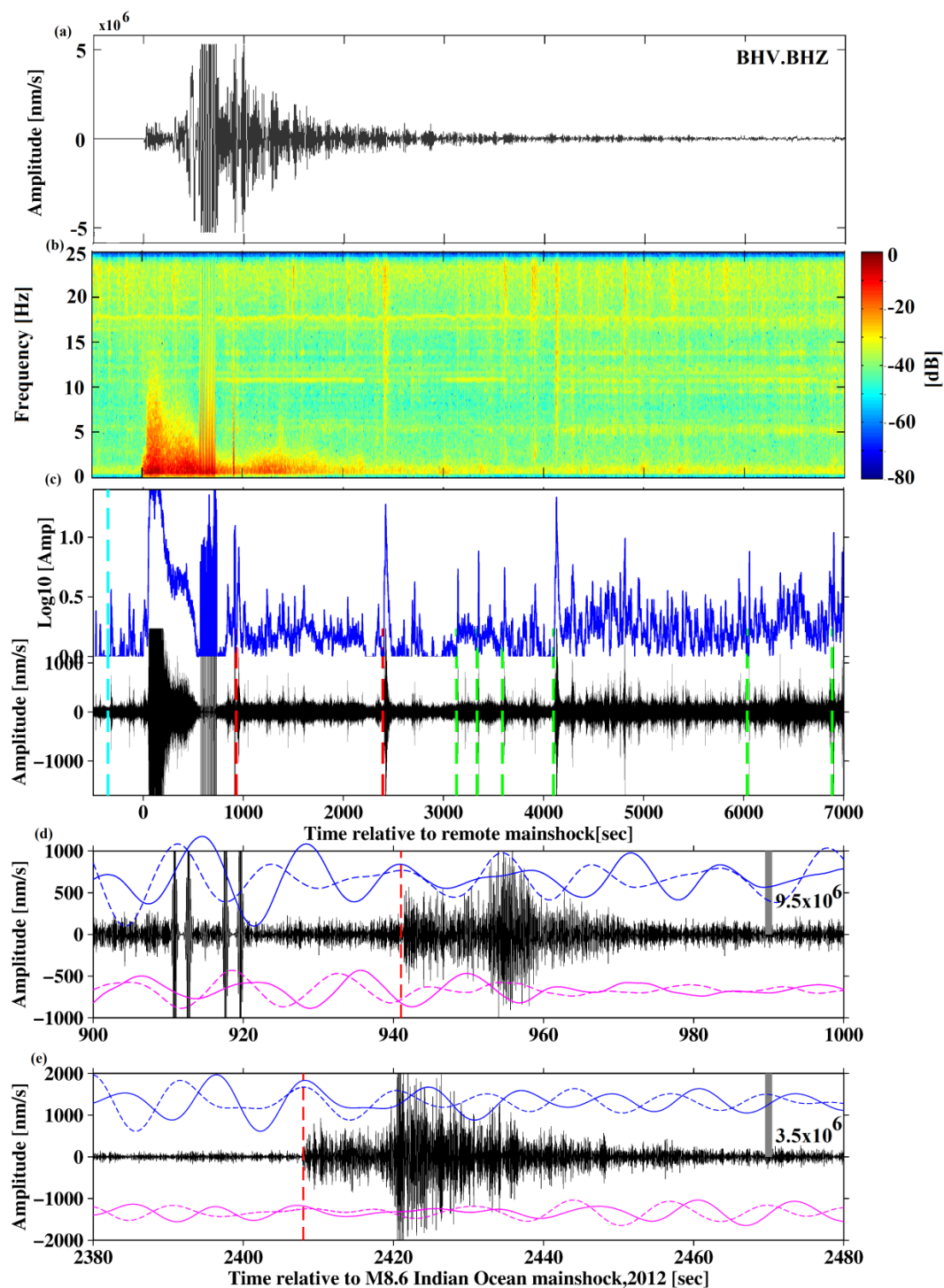


Fig. 1.20: Plot of triggered microearthquakes during and after the passage of waves related to the April 11, 2012, Indian Ocean earthquake (M8.6) recorded at BHV station. (a) Raw waveform data along with corresponding spectrogram in figure (b), (c) 5-16 Hz band pass filtered envelope function and waveform. The vertical red and green dashed lines mark the origin time of the triggered events during and after the surface wave, respectively. (d) The enlarged plot shows the broadband waveform and the triggered microearthquakes during the passage of surface waves of Indian Ocean earthquake. Blue and magenta waveforms are the rotated components of Rayleigh and Love wave, respectively. The solid and dashed waveforms represents the displacements before and after applying the time correction. Both microearthquakes are triggered by Rayleigh wave. Warm colours represent strong amplitude signal, whereas cool colours represent weak amplitude signal.

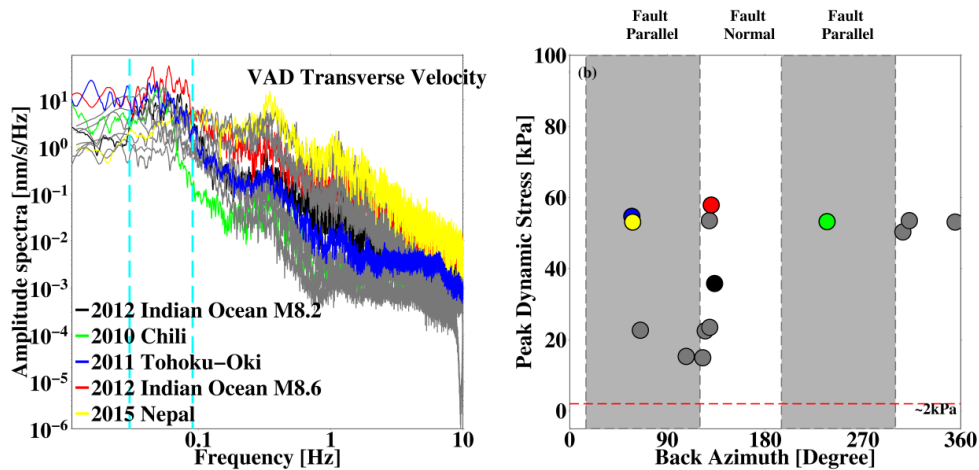


Fig. 1.21: (a) Comparison of the velocity spectra of the transverse component for the studied teleseismic events (dynamic stress ≥ 10 kPa). The zones between two vertical cyan lines are attributed to the individual higher amplitude. (b) Peak Dynamic stress plotted against back azimuth for remote mainshocks with dynamic stress ≥ 10 kPa, since 2007. The horizontal dashed line marks the stress level of ~ 2 kPa below which no remote mainshock triggers seismicity around the world.

1.12 Remote Dynamic Triggering in Hindukush Region following the Megaquakes ($M_w \geq 8.0$)

(Mayank Dixit)

Due to the scarcity of a dense seismic network, there are only few published records that have captured the phenomenon of remote triggering of earthquakes in the Himalayan arc. This zone, is situated in the western side of the densely populated New Delhi city, and has not observed a great ($>M_w 8.0$) earthquake for more than 1000 years, as per paleoseismological studies. Dynamic triggering can be used to quantitatively estimate the stress level along a fault plane and its spatiotemporal variation. In this study, we observed both dynamic and delayed triggering in the Hindukush region. Additionally, we have estimated stress changes, and a variety of statistical parameters for the dynamically triggered and delayed local events. Our goal is to generate one of the most comprehensive reviews on the mechanisms that drive dynamic and delayed triggering for this area. Furthermore, the abundance of teleseismically triggered local earthquakes contributes to our main earthquake catalog, aiding in revealing seismicity patterns and fault structure.

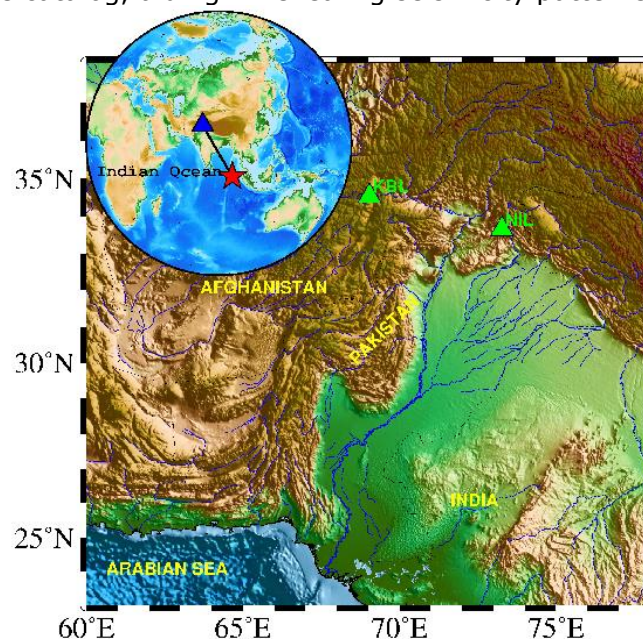


Fig. 1.22: Map of the Hindukush region of the Himalaya. The green triangles are broadband stations used in the study. In the top-left inset map, the epicentral location of triggering remote main shock

(red star), April 11, 2012, M8.6, Indian Ocean Earthquake is shown, along with the great circle path as a black line. The green triangles represent the NIL and KBL stations in Hindukush.

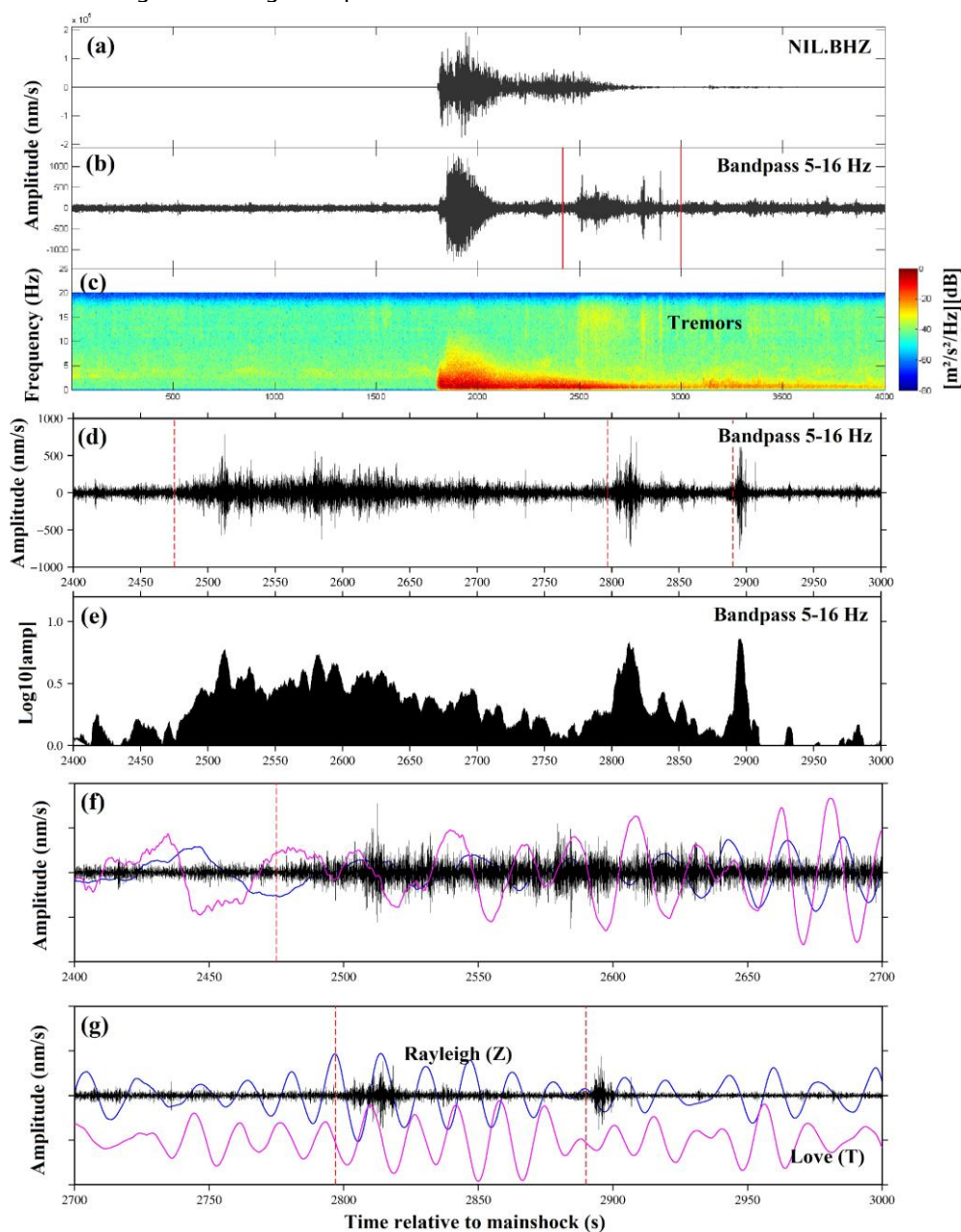


Fig. 1.23: (a) Waveform data of April 11, 2012, Indian Ocean Earthquake (M8.6) recorded on the vertical component at NIL station, (b) 5-16 Hz band-pass filtered data, (c) spectrogram of the vertical component. The enlarged portion of the vertical red lines are shown in figures (d) and (e). (d) 5-16 Hz bandpass data and its corresponding envelope function shown in figure (e). The dotted vertical lines are attributed to the origin time of triggered tremors. Figures (f) and (g) show an enlarged view of the 5-16 Hz bandpass broadband waveform and triggered tremors during the passage of surface waves. Blue and magenta lines are the rotated components of Rayleigh and Love wave, respectively.

1.13 Estimation of Source Parameters

(Ketan Singha Roy and Santosh Kumar)

Source parameters, namely, stress drop, corner frequency, seismic moment etc., have been estimated for small to moderate earthquakes in Arunachal Pradesh. We have used velocity records from 380 earthquakes (M1.7 – 5.0), that occurred in 2015. Most of the shocks have higher corner frequencies for P-waves, compared to S-waves. The stress drop

values lie in the range 0.05 – 94 bars and seem to be correlated with seismic moment (Fig. 1.24). The corner frequency varies between 1.9 and 7.86 Hz (Fig. 1.25).

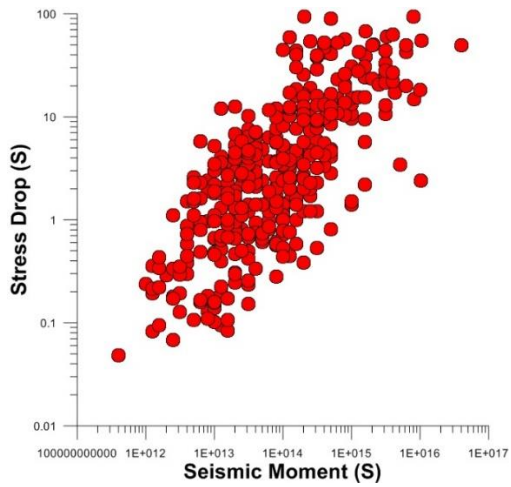


Fig. 1.24: Plot between stress drop and Seismic moment

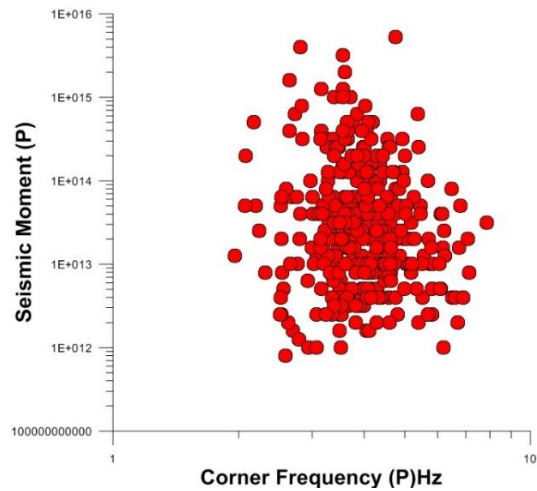


Fig. 1.25: Plot between corner frequency and Seismic moment

2. SEISMIC HAZARD ASSESSMENT AND MICROZONATION

2.1 Development of Site Specific Response Spectrum at Khavda windmill site, Kachchh

(Kapil Mohan, Sumer Chopra, Naveen Kumar, Madan Mohan and Shruti Dugar)

The M/s. Adani Green (Gujarat) Pvt. Ltd. has requested ISR to conduct site specific seismic hazard assessment and develop site-specific ground response spectra for Khavda windmill site, Kachchh, Gujarat (Fig. 2.1). The Soil Testing (ST) report from two boreholes drilled to ~100 m depth, prepared by M/s KCT Consultancy Services, Ahmedabad was provided to ISR. We conducted both Probabilistic Seismic Hazard Assessment (PSHA) and Deterministic Seismic Hazard Assessment (DSHA) to estimate the Seismic Hazard at the windmill site. The PSHA has been conducted for 2% (2475 yrs. return period) and 10% probability of exceedance in 50 years (475 yrs. return period) for C-type NEHRP soil condition.

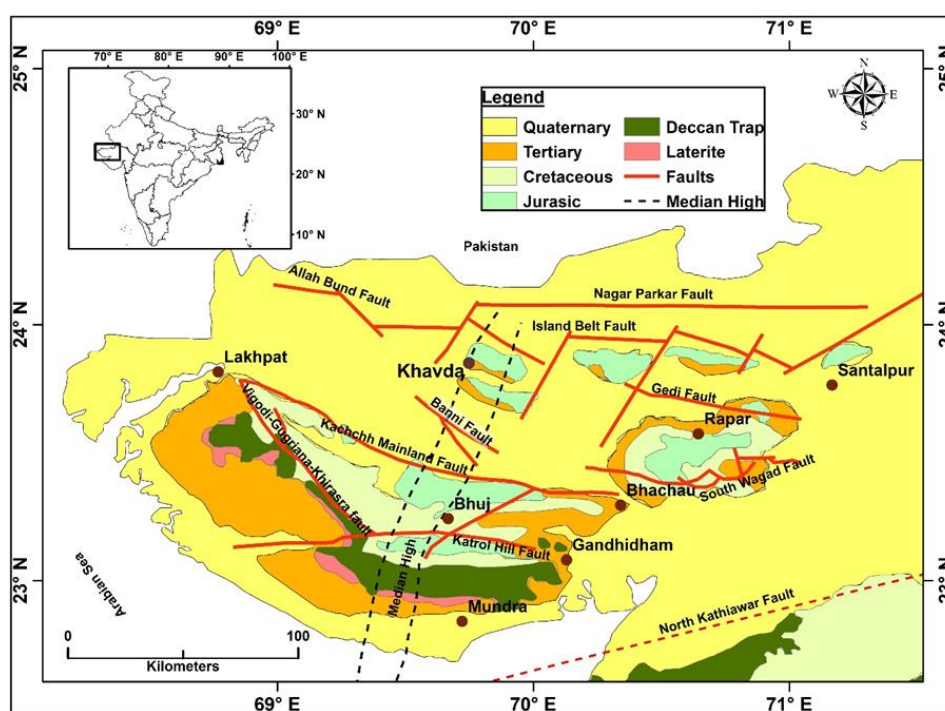


Fig. 2.1: The site location along with Geology and Tectonic map of Kachchh (after Biswas, 2016)

The DSHA is conducted considering a Mw 7.8 earthquake along the Allahbund fault, akin to that of 1819. The earthquake catalog for Gujarat region prepared by ISR from the year 1668 to 2016 has been used for the PSHA. Detailed calculations are carried out considering the inputs from both the boreholes drilled at the site and the Engineering Bed layer (EBL) is estimated based on Geophysical (MASW) and Geotechnical investigations. The EBL is marked at a depth of 63m in BH-01 and 80m at BH-02 with Vs of ~500m/s and N160 >100. The PGA has been estimated at the EBL using the Stochastic Finite Fault Modelling Technique (SFFMT). The ground motion at surface level has been estimated using 1D ground response analysis.

As for the PSHA, the PGAs have been estimated corresponding to return periods of 475 yrs, 2475 yrs at 520m/s (C-type soil). The NEHRP amplification factor is applied to estimate the surface (D-type soil) PGA. A total of nine input parametric combinations have been used to estimate the PGAs at each borehole at the EBL level using DSHA. The ground response analysis using SHAKE has been conducted to estimate the surface PGA and response spectra (Fig. 2.2) at each borehole. The deterministic ground motion values have

been found higher than the values estimated using PSHA. The mean amplification factor of 1.25 is computed (between EBL to surface) at the site through DSHA. The higher PGA values were considered for the computation of design spectra.

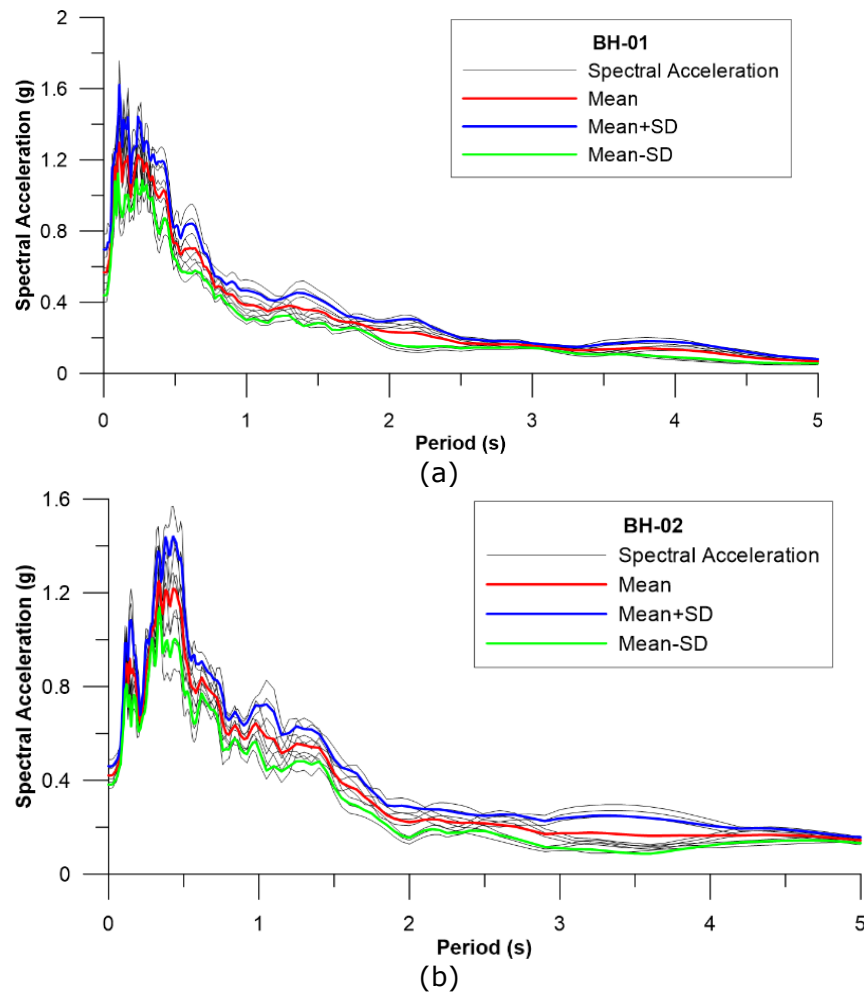


Fig. 2.2: The normalized response spectra (Mean, Mean+SD and Mean-SD) at 5% damping estimated at boreholes (a) BH-01 and (b) BH-02

2.2 Multi-criteria study for Seismic Hazard Assessment of UNESCO world heritage Ahmedabad city, Gujarat, Western India

(V. K. Dwivedi¹, R. K. Dubey², V. Pancholi¹, M. M. Rout¹, P. Singh¹, B. Sairam¹, S. Chopra¹ and B. K. Rastogi¹)

¹Institute of Seismological Research, Raisan, Gandhinagar, Gujarat 382009, India

²Indian Institute of Technology, Indian School of Mines IIT(ISM), Dhanbad

Ahmedabad, the most populous city of Gujarat, assigned zone III in the seismic zone map of India (BIS, 2002), has experienced moderate earthquakes in the past. Several high-rise buildings have collapsed or severely damaged in the city during the 2001 Bhuj earthquake (Mw 7.6), which was 240 km from the city. Keeping this in view, micro-level seismic hazard assessment in the city is carried out using geotechnical, geological and geophysical inputs, which may help in designing buildings and other civil engineering structures and will reduce the probability of loss of life and property in this region. A total of 23 boreholes (11 boreholes of 80m, 7 boreholes of 40m and 5 boreholes of 35m) were drilled at different locations in the city. To estimate the shear-wave velocity, we have employed direct and indirect methods. PS logging is carried out in 11 boreholes and shallow geophysical investigations (multi-channel analysis of surface waves, MASW) are carried out at 54 sites. The field and laboratory tests on soil samples, geophysical

investigations and seismotectonic information enabled us to estimate soil overburden thickness, shear-wave velocity, factor of safety against liquefaction, and site response in terms of amplification factor. The peak ground acceleration was estimated at engineering bed rock level ($V_s760\text{m/s}$) by PSHA. All this information is used in preparing an integrated seismic hazard (SH) map of the Ahmedabad city using an analytical hierarchical process. The seismic hazard map is characterized into three broad categories; low, moderate and high. The western part of Ahmedabad shows the highest hazard. The northern and the eastern parts show moderate seismic hazard. It is observed that the presence of sand and flood plain deposits along the Sabarmati river increases the hazard. The study has also highlighted that the presence of a paleochannel increases the overall hazard, which is clearly visible in the integrated hazard map.

2.3 Geotechnical characteristics of soils to identify liquefaction potential of the coastal area of the Bhavnagar, Gujarat, Western India

(V. Pancholi, P. Singh, M. M. Rout, N. Bhatt, V. K. Dwivedi, S. Chopra)

The Bhavnagar district falls under zone III of the seismic map of the India, where magnitude 6 and maximum intensity of VII or VIII can be expected due to regional or local earthquakes. The district is located in the southeastern part of the Saurashtra peninsula of Gujarat with a coastline of almost 145 km. Bhavnagar, Ghogha, Talajaand Mahuva are the important sea ports of the district. A major part of the district is occupied by basalt while loamy mixed, calcareous, fine and montmorillonite soils cover different geomorphological terrains of the district near the coastal region. The catalogue of earthquakes shows that the region has experienced an earthquake in February 1705, that had an intensity of XI (MMI) near Ghogha. During 2000, the region has experienced almost 132 earthquakes (3 earthquakes of >3.8 magnitude) in a span of almost 4 months (9 August to 15 December 2000). Among them, around 40 events are located in the southeast of Bhavnagar town. The damages due to this swarm activity are inexplicably high considering the magnitudes of the events. In this study, we have collected geotechnical information from coastal area of the district and evaluated liquefaction hazard. The boreholes are of minimum 18m and maximum 50m depth. The index properties of soil from these boreholes were estimated. With the help of density, plasticity index, ground water level, Peak Ground Acceleration (PGA), fine content and SPT N value, liquefaction hazard is estimated by standard methodologies. The study shows that the coastal area has moderate to high probability of the liquefaction during a major earthquake.

2.4 Geotechnical Investigation for estimation of the Liquefaction hazard for the capital city of Gujarat state, Western India

(V. Pancholi, V. K. Dwivedi, P. Choudhury, S. Chopra)

Gandhinagar, the capital city of Gujarat state, Western India is situated in the middle of the moderately active Cambay rift. The region lies under the seismic zone III of the seismic zoning map of India. The city rests on 250m – 300m thick flood plain deposits consisting of coarse sand, silt and clay. In this work, liquefaction hazard is assessed using geotechnical investigations. A total of 14 boreholes of 35 to 50m depth were drilled with sampling at every 1.5m depth interval (till termination depth) covering the entire Gandhinagar city. A standard penetration test (SPT N-value) was conducted at an interval of 3m depth in every borehole. We used 400 samples for the estimation of index properties of the soil in the study area. The lithological distribution in the city is also mapped based on the soil classification. The liquefaction hazard is estimated by standard methodologies using density, plasticity index, groundwater level, Peak Ground Acceleration (PGA), fine content and Standard penetration test (SPT) N value. The site-specific PGA values at the surface are estimated by carrying out ground response analysis. The study shows that the area comprises alternate layers of argillaceous and arenaceous soil. We found that in general the area has low liquefaction

potential but in case of heavy rainfall, the chances of liquefaction may increase as the soils are conducive to liquefaction.

2.5 Engineering Geological Mapping for Seismic Hazard Assessment of the Gandhinagar City, western India

(V. Pancholi ¹, V. K. Dwivedi ¹, B. Sairam ¹, P. Choudhury ¹, S. Chopra ¹, N.Y. Bhatt ²)

¹Institute of Seismological Research

²M.G. Science Institute

Gandhinagar is the capital of Gujarat state in western India and a center of intense economic and urban development activity, which requires a constant need for development and expansion. The city, having a total area of 57 km², is situated on the bank of the river Sabarmati. Geologically, the city is covered by alluvium deposits, and the top layer of 80 - 100 meters is composed of loose sandy and soft clayey soils. Most of the urban activities in the city are located on these subsoil strata. A geotechnical database is prepared at various locations of the city along with the geological and geomorphological details. In the framework of this study, 14 boreholes have been drilled, and detailed mapping of the city is done according to its lithology, soil properties, standard penetration test (N Value) and shear wave velocity (Vs). With the use of the average shear wave velocity, the amplification factor and peak ground acceleration (PGA) at surface are estimated and further used for the assessment of seismic hazard. The seismic hazard analysis is done by using published ground motion prediction equations (GMPE) developed for the Gujarat region. Four published GMPEs are used in a logic tree approach by taking magnitude 6.0 as the scenario earthquake for near field case. The distance of the source from each borehole is calculated and used in GMPEs. Two scenario earthquakes representing Mw7.7, 2001 Bhuj earthquake and M6.5 in the Narmada-Son region are also considered as far-field earthquakes. From the detailed analysis, soil map, SPT N value map, Vs map and PGA map are prepared and placed on Geographic Information system (GIS) platform to interpret the complex data for reliable interpolation. The study shows that the areas in the central and southwestern parts of the city are more prone to high ground shaking and related damage during a major earthquake in Gujarat. The results can be considered to guide further urban development and possible infrastructural development of the city.

2.6 Seismic Hazard assessment in northern Kachchh

(Vandna Patel, Harsh Limbachiya, Naveen Sharma, Tarun Solanki, Sumer Chopra)

M/S Adani Wind Energy (Gujarat) Pvt. Ltd (AWEPL) has requested the Institute of Seismological Research (ISR) to carry out seismic hazard assessment at their upcoming project site, north of Khavda, Kachchh district, Gujarat, very near to the international border. The area is around 589 sq.km to the north of road connecting India bridge with Vighakot, spreading roughly 25km in the north-south and 35 km in the east-west directions (Fig. 2.3). The region is almost flat and most parts remain water-logged during monsoon.

The project area falls in Zone V as per seismic zoning map of India of BIS, indicating maximum seismic hazard potential. The area hosted a large earthquake of magnitude 7.8 in 1819, which changed the topography of the region and uplifted an 80 km long stretch of land called Allah-Bund. ISR carried out geological mapping of the entire project area and then carried out shallow geophysical surveys comprising multi-channel analysis of surface waves (MASW) and microtremor investigations covering the entire project area. The field investigations started on Feb 13, 2020 and ended on March 21, 2020. Three teams participated in the survey for carrying out geological mapping, MASW survey and microtremor surveys. MASW survey is carried out at 40 sites and microtremor at 100 sites covering entire area uniformly.

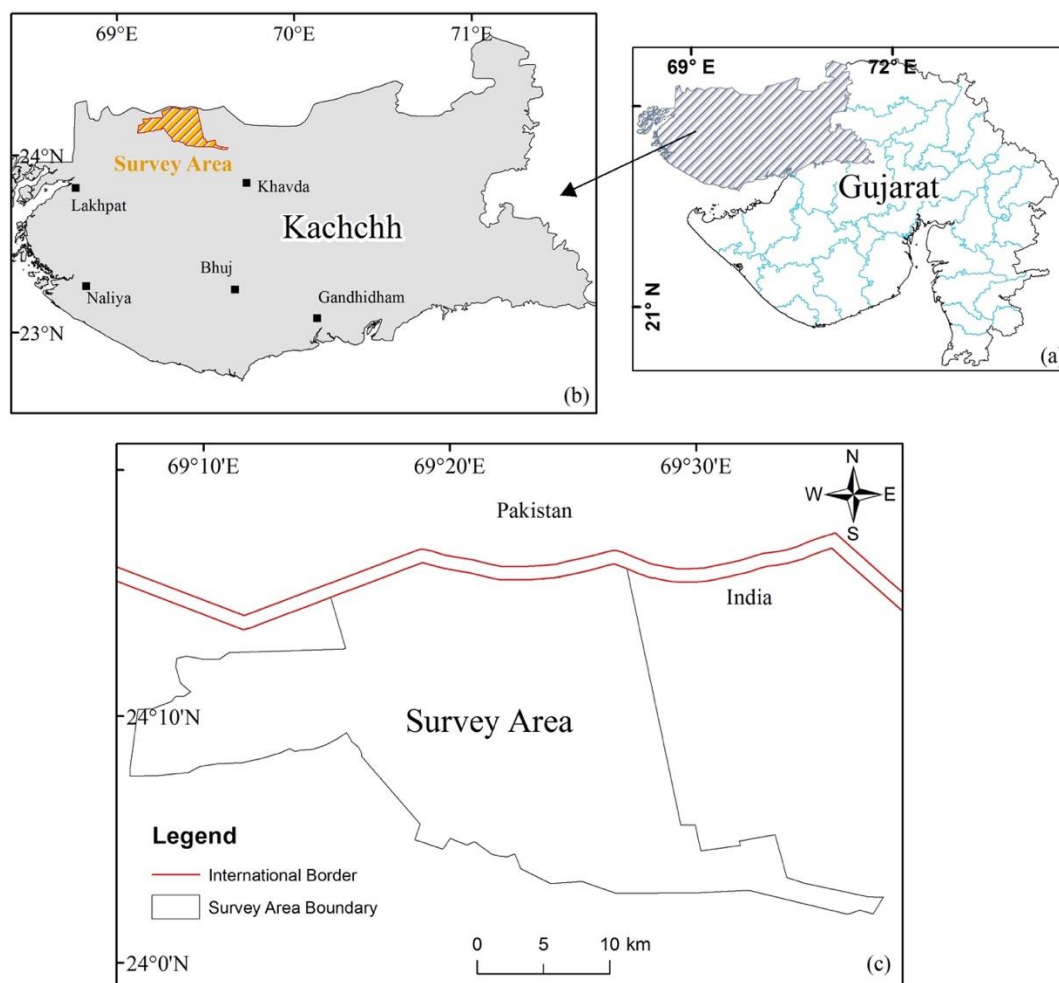


Fig. 2.3: Location map of the project site

2.7 Magnetotelluric investigation in the western part of Narmada Son lineament zone

(Peush Chaudhary and Kapil Mohan)

To characterize the Narmada North fault, MT data from twelve new sites have been acquired near the Bhadbhut area (Bharuch) along a N-S profile (Fig. 2.4), in addition to earlier eight sites. An interstation spacing of 3-4 km has been maintained during the survey, with a recording period of 3-4 days. The acquired data was processed to obtain the impedance tensor with the help of MAPROS processing software. A geoelectric strike direction of $N75^{\circ}E$ was estimated for the present MT data using Becken & Burkhardt (2004) approach. The data was then decomposed into the TE mode (parallel to strike) and TM mode (perpendicular to strike). After the decomposition, the MT data is subjected to 2D modelling with the help of WinGLink software. The preliminary 2D geoelectric depth section down to a depth of 25 km is shown in Fig. 2.5.

The 2D geoelectric depth section shows an upper layer of resistivity from 1 to 5 Ohm.m. This layer may represent the Tertiary sediments having maximum thickness in the southern part of the profile followed by the granitic basement. A conductive feature (C1) has also been observed in the southern part of the profile below sites 6 to 12 that might be the Narmada North Fault (NNF). However, these results are preliminary and more MT sites will be required in the southern part of the area for a detailed interpretation of the results.

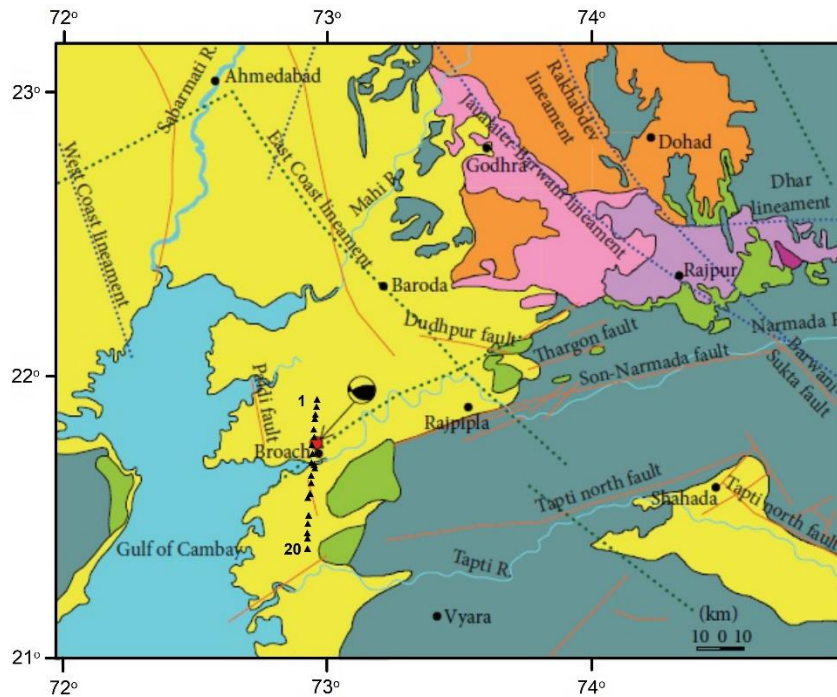


Fig. 2.4: Map showing the locations of acquired MT stations (black triangles) plotted on the tectonic map of the region (after Kothiyari and Rastogi, 2013)

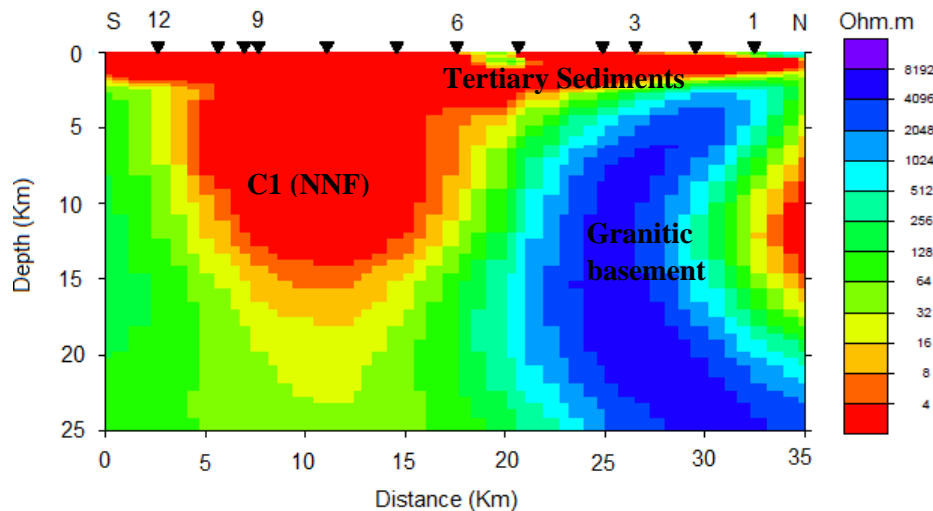


Fig. 2.5: Preliminary 2D geoelectric depth section of the MT data along the profile

2.8 2D modeling of the magnetotelluric data acquired in and around Bhadbhut area

(Peush Chaudhary, Kapil Mohan and Sumer Chopra)

Data from a total of 20 MT stations were acquired in the broad frequency range (0.001-1000s) with a recording duration of 72-96 hours, along a ~58 km long traverse (Fig.2.6). A geoelectric strike of N75°E has been calculated by using the ellipticity criteria of Becken & Burkhardt (2004), that matches well with the geological setting of the region. The data was then decomposed into the TE mode (parallel to strike) and TM modes (perpendicular to strike). After the decomposition of data into TE mode and TM modes, the MT data is subjected to 2D modeling with the help of WinGLink software.

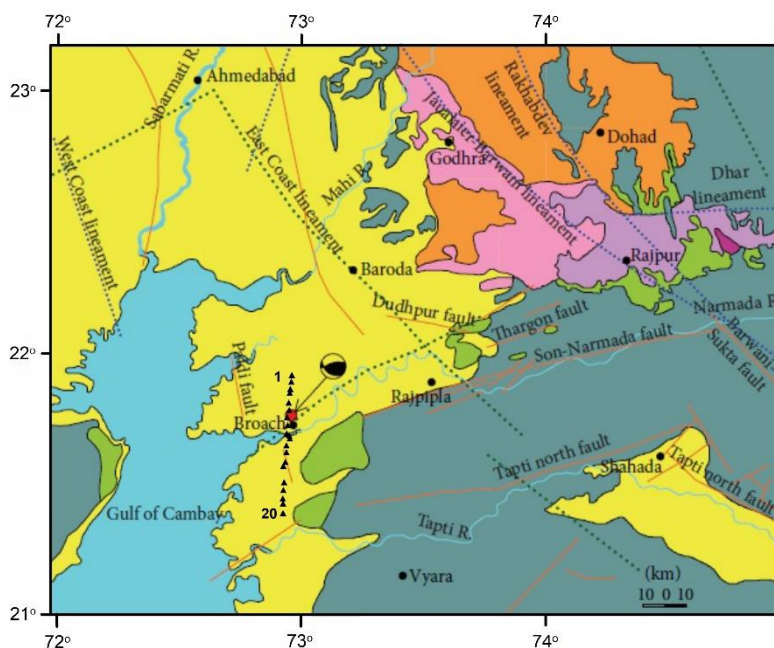


Fig. 2.6: Map showing the location of acquired MT stations (black triangles) plotted on a tectonic map of the region (after Kothyari and Rastogi, 2013).

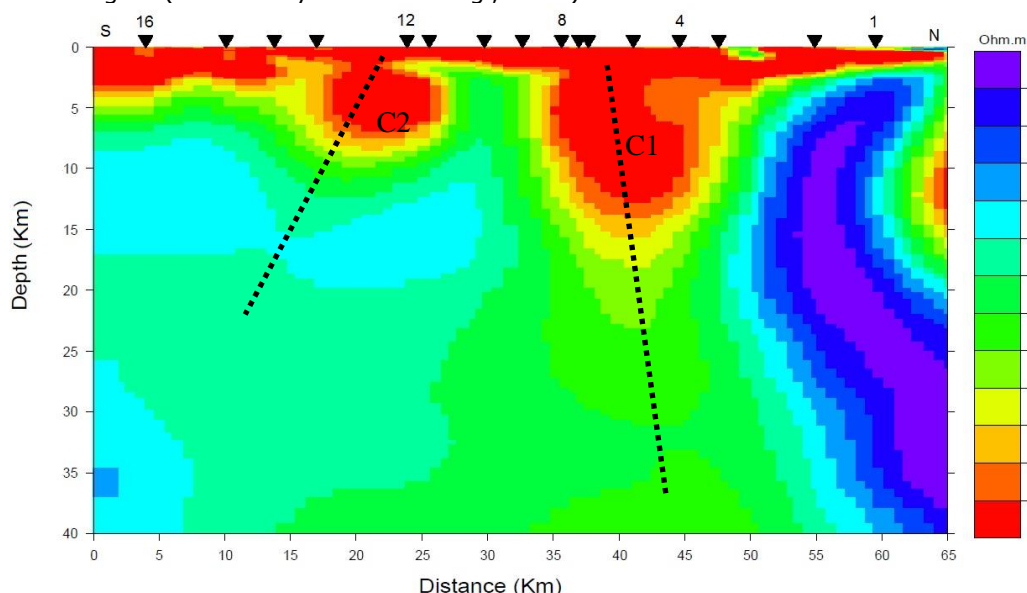


Fig. 2.7: Preliminary 2D geoelectric depth section of the MT data along the profile

From the 2D inversion of the MT data (Fig. 2.7), two conductive zones are identified. The first conductive zone C1 (with a resistivity of ~ 2 Ohm.m) has been found at ~ 20 km south of the first station (between site 3 and site 8) with a very steep-north/ near vertical dip, inferred as the Son-Narmada North Fault/ Son Narmada Fault. The second conductive zone C2 (with a resistivity of ~ 2 Ohm.m) has been found 15 km south of the first conductive zone (between site 12 and site 13, near Godadra village) with a very steep south dip, named as Godadra fault. However, these results are preliminary and further investigations are required for a detailed interpretation of subsurface structures in the region.

2.9 Electrical Resistivity Tomography (ERT) on the Ukai dam site (Dist. Tapi), Gujarat

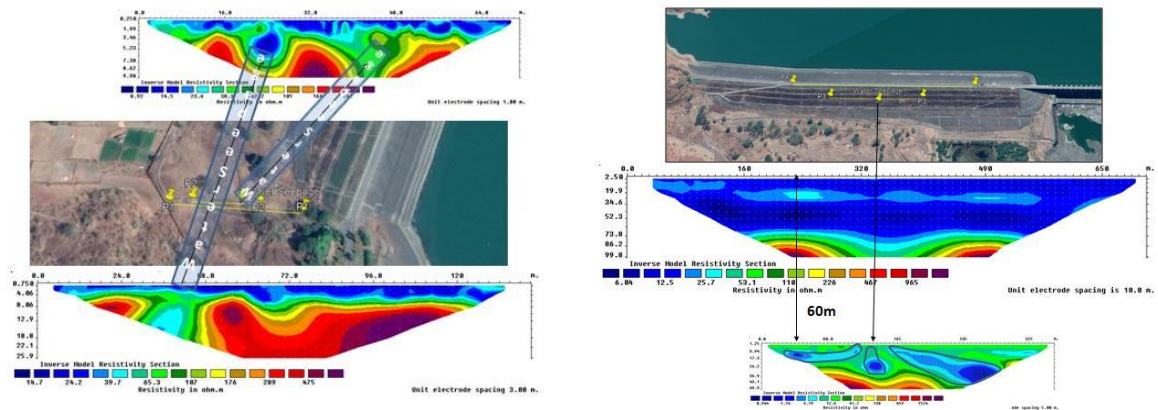
(P. Chaudhary P. Patel, D. Singh)

The Ukai Dam, constructed across the Tapi River, is the second-largest reservoir in Gujarat after the Sardar Sarovar Dam. This dam is located ~ 94 km from Surat and also

known as Vallabh Sagar. This dam was constructed in 1972 and is playing a key role in irrigation, power generation and flood control in the Gujarat state. It has a catchment area of about 62,255 km² and a water spread of about 52,000 hectares. After heavy rainfall in the year 2019, seepage started occurring in the Dam at different locations. To demarcate and identify possible locations of the seepage, Electrical Resistivity Tomography (ERT) was carried out at two different locations (Fig. 2.8a). Data along four ERT profiles have been acquired. In the preliminary investigations, some possible sources of the seepage were marked. However, a more detailed study is required to identify the possible sources of seepage in the Dam.



(a)



(b)

(c)

Fig. 2.8: (a) Locations of ERT survey at Ukai Dam. (b) Resistivity profile at first location. (c) Resistivity profile at second location

2.10 Magnetotelluric study in the Bhavnagar region of Saurashtra

(Dilip Kushwaha and Kapil Mohan)

The area around Bhavnagar is traversed by two major faults: the western margin Cambay basin fault, and the E-W oriented Shihor fault that has an offset from the western margin Cambay basin fault (Fig. 2.9). The surrounding area has experienced two earthquakes, one each on 10 August (M 3.6) and 12 September 2000 (M 3.8). The Tarshima and Malanka villages that experienced most of the tremors are in line with E-W trending Shihor fault (Bhattacharya et al., 2004). The Magnetotelluric (MT) investigations were carried out in Saurashtra near Bhavnagar district along the NW-SE profile, 24 km from Kamlej in the north to Ghogha village in the south for characterizing these faults (Fig. 2.9). The MT data

is acquired at 8 stations in a broad period range of 0.001 to 1000s for ~48 hr at each station. ADU-07 (manufactured by M/s Metronix, Germany) was used in the acquisition of the data. The magnetic field measurements were made using MFS-06e induction coils, and the electric field measurements were made using Pb-PbCl₂ electrodes. The regional strike direction, estimated through Becken & Burkhardt (2004) decomposition technique is found to be NNW-SSE, for a broad period range (Fig. 2.10b). The estimated strike direction is in good agreement with the tectonic setting of the study area. The dimensionality analysis of the MT data for a broad period range is estimated through Swift's and Bahr's skew technique. The Swift's skew and Bahr's skew plot shows values greater than 0.2 and 0.3 for periods greater than 10s, suggesting 2D/3D nature of the subsurface structure.

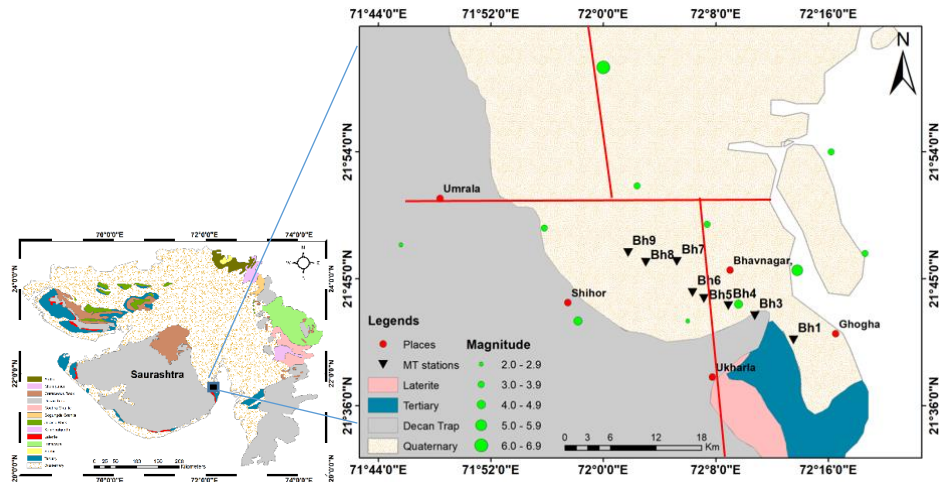


Fig. 2.9: Geological map of the Bhavnagar area along with the MT stations, faults and seismicity

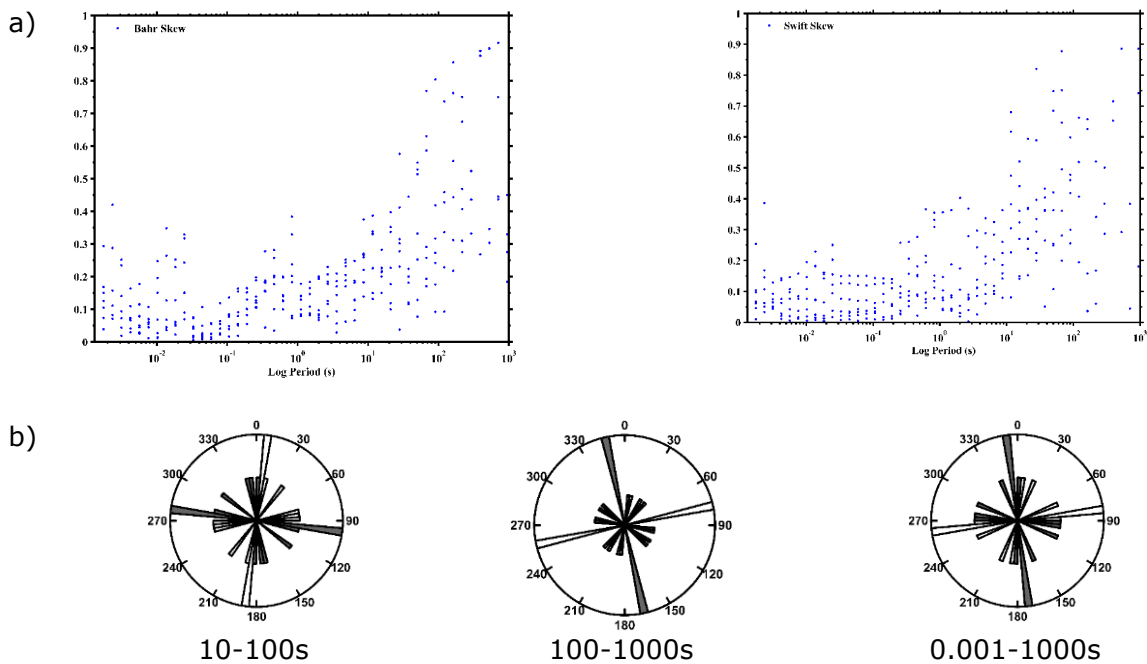


Fig. 2.10: (a) Dimensionality and (b) Directionality of the Magnetotelluric data

2.11 Magnetotelluric Investigation in the Talala area of Saurashtra

(Dilip S. Kushwaha and Kapil Mohan)

The Talala region of Saurashtra in Western India witnessed three moderate events of Mw 4.8 (2007), Mw 5.0 (2007) and Mw 5.1 (2011). To characterize the causative fault, data along a ~62km long NW-SE oriented profile of 16 MT stations has been acquired from

Sendarda village in the north to Hadmatiya village in the south (Fig. 2.11). The data is acquired in a broad period range (0.001 to 1000s), up to ~48hr at each station. The distortion parameters have been estimated using the Groom and Bailey (GB) approach. In this approach, the observed impedance (Z) = $RCZ2DRT$, where R is the rotational matrix, $Z2D$ is the regional undistorted impedance, C is the telluric matrix (which is a product of the shear, twist, anisotropy and site gain). The Multi-Site Multi-frequency (MSMF) analysis is performed for a period of 0.001-1000s. In the present analysis, the shear and twist values are observed below $\pm 45^\circ$ that suggest 2D nature of the data.

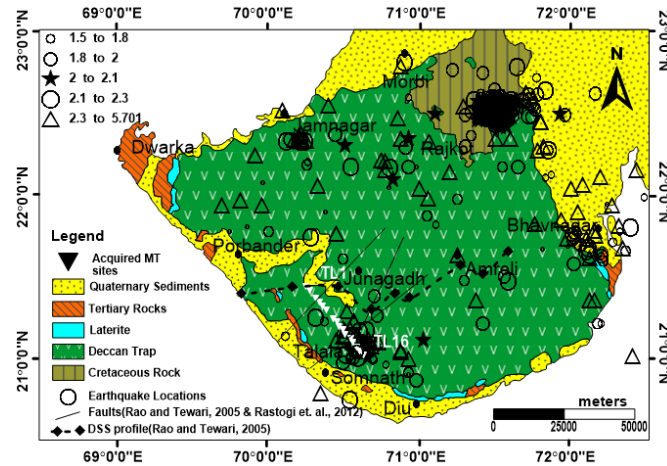


Fig. 2.11: Geological map of the study area. The MT stations and seismicity are plotted. The black solid lines are the faults (after Rao and Tewari, 2005 & Rastogi et al, 2012). (Geological map after Merh, 1995).

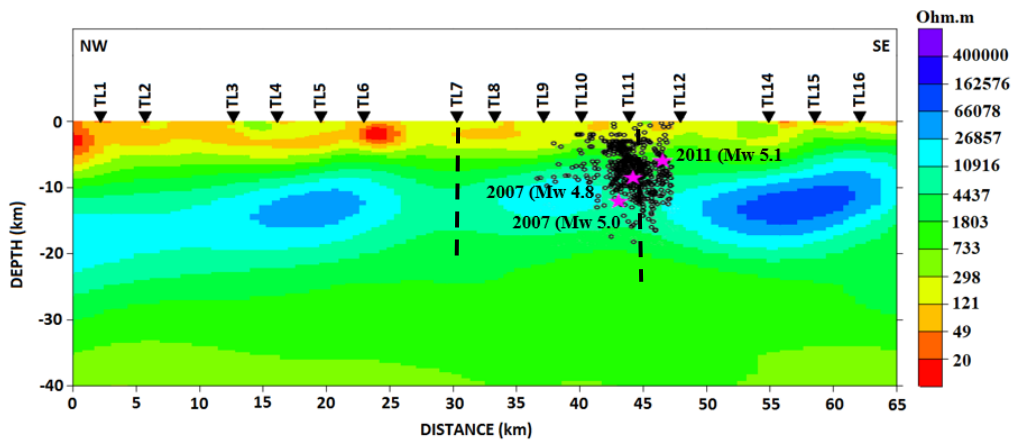


Fig. 2.12: 2D inversion model of joint TE+TM+Hz mode along with the earthquake epicentres. The dashed lines are the faults along the profile.

The decomposed and rotated impedance data have been subjected to 2-dimensional inversion analysis, using the 2D MT inversion program of Rodi and Mackie (2001) available in the data modeling package WinGlink. It finds regularized solutions (Tikhonov Regularization) to the 2-dimensional inversion problem for the MT data using the method of non-linear conjugate gradients (NLGG). The forward model simulations have been carried out using finite-difference equations generated by network analogues to the Maxwell's equations. In the NLGG method, the regularization parameter τ plays a significant role. The value of τ represents the measure of trade-off between the data fit and model smoothness. To find out an appropriate τ -value, the inversion was carried out with different τ -values. The RMS error obtained from each inversion has been plotted against model roughness. The L-curve criteria proposed by Hansen and O'Leary (1993) and Hansen (1998), which suggests that the τ value at the knee of the curve is most appropriate, has been adopted. Therefore, on the basis of L-curve plot, we have selected $\tau=3$. The error floor of 20% for apparent resistivity and 1.5° for the phase have been

assigned for the profile, which results in down weighting of the apparent resistivity with respect to the phase that helps in reducing the influence of the static shift in TE mode (Israil et al., 2008). The initial model was a uniform half-space with a resistivity of 100 Ω m. The inversions run about 150 iterations before attaining a pre-set RMS error levels. The RMS error is defined in the inversion scheme as RMS of the sum of misfit in rho and phase of TE and TM and the vertical magnetic field (Hz) is calculated. The 2D Geoelectric section down to 40 km depth for TE+TM+Hz mode is shown in Fig. 2.12.

In a 2D model (TE+TM+Hz), between stations 1 to 7, the first layer with a resistivity of < 30 Ohm.m is observed to a depth of about 3-4 km from the surface. The second layer with varying resistivity of about 100-500 Ohm.m is observed at a depth of about 5-10km in the NW portion of the profile, about ~5km depth in the centre and about ~2-3km in the SE part of the profile followed by a layer with resistivity > 10000 Ohm.m. The 2D model suggests a first layer of Quaternary sediments, the second layer of Deccan trap followed by the Precambrian basement rock. Between stations 6 to 8 and 10 to 12, two fractured zones are observed in the 2D model. The vertical fractured zone between stations 10 to 12 may be the Girnar fault. The seismicity is also overlapped on the 2D section (taken after Mahesh et al., 2016) and found concentrated at/ near the Girnar fault. The fault plane solutions of the area also indicate presence of strike slip fault. A new vertical fault is identified in the present study between stations 6 to 8, parallel to the Girnar fault.

2.12 Estimation of sedimentary thickness using 1D inversion of Magnetotelluric(MT) data

(P. Patel, K. Mohan)

In this study, an 8 layer model is used for Occam and Bostick inversions, whereas in the Least square inversion, a 22 layer model is used. The layered structure at each site using all the inversion algorithms is shown in Fig. 2.13, 2.14 and 2.15 over the 2D resistivity cross section from the 1D model. The 1D inversion algorithms from all three different inversion techniques show a segmented nature of the subsurface along the profile. In the north of the profile from site 1 to site 6 (Shervo to Nirona) the recent (Quaternary + Tertiary) sediments were found down to a depth of 900 m with the resistivity varying from 0.5 Ω .m to 2 Ω .m. In the south, from site 12 to site 18 (Bhadli to Dujapar), Deccan basalt with a thickness of 250 m to 600 m is found exposed on the surface with a resistivity from 50 Ω .m to 90 Ω .m. Mesozoic sediments underlie the recent (Quaternary + Tertiary) sediments in the north and under the Deccan basalt in the south of the profile with resistivity from 2 Ω .m to 15 Ω .m. Mesozoic sediments are exposed in the center of the profile from site 7 to site 11 (from Nirona to Bhadli). The thickness of Mesozoic sediments varies from 1 km to 2 km along the profile, which is well correlated with the ONGC borehole data (at Nirona village).

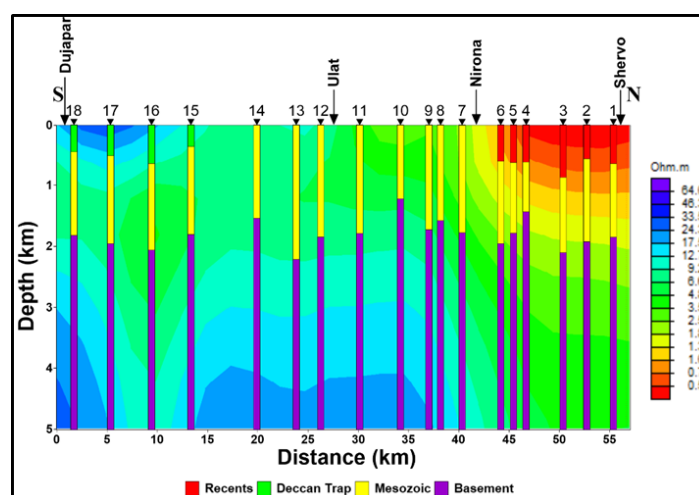


Fig. 2.13: Plot of layered structure at each site using Bostick inversion algorithm

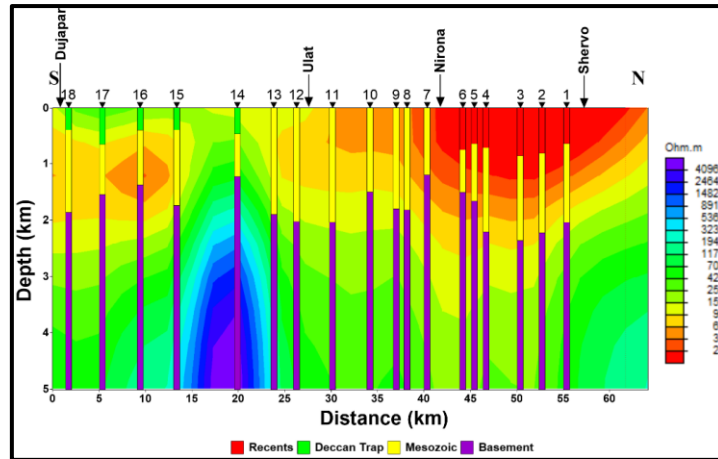


Fig. 2.14: Plot of layered structure at each site using Occam inversion algorithm

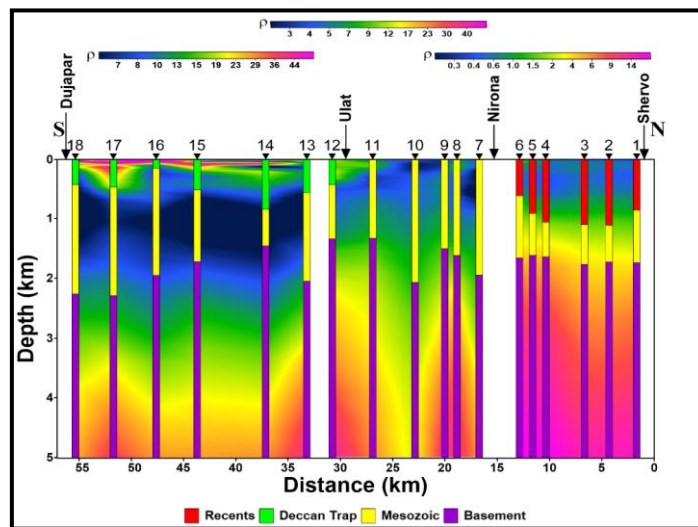


Fig. 2.15: Plot of layered structure at each site using Least square inversion algorithm

2.13 Electrical Resistivity Survey in Ahwa (Dist. Dang), Gujarat

(Pruthul Patel, Vasu Pancholi, Peush Chaudhary, Dilip Singh, Vinay Dwivedi, Pawan Singh, Rakesh Nikam)

The Dang district is situated in the southeastern part of Gujarat state and lies between $20^{\circ} 33'50''$ N to $21^{\circ} 04' 52''$ N latitudes and $73^{\circ} 27'58''$ E to $73^{\circ} 56'38''$ E longitudes. It is bounded by the Surat and Navsari districts of Gujarat state in the north and west while in the east and south, Maharashtra state delimits its extension. The Ahwa Taluka lies in the Dang district and comprises 311 Villages. The district occupies an area of 1,764 sq km and has a population of 2, 28,291(2011 census). The district is hilly, with a few high hills in the east and south, and the rest of the district is occupied by a mass of flat-topped low lying hills. The main rivers of this region are Gira, Purna, Khapri and Ambika. The average annual rainfall in this region is 1635 mm (Gupta, 2014), which is higher than the average rainfall of Gujarat state. In spite of high annual rainfall, the district is facing a severe shortage of water both for drinking and agriculture (almost 85% of the population depend on agriculture). To increase the irrigation potential and also for rain water harvesting, GWRDC has decided to dig approx. 2512 dug wells. Since the region is covered by hard rocks, geophysical survey (Electrical resistivity survey) is essential for selection of suitable sites for dug wells. In the first phase, geophysical surveys at around 1000 points in Ahwa Taluka are completed.

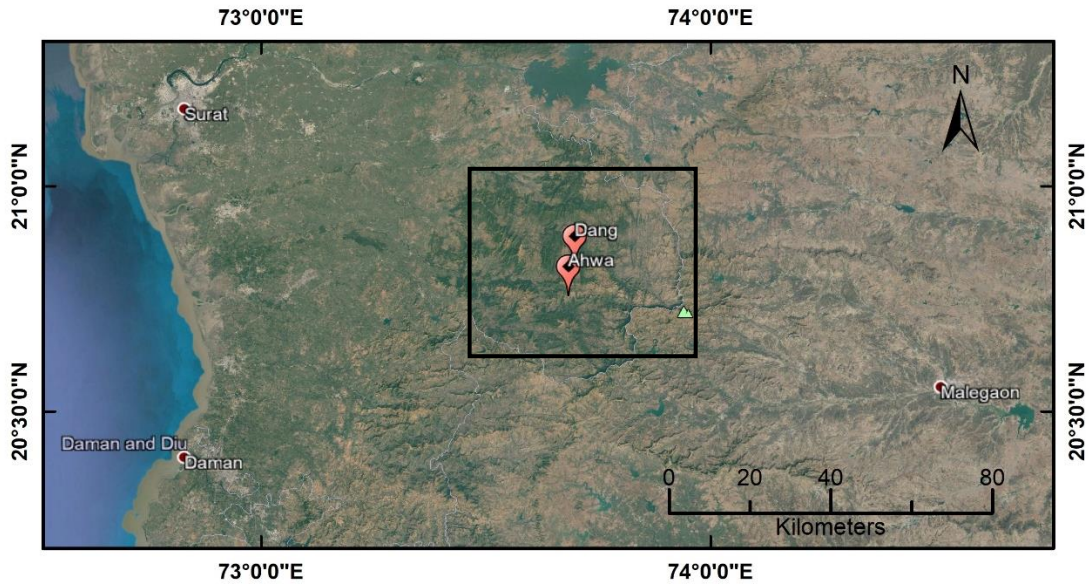


Figure 2.16: Location map of resistivity survey in Ahwa (Dist. Dang)

2.14 Conductive and Vp/Vs anomalies across the Cambay and Kachchh basins

(N. Danda, A. P. Singh)

An attempt has been made to compare the conductive anomalies obtained from MT data with the Vp/Vs anomalies, to track fluids, thermal imprints, and magmatic processes at various depths and the degree of plume-lithosphere interactions across the Kachchh and Cambay basins, western India. The conductive anomalies obtained from MT data match with the high Vp/Vs anomalies across the profile. This correlation infers presence of fluids within the Kachchh region (sites: 101-111), associated with seismicity in this region. The high Vp/Vs and conductive anomalies (116-124) beneath the Cambay basin suggest basaltic underplating and volatile enriched fluids associated with the plume-lithosphere interactions.

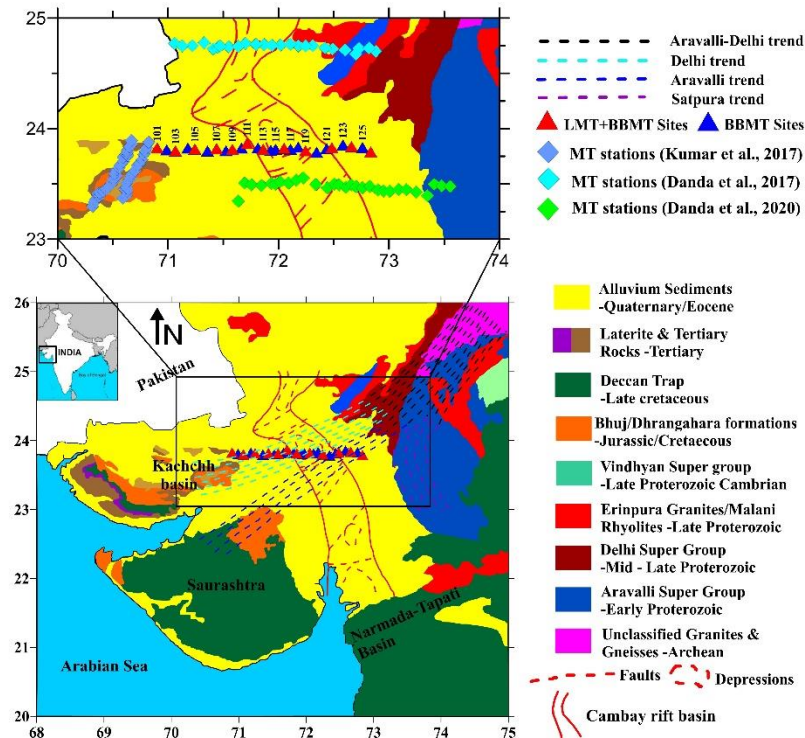


Figure 2.18: Geological map of western India. On top, MT profiles are shown

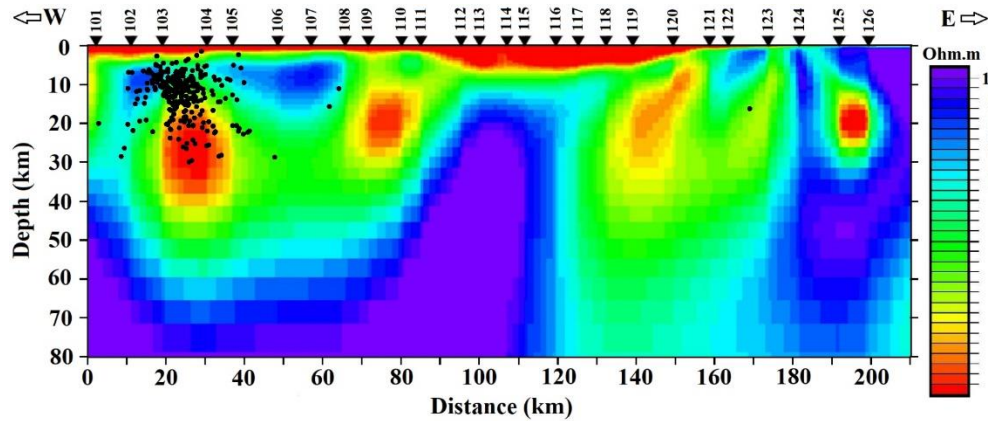


Figure 1.19: Geoelectric model obtained from MT data across the Kachchh and Cambay rift basins western India

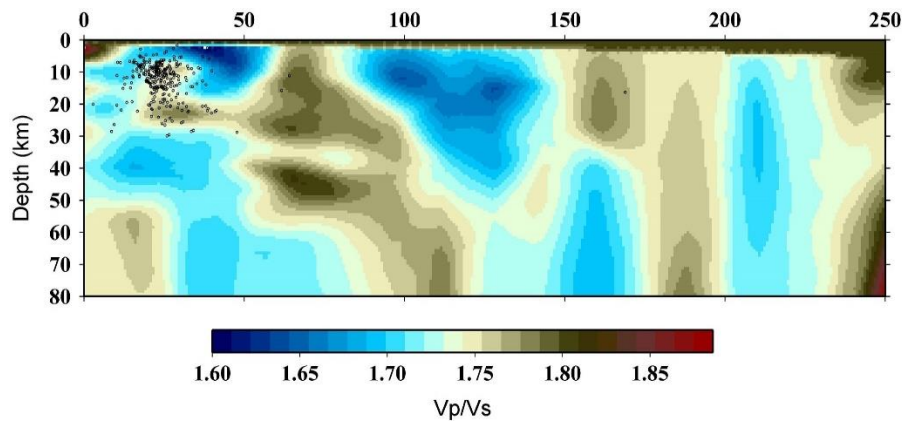


Figure 2.20: Vp/Vs anomalies across the MT profile as shown in figure 2.22. Black dots indicate the distribution of seismicity at distances that are less than 10 km from the profile.

2.15 Estimation of near surface attenuation parameter Kappa (κ) in Northwest and Northeast Himalaya region

(Vikas Kumar¹, Sumer Chopra², Pallabee Choudhury², Dinesh Kumar³)

¹ National Center for Seismology, Ministry of Earth Sciences, New Delhi-110003

² Institute of Seismology Research, Gandhinagar, Gujarat-382009

³ Department of Geophysics, Kurukshetra University, Kurukshetra-136119

We estimated the spectral decay parameter, kappa (κ) for the North-West Himalaya and the North-East India regions, using the strong motion records obtained from accelerographs installed in these regions. We estimated κ from horizontal as well as vertical records from 204 (3 component) accelerograms. It has been observed that in the NW Himalaya and the NE India, the values of κ vary considerably among different sites and with distance. This may be due to the lateral heterogeneity of the crust in these regions. The increasing value of κ with distance indicates that S-wave attenuation is more at shallower depths and less at deeper depths. The estimated values of κ for the NW Himalaya and the NE India region do not vary with magnitude, which means κ is independent of earthquake size. It was observed that the value of κ is more for horizontal components as compared to the vertical components. The local site conditions and tectonic regime influence the value of κ as it was found that κ was more at sites covered by alluvium than at rock sites, in both the regions. The average value (horizontal and vertical components) of κ for the NW Himalaya is $0.050 \pm 0.009s$ and $0.048 \pm 0.010s$, respectively, while for the NE India region, the average value of κ is $0.0368 \pm 0.0054s$ and $0.0334 \pm 0.0091s$, respectively. This indicates that the geological formations in NE region have more competence and are less attenuative. The high values of kappa in both these regions indicate that most of the high frequency energy will be removed during strong

earthquakes in these regions. The kappa values estimated for both the regions may be helpful for attenuation studies and updating hazard maps in these regions.

2.16 Site specific geological map of the Bhadbhut Barrage Site, Bharuch, Gujarat (Naveen Kumar)

A geological field survey has been conducted to assess the soil condition on the left and right banks of Bhadbhut barrage. On the basis of the field survey, the site specific geological map of the Barrage site is prepared (Fig.2.21). The nearly flat but gently sloping (westerly) Quaternary sediments occupy a major part of the area that has been divided into alluvial plains, river terrace deposits, channel deposits and tidal flats. The alluvial plains are found to be deposited as overbank fine sediments that comprise black clay and silty soil. The river terrace is a wide flat topped terrace surface of 5–10-m height, which occupies both the banks of Narmada River and mainly comprised of fine sand, silt and clay. The channel deposits are accumulated as an island in the middle of the Narmada river channel. The tidal flats are found along the coast of the Gulf of Khambhat.

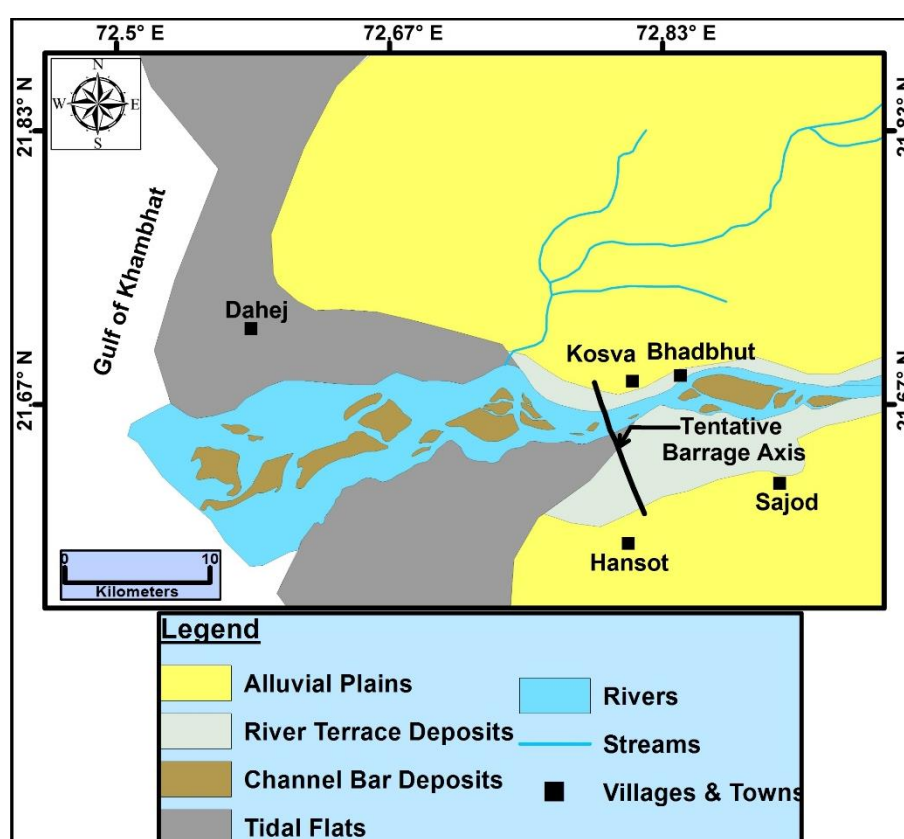


Fig. 2.21: Geomorphological map of the Bhadbhut Barrage site

2.17 Assessment of Relative Active Tectonics in Parts of Dadra and Nagar Haveli, Western India (Naveen Kumar)

In the present study, the results of integrated studies of landform development and geomorphic indices of drainage networks across the Panvel flexure seismic zone have been presented. The Panvel flexure zone is seismically active. Continued seismic activities of $M \geq 4$ levels were reported along the axis of flexure. In the west of the study area, the west coast fault and in the east, the western Ghats Escarpment are present. The fluvial terraces along the river Damanganga and its tributaries, incision, palaeochannels and offset of rivers suggest an active nature of the terrain. To assess the relative tectonic activity, morphometric indices, such as stream-gradient (SL) index, hypsometric integral (HI) have been analyzed. The landform development along the river valley in the study area suggests

the occurrence of neotectonic activities in the region. The results are used to divide the area from low to high relative tectonic activity classes, which is expressed as a relative tectonic activity index and according to the values, the western part of the study area is tectonically relatively more active than the remaining part of the area (Fig. 2.22). Field validation associated with the evidence highlighted by using geomorphic indices as well as stream deflection and lineament analysis reveal that the Damanganga watershed of Konkan coastal region, particularly the north-western flank, is most affected by the tectonic activity.

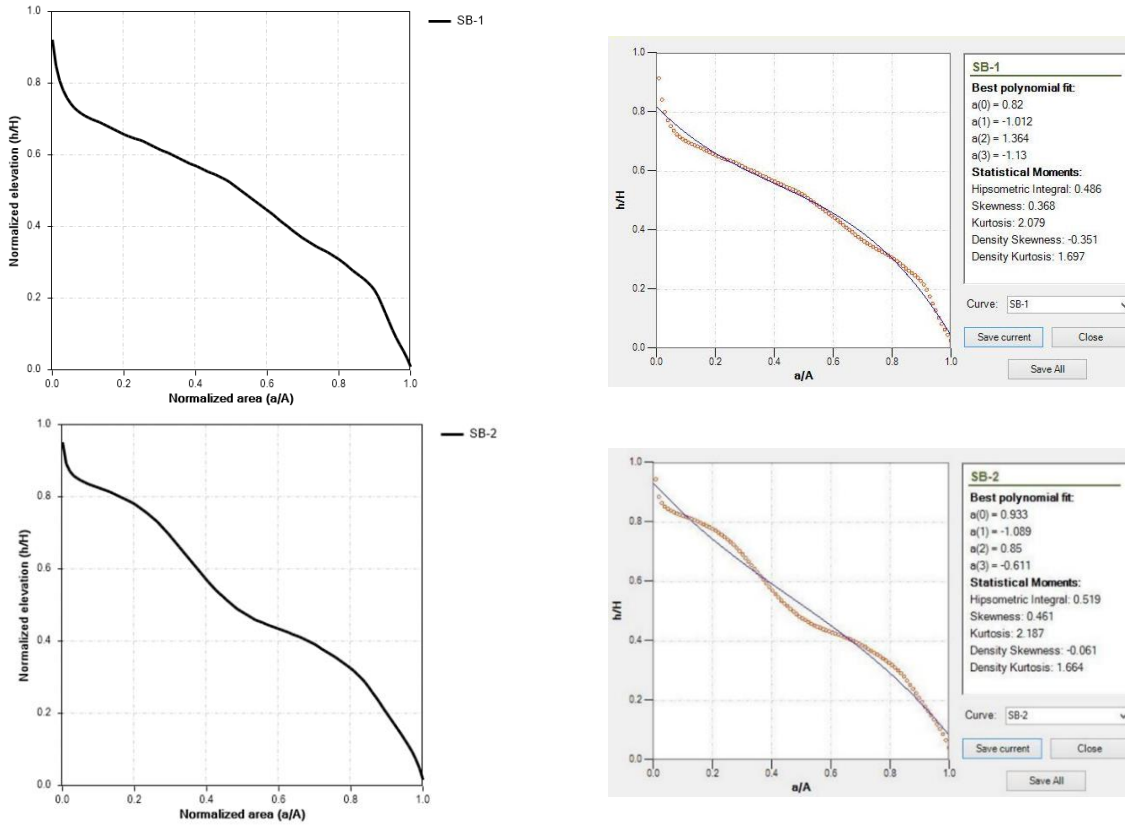


Fig. 2.22: Various geomorphic indices in SB-1 & SB-2 in the study area

3 SOLID EARTH GEOPHYSICS

3.1 Lowermost mantle (D'') anisotropy inferred from splitting of S, ScS and SK(K)S phases recorded by the Gujarat Seismic Network

(G. Srijayanthi, B. Padma Rao and M. Ravi Kumar)

The earth's interior is divided into concentric shells of different layers separated by a discontinuity marking a change in physical properties like velocity, density, temperature, pressure, etc. In 1940's Keith Edward Bullen coined the alphabets from A to G to define these shells and divided the lower mantle (670 km to 2900 km), the D layer, into D' and D'' layers based on differences in physical properties (seismic velocities) (Bullen, 1949, 1950). The very existence of D'' layer is ascertained by many studies, whose thickness varies from 100 to 300 km above the Core Mantle Boundary. However, its ubiquitous nature and its characteristics are yet to be established. The early global seismic tomography studies (Dziewonski et al., 1977; Dziewonski, 1984) indicated 1% higher velocities above the core mantle boundary (CMB) or the D'' layer. Later studies discovered a few more regions inside the earth with ultralow velocities ($\sim 30\%$ less) atop the CMB (Garnero et al., 1998). This region is assumed to play an important role in mantle dynamics. The lower mantle was believed to be isotropic until the first shear wave splitting observation from this region was published by Vinnik et al. 1989. Since then, many shear wave splitting studies from multiple shear phases (of the same event) shed light on the anisotropic characteristics of the bottom most 200 to 300 km of the lowermost mantle which distinctly differed from the isotropic lower mantle. The presence of high density slab graves and the large melt pockets of mantle convection system are believed to be the roots of seismic anisotropy chiefly associated with dislocation creep regime in this region. Further, a few studies (Garnero et al., 2004; Kendall & Silver, 1998) indicated that the D'' layer beneath the Atlantic and Pacific are either isotropic or feebly anisotropic. Therefore, the non-uniqueness and heterogeneous nature of this region is drawing the research interest globally. In the present study we utilised the teleseismic shear phases (S, SK(K)S, ScS) recorded by a network of stations in Gujarat, northwestern India to understand the seismic character of the lowermost mantle.

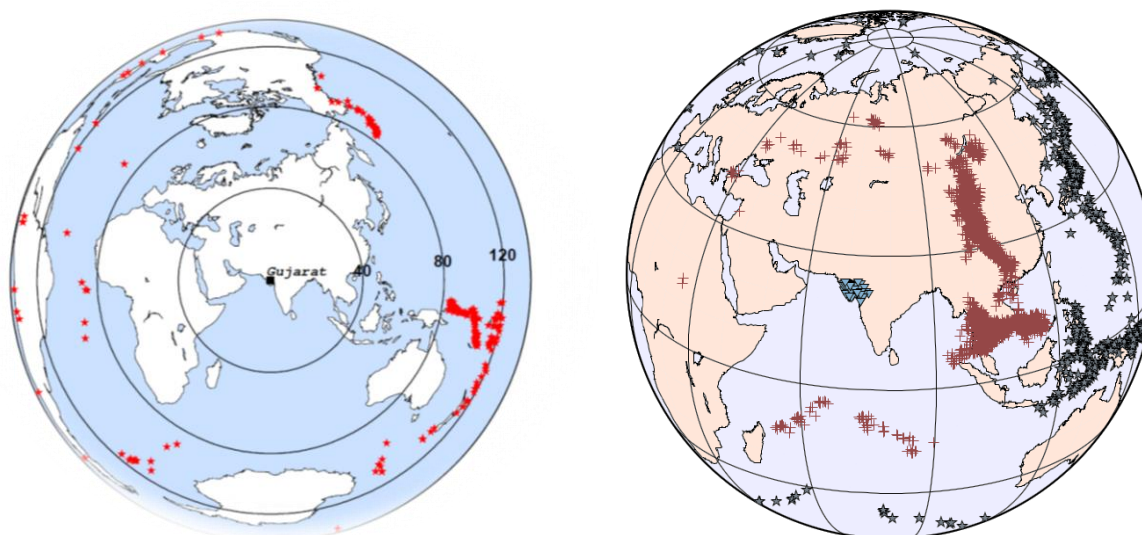


Fig. 3.1: Location of teleseismic earthquakes (red stars) used for SKS-SKKS method (left). The station, earthquakes and the ScS reflected points at the Core Mantle Boundary (brown crosses) used in S-ScS method (left).

The primary objective of the present study is to characterise the nature of anisotropy in the lowermost mantle using the teleseismic shear phases recorded by the GSNet seismological broadband network of 85 stations under the aegis of Institute of Seismological Research, Gujarat, India. There are many methods being adopted globally

to study the D'' layer anisotropy, presently we are using both the differential splitting methods namely, SKS-SKKS and S-ScS to investigate the anisotropy in the lowermost mantle. For the SKS-SKKS method, we extracted the teleseismic SK(K)S waveforms of earthquakes in the epicentral distance range of 84° to 145° (Fig. 3.1).

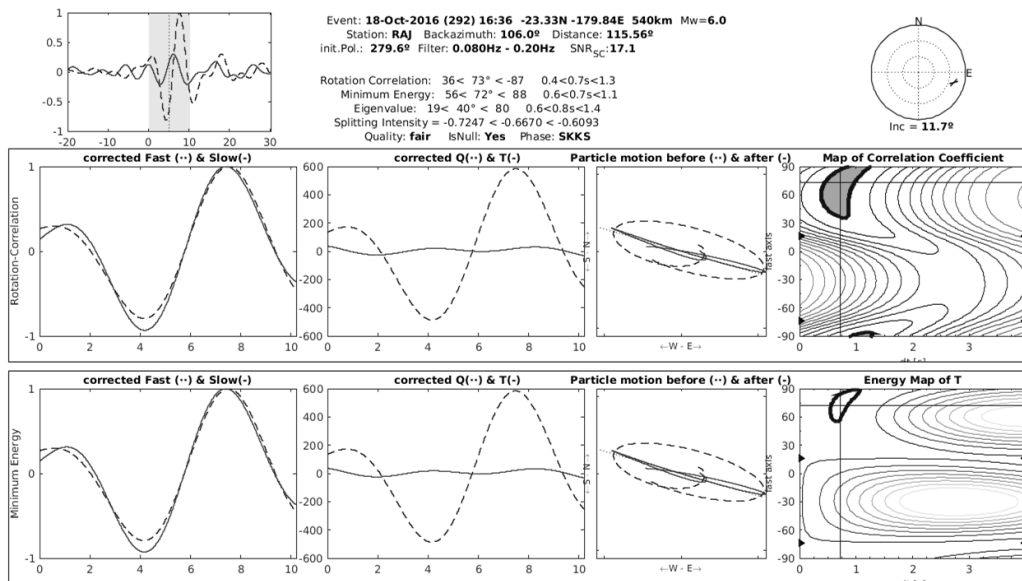


Fig. 3.2: Example of SKKS seismic anisotropy measurement at station RAJ.

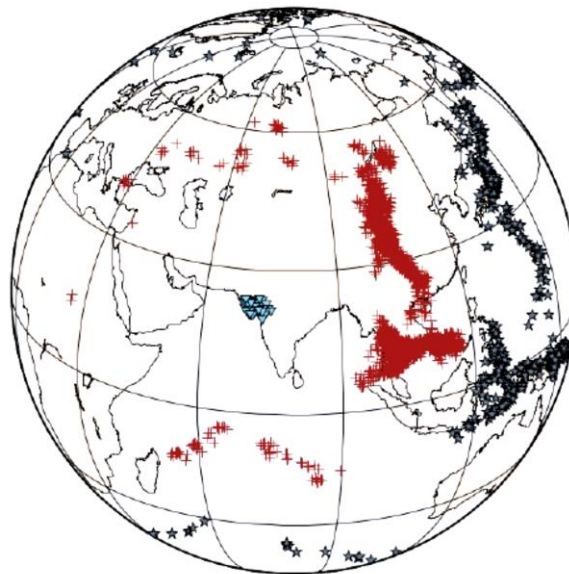


Fig. 3.3: The broadband seismological stations (inverted triangles) and earthquakes (stars) along with the ScS reflected points at the Core Mantle Boundary (red crosses).

Further, the S and ScS phases from teleseismic earthquakes having epicentral distance from 36° to 90° are utilised to characterise seismic anisotropy of the lowermost mantle beneath the midpoint of the event-station pairs from different backazimuths (Fig 3.3). Both the S-ScS differential travel times and S corrected ScS anisotropy method are used to explore the same.

In this study, the primary step is to correct the ScS waveforms for the both the receiver and source side anisotropy. It is well known that due to its travel path, the direct S phases experience a combined effect of upper mantle anisotropy at both the receiver and the source side. Initially, the S and ScS waveforms are accounted for the receiver side anisotropy using the SKS splitting parameters that are extracted either from previous

studies or from our own SKS splitting analysis (as mentioned before). Later, the ScS phases are corrected for the source side upper mantle anisotropy utilizing the receiver side corrected S splitting parameters (or the source side anisotropy parameters) to obtain the information on the characteristics of the anisotropy of the lowermost mantle. However, since the effect of anisotropy is non-commutative while calculating the ScS anisotropy for the lowermost mantle, the source side anisotropy correction is applied in each iteration of the grid search to finally obtain splitting parameters that represent the anisotropic character of the lowermost mantle.

The ScS-S method yielded 67 good quality measurements (Fig. 3.4) that provide results of lowermost mantle anisotropy from Northeast Asia. The splitting parameters are also obtained from Southeast Asia where the presence of D" layer is established by previous studies (Roy et al., 2014)

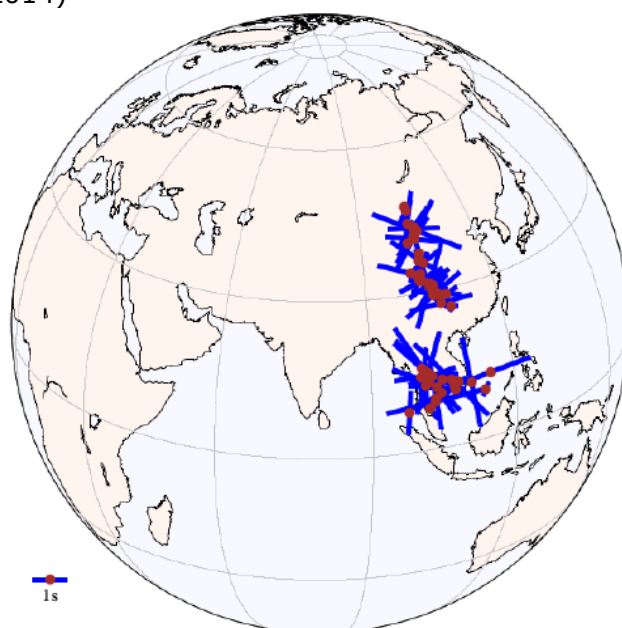


Fig. 3.4: The fast polarization directions in the lower most mantle inferred from source and receiver corrected ScS splitting measurements.

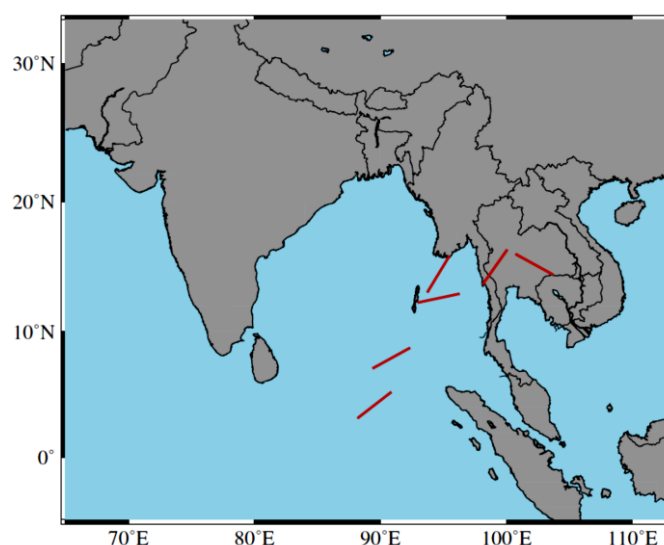


Fig. 3.5: Shear wave splitting results of SKS-SKKS discrepant pairs plotted at CMB piercing points.

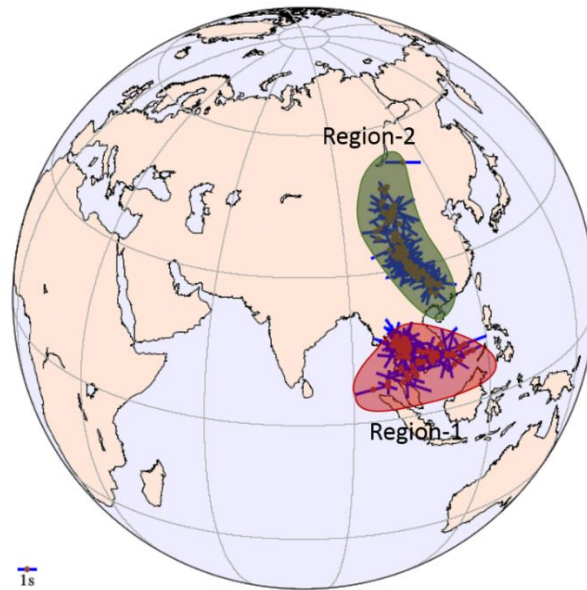


Fig. 3.6: The residual ScS splitting parameters i.e., fast polarization azimuth and delay time (Φ & δt) plotted at the ScS reflection points on the CMB.

A total of 5 average quality SKS-SKKS discrepant pairs were obtained after detailed analysis of shear wave splitting, which samples the lowermost mantle of a small region in Southeast Asia (or eastern Indian Ocean) (Fig. 3.5).

The results from both the ScS-S and SKS-SKKS method clearly indicate the anisotropic nature of the D'' region beneath NE (region-1) & SE Asia (region-2) between 100° E to 115° E longitude and 5° N to 50° N latitude (Fig. 3.6). The delay time (δt) varies from 0.07 to 3 s and 0.1 to 2.95 s in region 1, 2 respectively. The fast polarisation azimuth (φ) varies from 12° to 197° in region-1 and -35° to 160° in region-2. Globally, both the existence of the D'' layer and its seismic characteristics are debated and the nature of anisotropy is identified at a few regions. However, D'' layer appears to be ubiquitous with quite variable seismic anisotropy. The results from present study demarcate a new region, establishing a strong anisotropic nature of D'' layer in northeast Asia. Detailed analysis and interpretation of the obtained results can provide important understanding on the D'' layer anisotropy beneath region-1 and region-2.

3.2 Shear Wave Velocity Structure Beneath the Northwestern Deccan Volcanic Province from Joint and Separate Inversion of the Rayleigh and Love waves

(Jyoti Sharma)

The northwestern portion of the Indian peninsula is occupied by ~65 Ma tholeiitic flood basalts, the region popularly known as the Deccan Volcanic Province (DVP) (Figure 3.7). The Deccan Traps comprise a large volume of basalt of about 2 million km³, which erupted at the Cretaceous/Tertiary boundary, in a short period of less than a 1 Myr. It is estimated that ~80% of the flows erupted in less than 0.5 Myr. The massive outpouring of basalts in the DVP is linked with the interaction of the Indian continental lithosphere with the Reunion plume. In the present study, the shear wave velocity (V_{SV} and V_{SH}) structure of the crust and upper mantle is estimated beneath the tectonically active northwestern DVP (Lat.:19°-25°, Lon.:68°-76°) by inverting the Rayleigh and Love waves, jointly and separately, using regional surface wave tomography (SWT) technique. The total of 2334 dispersion curves includes 1286 dispersion curves derived from Rayleigh waves and 1048 from Love waves using waveforms of 77 regional earthquakes (4.8 ≤ M < 7.0). These earthquakes occurred in the Indian subcontinent and nearby regions, namely, Himalaya, Hindukush, Indo-Burmese ranges, Katawaz basin, Andaman-Sumatra Subduction zone and Carlsberg Ridge, during 2010-2015, and recorded at 38 online broadband seismological (BBS) stations of ISR. Earthquakes within short epicentral distances (< 300

km) and focal depths greater than 100 km were discarded to ensure well-developed surface wave trains, and avoid interference of the higher modes with the fundamental mode surface waves. Earthquakes with epicentral distances in the range of 300 to 3500 km were preferred, to enable reliable estimates of group velocity at short and intermediate periods. The earthquakes were chosen in such a way that the ray paths provide a good azimuthal coverage of the study area and hence good resolution tomographic images. The good quality seismograms were manually picked with an emphasis on the amplitude of the fundamental mode, which should be well above the background noise. The 2-D regionalized group velocity maps of Rayleigh and Love waves at different periods in the range of 6 to 100 s, are constructed to evaluate the lateral variations. The group velocity maps for Rayleigh and Love waves at different periods exhibit a similar kind of pattern. However, Love waves have higher group velocities in comparison to Rayleigh waves, probably due to the effect of anisotropy. The maps reveal significant variations, corresponding to each of these periods, with a reliable (where the path coverage is good) variation smaller than 0.3% with respect to the mean group velocity calculated over the whole area.

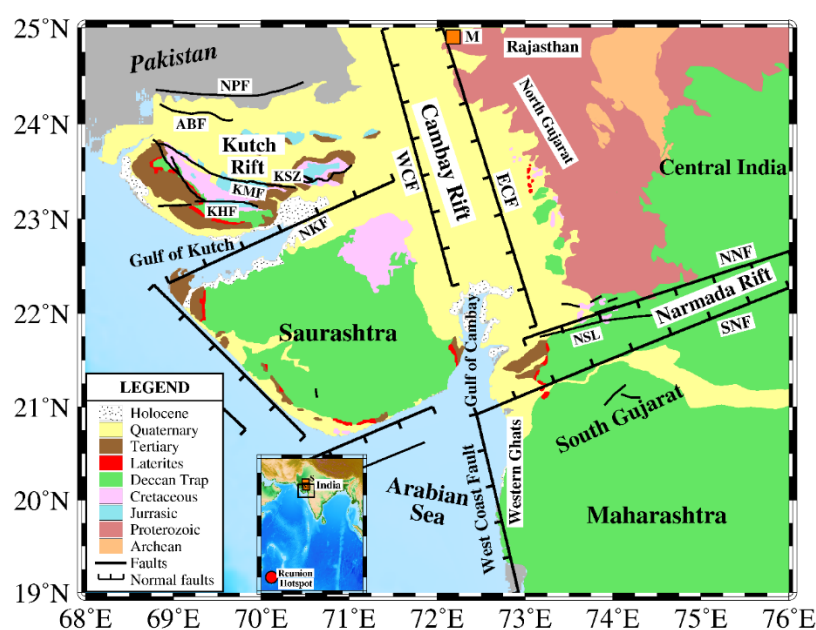


Fig. 3.7: Map showing the geological and tectonic features of the northwestern Deccan Volcanic Province (DVP), India (Geological Survey of India, 2000; Biswas, 2005). The major faults in the study region are Allah Bund Fault (ABF), Kutch Mainland Fault (KMF), Katrol Hill Fault (KHF), Nagar Parkar Fault (NPF), North Kathiwar Fault (NKF), East Cambay Fault (ECF), West Cambay Fault (WCF), West Coast Fault (WCF), North Narmada Fault (NNF), South Narmada Fault (SNF) and Narmada-Son Lineament (NSL). Inset shows the Indian subcontinent, Reunion Hotspot (red coloured circle) and study area (black coloured rectangle). Regions of alkaline magmatism Mer-Mundwara (M) and Sarnu-Dendali (S) mentioned in the text are shown as orange coloured squares.

The 2-D seismic tomography maps provide only a general view of the velocity distribution around the depths sampled by the considered period. To obtain a complete overview of the shear-wave velocity depth distribution, inversion of regionalized group velocities is performed at 1° by 1° grid cells, based on the lateral resolution. The regionalized 2-D tomography maps were prepared at 20 different periods, between 6 and 100 s. These were used for Rayleigh and Love wave inversion, to obtain the V_{sv} and V_{SH} models for 33 cells of $1^\circ \times 1^\circ$ grid size spanning the northwestern DVP. The non-linear Genetic Algorithm (GA) technique was applied during inversion to derive the best possible model by minimizing the error between the observed and theoretical dispersion curves. The GA works simultaneously on a population of models with user defined search space and uses stochastic processes to arrive at the best model (with the lowest misfit) in each generation of the models. The group velocities between 6 to 10 s period sample the sediments and top-crustal structure, between 10 to 35 s, the structure down to the Moho and those in

the range of 35 to 100 s enable determination of the shear-wave velocity structure down to ~ 220 km depth (lithosphere and the mantle below). In this study, a nine-layered model was chosen, where layer 1 corresponds to sediments or Deccan basalt; layer 2 corresponds to the basement/shallow crust; layer 3 corresponds to the upper crust; layer 4 corresponds to the lower crust; layers 5 and 6 represent the lid, except in rift regions where a thin lithosphere is observed; layer 7 represents the low velocity zone (LVZ) and layer 8 represents LVZ in some parts and high velocity upper mantle in the others (Figure 3.8).

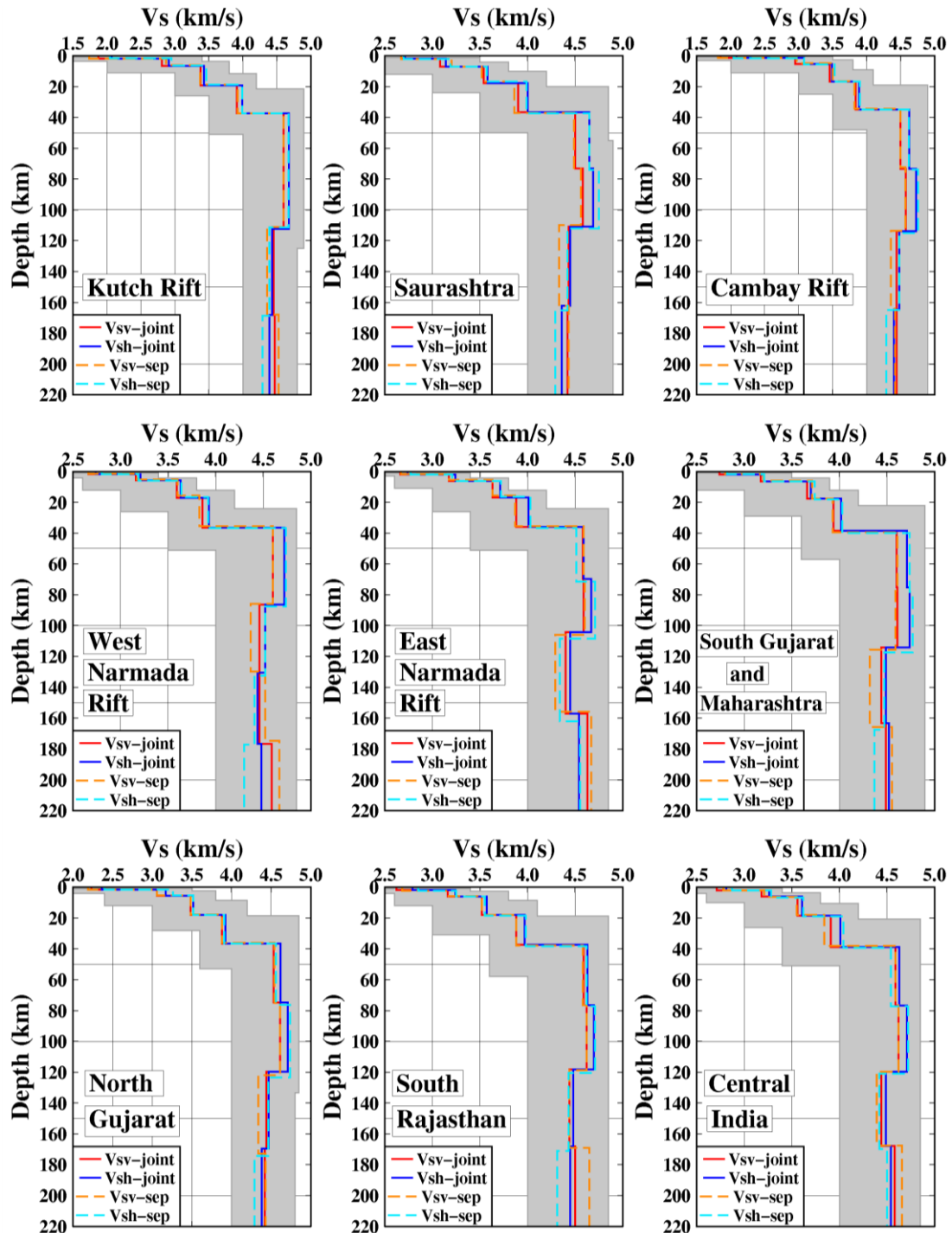


Fig. 3.8: Comparison of average S-wave velocity models (V_{SV} and V_{SH}) obtained from separate and joint inversion of Rayleigh and Love waves for the major sub-regions of northwestern DVP.

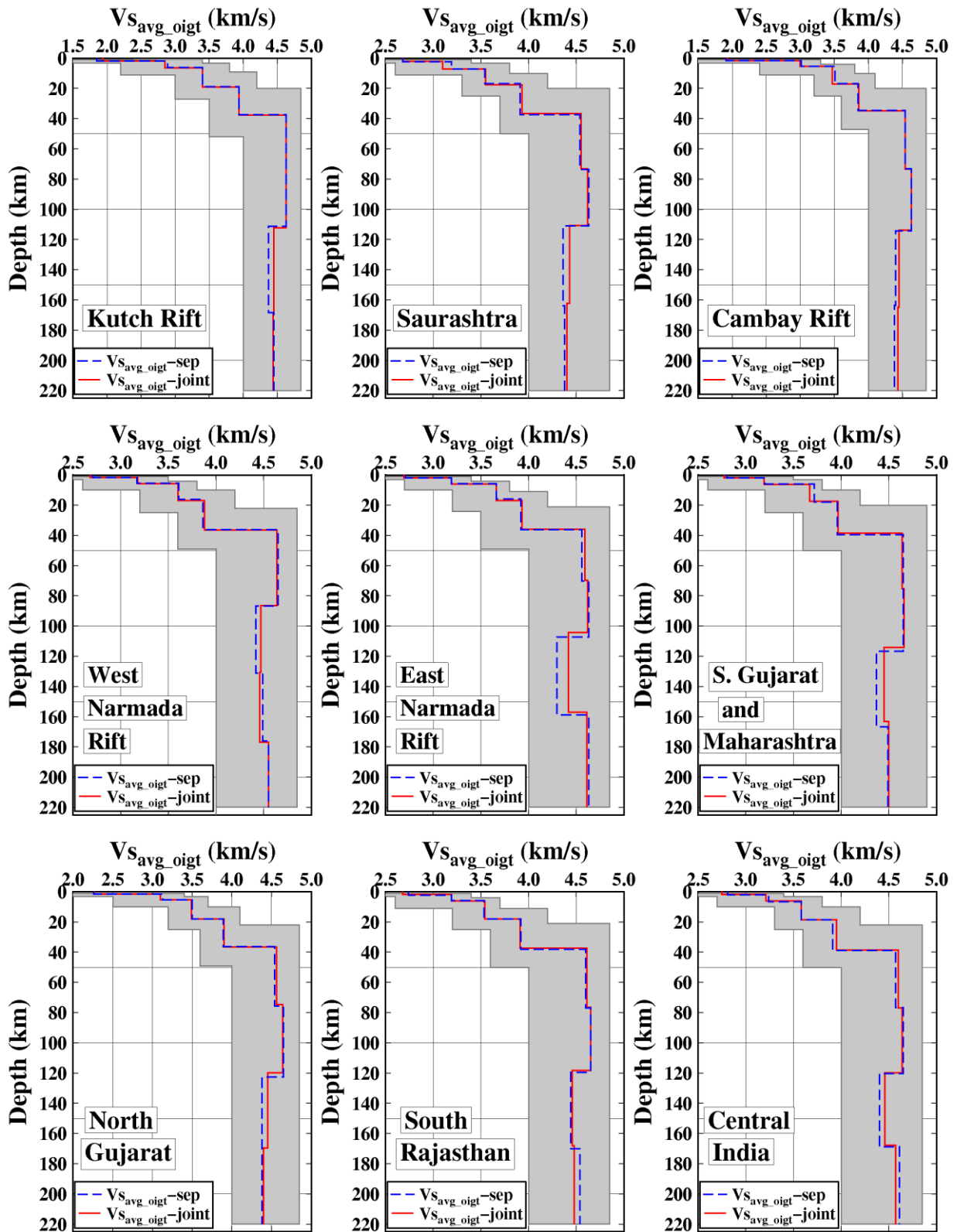


Fig. 3.9: Comparison of average isotropic S-wave velocity models ($V_{s_{avg_oigt}}$) obtained from separate and joint inversion of Rayleigh and Love waves for the major sub-regions of northwestern DVP.

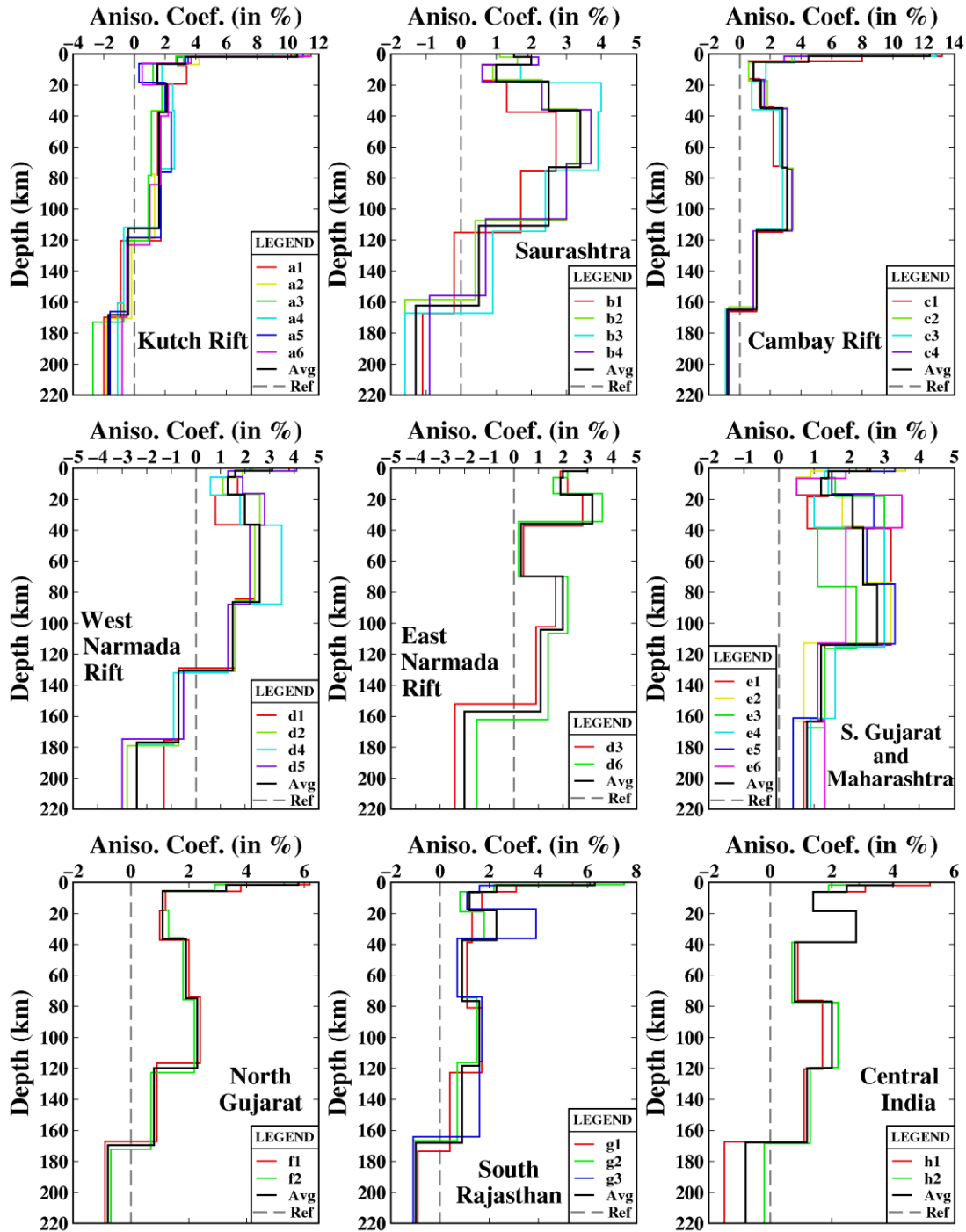


Fig. 3.10: Radial anisotropic coefficient (ξ_{0igt} in %) models for all the grid cells representing the major sub-regions of DVP.

Signatures of magmatic underplating have been recognized in terms of a high V_s (≥ 4.0 km) and a thick crust (≥ 40 km) beneath the KSZ and Western Ghats in the southern DVP, indicating presence of high-velocity lower crust with a mafic/ultramafic composition. Inversion of Rayleigh wave dispersion data shows that the crustal thickness varies from 35 to 40 km in Kutch, 32 to 36 km in Cambay, 34 to 37 km in Narmada Rift, 36 to 40 km in South Rajasthan and Central India, and 34 to 42 km in Saurashtra, South Gujarat and Maharashtra regions. Through joint inversion of Rayleigh and Love waves, a comparatively uniform distribution of Moho depth is observed. The crustal thickness is found between 36 and 40 km in the Kutch rift, 34 to 36 km in Cambay, 36 to 39 km in South Rajasthan and Central India, and 35 to 39 km in Saurashtra, South Gujarat and other parts of DVP. The lithospheric thickness varies from 80 to 124 km, being thinnest at the junction of Cambay

and Narmada rifts (~ 80 km), which could be the source zone of volcanic eruption, since rifting along Narmada was initiated just prior to flood basalt volcanism during the late Cretaceous and high heat flux values ($92\text{-}96$ mW/m²) are observed near the Gulf of Cambay. A thin lithosphere ~ 82 km has also been observed beneath the KSZ. A LVZ at shallow depths can be related with upwarping of the asthenosphere and/or presence of partial melts. A thin lithosphere beneath northwestern DVP could be a result of weakening due to plume-lithosphere interaction ~ 65 Ma, that facilitated volcanism through pre-existing rift zones. A prominent low shear-wave velocity zone has been delineated in the upper mantle (~ 162 km depth) beneath the Cambay and Saurashtra regions from the inversion of Rayleigh wave dispersion data. However, a broader low velocity zone is delineated through inversion of Love waves and joint inversion of Rayleigh and Love waves. A predominant LVZ beneath the Cambay, Saurashtra and adjoining regions, could be the effect of a residual thermal anomaly. A comparison of the V_{sv} and V_{SH} models obtained through separate and joint inversions indicates a major difference in the asthenospheric LVL and the layer underlying the LVL, specifically in the V_{SH} values (Figure 3.8). The shear wave models obtained through joint inversion are well constrained in comparison to the models obtained via separate inversion of Rayleigh and Love waves. There are no drastic variations in velocities and depths, and an almost uniform variation is observed for the sub-regions of different tectonic and geological environments. In this study, the averaged isotropic velocity $V_{S_{oigt}}$ models are also obtained through joint and separate inversion of Rayleigh and Love waves (Figure 3.9).

The radial anisotropy coefficient (ξ_{oigt}) is also estimated for the crust and upper mantle structure beneath the northwestern DVP, through joint inversion of the regionalized Rayleigh and Love wave group velocities (Figure 3.10). In the top sedimentary layers of Kutch and Cambay regions, ξ_{oigt} varies from 9 to 13 %, implying strong positive radial anisotropy. This could be due to the presence of consecutive sedimentary bedding planes and/or fractures near active faults. However, in the Deccan trap covered regions, a small value of the ξ_{oigt} is observed in the top layer, viz., 1-2 % in Saurashtra, 2-4 % in the Narmada rift, South Gujarat and Maharashtra regions. The radial anisotropy is positive in the lithospheric layers. However, a weak positive radial anisotropy and negative anisotropy is observed in the asthenospheric layer and the layer below the low velocity layer (LVL), and could be correlated as a combined effect of past and present geodynamic changes in the upper mantle of the Indian plate. Results from the present study reveal that the crustal and upper mantle structure beneath the northwestern India is substantially altered by volcanism. LVZs in the upper mantle probably reflect imprints of interaction of the Indian continental lithosphere with the Reunion mantle plume.

3.3 Low Velocity Zones and Negative Radial Anisotropy beneath the Northwestern Deccan Volcanic Province

(Jyoti Sharma, M. Ravi Kumar and Ketan Singha Roy)

The Deccan Volcanic Province (DVP) witnessed a massive outpouring of flood basalts of ~ 2 million km³ volume at ~ 65 Ma, in less than a Myr. The volcanic eruption is concomitant with crustal extension, lithospheric thinning and magma influx beneath the major rift systems namely Cambay, Narmada, and Kutch. In this study, we investigate the anisotropic and isotropic variations within the crust and upper mantle beneath the northwestern DVP by estimating the shear wave velocity (V_{sv} , V_{SH} and V_{Soigt}) and radial anisotropy (ξ_{oigt}) models using Surface Wave Tomography technique. A joint inversion of the regionalized Rayleigh and Love wave group velocities is performed, using the genetic algorithm technique. Our results reveal different intracrustal layers, lid, and asthenospheric low velocity zone (LVZ). The LVZ comprises of a uniform asthenospheric low velocity layer (LVL) of average V_{sv} 4.44 km/s and V_{SH} 4.47 km/s, and another LVL below, of average V_{sv} 4.45 km/s and V_{SH} 4.41 km/s. Further, the LVZ represents a negative anomaly with reference to different global models (AK135, STW105, PREM and S2.9EA). A negative ξ_{oigt} is observed in the LVZ, indicating dominance of vertical flow. This could be related to presence of partial melts, volatile materials and/or a thermal anomaly. We also

identified the Moho ($\sim 34\text{-}40$ km) and lithosphere-asthenosphere boundary ($\sim 84\text{-}123$ km). The low V_s values, negative ξ_{oigt} and thin lithosphere (~ 84 km) in the vicinity of Gulf of Cambay affirm the presence of a plume head beneath it, in concurrence with the hypothesis of Indian Plate-Reunion plume interaction.

3.4 Magnetotelluric (MT) investigations in the Great Rann of Kachchh to map the Allah Bund Fault

(Mehul Nagar, Rakesh Nikam, Himanshu Chaube, Dinesh Singh)

MT data from 22 sites have been acquired in the Greater Rann of Kachchh at a recording period of 2-3 days in the broadband frequency range (0.001-1000s) along three profiles (Fig. 3.11). Among the three, one N-S profile is across the Allah Bund Fault (ABF) and another profile is oriented E-W for identifying possible transverse faults. In both the profiles, we acquired 10 MT sites each. The third (N-S) profile was taken further west, in which we acquired MT data only at two sites. Preliminary data processing has been done for the two profiles. Fig. 3.12 shows the data quality.

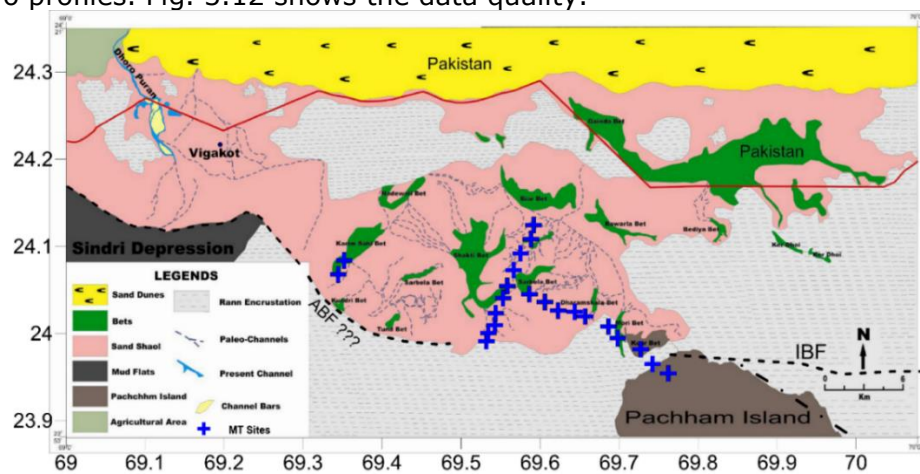


Fig. 3.11: Location map of the acquired MT sites

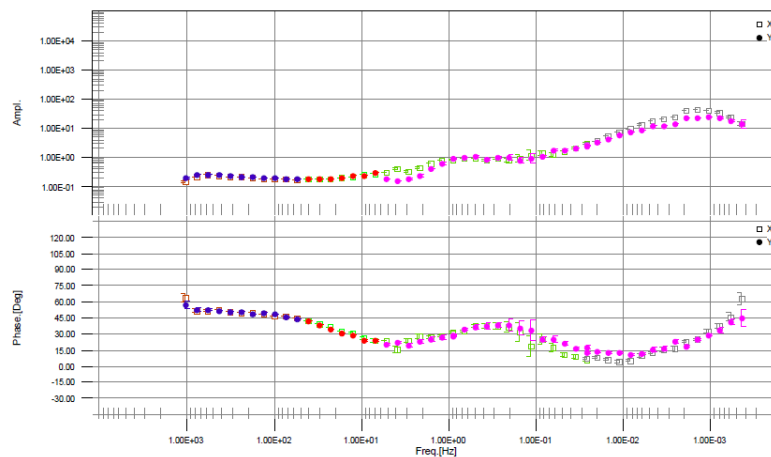


Fig. 3.12: Apparent resistivity and Phase vs Frequency (Hz)

3.5 Shallow Imaging of the Himalayan Frontal Thrust

(Nagarjuna Danda, Siddhartha Prizomwala, Aashna Tondon)

The shallow subsurface resistive structure across the Himalayan Frontal Thrust (HFT) region is characterized by a significant resistivity contrast on the geomorphologically marked hanging and footwalls of the HFT on north and south sides, respectively. The HFT is marked between stations 2 and 3 from profile-1 with a vertical resistivity contrast of ~ 200 Ohm.m from top surface to ~ 300 m depth. The resistivity contrast between hanging and foot walls on the top surface ~ 50 m is provisionally interpreted as Quaternary sediments. However,

a detailed investigation is required further to characterize this resistive contrast to verify whether it corresponds to any faults or sediments. The model obtained from profile-2 also shows a significant contrast in resistivity. However, it is hard to interpret these changes due to large station spacing.

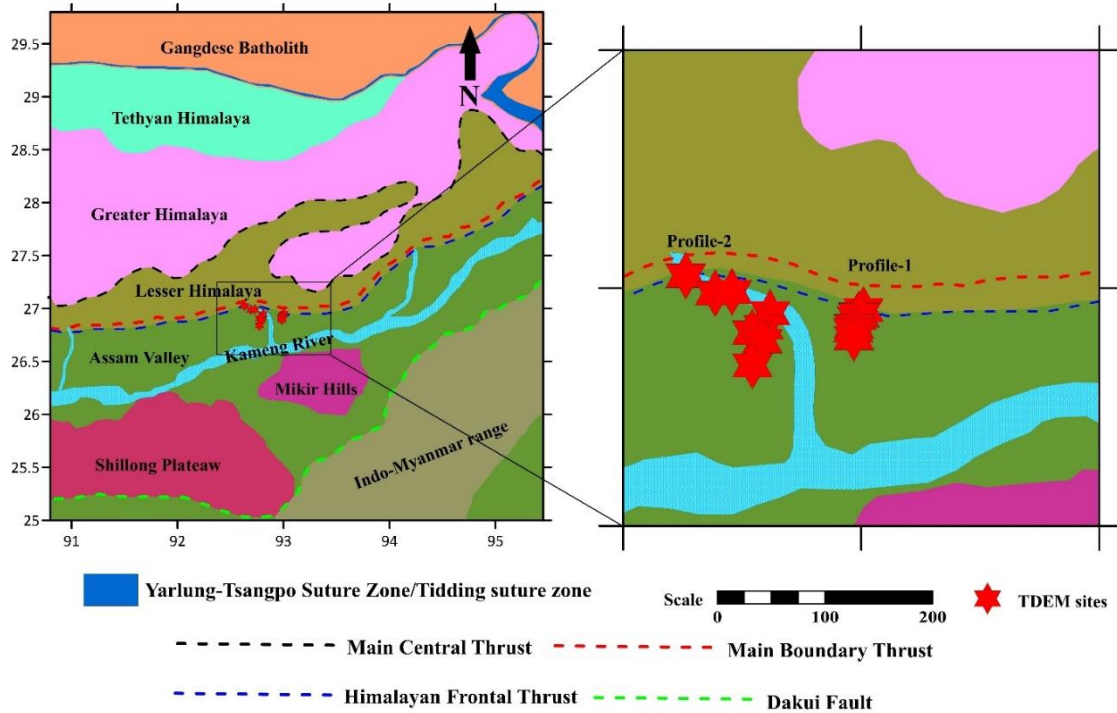


Fig. 3.13: Geological map showing the Himalayan region. Red coloured symbols are the TDEM sites (after Ningthoujam et al., 2015).

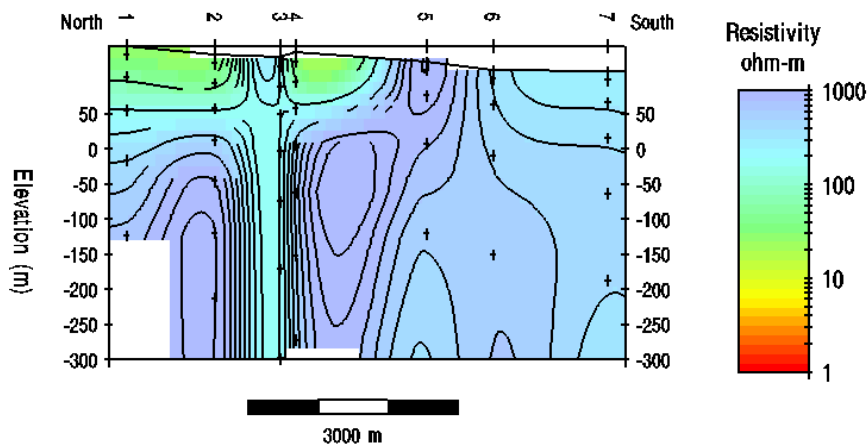


Fig. 3.14: Shallow subsurface electrical structure of the HFT along profile-1. Location of profile-1 is marked on the geological map in figure 3.13.

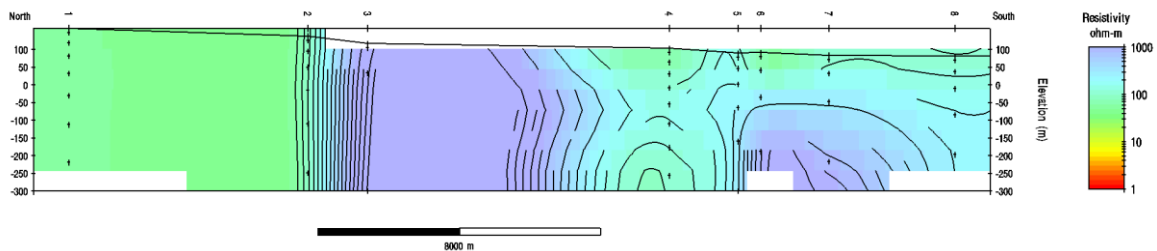


Fig. 3.15: Shallow subsurface electrical structure of the HFT along profile-2. Location of profile-2 is marked on the geological map in figure 3.13.

3.6 Lithospheric structure of Kaladgi rift basin and adjoining regions, southwestern India through Magnetotelluric perspective

(Amit Kumar, Nagarjuna Danda, C. K. Rao)

The top conductive layer in basement section indicates presence of sediments within the basin and basement undulations beneath the MT profiles (Figures 3.16 and 3.17a). The conductive anomalies C1-C2 indicate carbon and sulphur-rich fluids in the deep crust beneath the central part of the Kaladgi Basin and further extended in the southwest region, which might have risen through the fractured parts of the upper crust, down to 40 km depth. The conductive anomaly C3, northeast dipping, L-shape conductor may have been caused by enriched volatiles associated with plume-lithosphere interaction. Highly resistive structures (R1-R3) dipping in the south-westward direction along the entire profile in the upper crust are interpreted as tonalite-trondhjemite-granodiorite. Based on the 2-D lithospheric model, a near vertical conductive feature (C4) is delineated at the collision shear zone between the Mesowestern Dharwad craton and Neeoeastern Dharwad craton that represents the Archean suture. The lithosphere-asthenosphere boundary is marked at ~220 km depth, which is consistent with other geophysical observations in this region.

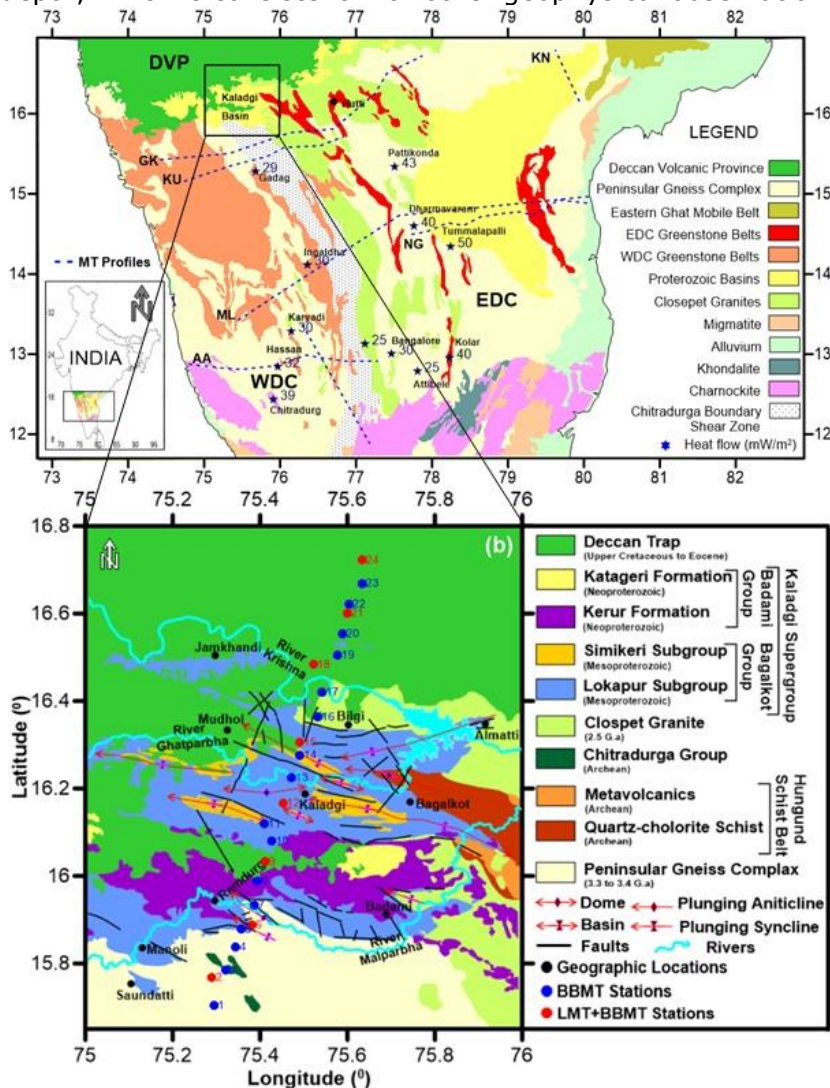


Fig. 3.16: (a) Geological map of the southwestern India (after Jayaprakash et al., 1987; Kala et al., 1999), (b) Geological map of the Kaladgi Basin and adjoining regions showing the MT site locations.

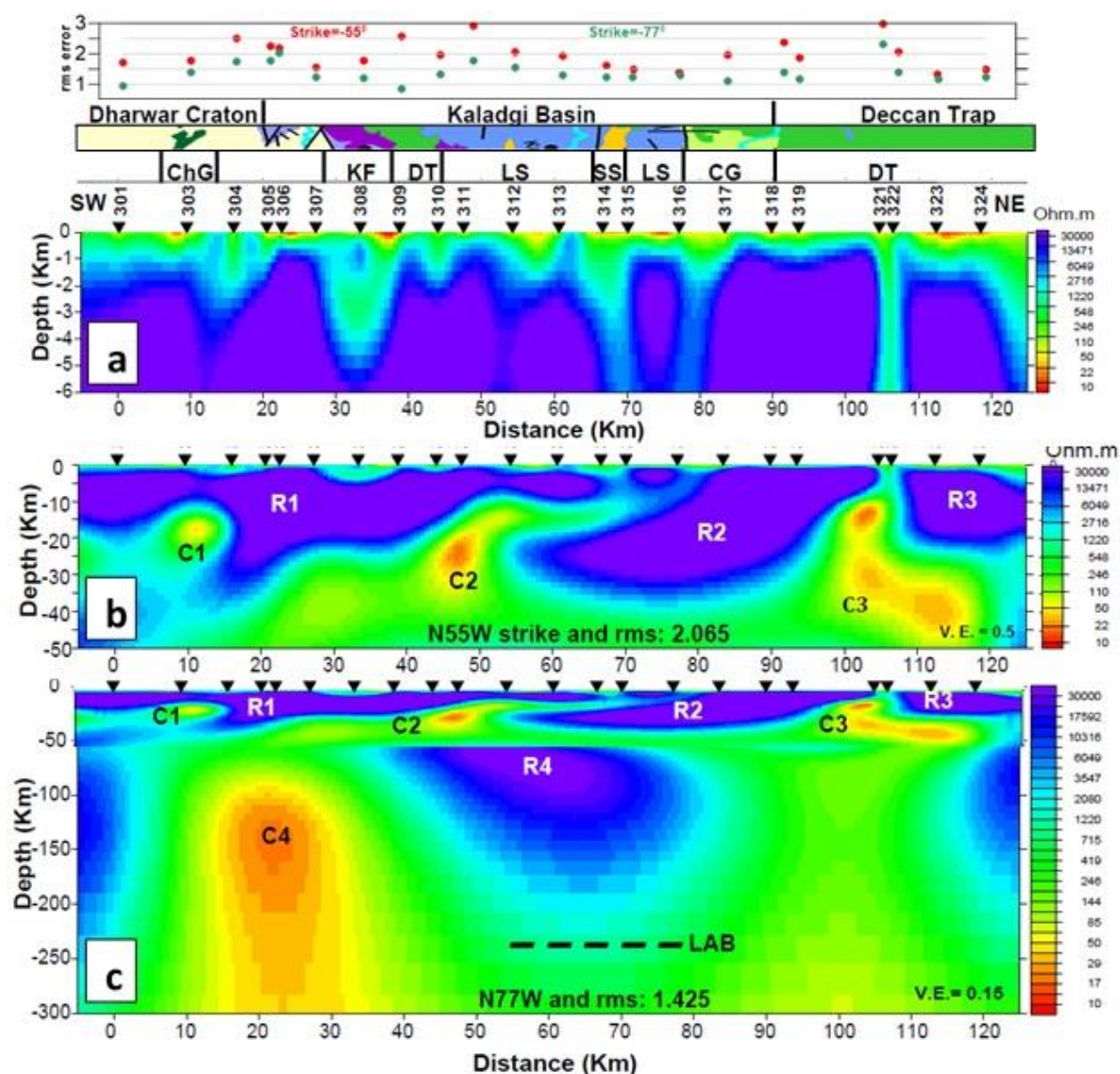


Fig. 3.17: Geoelectric cross-section along MT profile obtained from the TE and TM mode joint 2D inversion (a) Basement section (b) up to 50 km depth with regional strike N55W; (c) up to 300 Km depth with regional strike N77W. On the top, RMS misfit values of the joint TE and TM modes inverted for two different regional strikes are shown. Following are the abbreviations used for the major geological features, ChG: Chitradurga group, KF: Kerur Formation, LS: Lokapur Subgroup, SS: Simikeri Subgroup, CG: Closepet granites, DT: Deccan trap.

3.7 Delineation of intertrappean layers beneath the Deccan Volcanic province of western India through Microtremor analysis

(A.P. Singh, Gaurav Dave)

In the present study, ambient noise is used to determine the shallow subsurface structure of the Saurashtra horst. The microtremor measurements have been carried out at 50 well distributed sites in Saurashtra and the site amplification corresponding to the amplified frequencies and the relevant shear wave velocity profile, are estimated. The results show a plateau like shape with no sharp peak. The phase velocity dispersion of Rayleigh waves is calculated from array data using the spatial autocorrelation method, and a 1-D wave velocity structure is determined by means of the inversion processes. The Neighbourhood algorithm has been chosen to perform inversion of the dispersion curves. Forward modelling has also been done to validate the inversion results. Thicknesses of the Deccan intertrappean beds inferred from HVSr range from 34 to 39m. The H/V spectral ratios at all the sites indicate amplification of 2.9 to 3.5 and 2.0-2.2 for the frequency bands of 1.8

- 2.5 Hz and 4.0-6.0 Hz, respectively. A three layer model (one soil layer with the power law variation of velocity over the substratum) was used as the initial model for the inversion. It is seen that the uppermost layer down to 12m has a low shear velocity between 175 and 400 m/s. The second layer is at a depth of 25-40m with shear velocity 450-800 m/s and the third layer is at 70-80 m with shear velocity in the range of 850-1350 m/s. The results of the single and array measurements have been compared with the results of the multi-channel analysis of surface wave (MASW) data. The estimated shallow subsurface velocity structure in the city shows a good correlation with the geomorphological data.

3.8 Shallow Subsurface Imaging of Anjar Taluka, Kachchh using Transient Electromagnetic Studies

(Rakesh Nikam, Mehul Nagar, Indu Chaudhary, Himanshu Chaube, Dinesh Singh and P. Mahesh)

To image the deep groundwater aquifers, we carried out Transient Electromagnetic (TDEM) investigations in the Anjar taluka of Kachchh. TDEM data from 43 sites (Fig. 3.18) have been acquired by an in-loop configuration. At each site, 100 m sided transmitter loop was laid and ~ 9.2 amp of current was injected into the loop with different transmitter current frequencies (32, 16, 8, 4, 2 and 1 Hz). Induced voltage due to sudden change in the transmitter current was measured at the centre of the loop as a function of decay time, using a magnetic coil. A 1-D inversion was carried out using apparent resistivity rather than normalized voltages. One dimensional inversion modelling is performed by considering the horizontally layered earth model with homogeneous and isotropic layers (Mills et al., 1988). Elevation data at each site is incorporated during the inversion routine. For the present study, we use STEMINV (Zonge, USA) program to estimate the layered-earth resistivity models. The algorithm uses an iterative best-fit technique to minimize the RMS (root mean square) residuals between the observed and calculated rate of the magnetic field that reflects as the induced voltage at each station. The 1-D models at each site are generated and some of these are shown in Fig. 3.19.

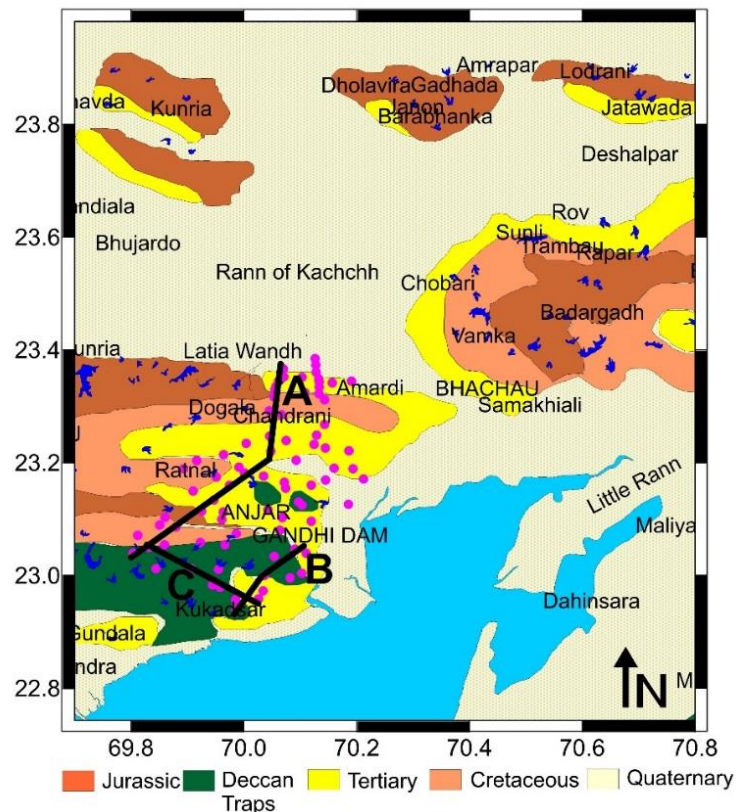


Fig. 3.18: Location Map of the TDEM sites (pink circles) and Profiles (thick black lines)

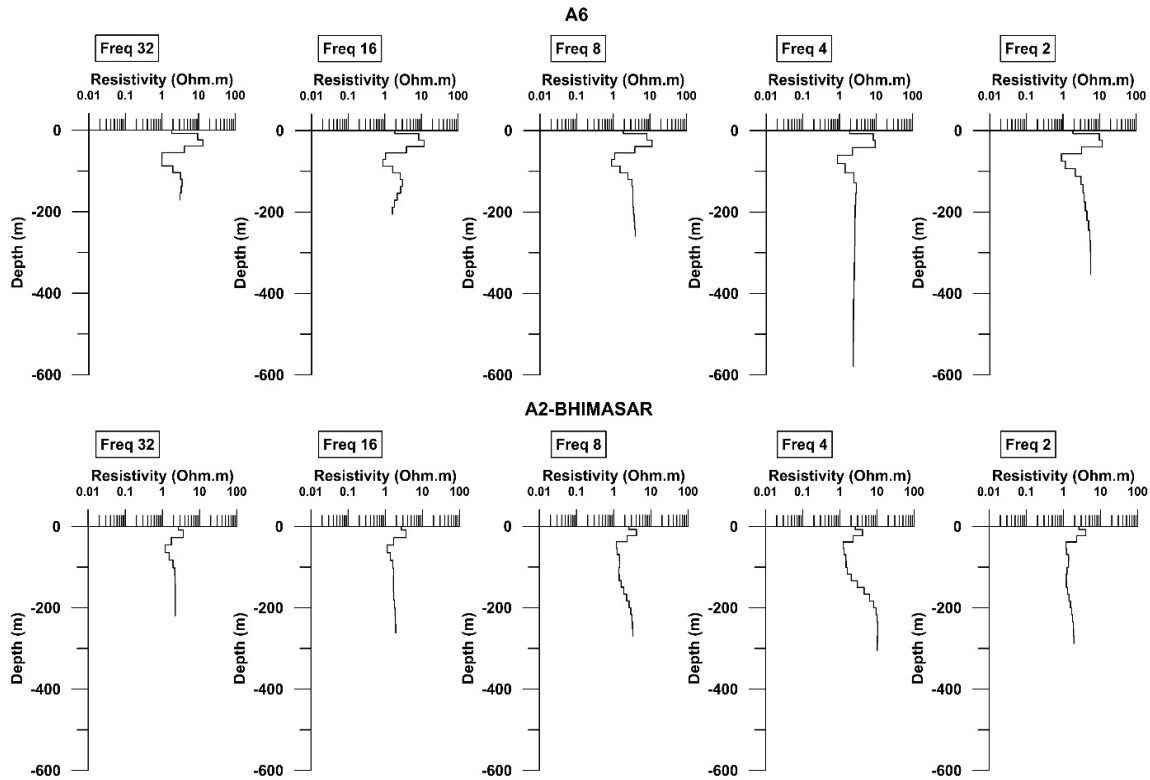


Fig.3.19: 1-D resistivity models for the TDEM sites in the Anjar Taluka

We plotted resistivity sections along three different profiles A, B and C (as shown in Fig. 3.19) by combining 1-D models from the sites falling in each profile to map the possible aquifer layer in the region (Fig. 3.20-3.22).

Profile A: In this profile, the resistivity values below sites 1-3 closely represent the quaternary sediments of Banni plains, separated from the Mesozoic rocks at sites 3 & 4. We observed a sharp contrast of resistivity between sites 6 & 7, which represents the tertiary formations within the cretaceous rocks. The sites 9-14 lie on the tertiary sediments. Again sites 14 & 15 show a significant resistivity difference separated by two different lithological units namely, tertiary and cretaceous. Also, the last two sites 17 & 18 are sited on the Deccan trap province. Interestingly, a sharp resistivity contrast between 10 and 11 separates two lithological units along with a zone with $\sim 100 \Omega\text{m}$ resistivity.

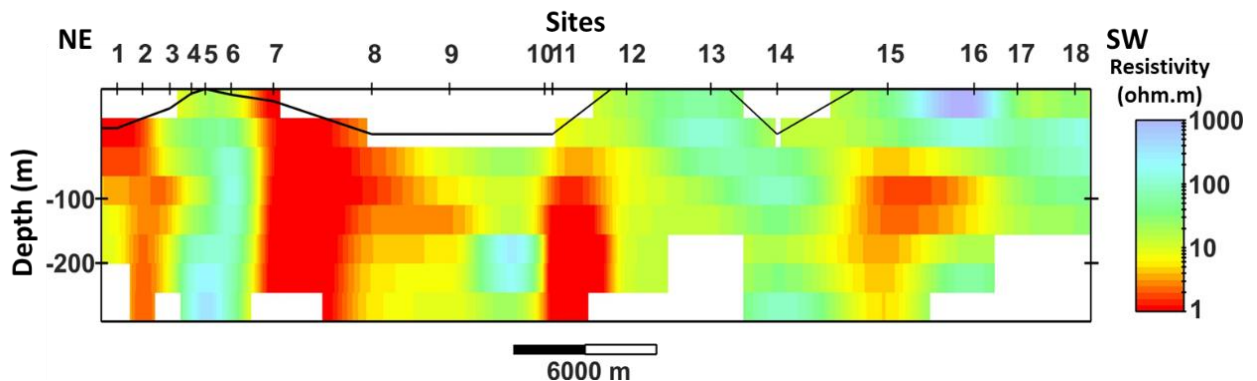


Fig. 3.20: Geoelectric section of profile A.

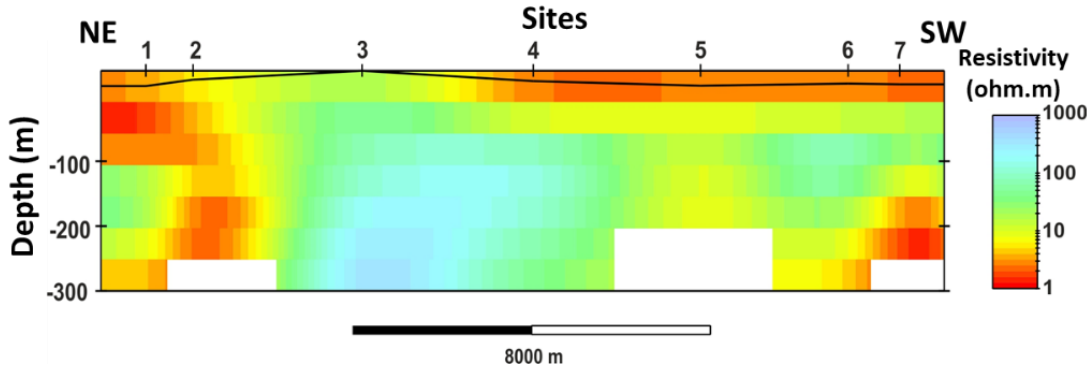


Fig. 3.21: Goelectric section of profile B

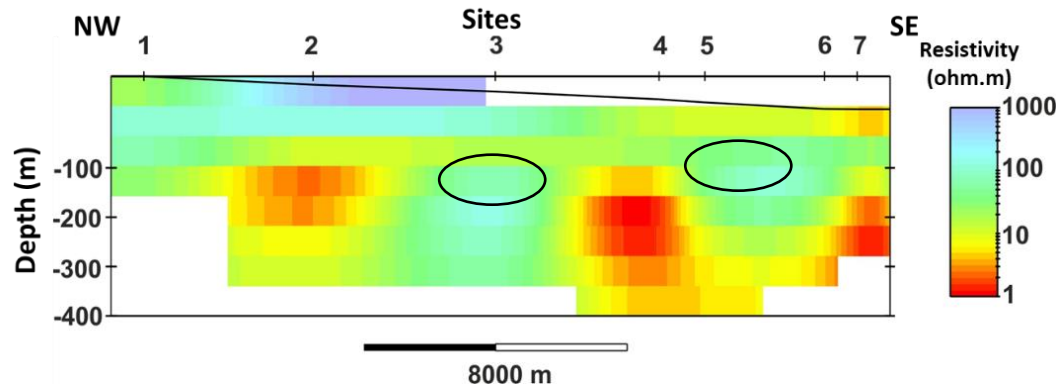


Fig. 3.22: Goelectric section of profile C.

Profiles B and C: Results from profile B (Fig. 3.21) show a conductive nature for the sites 1, 2, 6 and 7 because of the presence of tertiary sediments while the sites 3 & 4 are located on the Deccan trap that show a highly resistive nature. The thin highly conductive surface layer may be an impression of the recent unconsolidated sediments. The first three sites of profile C (Fig. 3.22) are located on the Deccan trap, hence show a high resistivity. The southeastern part of this profile reveals a zone of 100-1000 Ωm resistivity. In this profile, between sites 5 and 7, the Wagad sandstone layer of Mesozoic era is imaged as a moderately resistive layer that can be a prominent groundwater zone.

3.9 Delineation of lineaments in the Cambay rift and surrounding regions of NW India utilizing satellite derived EIGEN6C4 gravity data

(Avinash Kumar Chouhan)

The present study is an attempt to delineate the lineaments in the Cambay rift (CR), northwestern India, using satellite-derived EIGEN6C4 gravity data. A comparative study between the EIGEN6C4 and the ground based Bouguer anomalies, performed to validate the satellite data over the CR, shows a good correlation between them. Modern gravity data processing techniques (Total Horizontal Derivative, Analytical Signal, Tilt Derivative, and Euler deconvolution) are used to delineate the lineaments and estimate their source depth. Majority of the identified lineaments are trending in NW-SE and NE-SW directions and their source depth varies between 4.4 and 15 km. The NE-SW trending Diyodar and Tharad ridges in the CR are identified for the first time using gravity data. Based on the results of the present study, an updated tectonic map of the study area is presented.

3.10 Lithospheric structure beneath the seismically active northwestern Deccan volcanic province, India: Insight from the gravity data

(Avinash Chouhan)

Understanding of the Precambrian basement, Moho and Lithosphere-Asthenosphere boundary (LAB) remains limited due to sparse and lack of adequate geophysical data. To image the lithospheric structure beneath the seismically active northwestern Deccan

volcanic province (NWDVP), India, satellite-derived gravity data are utilized. The Precambrian basement depth has been estimated using two-dimensional radially averaged power spectrum (RAPS) analysis of the Bouguer anomaly. The basement depth varies from 0.5 to 7.2 km and is deepest along the central part of Cambay rift. Inversion of the Bouguer anomaly is used to calculate the topographical variation of the Moho and LAB. Inversion is performed over the band-pass (cut-off wavelength 100 and 200 km) and low-pass (cut-off wavelength 200 km) filtered Bouguer anomalies with the assumption of constant density contrast between the Moho and LAB interfaces. Results of the inversion reveal significant variation of the Moho and LAB depths over the NWDVP that vary between (1) 33-42 km and 82-124 km in the Kachchh rift, (2) 34-42 km and 68-110 km in the Cambay rift and north Gujarat, (3) 36-44 km and 80-95 km in the Narmada rift and south Gujarat and (4) 34-41 km and 85-135 km in the Saurashtra peninsula, respectively.

3.11 Structural fabric over the seismically active Kachchh rift basin, India: Insight from world gravity model 2012

(Avinash Chouhan)

The present study is an attempt to map the subsurface structural features using wavelength filtering and total horizontal derivative (THD) of gravity data. Power spectrum analysis of gravity data gives a cut-off wavelength of 100 km that has been used for wavelength filtering for regional-residual separation. The residual gravity anomaly significantly enhances the shallow features (like Allah-Bund fault, Kachchh mainland uplift, Wagad uplift, and Pachham uplift) and yields a NW-SE structural trend. Interpretation of the regional gravity suggests that the regional slope of the Moho in the KRB is in the SW direction. The predominant directions of the major lineaments derived by the THD of gravity data show EEN-WWS, NE-SW and NW-SE trends. A plausible explanation of the seismicity over the KRB has also been provided based on the structural features delineated in the present study.

3.12 Upper crustal structure of the North Cambay rift, India deduced from integrated study of gravity, seismic and borehole data

(Avinash Chouhan)

The Cambay rift, an intracratonic basin, situated in the northwestern Deccan volcanic province, is formed during the different stages of Mesozoic and Cenozoic era. To understand the detailed upper crustal geometry beneath the northern part of Cambay rift, gravity modelling is performed. The variation in the Bouguer anomaly (BA) is between -40 and +28 mGal. The total horizontal derivative of BA is calculated to study the lineaments/faults, which indicates that majority of the structural features are NW-SE oriented. Radially averaged power spectrum analysis reveals three layers at 2, 5.5 and 15 km depths. High pass filter with a cut-off wavelength of 100 km is used to extract the residual anomaly from BA. To study the upper crustal architecture, four density models have been constructed using residual BA that are constrained by Deep Seismic sounding, deep borehole and seismological data. Results of the density modelling reveal that the average thickness of Quaternary and Tertiary sediments is between 0.5 and 6 km, while the Deccan trap thickness varies between 0.5 and 3 km. The present study confirms the presence of Mesozoic sediments below the Deccan trap in the zone of marginal faults, having a maximum thickness of 0.6 km. Based on the results of the residual Bouguer and density modelling, the NE-SW trending Unhawa ridge and the N-S trending Mehsana uplift are delineated. Evidence of a magmatic underplating layer is also found in the middle crust along the central part of the rift, which further continues into the lower crust.

3.13 Determination of the local earthquake locations and velocity model for the Arunachal Himalaya using Joint Hypocentral Determination technique

(G. Srijayanthi and Nitu Yadav)

The Arunachal Himalaya that occupies the eastern most segment of the Himalaya between 26.66°N to 29.45°N latitude and 89°E to 98°E longitude is classified as zone V in the seismic zonation map of India (Bureau of Indian standards, 2002). Although two large earthquakes of M 7.3 and M 8.6 occurred in a span of just three years (Fig. 3.23), this region is least studied in terms of seismicity and also structure. It is important to understand the obtained seismicity and its correlation with any of the major geological features like MBT or MCT and whether the earthquakes in this region follow the theory of bimodal distribution of brittle strength in the crust and upper mantle, as observed along other segments of the Himalayan convergence zone or the earthquakes are restricted to the continental crust? In the adjacent Nepal Himalaya, the occurrence of earthquakes at sub-moho depths favours the idea brittle deformation in the upper mantle (Monsalve et al., 2006). Further the dominance of strike slip earthquakes in Nepal as well as adjacent Sikkim Himalaya strongly indicates active role of transverse tectonics (Hazarika et al., 2010; de la Torre et al., 2007).

Precise earthquake location requires accurately picked P, S wave arrival times and also an appropriate velocity model. A total of 1219 earthquakes were identified and analysed from December 2009 to December 2016. Since, no published velocity model exists for the study region we used 5 different velocity models from the Himalayas namely, Gupta et al., (1984), Mc Namara et al., (2017), Singer et al., (2017), De and Kayal, (1990) and Bhattachacharya, et al., (2007) and estimated earthquake location parameters and the corresponding errors/accuracies. The RMS and the location errors considerably reduce (< 0.5 s) when the apriori velocity model proposed for the adjacent Burma Himalayan region is used (Singer et al., 2017), compared to other velocity models. It is observed that most of the seismicity is outside the station network for which the location errors are high. Therefore, only a subset of 156 well located local earthquakes having azimuth gaps of $< 180^{\circ}$ are considered for estimation of velocity model using joint hypocentral determination technique (Kissling, 1995). It is also observed that the obtained velocity model mimics the initial velocity model (Fig. 3.24) (Singer et al., 2017) and also reduces the RMS error range from 0.5 s to 0.4 s. The obtained new velocity model was then used to locate the 1219 earthquakes that occurred in the region. A majority ($\sim 92\%$) of these earthquakes occurred above the Moho discontinuity at 60 km. A prominent number of events trend NW-SW trending along the Kopili fault. The earthquake locations in general are found to be concentrated across the Himalayan arc, rather than along it. The seismicity seems to be controlled significantly by the possible extension of the Kopili Fault into the Himalaya in the west and the syntaxial zone in the east, with the central portion being relatively quiescent.

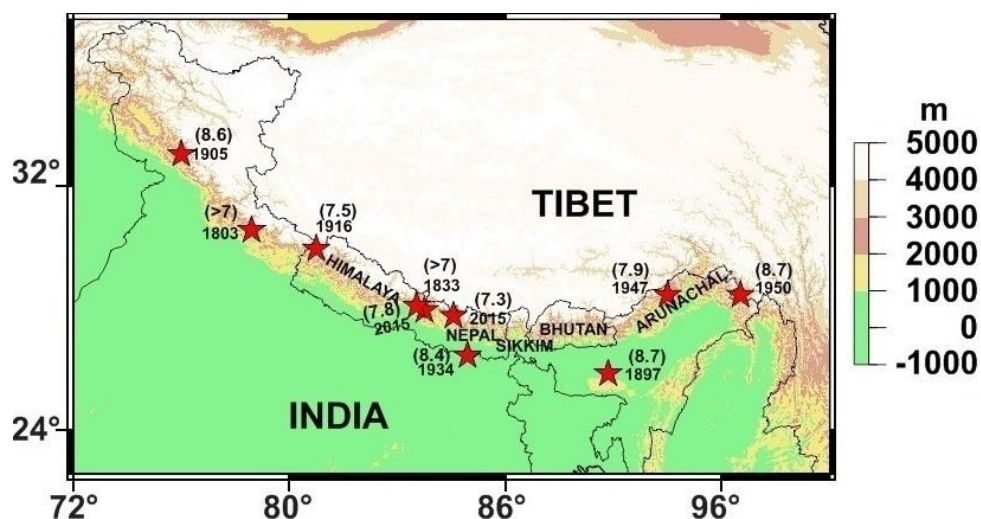


Fig. 3.23: Topographic map of the Himalaya–Tibet region showing large earthquakes (solid stars) $M > 7.0$ including two great ($M \sim 8.7$) earthquakes in the NE India. The two large earthquakes occurred in Nepal-Himalaya in the year 2015 is also shown.

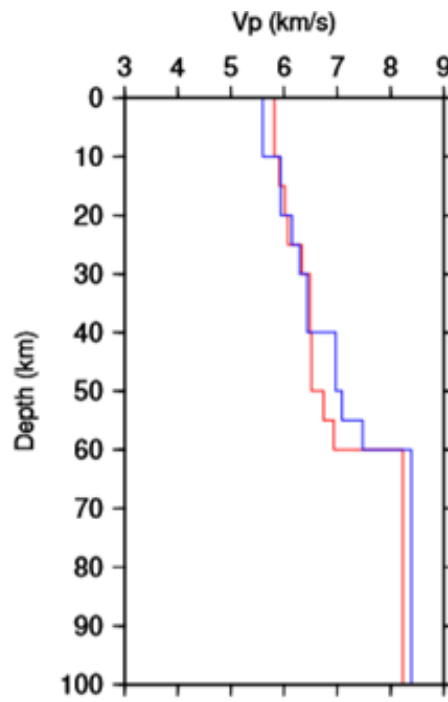


Fig. 3.24: Initial velocity model (red colour) and the final velocity model obtained from VELEST (blue colour).

4 EARTHQUAKE PRECURSORY RESEARCH

4.1 Source Characteristics of observed low latitude magnetic pulsations Pc3-4s

(Prasanna Simha, Jayashree Bulusu, Kusumita Arora and K.M.Rao)

In order to investigate the dependence of observed Pc4 on cone angle, we estimate the cone angle using the relation $\theta_{xB} = \cos^{-1} \frac{|B_x|}{B_{avg}}$ (Bolshakova and Troitskaya, 1968). It is earlier established that a low cone angle ($\theta_{xB} < 45^\circ$) facilitates occurrence of upstream waves that can drive Pc3-4 oscillations. For each event, the cone angle dependence is estimated and all events are classified into bins of 25 degrees each. The maximum number of Pc4 is found in the 50-75° bin (Fig. 4.1a). Very less number of events are observed in the cone angle limit of 25°. The amplitude and frequency of Pc4s are clearly independent of IMF cone angle (Fig. 4.1b and Fig. 4.1c).

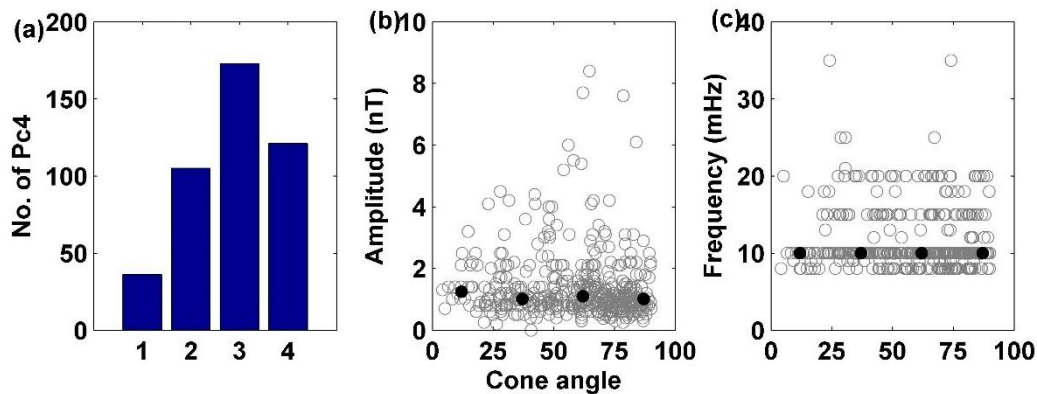


Fig. 4.1: Variation of Pc4 as a function of cone angle in bins of 25 degrees (indices 1 to 4 denote the 0-25°, 25-50°, 50-75° and 75-90° respectively) (a) Occurrence pattern, (b) Amplitude and (c) Frequency of Pc4.

Out of the four case studies presented above, we plot the variation of cone angle and other solar wind parameters during the events of 12 January 2013 in Fig. 4.2 and 6 May 2013 in Fig. 4.3, respectively. In Fig. 4.2, the top panels denote the spectral content in the X and Y components along with the superimposed cone angle estimates in the right axis (yellow colour). It is interesting to note that the cone angle shows a gradual increase from 10° to 45° during 0900-1000 UT, when a Pc4 event was observed at DSP. The corresponding interplanetary parameters, namely, average B field, solar wind speed and dynamic pressure, do not show an appreciable change. The variation in average B field < 5 nT, $V_{sw} < 400$ km/s, $|B_z| < 2$ nT, planetary activity index $k_p=0.33$, and the storm time index $Dst \sim 10$ nT suggest that the observed Pc4 event occurred during quiet geomagnetic conditions. As the cone angle is within 45°, we attribute upstream waves as the source of this event.

A similar investigation is also performed for the event that occurred on 6 May 2013 during 1130-1330 UT. The activity indices of $k_p=2.33$, $Dst=2$ nT, interplanetary activity index $B > 5$ nT, $|B_z| > 7$ nT, solar wind speed $V_{sw} > 500$ km/s suggest that the event occurred during disturbed geomagnetic conditions. During this event, the X component did not show Pc4 event whereas a peak frequency of 15 mHz was seen in the Y component. It is interesting to note that the cone angle estimate during this event varied within 50 to 70°, which suggests that the observed event may not be the result of upstream waves, generated outside the magnetosphere. The solar wind speed V_{sw} was high (~ 520 km/s), which results in the KH instability at the magnetopause boundary. This may generate surface waves (Southwood, 1968; Pu and Kivelson, 1983) as well as wave guide mode (Samson et al., 1992; Mann et al., 1999; Mills et al., 1999) that couple to a transverse mode at the inner turning point (Chen and Hasegawa, 1974; Southwood,

1974; Southwood and Kivelson, 1990; Mills and Wright, 1999), which gave rise to the pulsation event in the east-west component.

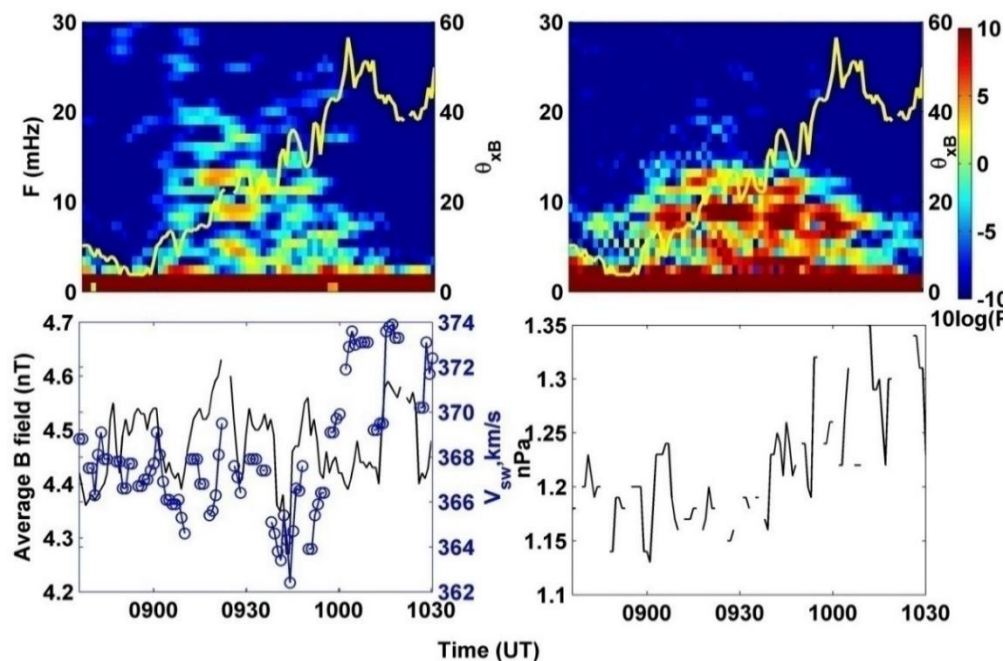


Fig. 4.2: Top panels denote spectral Pc4 characteristics observed in X and Y components superimposed with the cone angle estimates (yellow curve) during 0830-1030 UT on 12 Jan 2013. Lower panels denote variation of average IMF B field and solar wind speed (bottom left panels) and dynamic pressure (right bottom panel).

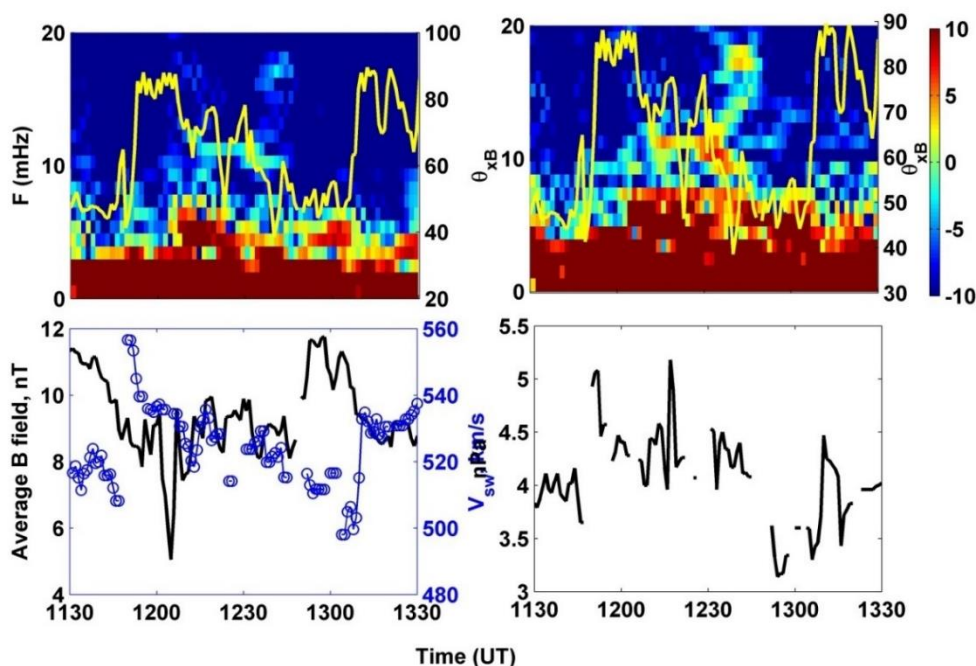


Fig. 4.3: Same as Fig. 4.2 for 6 May 2013 event

4.2 Analysis of anomalous variations of Surface Latent Heat flux, Air temperature at 2m and Outgoing Long wave Radiation prior to the New Zealand earthquake
(Prasanna Simha and K.M.Rao)

An earthquake with a magnitude of 7.8 occurred on November 13, 2016, at 54 km NNE of Amberley, New Zealand (Latitude: 42.73°S and Longitude: 173.054°E) (NEIC, USGS).

From the analysis of atmospheric parameters like Surface Latent Heat flux (SLHF), air temperature at 2 m from the surface (AT2m) and outgoing long-wave radiation (OLR), it was observed that anomalous variations were observed, before the occurrence of an earthquake, near the epicenter region. An anomalous spike in SLHF was first observed on October 7, 2018 with an SLHF value of 117.75 W/m^2 , which is 10.794 W/m^2 more than $+2\sigma$ level of mean SLHF value calculated from the preceding 10 years (Fig. 4.4). The second anomaly in SLHF was observed after the observation of anomalous variations in AT2m and OLR. On October 26, 2018, the second anomalous variation in SLHF was observed, but this time the deviation from the mean SLHF value is only 4.2766 W/m^2 (Fig. 4.4).

Anomalous variations in AT2m were observed twice prior to the earthquake at 54 km NNE of Amberley, New Zealand. At the location 42.8564° S latitude and 174.375° E longitude, anomalous variations in AT2m was observed on October 18, 2016 for the first time and the anomalous spike was recorded on the next day (October 19, 2016) also (Fig. 4.5). On October 18, 2016, an air temperature of 286.25 K was recorded at 2m from surface level, which is 3.0575 K more than the ten year average and "EEFI" of 2.1839. The next day (October 19, 2016), the air temperature recorded at 2m from the surface level was 285.899 K , while the ten years average of air temperature at 2m level was 283.1209 K and the EEFI was 2.7808.

Four days prior to the occurrence of the earthquake (November 9, 2016), anomalous variations in AT2m were observed for the second time. On November 9, 2016, an air temperature of 287.175 K was observed with an EEFI value of 2.078. The anomalous flux in OLR was observed only once prior to the earthquake. The anomalous flux was observed on October 21, 2016, with the OLR flux value of 266.727 W/m^2 , which is 40.22 W/m^2 more than the ten years average (Fig. 4.6). Even though on November 5, 2018, the current OLR value is 40.326 W/m^2 more than the ten years average, it was not above the $+2\sigma$ level. From the time series analysis, it can be noted that the current OLR value observed during November 9-12, 2016 was more than the ten years average, but the current OLR value was never more than the $+2\sigma$ level. Also, the current OLR value on the event day (i.e.) November 13, 2016, was 29.313 W/m^2 less than the ten year average.

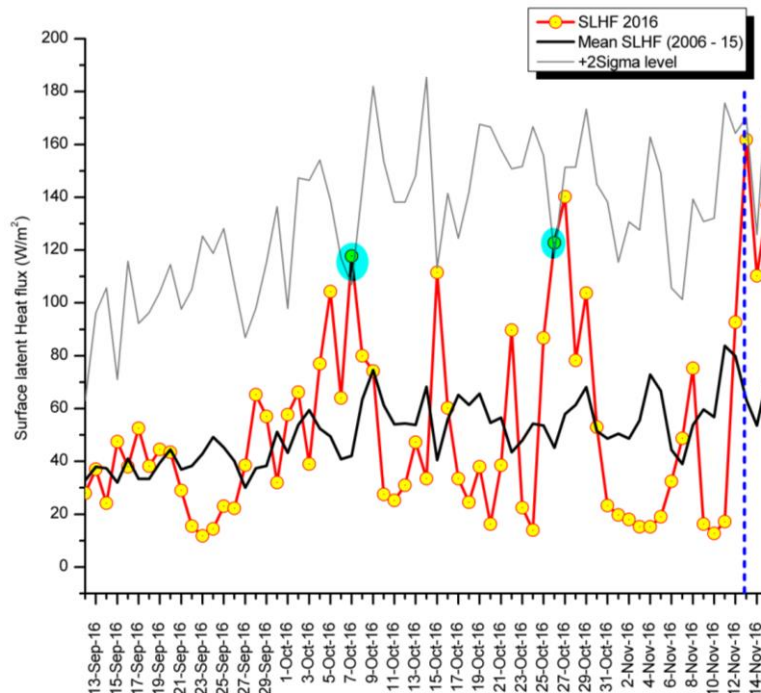


Fig. 4.4: Time series analysis showing variations in SLHF prior to the occurrence of New Zealand earthquake.

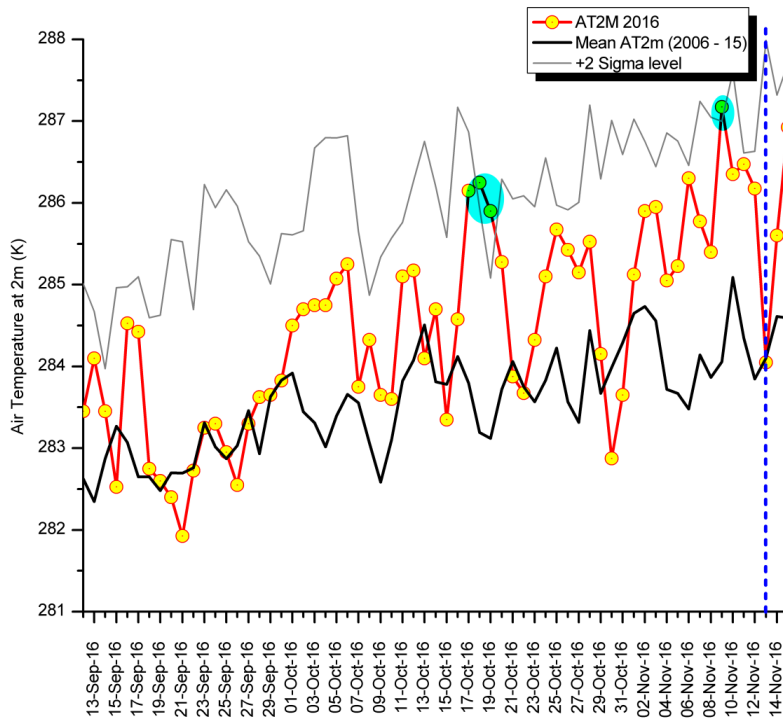


Fig. 4.5: Time series analysis of AT2m prior to the occurrence of New Zealand earthquake on Nov 13, 2016, compared to ten years' average and showing anomalous spikes on Oct 18, Oct 19 and Nov 9, 2016.

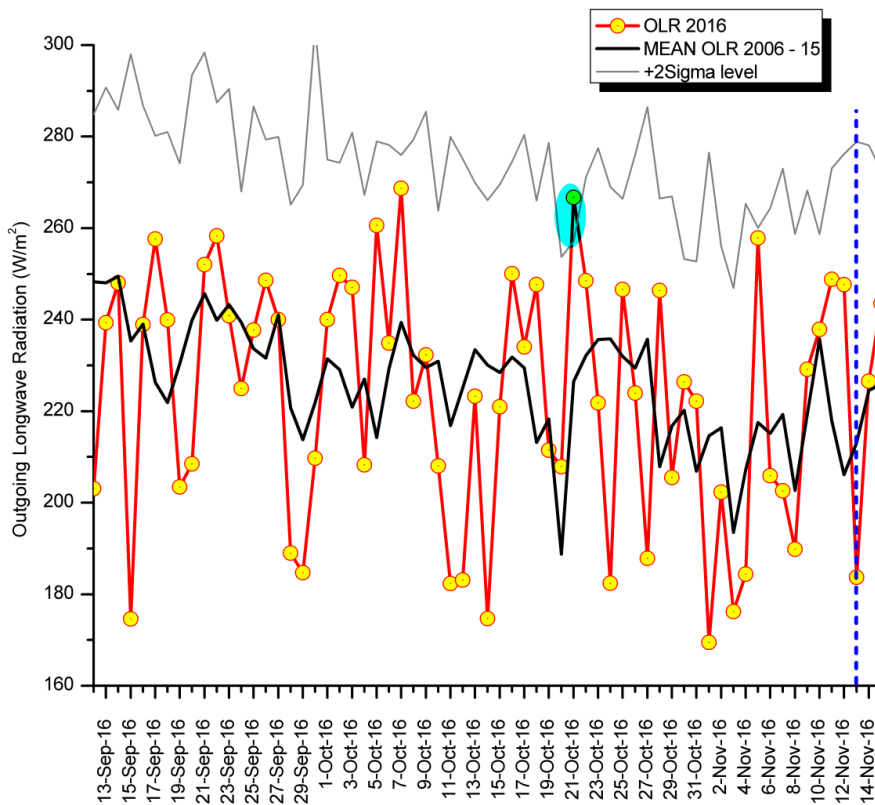


Fig. 4.6: Time series analysis of OLR scenario before the occurrence of New Zealand earthquake. An anomalous flux variation in OLR was observed on October 21, 2016.

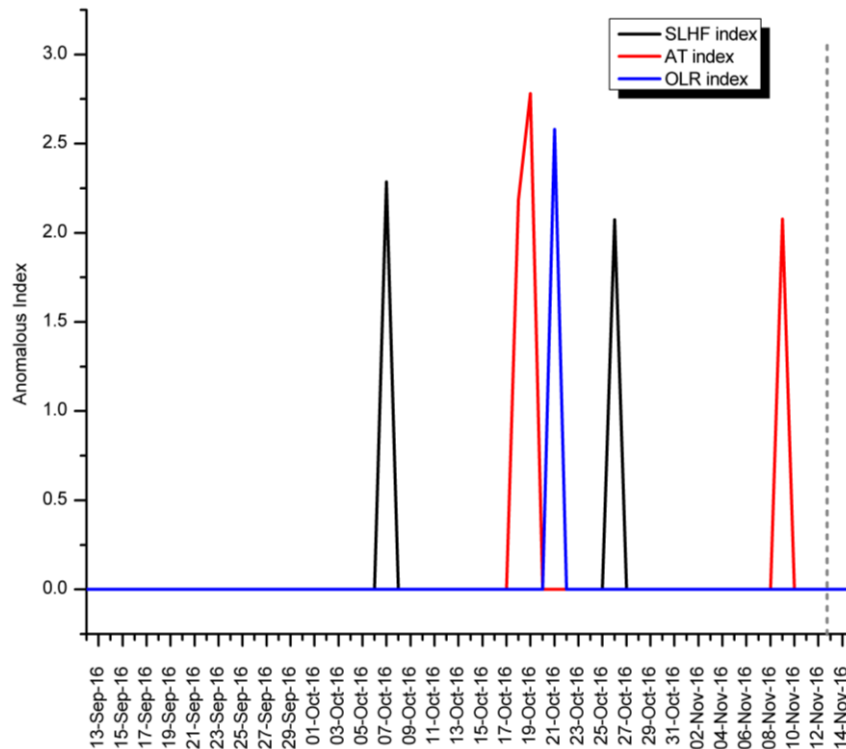


Fig. 4.7: Comparison between EEFI of SLHF, AT2m and OLR. Anomalous variations were observed first in SLHF, then in AT2m and OLR.

From an analysis of the above atmospheric parameters, it can be inferred that the increased tectonic activity triggered emission of gasses like radioactive radon. Increase in tectonic activity increases the stress along the plate/fault interface. Hence, the volume of voids of the rocks under stress reduces their volume, which in turn releases gases like radon from it. The radioactive radon from the voids of the rocks moves up and ionizes atmospheric air molecules at the earth's surface. These ions attract water vapour due to the polar nature of the water molecules and get condensed over these ions by releasing the latent heat energy into the atmosphere. This release of latent heat energy leads to the increase of air temperature at surface level first and then at higher altitudes as the air molecules move vertically up due to the convection process, thus finally, anomalous OLR flux above $+2\sigma$ level is observed. This can be inferred from the increase in SLHF level first, followed by temperature of air at 2m from the earth's surface and anomalous increase in OLR respectively (Fig. 4.7). From the results of SLHF, AT2m and OLR, it is understood that the seismically active regions can be identified on short term basis if we can continuously monitor the atmospheric scenario using satellite technology.

4.3 Observation of Seismo-Geomagnetic Pulsations using LEMI 30 at Badargadh, Kutch

(Prasanna Simha and K.M.Rao)

The variations in geomagnetic field are classified as external and internal, with respect to the surface of the Earth. The solar wind, magnetosphere and ionosphere are considered as the major causes of the external geomagnetic changes, while the internal geomagnetic variations are linked with the tectonic processes and generally related to the magnetization of the crustal rocks (Merrill et al., 1996, Manda and Purucker, 2005). The response of magnetic minerals to the variation in the external field and also their reaction to the crustal stress field can cause local crustal geomagnetic anomalies, which vary on all spatial scales. Previous studies about the characteristics of earthquake precursors show that the amplitude of the observed anomalous variations could be correlated with the magnitude of seismic event. In other words, large precursory signals can be recorded in association with big seismic events (Cicerone et al., 2009). However, the occurrence of major

earthquakes can be preceded by anomalous variations in several geophysical parameters such as anomalous changes in the geomagnetic field (Vere-Jones, 1995). Many discussions and arguments are still arising about the signature and influence of earthquakes on the geomagnetic field measurements

In order to see the background global geomagnetic activity levels, the Planetary Index (Kp) and Disturbance of Storm Time Index (Dst) are analysed during the corresponding period (Fig.4.8). The Seismo Geomagnetic pulsations are identified using the data of Induction Coil Magnetometer at Deslapar and Badargadh MPOs during two local earthquakes of magnitude 4.3 and 3.7 on 8 and 30 July 2019 (Fig. 4.9 and 4.10).

The simultaneous magnetic pulsations Pc3 and PI1 have been identified on 8 July and 30 July 2019 (Fig. 4.9). Similar observation is found after the local earthquake on 30 July 2019. With minor geomagnetic activity, the recurring Pc3 is one of the identified features during the event. According to Hayakawa et al. (2007), natural ULF emissions can be emitted from the centre of the seismic activities due to several effects, such as piezo-magnetic, electro-kinetic and micro-fracturing during their preparation stage. Moreover, the changes of the underground conductivity can cause an enhancement of the observed ULF signals (Mogi, 1985).

The time of the local earthquake has been indicated by a red dotted line in Fig. 4.8. The Geomagnetic field is less compressed on 8 July 2019, during the event period and being released after 18 UT. Kp and AP also showed some minor geomagnetic activities. The geomagnetic pulsations recorded during the event period are as shown in Fig 4.9 and 4.10.

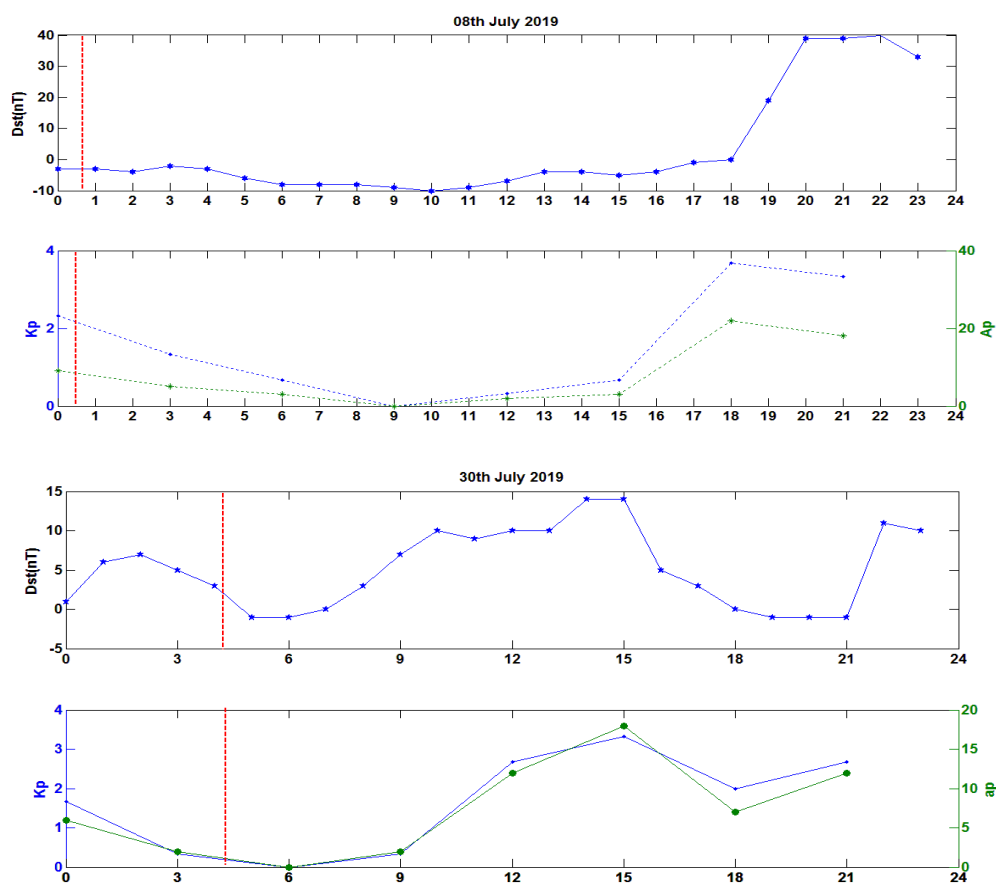


Fig. 4.8: Global Planetary Index (Kp) and Disturbance of Storm Time Index (Dst) on 8 and 30 July 2019

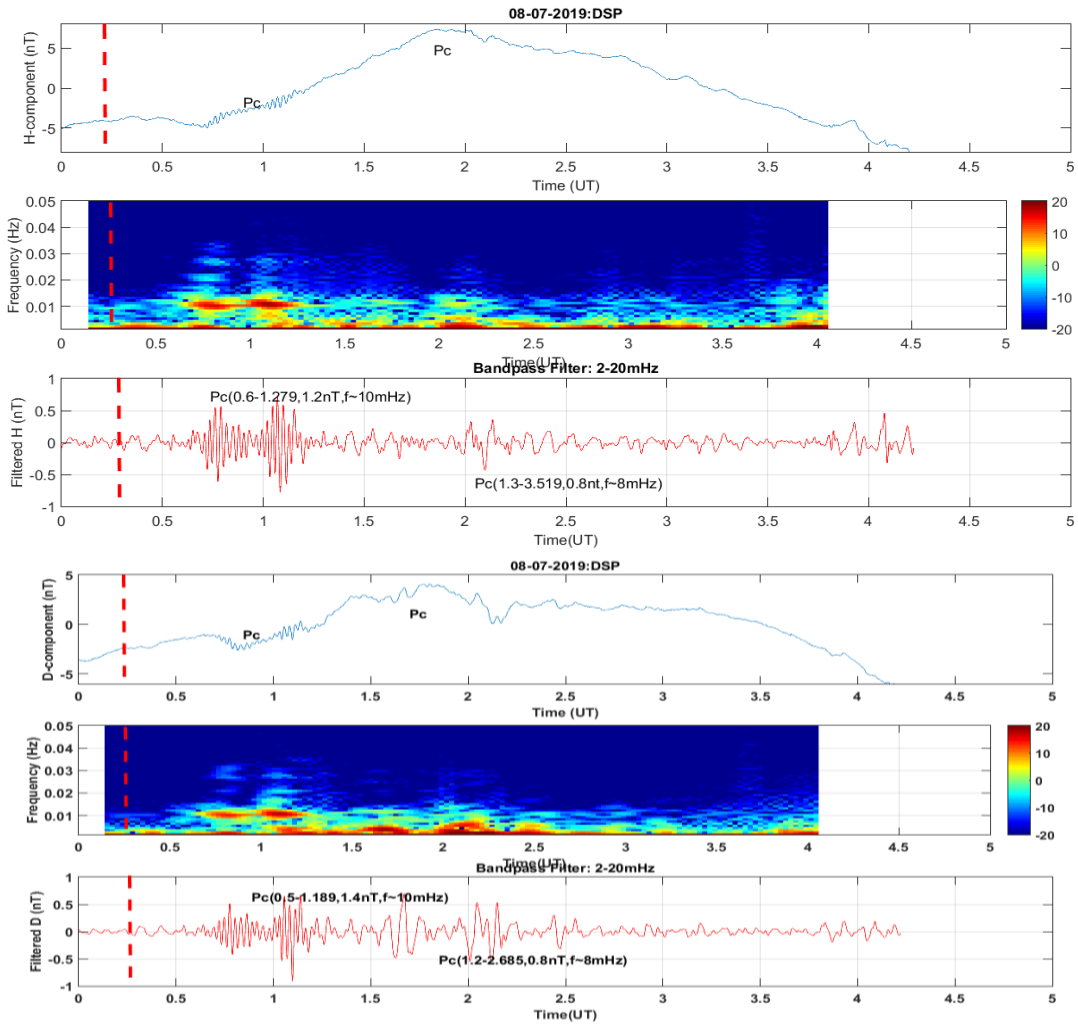
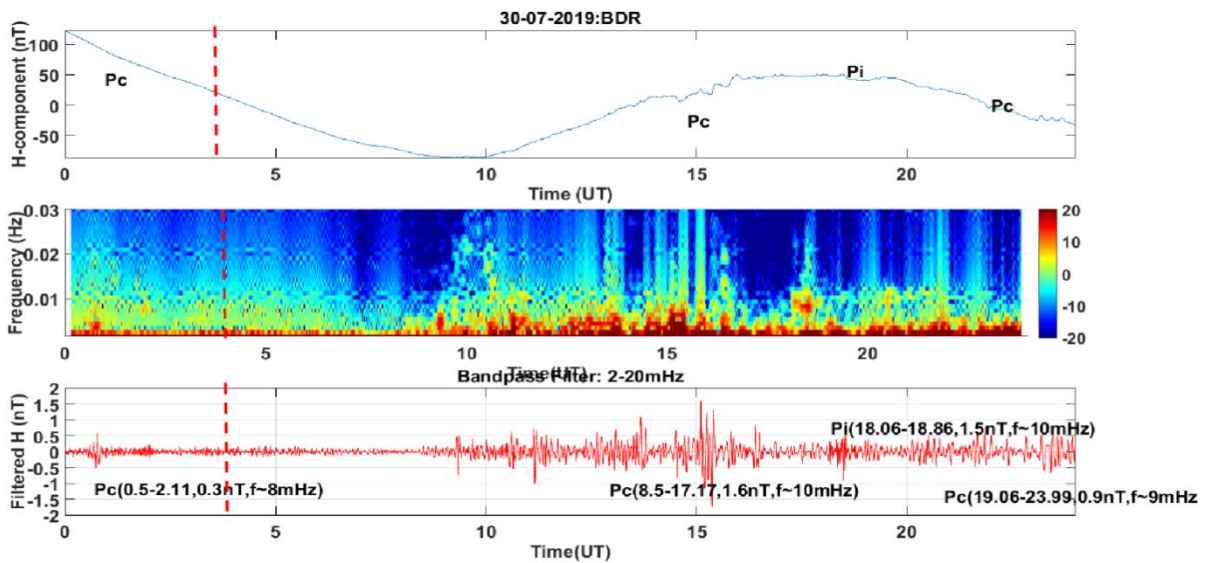


Fig. 4.9: Geomagnetic Pulsations at the Deslapar site after the 4.3 Magnitude earthquake on 8 July 2019. The red (dashed) line is the event time of the earthquake in UTC.



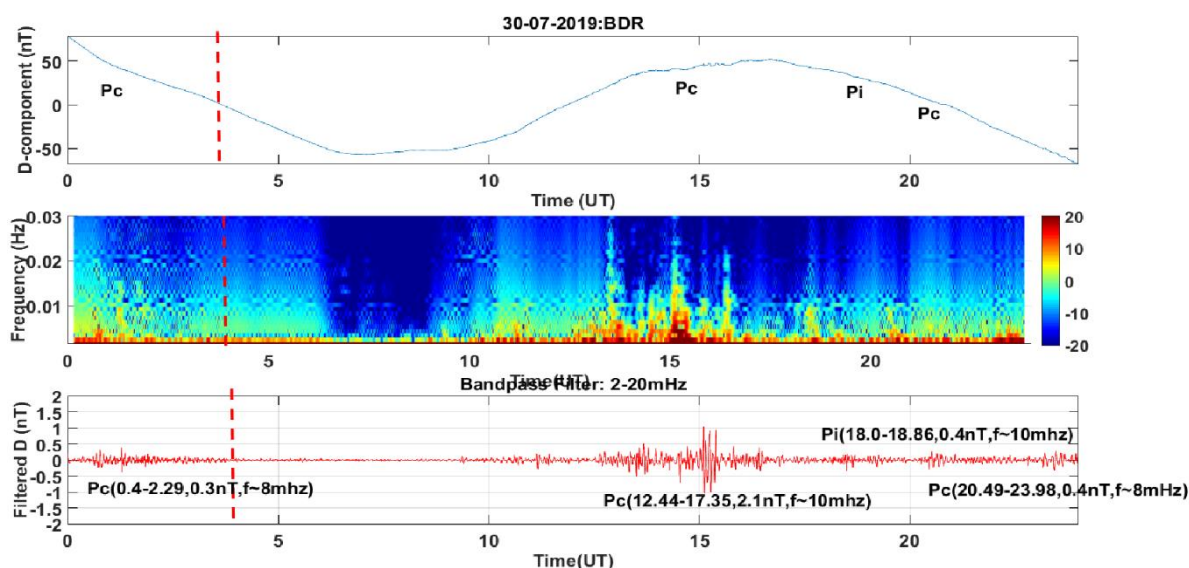


Fig. 4.10: Same as Fig. 4.9 but for the M3.7 earthquake on 30 July 2019

4.4 Local Trend Analysis of Irregular pulsations (Pi2:6-25 mHz) at low latitude station Desalpar, Kachchh

(Prasanna Simha and K.M.Rao)

Geomagnetic pulsations are studied using ground magnetometer data of Induction coil magnetometer, at Desalpar MGO. We report the morphology of Pi2 pulsation bursts (6-25 mHz) and its local time variations during the year 2013. The investigation is carried out to address the effect of sun earth interaction on these Pi2s. The local trend analysis has been carried out by classifying the data into 3 hour local time bins (LT=UT+0530). Pi2 periods and occurrence rate during the local time in 2013 show maximum number of events in the early morning and midnight times, and very less number during the noon times (Fig. 4.11a). The maximum number of events that occurred in the D component and H components are 44 and 29 in the midnight and early morning hours, might be because of the tail currents at the magnetic reconnection during the night time. We observed more number of events in the D component in comparison with the H component, while the observed periods of the H component are more compared to the D component (Fig. 4.11b). The ranges of periodicity of the H and the D components are around 50-150s and 59-99s, respectively. The periodicity of Pi2 has been enhanced during 18-19 LT. The periodicity in H component increased from 6 LT and attained a maximum during 18-19 LT, and decreased after that (Fig. 4.11b). The maximum amplitude is noticed during the 6LT. The amplitude of D component is more than that of the H component (Fig. 4.11c).

The number of events, amplitude and period are correlated with the interplanetary parameters, such as Planetary Index (K_p) (Fig. 4.12a), Interplanetary Magnetic Field (IMF) (Fig. 4.12b), Solar Wind Speed (Fig. 4.12c) and proton Density (Fig. 4.12d). 200-250 Pi2 have been noticed during the lower K_p values. This could be because of the particle injection through the polar cusp during the daytime being intensified pole ward. The amplitude has been enhanced when the activity is increased; when K_p values are increasing, the median of the amplitude and the frequency show continuous enhancement (Fig. 4.12a). High numbers of events have been noticed when the IMF is greater than 5nT and its amplitude and frequency have increased linearly during the increase of IMF (Fig. 4.12b). Similar conditions have been noticed when the solar wind speed is around 400km/s and proton density is around 5 to 10 N/cc (Fig. 4.12c & d).

The morphology to identify the pulsation bursts during the quiet and disturbed time is shown in Fig. 4.13. The observed quiet and disturbed period Pi2s of the magnetic data of Desalpar are compared with the 1Hz fluxgate magnetic data of Intermagnet low latitude stations, i.e., HON and PHU. Time-frequency analysis was applied to the down sampled

time series of magnetic data. The identified events were filtered in the range of 3-25 mHz so that pulses of Pi2 and respective amplitudes are extracted. The peak to peak amplitude during the quiet day (22 Jan 2013, Kp~0) is around 0.34 nT (Fig. 4.13 a & b) and 0.9 nT during disturbed days (28 Feb 2013, AL=-109nT) (Fig. 4.13 c & d).

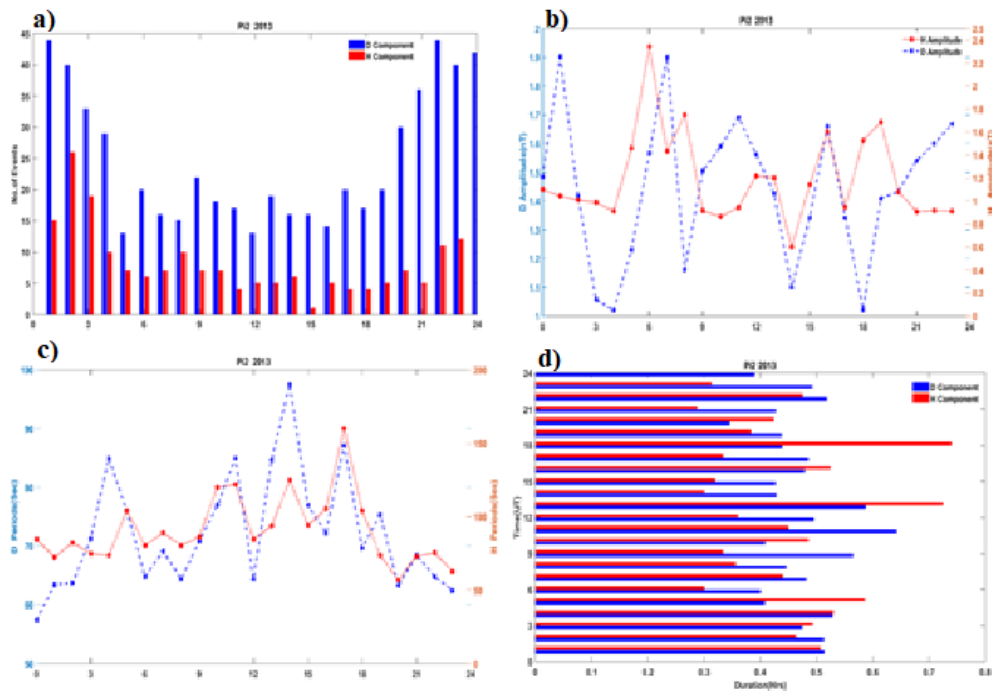


Fig. 4.11: The local trends of Pi2 events as a function of (a) occurrence, (b) peak to peak amplitude (c) periods (d) duration of X (blue) and Y (red) components respectively.

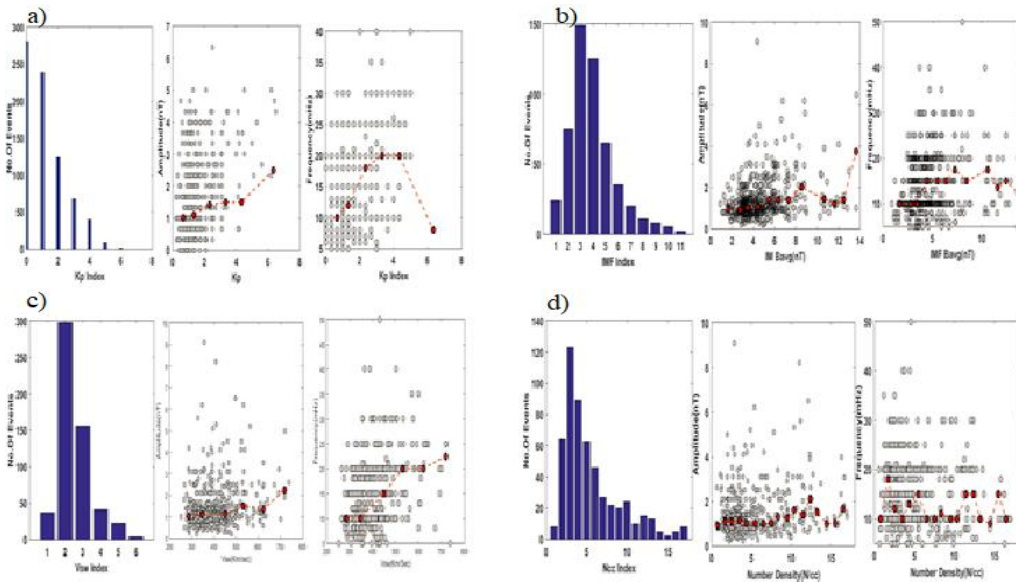


Fig. 4.12: Variation of Pi2 as a function of (a) Kp, (b) IMF Bavg, (c) solar wind speed, (d) Proton density. The occurrence, amplitude and frequency have been plotted. Grey and black dots indicate the individual samples of the amplitude and frequency in each subpanel, whereas the red dots indicate the median values.

We computed the confidence interval using the formula given by Torrence and Compo (1998) and obtained the power spectral densities of H and D components in the quiet and sub storm periods (Fig. 4.13 a & b). We identified the peaks, which exceed the confidence interval during the quiet day. We noticed more pronounced signal in the D component compared to the H component at around 10 mHz. During the sub storm period, we have

noticed good signal both in H and D components. The present analysis deals with the pulsation bursts noticed during 2013, using highly sensitive Induction coil magnetometer (LEMI 30) data at Desalpar and the analysis of Pi2s local trend in association with the Interplanetary Parameters is carried out. The periodicity of Pi2 has been enhanced during 18-19 LT. The periodicity in H component is increased from 6 LT and attains a maximum during 18-19 LT and then decreased. The maximum amplitude is noticed during the 6 LT. Maximum number of Pi2s have been observed when the Kp values are lower and the IMF B average is around 5nT, solar wind speed is around 400km/s, and the proton density is around 5 to 10 N/cc. The investigation of Pi2s that occur during quiet geomagnetic conditions without the association of sub storms have gained a lot of importance (Bulusu et al., 2017, Kosaka et al., 2002; Kwon et al., 2013). The Pole ward Boundary Intensification (PBIs) is one such mechanism that explains the geomagnetic quiet conditions. We made an attempt to study the Pi2s during quiet condition on 22 Jan 2013, where Kp is around 0. We noticed very good signals in D component compared to the H component.

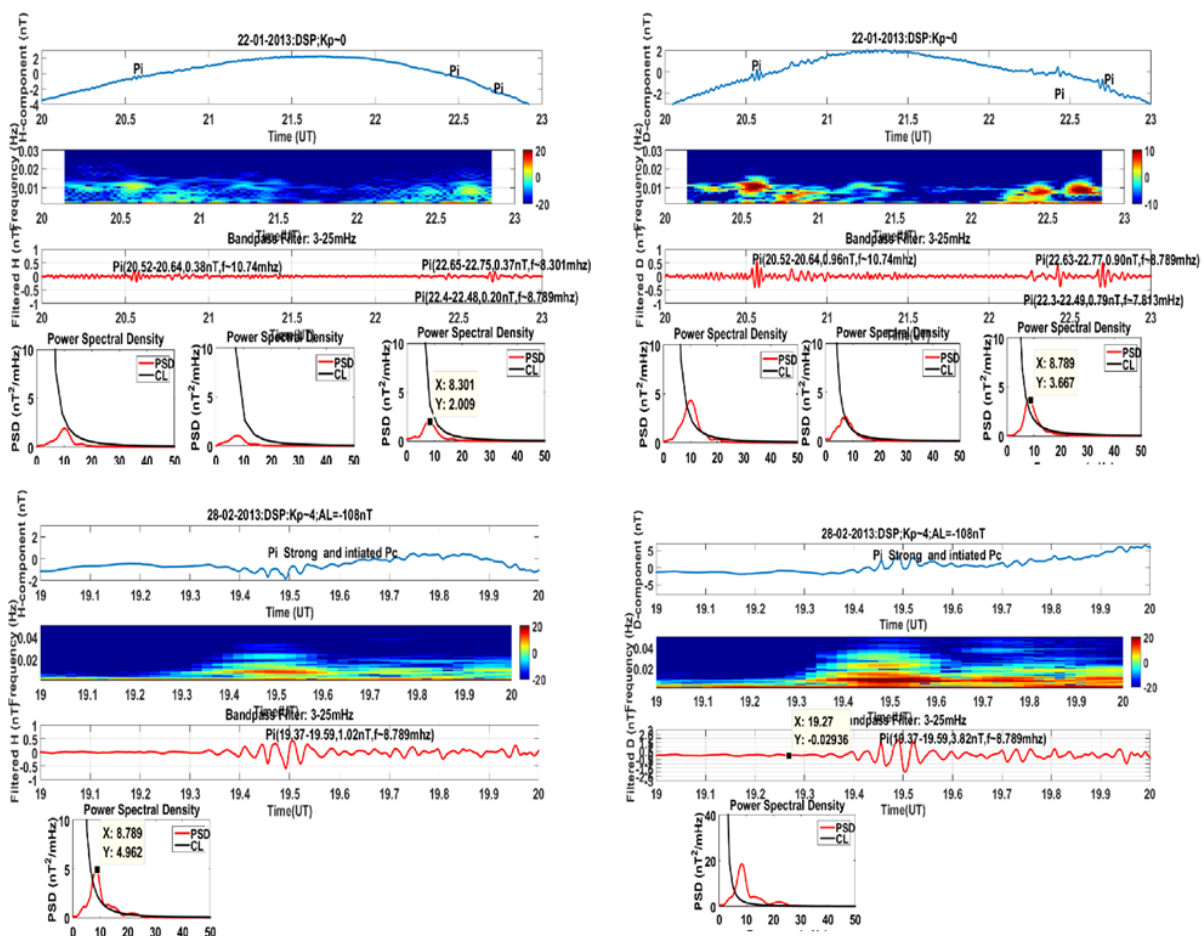


Fig. 4.13: Quiet and storm time Pi2s in H and D components recorded at Desalpar

4.5 Classification of Geomagnetic Pulsations during a moderate Geomagnetic storm

(Prasanna Simha and K.M.Rao)

A magnetic storm is an interval of several days duration during which there is a large reduction in the horizontal component of the geomagnetic field at the Earth’s surface (Gonzalez et al., 1994). A classic magnetic storm begins with a sudden commencement and a prolonged initial phase. These are caused by a sudden increase in the dynamic pressure of the solar wind as high speed and high-density plasma from the Sun suddenly

arrive at the Earth. The magnetopause is pushed earthward, strengthening its current and its positive effect on the ground. The sudden commencement is a packet of waves triggered by the sudden displacement of the field lines in the magnetosphere that resonate in response to the change. The initial phase lasts from a few minutes to many hours, and is usually followed by a rapid decrease in the surface field. This decrease is called the main phase of the magnetic storm. A weak storm consists of only a 50 nT decrease, a moderate storm about 150 nT, a strong storm up to 300 nT, and a great storm more than 500 nT. We analysed the global parameters along with the observed geomagnetic pulsations which are determined using the data of induction coil magnetometer of Deslappar, Kachchh, Gujarat during a moderate geomagnetic storm during 27-29 June 2013.

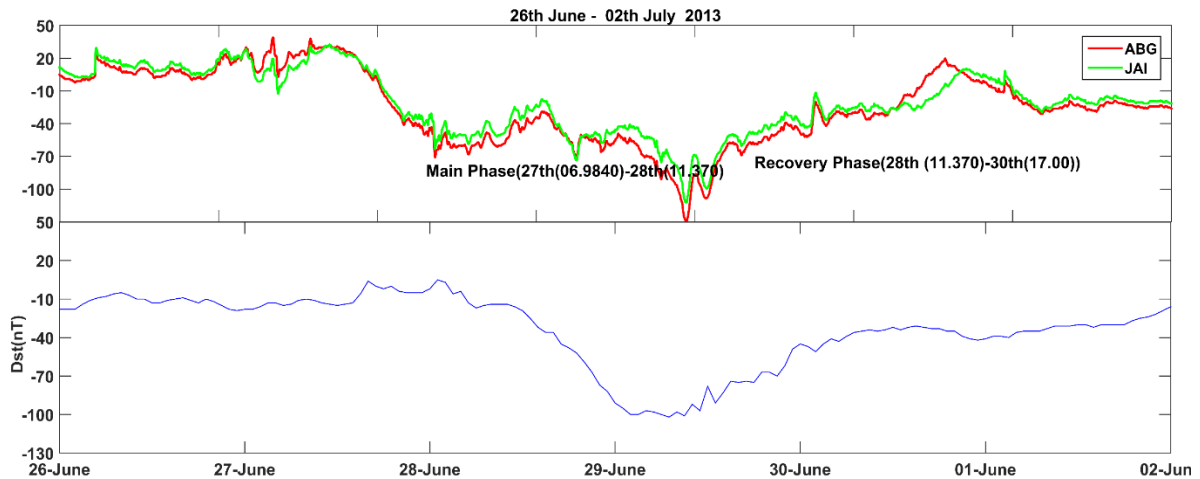


Fig. 4.14: H-component of geomagnetic field at the two intermagnet stations along with Disturbance of storm time index (Dst).

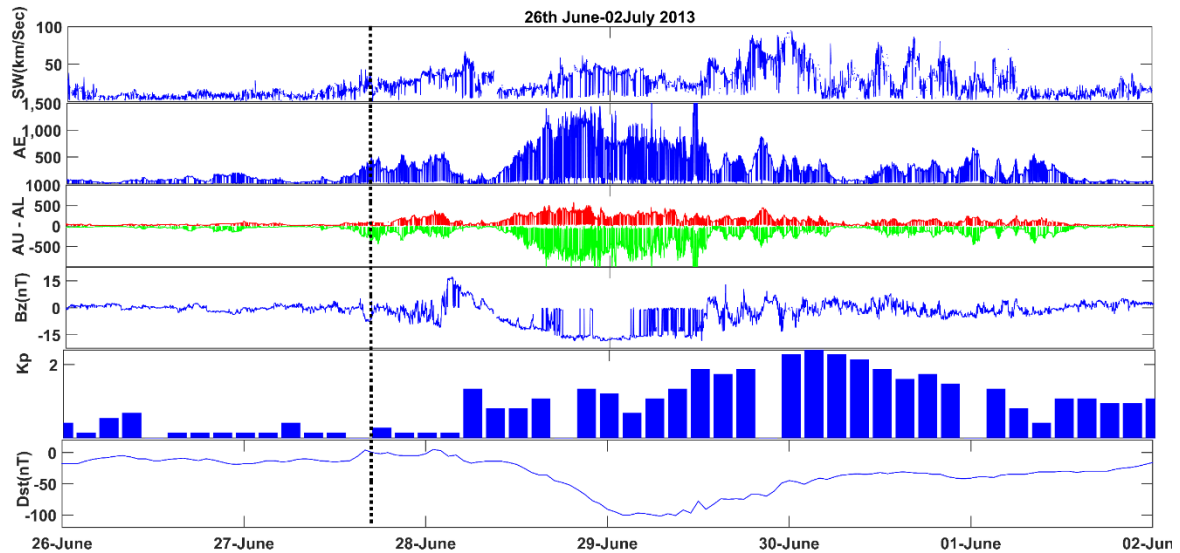


Fig. 4.15: Global Parameters during 26 Jun- 2 Jul 2013. Dotted line indicates the main phase initiation.

The phases of magnetic storm are identified using H-component of the geomagnetic field recorded at Alibag and Jaipur intermagnet stations. The H-component of geomagnetic field of these stations and Dst time series are plotted in Fig. 4.14. Here, the main phase lasts for 5 hours and no considerable storm sudden commencement (SSC) is noticed. The main phase of the storm started at 06.98 UTC of 27 June and ended on 28 June around 11.370 UTC. The present storm was initiated by an interplanetary shock arrival at $\sim 15:00$ UT on 27 June. The IMF Bz fluctuated around 0, but after $\sim 08:00$ UT on 28 June, the IMF Bz gradually turned southward (<0) and remained steady at about -10 nT until $\sim 12:00$ UT

on 29 June. The persistent southward IMF drove the magnetosphere into a magnetic storm, during which geomagnetic indices reached maximal values of $|Dst| \sim 120$ nT and $AE \sim 1000$ nT (Fig. 4.15).

The identification of magnetic pulsations has been done using the time-frequency analysis. In this process, we first down sampled and de-noised data using a spectrogram, with a hamming window of length 1024s and 50% overlap. The identified events were filtered in the broad band of 2-30 and 6-22 mHz so that pulses of Pc4, Pi2 and respective amplitudes are extracted. The identification of magnetic pulsation during main phase of magnetic storm is shown in Fig.4.16 and recovery phase is shown in Fig. 4.17.

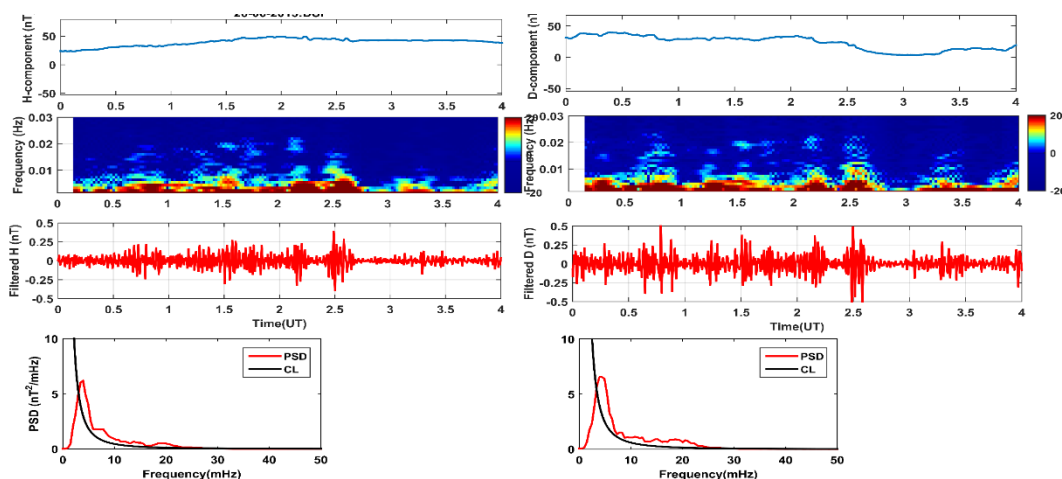


Fig. 4.16: Identification of Pulsations Continuous during the main phase of the storm

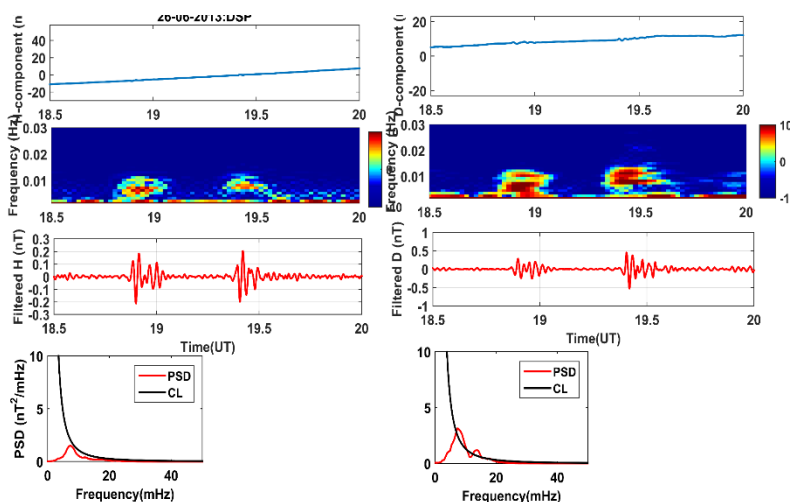


Fig. 4.17: Identification of Pulsations Irregular during the recovery phase.

The growth of ring currents around the earth generates the main phase of the storm. This is traditionally thought to be a doughnut-shaped region around the Earth containing a strong westward current. This current is primarily created by ions including protons, helium ions, and oxygen ions drifting westward around the Earth from midnight towards dusk and onward. This current acts much like a large solenoid around the Earth producing a magnetic disturbance that is southward along the Earth's dipole axis, whereas the geomagnetic field itself is northward.

The Pc4 and Pc5 pulsations have been identified during the main phase and their amplitudes are found to be enhanced to 2.48 nT. These Pulsations are triggered by Poloidal ULF waves which are magnetic field line oscillations with a strong displacement in the radial direction. With a dominant azimuthal wave electric field that is along the drift motion

of magnetospheric particles, the poloidal wave can effectively interact with energetic particles in the ring current and the radiation belt. Energetic particles can be accelerated or decelerated by the wave electric field through the drift/drift-bounce resonance (Southwood, 1976). The filtered induction coil data during the main phase of storm is shown in Fig. 4.18. The details of pulsations identified are shown in table 4.1.

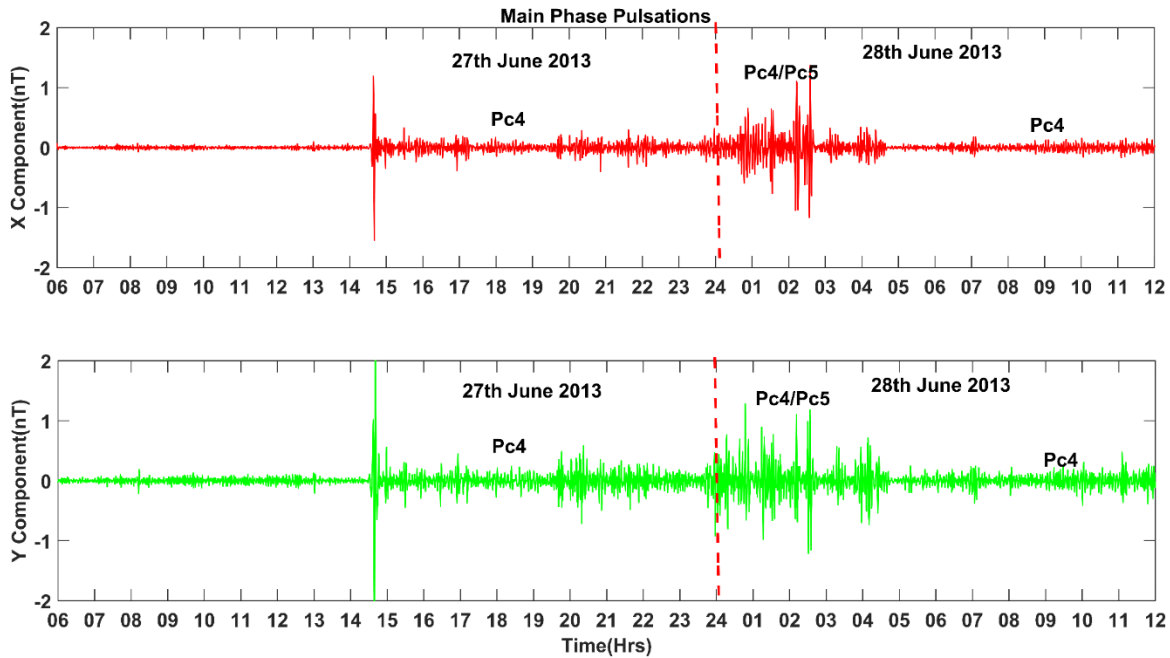


Fig. 4.18: Main phase Geomagnetic pulsations recorded at induction coil magnetometer

Table 4.1: Details magnetic pulsations during the main phase of storm

| Date | Main Phase Pulsations | | | | | | | | | |
|--------------|-----------------------|-------|------|-----------|---------|------------------|-------|------|-----------|---------|
| | X Component (nT) | | | | | Y Component (nT) | | | | |
| | Start | End | Amp | Frequency | Type | Start | End | Amp | Frequency | Type |
| 27 June 2019 | 14.86 | 23.99 | 0.6 | 14.16 | Pc4 | 14.86 | 23.99 | 0.92 | 14.86 | Pc4 |
| 28 June 2019 | 0 | 4.791 | 2.48 | 3.9/7.8 | Pc5/Pc4 | 0 | 4.8 | 2.36 | 4.4/15.14 | Pc5/Pc4 |
| | 7.7 | 12 | 0.32 | 4.88 | Pc5 | 5 | 12 | 0.63 | 4.883 | Pc5 |

The recovery phase of the storm is caused by the loss of these ions. Until recently, it was thought that the main loss process for the ions was charge exchange. As the ions approach the atmosphere in their bounce motion, there is a high probability of interaction with an atmospheric neutral atom. An electron from the cold atmospheric atom is exchanged with the hot ion. The hot ion becomes an energetic neutral atom that is no longer confined by the field. The cold atom is transformed into a cold ion that contributes little to the current. The creation of ring current is caused by a prolonged interval of strong southward magnetic field and high solar wind velocity. These are precisely the conditions that cause magnetic reconnection on the dayside and intense convection in the magnetosphere. The ions creating the current are brought in from the tail and energized by the magnetospheric electric field associated with convection. There is growing evidence that most of these ions simply drift through the magnetosphere and exit through the dayside boundary (Liemohn et al., 2001). Only after the recovery phase begins some of these ions come onto closed drift paths that circle the Earth. There is also growing evidence that ion cyclotron waves may play an important role in ring current decay. These waves scatter ions in pitch angle towards the loss cone. This allows the ions to come closer to the atmosphere where the probability of interacting with a neutral particle is higher. There is no type of ULF wave that has been identified as specifically created by a storm-time ring current. The

instabilities that can occur in a cloud of drifting protons also occur during intervals that is, not strong high-density plasma from the Sun suddenly arrive at the Earth. The Recovery Phase Pulsations identified using Induction Coil Magnetometer are shown in Fig. 4.19.

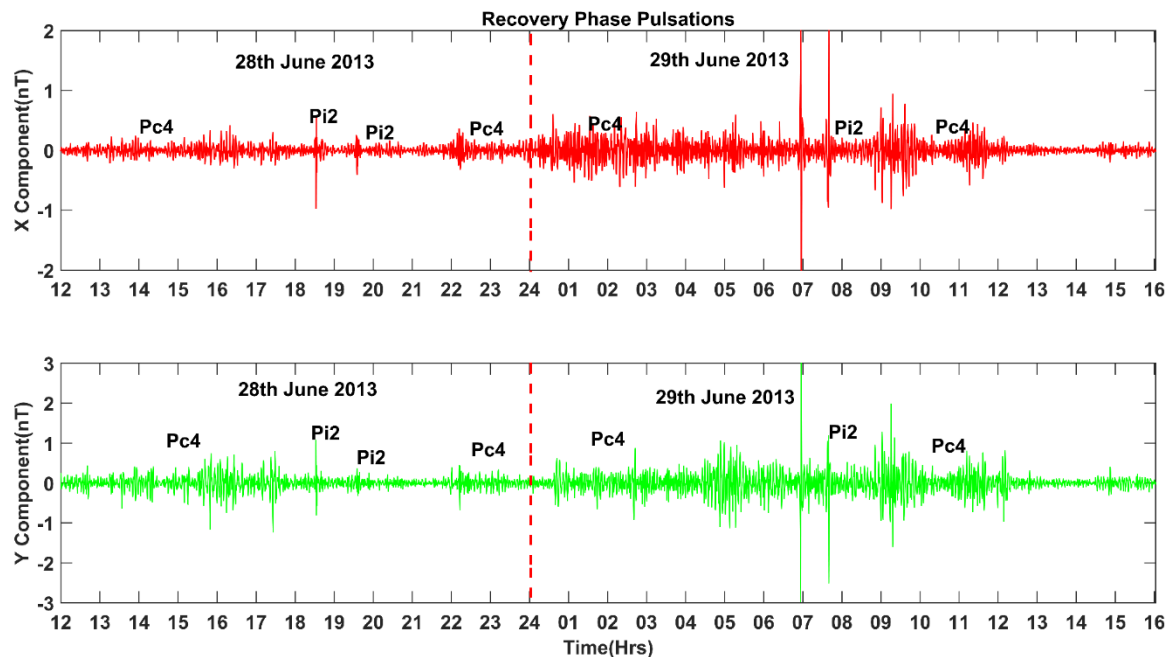


Fig. 4.19: Recovery Phase Pulsations identified using Induction Coil Magnetometer

Table 4.2: Details magnetic pulsations during Recovery phase of storm

| Date | Recovery Phase Pulsations | | | | | | | | | |
|--------------|---------------------------|-------|------|-----------|------|------------------|-------|------|-----------|------|
| | X Component (nT) | | | | | Y Component (nT) | | | | |
| | Start | End | Amp | Frequency | Type | Start | End | Amp | Frequency | Type |
| 28 June 2019 | 12.13 | 17.85 | 0.72 | 10.25 | Pc4 | 12.1 | 17.93 | 1.39 | 10.25 | Pc4 |
| | 18.4 | 18.63 | 1.43 | 16.6 | Pi2 | 18.4 | 18.61 | 1.89 | 18.07 | Pi2 |
| | 19.5 | 19.67 | 0.65 | 18.07 | Pi2 | 19.54 | 19.62 | 1.02 | 19.14 | Pi2 |
| | 21.6 | 24 | 0.65 | 12.21 | Pc4 | 21.51 | 24 | 1.09 | 12.21 | Pc4 |
| 29 June 2019 | 0 | 6.48 | 0.92 | 9.27 | Pc4 | 0 | 6.68 | 2.01 | 7.32 | Pc4 |
| | 7.62 | 7.7 | 2.95 | 9.76 | Pi2 | 7.25 | 7.76 | 3.7 | 9.76 | Pi2 |
| | 8.75 | 12.29 | 1.53 | 8.79 | Pc4 | 8.5 | 12.31 | 2.15 | 9.28 | Pc4 |

4.6 Pi2 Pulsations during Quiet and Disturbed Geomagnetic Conditions: Low latitude Observations

(Prasanna Simha and K.M.Rao)

Irregular ultra-low frequency oscillations take the form of separate transient wave packets, which belong to the Pi2 geomagnetic pulses (Saito, 1969; Pudovkin et al., 1976). The pattern of Pi2 has been observed in wave trains damped over a period of 40 to 150 seconds and their duration from 5 to 20 minutes. The characteristic of the Pi2 pulses can be observed both in the form of isolated bursts and in the form of sequences of bursts made up of several packets of waves. The onset of each partial magnetospheric storm is accompanied by Pi2 pulsations (Saito, 1969). We analyzed the bursts of magnetic pulsations observed with the high precision induction coil magnetometer (LEMI 30) deployed at the MPGO of Desalpar, Kutch, Gujarat during the period 2013 to 2017.

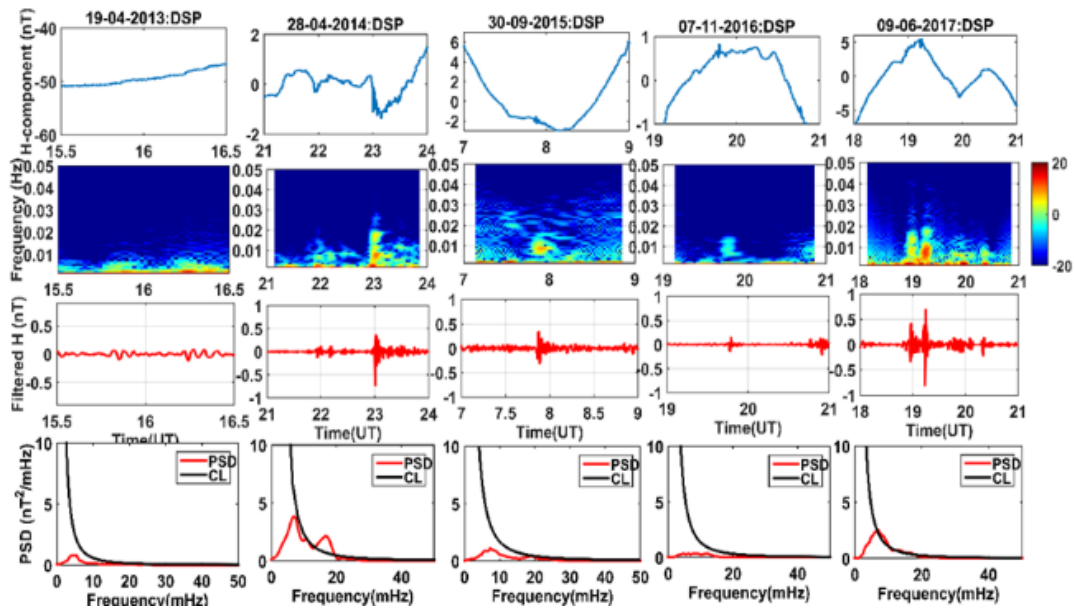


Fig. 4.20: Case study of Pi2 burst during 2013-2017 Quiet period in H-component (IMF is between 0-5nT, Solar wind speed less than 300km/sec, Kp is around 0).

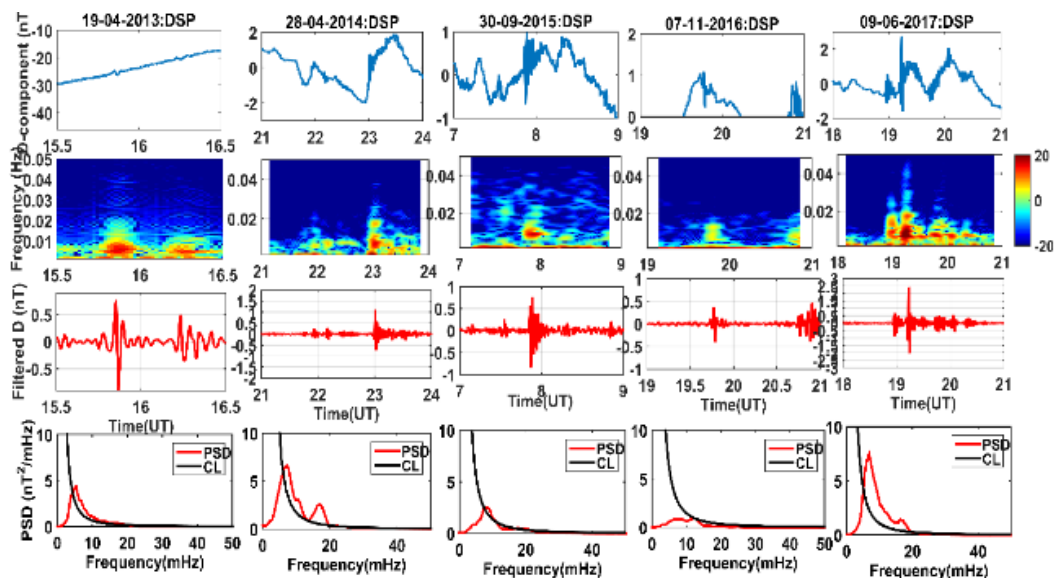


Fig. 4.21: Case study of Pi2 burst during 2013-2017 Quiet period in Z-component (IMF is between 0-5nT, Solar wind speed is less than 300km/sec, Kp is around 0).

Figures 4.20 and 4.21 show the morphological identification of the burst Pi2 in the H and Z components of the Desalpar magnetic data. Careful observation of the raw geomagnetic signal every six hours is very important in order to characterize the raw data as noise, data jump or geomagnetic pulsation. The spectral parameters of the raw data were obtained from their spectrogram, which provides information on the time, frequency and intensity of the PSD during the period of the event. The lower and upper cut-off frequencies of the spectrogram were applied in the butter worth filter in order to obtain the filtered signal. Parameters such as the duration of the event (time), the peak-to-peak amplitude, the frequency up to which the signal persists are recorded in the database.

We also analyzed their source parameters according to global parameters such as IMF B, solar wind density, solar wind speed, proton density, the number of Kp and sunspots for the present study period. The study period 2013-2017 includes the ascending and

descending phases of the solar cycle (the ascending phase 2013-2016 and the descending period 2017). Figure 4.22 shows various global parameters such as SSN, Kp and interplanetary electric field (IEy) of OMNI websites. The red dotted line shows the global parameters and the blue dotted line shows the number of Pi2 observed during this period. There is a clear anti-correlation between the number of sunspots and the presence of Pi2. Previous studies also report this inverse relationship for the occurrence of Pi2 and the solar cycles during solar cycles 20 and 21 (Rao and Sarma, 2003 and Saito, 1969). Previous studies have also shown that the periods during solar minimum year are much larger than those during solar maximum years (Troitskaya, 1967; Kwon et al., 2013).

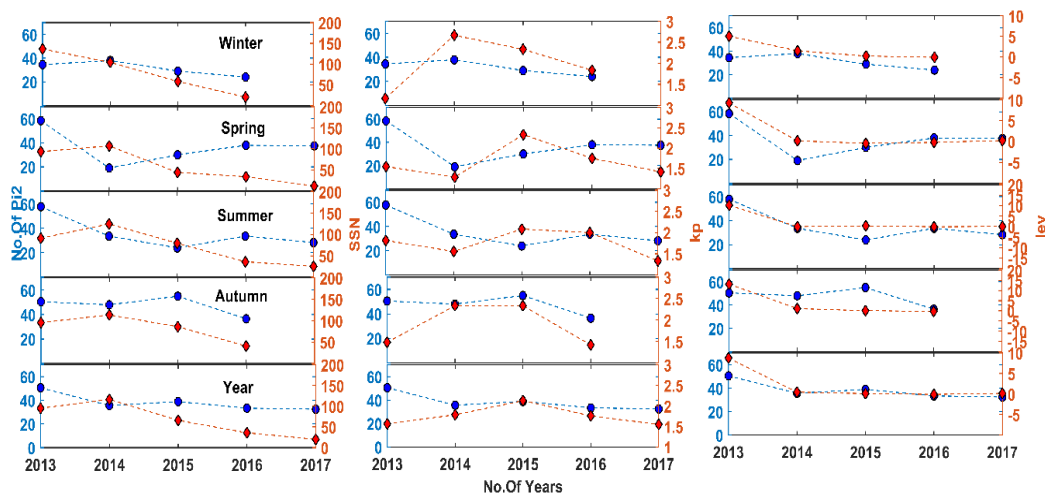


Fig. 4.22: The temporal variations of number of Pi2s observed annually and in various seasons with respect to SSN, Kp, and IEy.

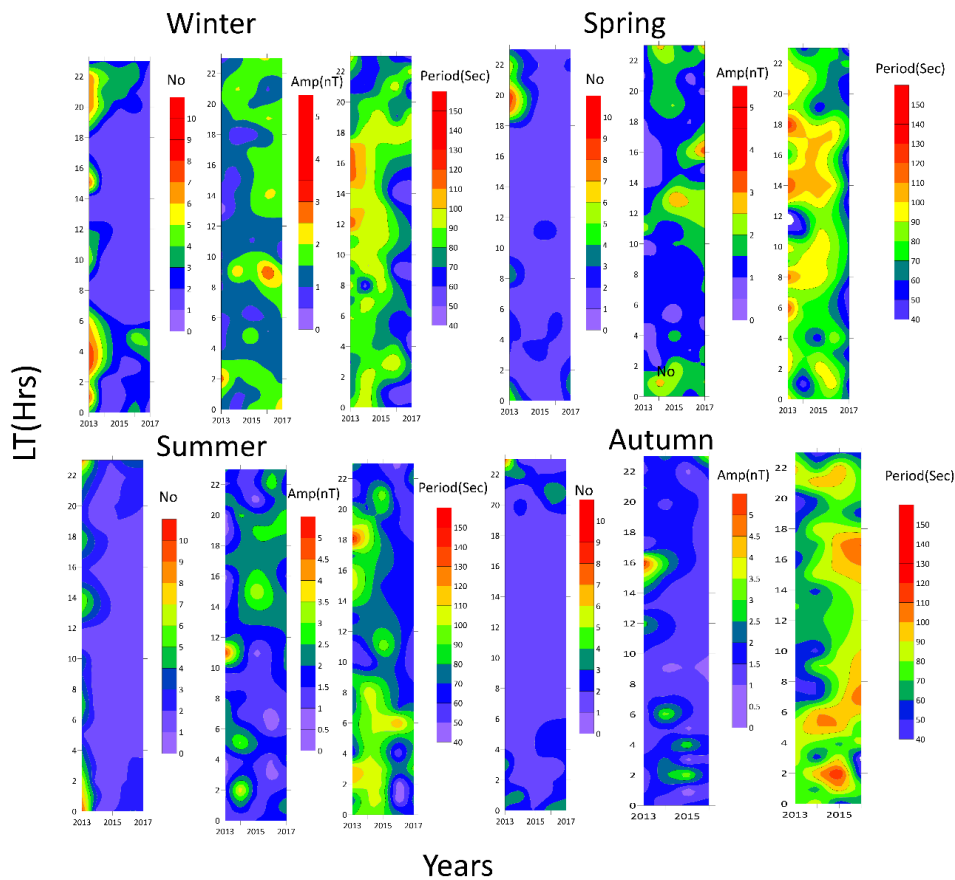


Fig. 4.23: Contour plots of Local Time variations for the period 2013-2017 along with the number, amplitude, and period.

This observed inverse relationship can be explained on the basis of Alfvén's resonance theory, which is generated due to the change in ionospheric conductivity and the intensity of solar wind waves. It is the combined effect of the interplanetary magnetic field and the speed of the solar wind that influences this resonance. In Dungey's open magnetosphere model, this resonance theory is explained on the basis of the electric field of the solar wind, which is a combined effect of the interplanetary magnetic field and the speed of the solar wind. We analyzed the annual average of the interplanetary electric field (IEF) using the magnetic field and speed of the solar wind in the interplanetary medium during the period 2013-2017. During the spring and summer seasons, we clearly found an anti-correlation compared to winter and autumn seasons. Annual fluctuations have also shown anti-correlations.

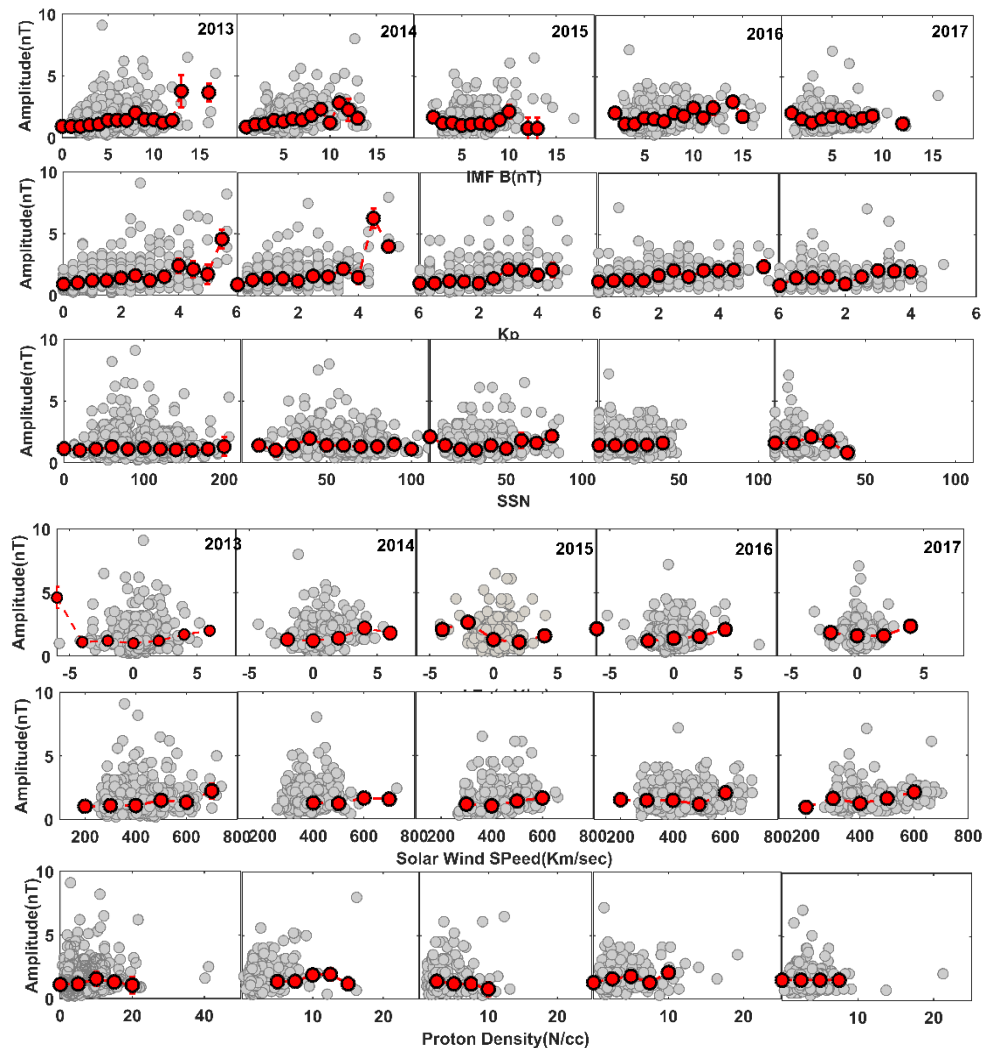


Fig. 4.24: Amplitudes versus Global parameters.

Figure 4.23 shows the contour plots of local temporal variations over the years (2013-2017) as well as the number of Pi2, the amplitude and the period. This figure clearly shows that Pi2 mostly occurs early in the morning and at midnight. In addition, a maximum occurrence of Pi2 was found in 2013 and a minimum occurrence in 2017, which corresponds to a lower solar activity. The increased amplitudes were also observed in the morning and at midnight, but high amplitude was observed during 12 LT, which is due to the maximum of the sun intensity during this time. The maximum duration is determined during the 14-18LT in spring compared to other seasons. Local time and annual contour analysis show that a maximum period was found in the spring and that the maximum amplitudes and occurrences of Pi2 were found during the winter season. The Pi2 amplitudes, periods and events are directly linked to the maximum solar activity.

The intensity of the storm has a strong influence on the solar wind parameters such as the B_z component (Arnoldy, 1971), the B_y component (Hakamada et al., 1980) of the interplanetary magnetic field (IMF); Solar wind speed (V) (Snyder et al., 1963; Murayama and Hakamada, 1975) and interplanetary electric field (Sobolev, 1994). The intensification of the sub-storm increases approximately linearly with the decrease of the B_z component of the interplanetary magnetic field (IMF) for the range of $B_z < 4$ nT (southern component of the interplanetary magnetic field). They have also shown that the frequency of occurrence increases with increasing solar wind speed (V) (Takao, 1996). Figure 4.24 shows the amplitudes in relation to the global parameters. The gray dots are the amplitudes and the global parameters, and the red connecting lines are the median according to the index. Amplitudes increase with IMF B , and maximum amplitudes were found for 5-10 nT, K_p of 2-4, SSN of 100-150.

4.7 Spatio-temporal variation of Total electron content prior to Jamaica earthquake ($M=7.7$) on 28 Jan 2020

(Prasanna Simha and K.M.Rao)

The temporal and spatial distribution of the TEC was examined using the GAIM modelled TEC and ground based TEC of ground based dual frequency GPS receivers of IGS network to search for anomalies before the magnitude 7.7 earthquake in Jamaica on January 28, 2020 at 19 UTC. The GPS stations RDSD, CRO1 and ABMF of the IGS network are located within the radius of the earthquake preparation zone. The stations along with the epicentre of this earthquake are shown in Fig. 4.25 and locations of GPS stations are listed in Table 4.3.



Fig. 4.25: Study area of Earthquake (IGS GPS sites denoted by blue colour). The event is denoted by red star

The eastern part of the Cayman basin is part of the Gonave microtiter plate, which is located between the North American plate and the Caribbean plate. It is bounded in both north and south by large faults, which together take into account the relative displacement of the two main plates. In the north, the border is the western part of the north-oriented fault zone, which absorbs 6 to 11 mm of plate boundary movement per year, while in the south, the border between the Walton fault zone at the western Jamaica and the Enriquillo-Plantain Garden fault zone to the east with about 8 mm per year. This earthquake has a magnitude of 7.7 Mw and an estimated focal depth of 14.8 km. The focal mechanism, combined with analysis of seismic waveforms, is consistent with strike-slip motion on the Septentrional-Oriente fault zone. The main shock was followed by a series of aftershocks,

with the largest being a Mw 6.1 event that occurred less than three hours later, to the southeast of Grand Cayman. The modelled rupture zone extends from just west of the epicentre of the M 6.1 aftershock to just east of the main shock epicentre, suggesting unilateral westward propagation.

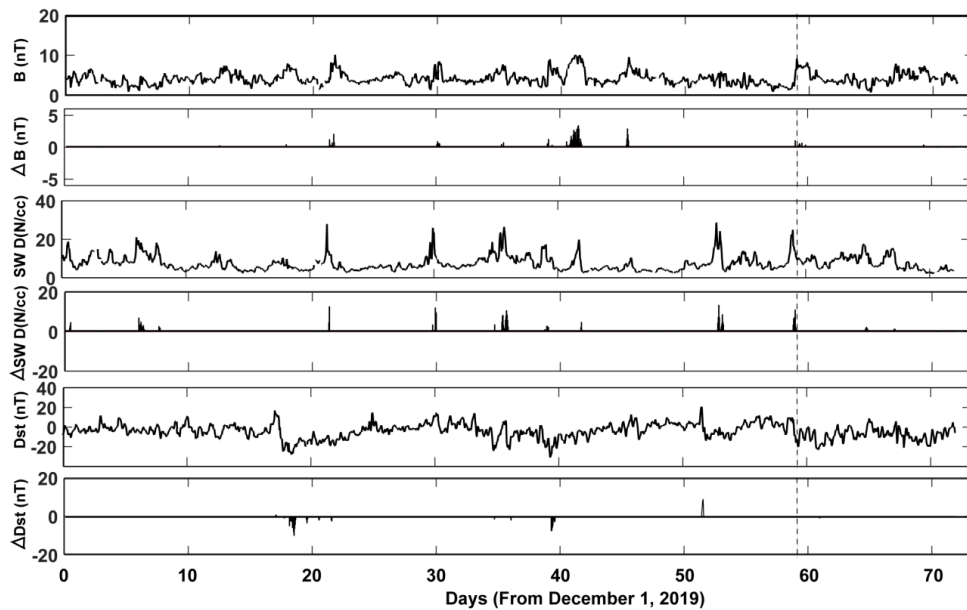


Fig. 4.26: Global Geomagnetic parameters such as IMF B, Solar wind Density (N/cc) and Disturbance of storm time Index (Dst).

Table 4.3: Details of GPS stations of IGS network

| S.No | IGS Site | Lat | Lon | Epi Dist (km) |
|------|----------|--------|---------|---------------|
| 1 | RSDS | 18.416 | -69.913 | 670 |
| 2 | CRO1 | 17.756 | -64.584 | 1260 |
| 3 | ABMF | 16.262 | -61.52 | 1620 |

To understand the global geomagnetic conditions during this period, we analyzed global geomagnetic parameters such as the interplanetary magnetic field (B), the density of the solar wind (N/cc) and the disturbance index (Dst) during the period 1 Dec-10 Feb 2019. The global parameters were determined using the sliding interquartile range method. These abnormal indices were mentioned as the delta of the respective parameters. Figure 4.26 shows the time series of these parameters as well as the delta of the respective parameters. The activity of the geomagnetic storm was recorded on 19, 39 and 51 days before the earthquake.

The raw VTEC data with Dst are presented in Figure 4.27. The propagation of pressure waves with the speed of infrasound in the atmosphere is induced by the vertical displacements of the ground by atmospheric explosions and shallow earthquakes. At ionospheric heights, low frequency sound waves are coupled to ionospheric gravitational waves and induce variations in the ionospheric electronic density (Calais and Minster, 1995). They observe an abnormal signal which begins a few minutes after the earthquake, with delays which increase with the distance from the epicentre. Abnormal Ionospheric TEC signals were observed days and hours before major earthquakes in the earthquake preparation area (Oikonomou et al., 2016; Pundhir et al., 2017; Ulukavak and Yalcinkaya, 2017). Earthquakes with strike slip and thrust fault mechanisms with magnitude 6-7 are perceptible to seismo-ionospheric disturbances. The ionospheric anomalies have been observed 5 days prior to several global earthquakes for positive and negative anomalies during the period 1998-2014 (Shah and Jin, 2015).

To identify anomalous signals of the TEC variation, a quartile-based statistical analysis is performed which is similar to that used by Liu et al. (2010). We compute the median M of every successive 15-day values and find the deviation between the observed one on the 16th day and the computed median M . To provide the information about the deviation, we also calculate the first (or lower) and the third (or upper) quartiles, denoted by LQ and UQ , respectively. Under the assumption of a normal distribution with mean μ and standard deviation r for the VTEC, the expected value of M and LQ or UQ is μ and $1.34r$, respectively (Klotz and Johnson, 1983). According to this criterion, we set the lower bound, $LB = M - 1.5IQR$ and upper bound, $UB = M + 1.5IQR$ (Neter et al., 1988). Figure 4.28 shows the raw VTEC data (red) along with the upper bound (blue) and lower bound (green) from three IGS GPS Stations.

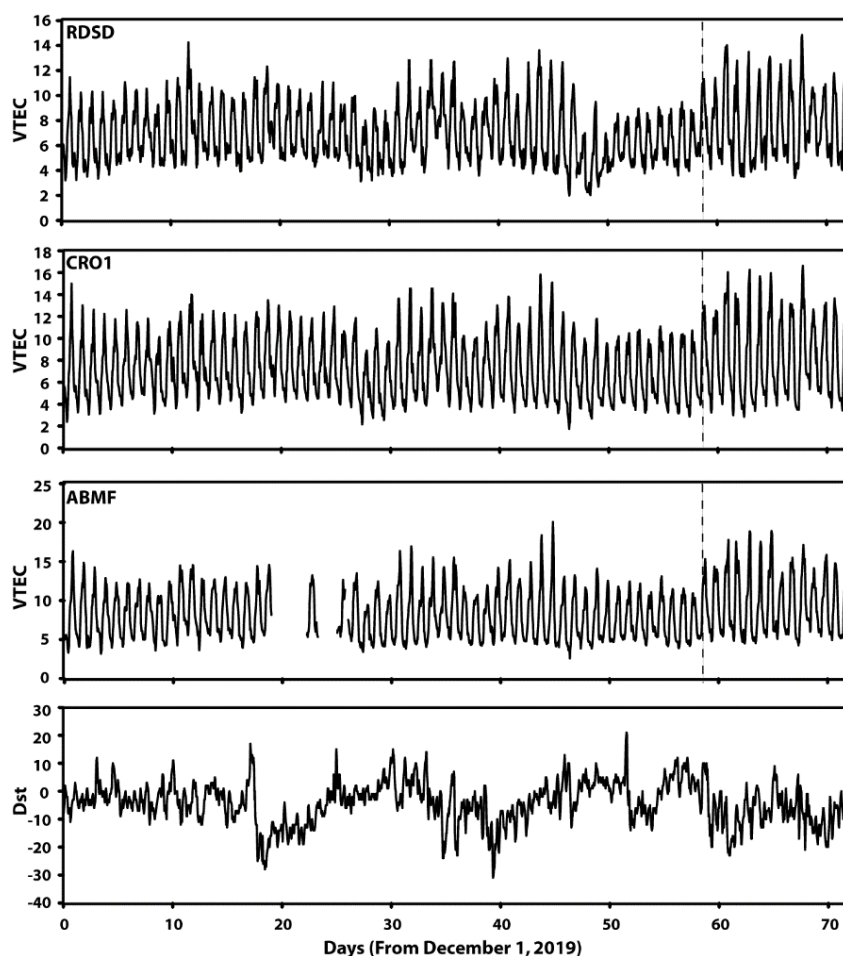


Fig. 4.27: Raw VTEC data from three IGS GPS stations along with the Disturbance of storm time Index (Dst).

The abnormal signals were observed on the 11th, 40th to 44th and 60th to 67th days. The dotted line shows the day of the earthquake in Jamaica on January 28, 2020. The ionosphere is so conducive and has good influence on external and internal effects. The anomalies of the present earthquake are also a mixture of both, after thorough inspection of global parameters and the signal of VTEC. The anomalous signals on 11th, 41-42th day are of seismo-genic origin, other signals are triggered by sun-earth interactions. The signals are strongly noticed on 11th and 41-42th day in the nearest station as compared to the far station. RDSB has shown a good anomaly compared to the far stations. The spatial DTEC have been compiled over the earthquake preparation zone for the present event in combination with the temporal TEC from 10 to 21 UT on 28 January 2020. In order to map the most severe TEC, the spatial TECs are plotted over the epicentre.

The difference values are minimal before the event time and they suddenly get enhanced a few hours before the earthquake and persist after the earthquake. The spatial maps

have been obtained by taking the Spatial TEC data from the GAIM TEC and data have been interpolated using the natural nearest neighbourhood method. The spatial DTEC over the epicentre of the present earthquake have shown an abnormal electron density 3 hours prior to the event. These electron clouds persist over the EQ breed zone from UT = 16:00–21:00 h, compared to the quiet geomagnetic day (20 Jan 2020) (Fig. 4.29). Ryu et al. (2014) also reported ionospheric anomalies in TEC during UT = 04:00 before the main shock of the Wenchuan EQ.

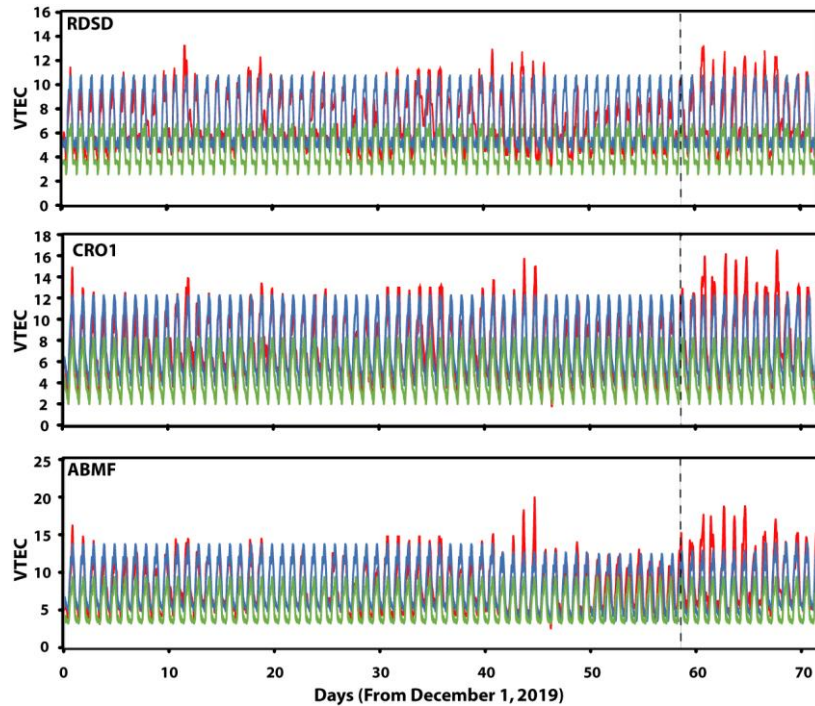


Fig. 4.28: Raw Data of VTEC (red) along with the upper bound (blue) and lower bound (green) from three IGS GPS Stations.

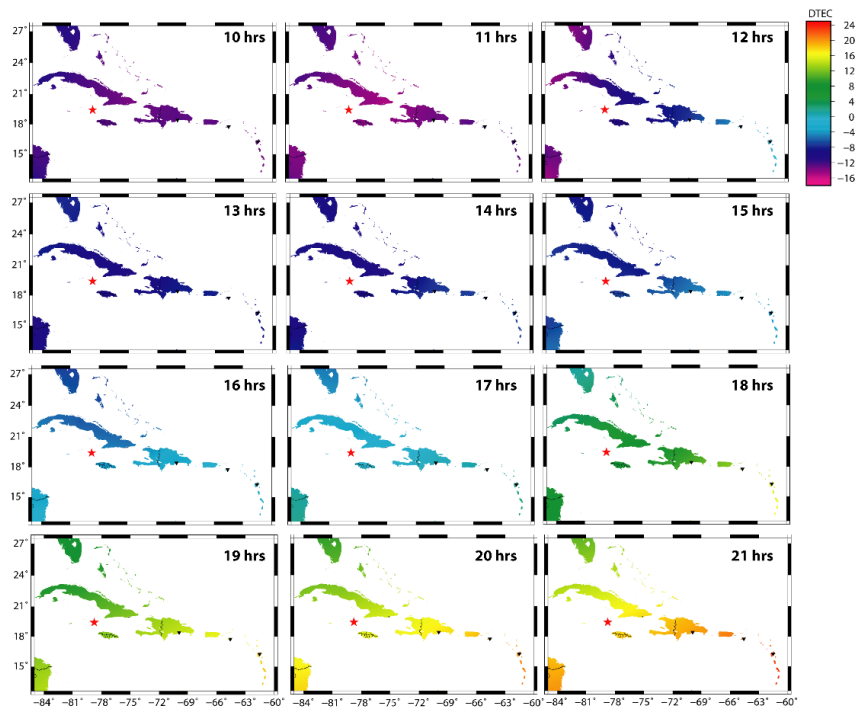


Fig. 4.29: The spatial DTEC map of seismo-ionospheric anomalies over the epicentre for different UT hours on 28 Jan 2020.

4.8 Deterministic Analysis of the soil radon along with all the other meteorological parameters

(Sushanta Kumar Sahoo and K.M.Rao)

A deterministic analysis of the soil radon along with the other meteorological parameters has been carried out to understand the long range memory present in the corresponding datasets. The emission of soil radon is regarded as a non-linear and complex process due to its dependency on different chaotic variables like pressure, temperature, humidity etc. (Planinic et al., 2004; Barbosa et al., 2007; K ulahc ; Ően, 2014). To determine the long memory character, the rescaled range analysis (R/S) of soil radon and other parameters is conducted. In the R/S analysis, a parameter known as the Hurst exponent (H) or the index of dependence is derived. The value of H is confined between 0 and 1. Based on the range of its value, the Hurst exponent divides the input time series into three categories, i.e., anti-persistent ($0 < H < 0.5$), random ($H = 0.5$) and persistent ($0.5 < H < 1$) (Tatli, 2015; Gkarlaouni et al., 2017). In case of the random walk, the time series does not possess any long memory effect. In the anti-persistent category, the trend reversion is more probable than the trend continuation. For the persistent type, i.e., when the H value is confined between 0.5 and 1, the time series exhibits a long range correlation.

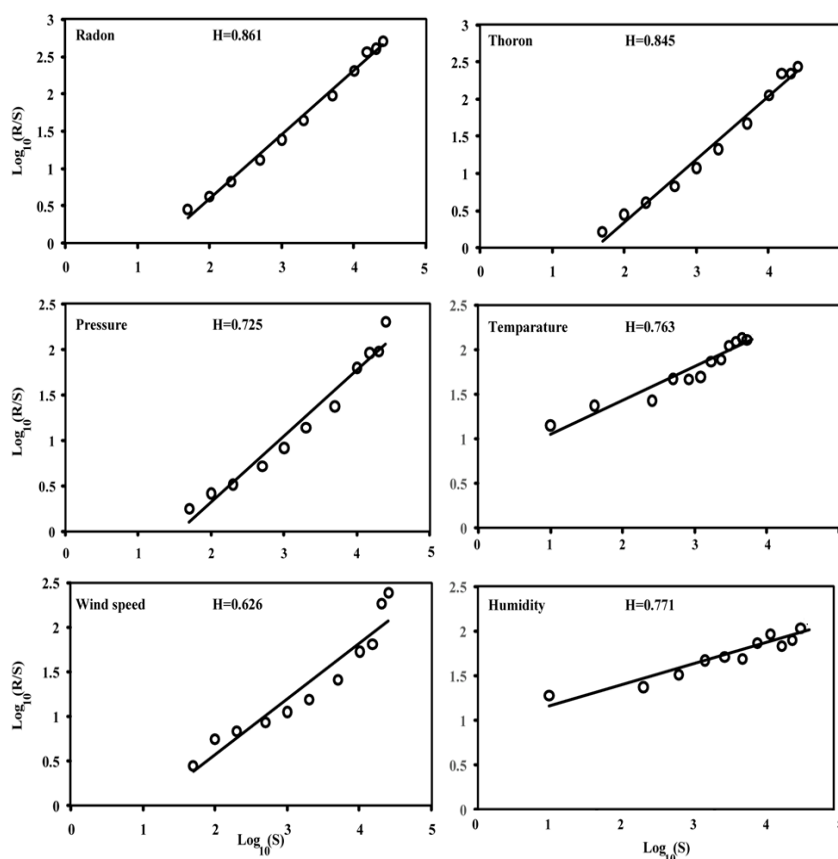


Fig. 4.30: Hurst exponent of radon and meteorological parameters

Table 4.4: Different paramaters and their Hurst exponent (H)

| Parameter | Hurst exponent(H) |
|-------------|-------------------|
| Radon | 0.861 |
| Pressure | 0.725 |
| Temperature | 0.763 |
| Humidity | 0.771 |
| Wind speed | 0.626 |
| Thoron | 0.845 |

The Hurst exponent of each and every parameter was computed. From the analysis, it has been observed that the H values in the present study vary from 0.5 to 1 for all the parameters (Fig. 4.30). Based upon the value of the Hurst exponent (H), it can be concluded that all the parameters have long memory characteristics.

4.9 Scaling characteristics of the Earth's magnetic field data of Desalpar in association with local earthquakes

(Sushant Kumar Sahoo and K.M.Rao)

In the present study, Detrended Fluctuation Analysis (DFA) has been applied on the horizontal (H) and vertical (Z) components of Earth's magnetic field, recorded at Desalpar observatory in the Kutch region. The raw data of the geomagnetic field for the period 1 January to 13 August 2012 has been selected for the analysis. The sampling period of the data acquisition has been maintained at 1s throughout the monitoring period. To avoid the influence of anthropogenic activities and solar variations, the raw data of both components (H and Z) during night hours (18:00 to 21:00 UT, 23:30 to 02:30 LT) have been examined and their scaling characteristics are analyzed depending upon the geomagnetic and local conditions. The real time distribution of the planetary index (K_p) was also plotted during the monitoring period. It was observed that the scaling exponent of the H component shows a good correlation with the K_p value and thereby explains its origin due to the geomagnetic activities in the ionosphere. Again, some local variations were also observed in the scaling exponent of the Z component during the study period and attempts are made to explain this unique feature with artificial and/or natural sources including the enhanced earthquake activity.

For a signal having long range correlation, the fluctuation function behaves as a power law of the time-scales and thus, its slope should be constant, denoted as α index (scaling exponent). The DFA approach has already been applied to magnetic field data at various places (Currenti *et al.* 2005, Telesca and Hattori 2007, Telesca *et al.* 2008, Varotsos *et al.* 2010). It has already indicated that the scaling exponents of the Z and H components of the Earth's magnetic field vary in a similar way. This means that their ratio is more or less constant if they are due to external impacts (as the solar wind-earth magnetosphere interaction mechanisms).

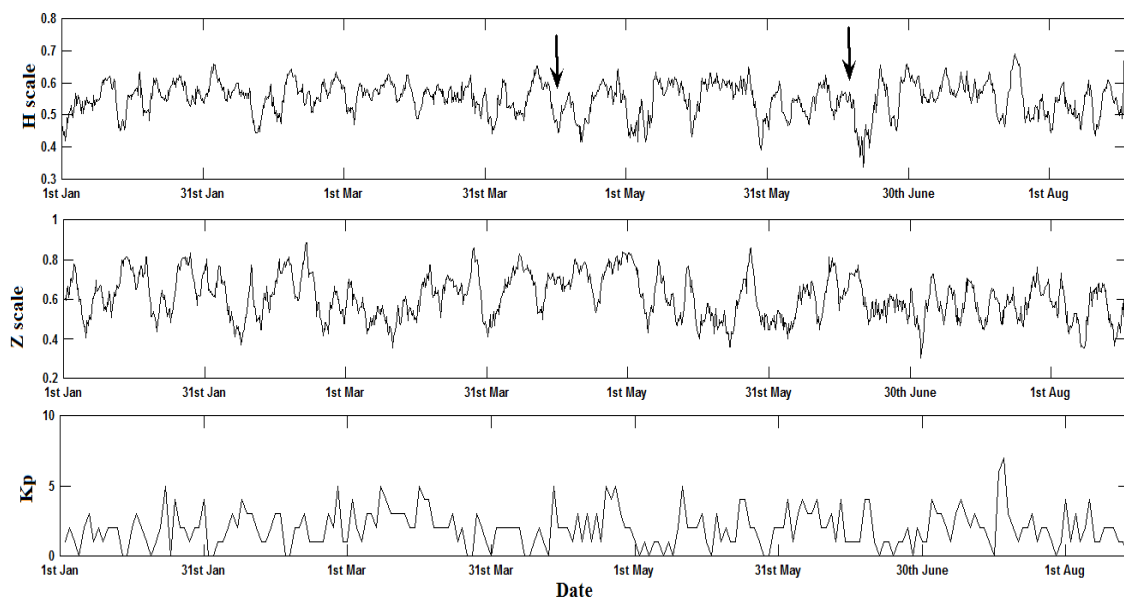


Fig. 4.31: Scaling exponents of H and Z components with the K_p value for the period 1 January-13 August 2012

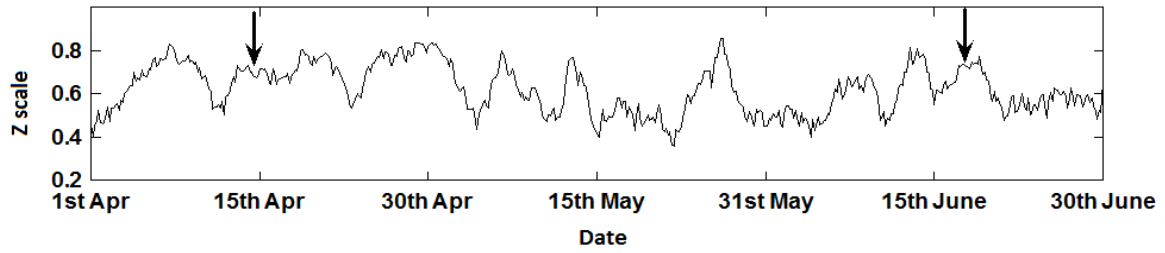


Fig. 4.32: Scaling exponents of the Z component for the period 1 April- 30 June 2012

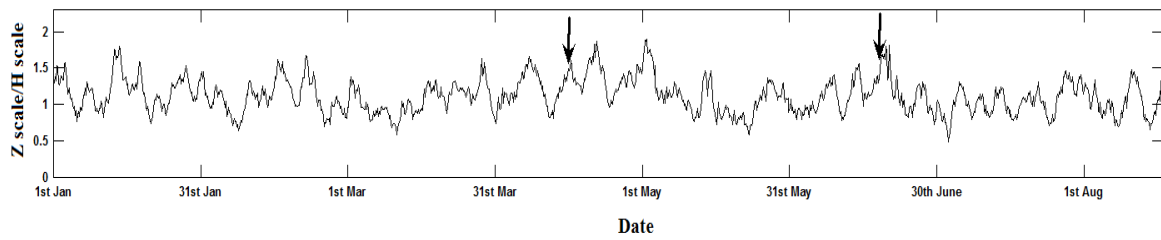


Fig. 4.33: Ratio of scaling exponents of Z and H components for the period 1 January- 13 August 2012

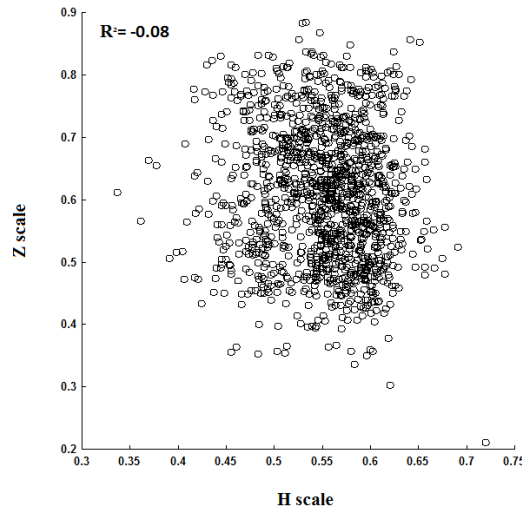


Fig. 4.34: Correlation between the scaling exponents of H and Z components

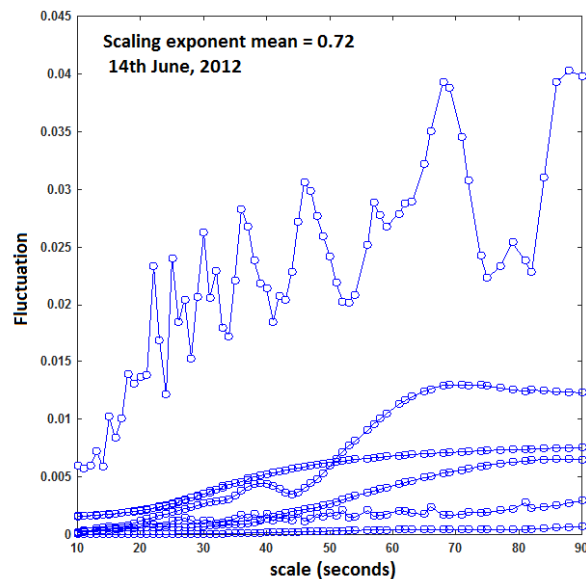


Fig. 4.35: Fluctuation functions (evaluated for ULF range, scales 10-90s, over 6 half-hour intervals in the time 00-03(UT) on 14th June 2012 (Z component) are depicted

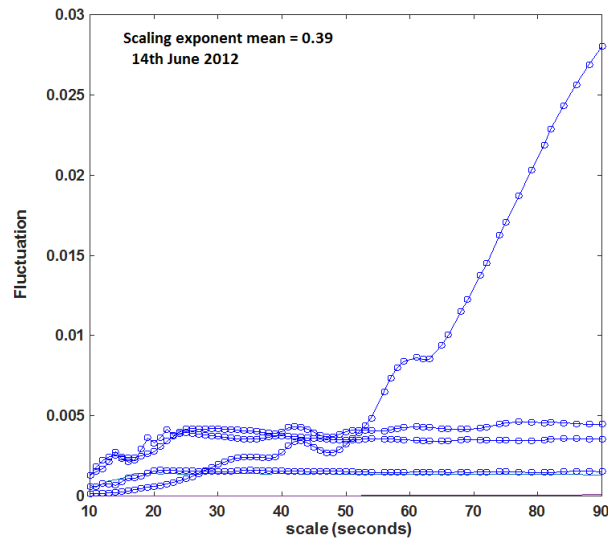


Fig. 4.36: Same as Fig. 4.35 but for the H component

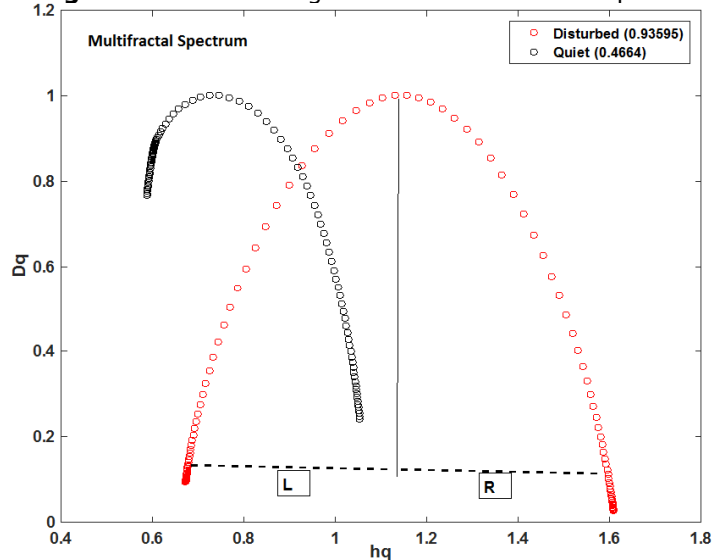


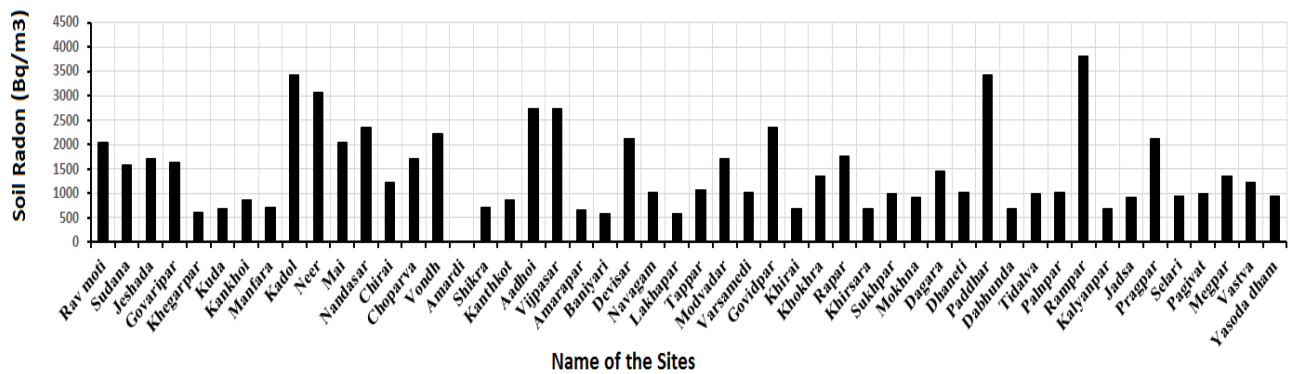
Fig. 4.37: Multifractal spectrum of the disturbed (14th June 2012) and quiet (11th June 2012) phases of the Z component

The scaling exponents of the H and Z components of Earth's magnetic field data at Desalpar have been determined and graphically presented with respect to time (Fig. 4.31). During the monitoring period, the K_p value of the night hour (18:00 to 21:00 UT, 23:30 to 02:30 LT) has been collected from the Kyoto observatory of Japan and presented (Fig. 4.31). From the figure, it has been observed that the scaling exponent of H shows a good correlation with the K_p value during the monitoring period. A good correlation between K_p and H indicates that the variation of H owes its origin to the far field effect due to the ionospheric activities. Again, to check the trend of similarity, a cross correlation is conducted between the scaling exponents of both H and Z components (Fig. 4.34) and it is found that there is negligible correlation ($R^2 = -0.08$). The lack of correlation between those two components (H and Z) encouraged us to investigate the source of the variation of the scaling exponent of the vertical component. During the monitoring period, two moderate earthquakes occurred nearer to the observatory and we have correlated the variation of the scaling exponent of the vertical component with reference to those earthquakes. It has been observed that the scaling exponent of the Z component is enhanced before one to two weeks of the occurrence of the earthquakes (Fig. 4.32).

Similarly, the ratio of scaling exponents of Z and H components for the period 1 January-13 August 2012 is depicted in Fig 4.33. This shows small enhancement in Z/H ratio before

Table 4.5: Soil radon concentration (in Bq/m³) recorded during the survey

| Station | Avg | Max | Min | Station | Avg | Max | Min |
|-----------|--------|------|-----|----------------|--------|------|-----|
| Aadhoi | 782.38 | 2736 | 342 | Megpar | 157.65 | 1368 | 342 |
| Amarapar | 120 | 660 | 330 | Modvadar | 114.85 | 1710 | 342 |
| Baniyari | 72.87 | 588 | 294 | Mokhna | 236.75 | 918 | 306 |
| Chirai | 215.5 | 1224 | 306 | Nandasar | 369.66 | 2352 | 294 |
| Choparva | 272.4 | 1710 | 342 | Navagam | 63.55 | 1026 | 342 |
| Dabhunda | 52.09 | 684 | 342 | Neer | 493.41 | 3078 | 342 |
| Dagara | 255.65 | 1470 | 294 | Paddhar | 928.4 | 3420 | 342 |
| Devisar | 344.51 | 2124 | 354 | Pagivat | 84.28 | 990 | 330 |
| Dhaneti | 127.52 | 1026 | 342 | Palnpar | 65.67 | 1026 | 342 |
| Govaripar | 294.46 | 1650 | 330 | Pragpar | 478.9 | 2124 | 354 |
| Govidpar | 786.7 | 2352 | 294 | Rampar | 1114 | 3822 | 294 |
| Jadsa | 102 | 918 | 306 | Rapar | 291.84 | 1764 | 294 |
| Jeshada | 378.54 | 1710 | 342 | Rav moti | 383.09 | 2058 | 294 |
| Kadol | 1142.5 | 3420 | 342 | Selari | 147.6 | 954 | 318 |
| Kalyanpar | 75.19 | 684 | 342 | Shikra | 98.6 | 708 | 354 |
| Kankhoi | 106.92 | 882 | 294 | Sudana | 359.2 | 1590 | 318 |
| Kanthkot | 93.06 | 882 | 294 | Sukhpar | 249.28 | 990 | 330 |
| Khegarpar | 81.285 | 612 | 306 | Tappar | 91.68 | 1062 | 354 |
| Khirai | 77 | 684 | 342 | Tidalva | 128.09 | 990 | 330 |
| Khirsara | 90.79 | 684 | 342 | Varsamedi | 86.1 | 1026 | 342 |
| Khokhra | 307.05 | 1368 | 342 | Vastva | 275.19 | 1224 | 306 |
| Kuda | 127.92 | 684 | 342 | Vijpasar | 441.75 | 2736 | 342 |
| Lakharpar | 78.82 | 588 | 294 | Vondh | 369.95 | 2226 | 318 |
| Mai | 357.97 | 2052 | 342 | Yasoda dham | 163.81 | 954 | 318 |
| Manfara | 56.31 | 708 | 354 | | | | |

**Fig. 4.39:** The maximum radon concentration of the sites

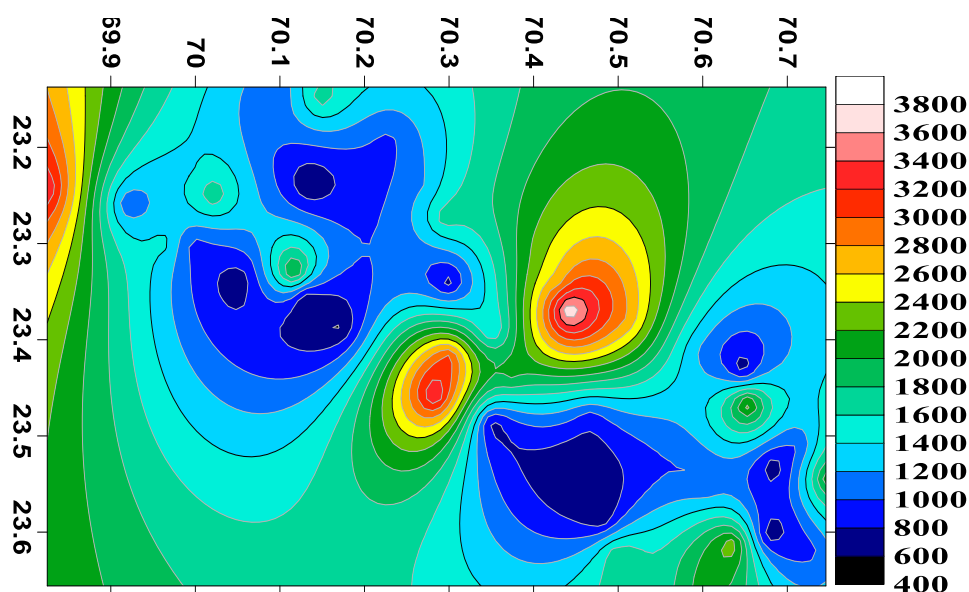


Fig. 4.40: Distribution of the maximum radon concentration

4.11 Installation of 10 Soil Radon monitors (Barasol BMC2) in Kachchh

(Sushant Kumar Sahoo and K.M.Rao)

We have conducted a soil radon survey along the seismic array stations in Kachchh region of Gujarat to decipher potential sites for permanent installation of new radon monitoring probes (Barasol BMC2). During the survey, we have collected soil radon data of 49 stations with an average duration of 20 hours at each station. The sampling interval of the data acquisition was kept 10 minutes at every station. The descriptive statistics of the soil gas radon obtained during the survey are analysed. We observe that the radon value varies between 0 and an average of 3800 Bq/m³ during the survey period. Stations like Rampar, Paddar, Kadol, Neer, Nandasar have recorded a high value of radon during the survey. This is due to the well condition of soil distribution and the location near active faults like KMF, South wagad fault. Along with the soil radon, pressure and temperature are also recorded simultaneously by the instrument (Barasol BMC2). Based on the survey conducted in the month of October, 10 stations in the Kutch region were selected for the permanent installation of Barasol BMC2. The locations of the selected stations are shown in Fig. 4.41. The installation was completed by last week of November.

Table 4.6 Descriptive Statistics of Soil Radon at all the stations

| Station | Average (Bq/m ³) | Standard Deviation(Bq/m ³) |
|-----------|------------------------------|--|
| Badargarh | 164.42 | 74.73 |
| Desalpar | 682.14 | 97.23 |
| Devisar | 114.28 | 95.34 |
| Kadol | 3374.89 | 425.24 |
| Modvadar | 1630.38 | 569.44 |
| Nandasar | 4453.12 | 1308.98 |
| Paddar | 2504.35 | 1122.38 |
| Pragpar | 1371.64 | 1208.95 |
| Rampar | 3501.35 | 1097.86 |
| Rapar | 7714.17 | 1544.94 |

During the installation, a 3 ft deep hole was dug in the soil at each site and the probe was inserted inside the hole and kept in a hanging position (Fig. 4.42). The bottom of the hole was covered with gravels to avoid contamination due to water.

The raw data of all the stations was collected during 16-24 Jan, 2020. The descriptive statistics of the radon data is given in the Table 4.6. The average radon level of 10 sites

is illustrated in Fig. 4.43. The raw data of other stations are presented in Fig. 4.44. From this figure, it is observed that the soil gas radon has reached a maximum of 7000 Bq/m³ at Rampar station. Again, it can be marked that the range of soil radon at each station increased compared to that obtained during the survey. It has also been observed that stations like Rapar, Rampar, Kadol etc. have recorded a high value of soil radon, i.e. more than 5000 Bq/m³.

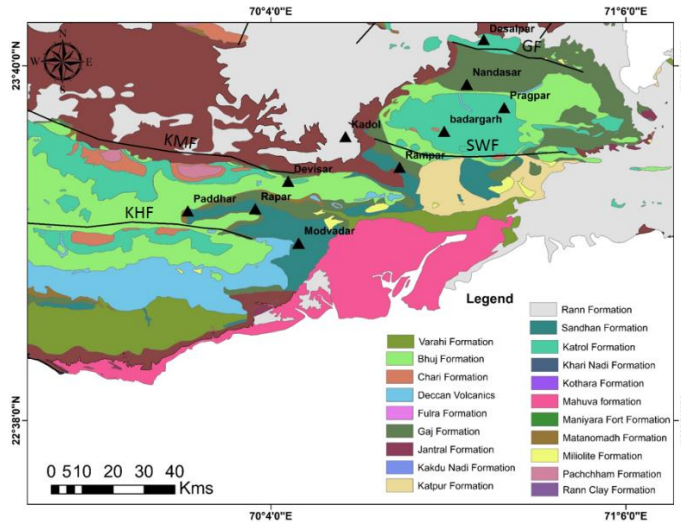


Fig. 4.41: Location map showing the Soil radon measuring stations

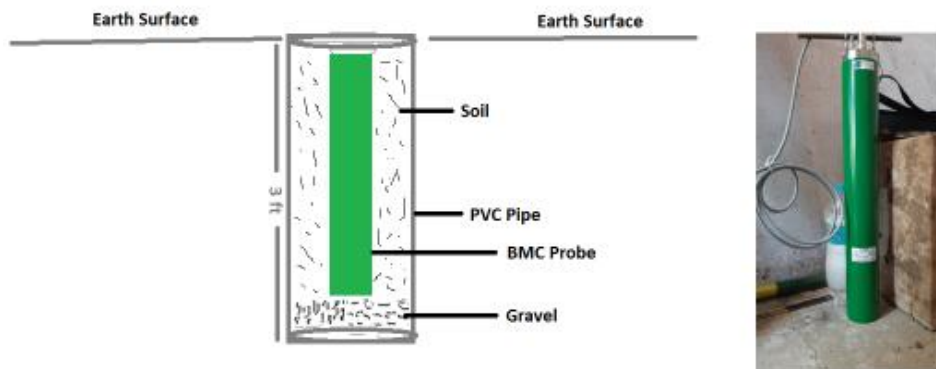


Fig. 4.42: Sketch of installation of BMC probe at the sites

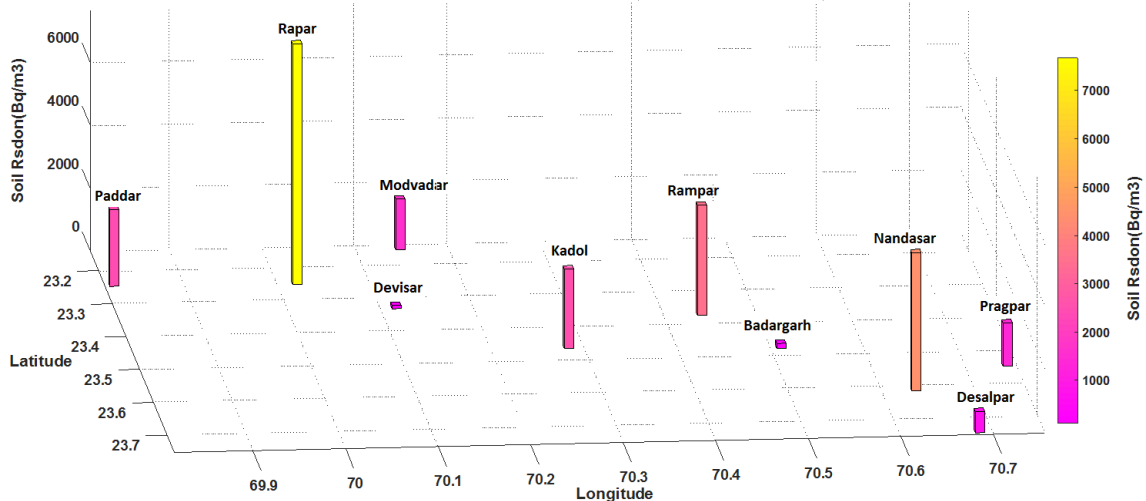


Fig. 4.43: Average soil radon at all the 10 stations

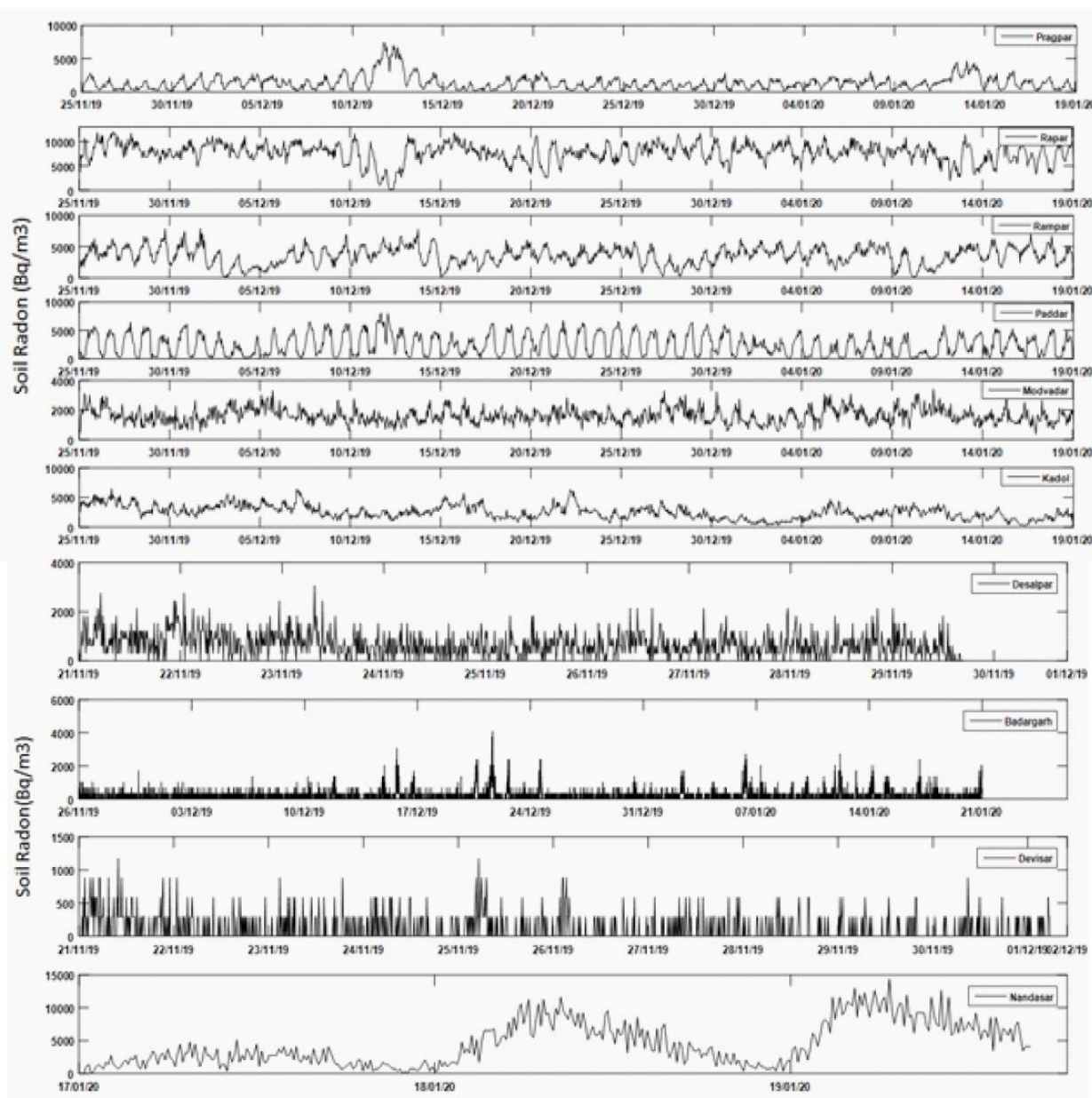


Fig. 4.44: Soil radon recorded at all the stations after installation

4.12 Observation of the ULF Electromagnetic emissions prior to the New Zealand Earthquake of M 7.8 on 13th November 2016

(Sushant Kumar Sahoo and K.M.Rao)

We analyzed the ground geomagnetic data obtained from the 3-component fluxgate magnetometer at from Eyrewell, New Zealand (43.40 °S, 172.40 °E) for the period October 1 to December 31, 2016, to study the electromagnetic precursors associated with the M 7.8 New Zealand earthquake that occurred on 13 November 2016. The locations of the epicenter of New Zealand earthquake and the Magnetic Observatory are shown in Figure 4.45. This station is maintained by the Institute of Geological and Nuclear Sciences and is part of intermagnet network. Intermagnet network is promoting high standards of magnetic observatory practice and providing the magnetic data for research purposes (www.intermagnet.org). This earthquake occurred 54 km northeast of Amberely in New Zealand, 158 km from Eyrewell monitoring station.

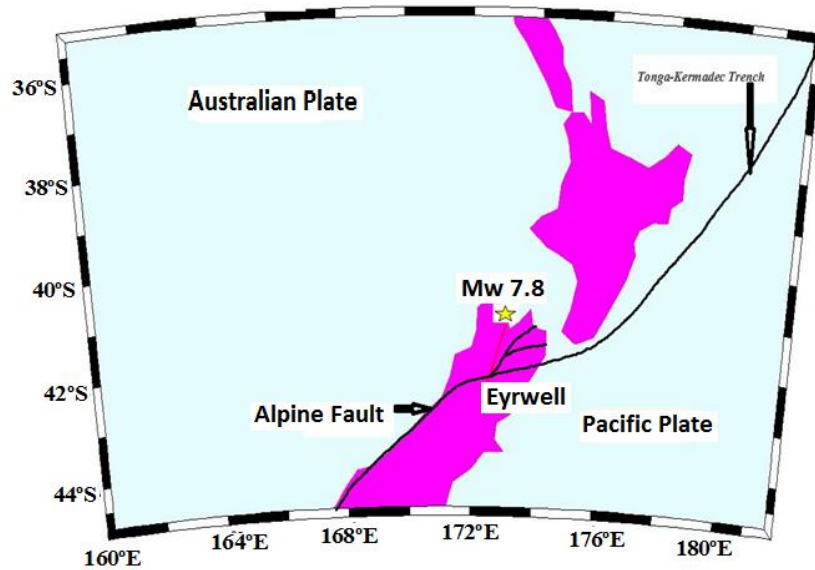


Fig. 4.45: Location of the epicenter of New Zealand earthquake and the Magnetic Observatory

To reduce the influence of anthropogenic and cultural disturbance, we have selected the magnetic data during the mid-night (23:00-02:00 LT) for analysis. The global parameters i.e. Kp and Dst index are obtained from world data center, Kyoto, Japan (<http://wdc.kugi.kyoto-u.ac.jp>). The Kp values and Magnetic data of X, Y, Z comp recorded at Eyrewell station are shown in Figure 4.46. The polarization ratios are generally lower for the far field than for the near. The polarization ratio (Z/G) is less than 1 for the far field effect, however, it is almost equal to 1 or more for the near field effect that is based on the electromagnetic emissions from the lithosphere due to microcracks or to the electrokinetic effect associated with the occurrence of earthquakes (Hayakawa et al., 2007).

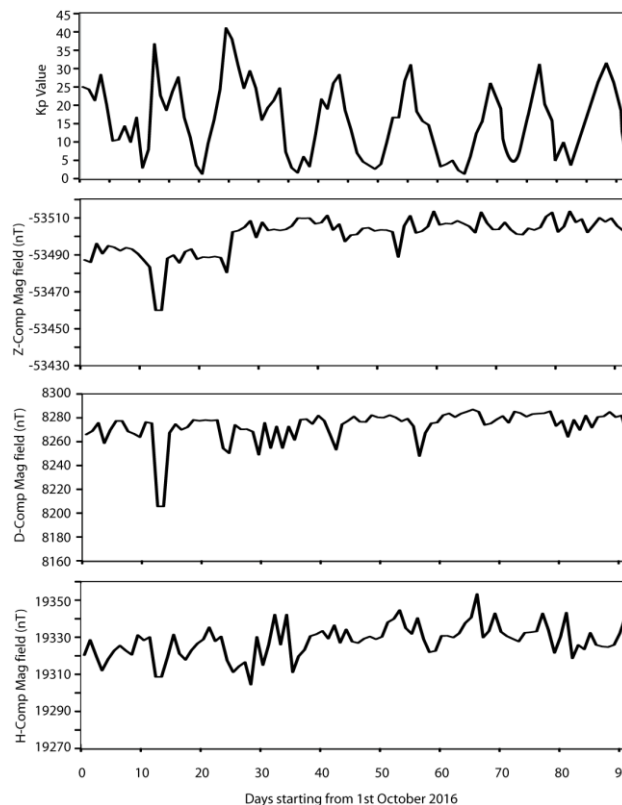


Fig. 4.46: Kp values and Magnetic data of X, Y, Z comp recorded at Eyrewell station

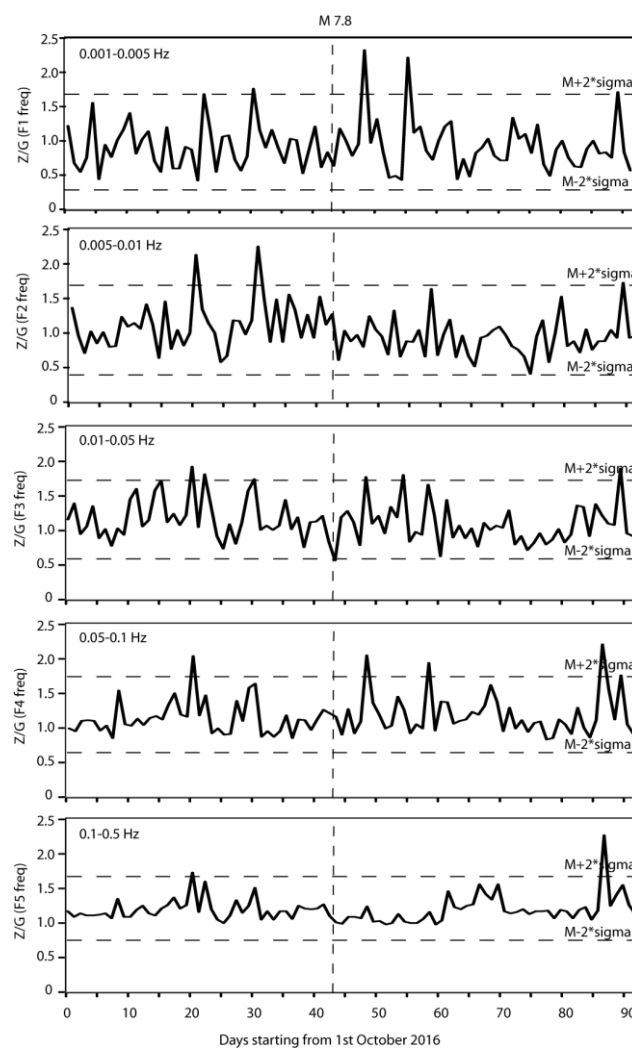


Fig. 4.47: Plot of the Polarization ratio (Z/G)

We can relate the enhancements on October 20, October 30, 2016 with the electromagnetic emissions inside the earth due to the micro-fracturing occurred during the preparation phase of the New Zealand earthquake. We measure the fractal dimension of three orthogonal components of the variations of the geomagnetic field, which makes it possible to obtain three sequences of the temporal variations of the fractal dimensions corresponding to the components X (NS), Y (EW) and Z (vertical). Figure 4.49 shows the time evolution of the fractal dimensions of the geomagnetic components (H, D and Z) and the Dst value. The fractal dimension of D and Z components of magnetic data has decreased initially and increased sharply 3 days before the New Zealand earthquake.

The electromagnetic signal in the ULF range was selected for polarization analysis (Hayakawa et al., 2007). This study dealt with calculation of Z/G in the ULF range (0.001-0.5 Hz) in five frequency bands, i.e. f1 (0.001-0.005 Hz), f2 (0.005-0.01 Hz), f3 (0.01-0.05 Hz), f4 (0.05-0.1 Hz) and f5 (0.1-0.5 Hz) for three months during October 1 to December 31, 2016. Figure 4.47 illustrates the polarization ratios of five frequency bands during study period. In this figure, the temporal evolution of the polarization ratio (Z/G) of the geomagnetic field of the midnight (23:00-02:00 LT) time recorded at the Eyrell monitoring station, has been plotted in five different frequency bands of ULF range, for 3 months. The time of New Zealand earthquake is shown as a dashed line. The time series of polarization ratio has shown enhanced polarization two times, i.e., on 20 Oct and 30 Oct 2016 before the occurrence of New Zealand earthquake and shows a value ~ 1 or more during these instances. Since the global geomagnetic indices Kp and Dst are normal in these cases, the enhanced polarization ratio may be related to the earthquake

preparation phase of the New Zealand earthquake. The most characteristic frequency of the Seismo ULF emissions observed is 0.005 to 0.1 Hz, similar to the results obtained by previous researchers for Spitak (Kopytenko et al., 1990); Loma Prieta (Fraser-Smith et al., 1990); Guam (Hayakawa et al., 1996); Biak (Hayakawa et al., 2000) earthquakes.

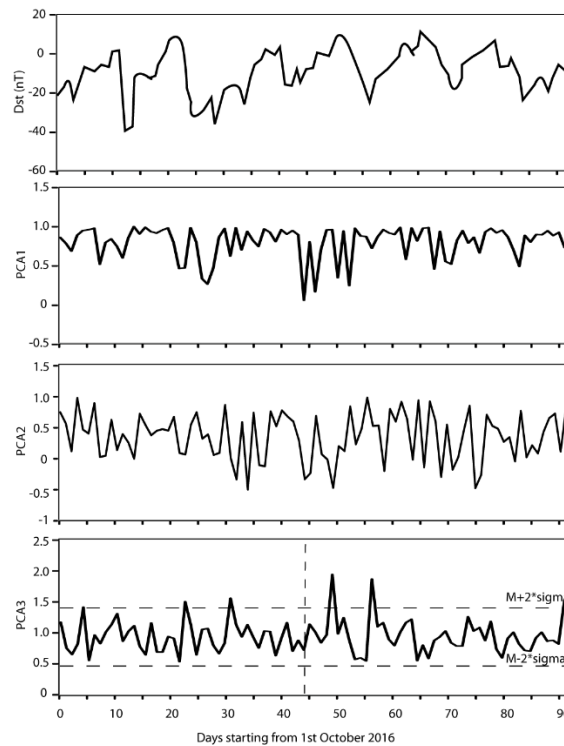


Fig. 4.48: Principal Components of H-component of Magnetic Field with the Dst

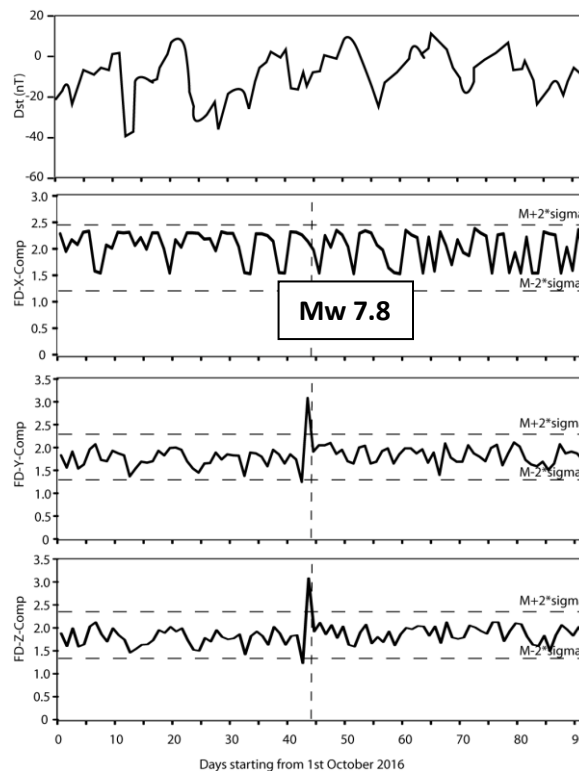


Fig. 4.49: Fractal dimension variability determined by Berry's method during 1 Oct- 31 Dec 2016.

To further classify them, we applied principal component analysis to the magnetic data of the H-component. The first three principal components showed more than 90% of the variance of the original ULF magnetic field time series. Figure 4.48 illustrates the three principal components with Dst values during 1 Oct- 31 Dec 2016. The variation of the eigenvalue of the first principal component is strongly correlated with the Dst value compared to the two other components. We may assume that the first principal component of the observed signal is due to the contribution of the global magnetic signal, which is obtained from terrestrial solar activity. The eigenvalue of the second main component was found to show a daily variation of 24 hours during the monitoring period with maximum in the day and minimum in the night. The temporal variation of the third principal component was analyzed to verify a possible correlation between ULF emissions and the occurrence of the earthquake. It has been observed that the Eigen-value of the third principal component is enhanced on October 20, October 30, November 20, November 28 and December 20, 2016. These enhancements in PCA are similar to enhancements of polarization ratios.

5 ACTIVE TECTONICS

5.1 Geodetic monitoring of Landslide movement at two sites in the Garhwal Himalaya

(R K Yadav, V K Gahalaut, P Gautam, R Jayangondaperumal, K M Sreejith, I Singh, A Kumar, V Jovivek, R Agrawal, J K Catherine, S P Sati)

We report anomalous motion at three continuous GPS (Global Positioning System) stations BHTW, RATH and GUPT situated in the Garhwal Himalaya (Fig. 5.1a). Sites RATH and GUPT are operating since 2012 and site BHTW is running since 2006. Two adjacent sites at Bhatwari (BHTW) and Raithal (RATH) villages lie in the landslide prone Main Central Thrust (MCT) zone in the Bhagirathi valley of Uttarkashi district (Fig. 5.1b) and another site at Guptkashi (GUPT) of Rudraprayag district lies in the Mandakini valley, ~50 km southeast of Uttarkashi region. The motion derived from GPS observations is more than the plate motion at these sites and it deviates significantly from the measured motion at nearby sites in the same tectonic environment. To investigate the processes responsible for this anomalous behaviour, the probable tectonic motion, calculated from the motion at nearby sites lying in a similar tectonic environment, has been subtracted from the observed motion at these sites. The estimated residual motion at site BHTW is ~12 mm/yr of eastward motion from 2006 to 2012 which increased to ~22 mm/yr in 2016 (Fig. 5.1c). The northward residual motion is ~1-3 mm/yr. There was an insignificant vertical residual motion before 2012 and further, subsidence of ~6 mm/yr has been observed. Site RATH, located 1.4 km away from BHTW, shows residual motion similar to that at site BHTW. However, the site RATH, located at the crown is moving at a slower rate than the site BHTW in the toe, since 2006. The relative motion between these two sites appears to be increasing with time and it is consistent with the ground deformation features observed in the region. The residual motion at site GUPT is ~15 mm/yr of north-eastward motion and an insignificant motion in the vertical component (Fig.5.1d).

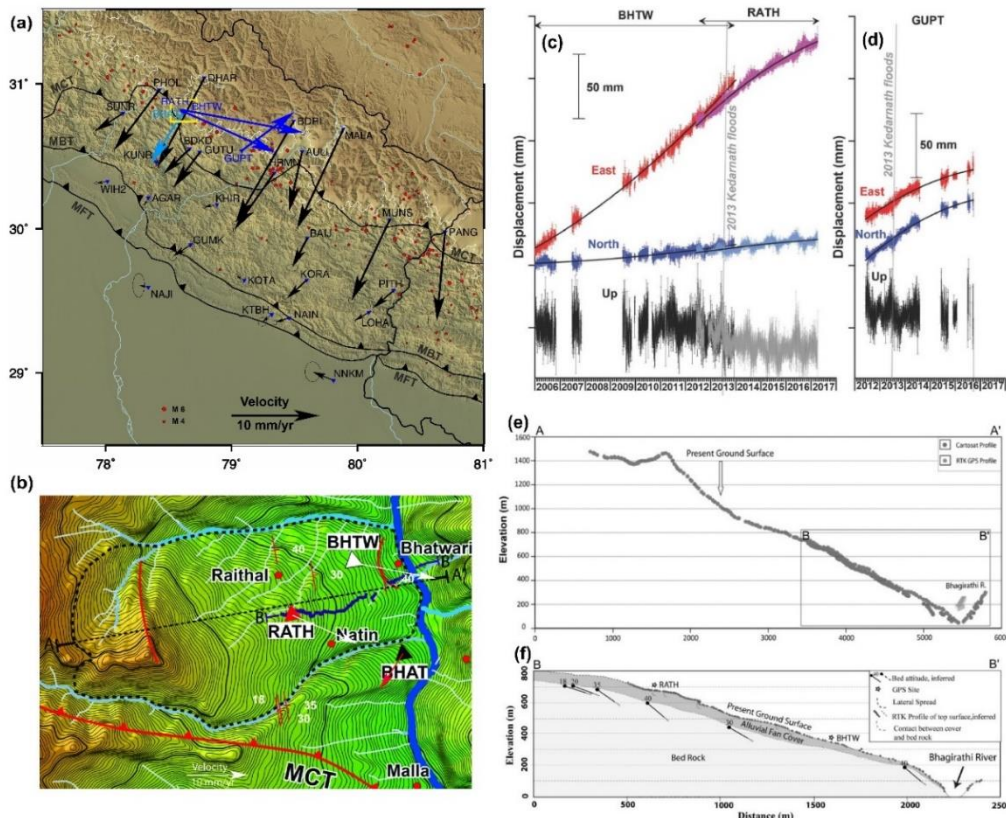


Fig. 5.1: (a) Site velocity (black vectors) in the Kumaun Garhwal Himalaya with respect to a fixed India plate. The sites RATH, BHTW and GUPT show distinct site motion (blue vectors) as compared

to the surrounding sites that lies in a similar tectonic environment. However, the motion at site BHAT close to BHTW and RATH is consistent with the tectonic motion. (b) Digital elevation model of the landslide region of Bhatwari. Blue colour traces the Bhagirathi River and its small streams. Note that site BHAT is located outside the landslide zone. (c) Temporal variation in the displacement components at GPS sites BHTW and RATH derived after removal of expected tectonic motion at sites with the help of motion at sites that lies in a similar tectonic setup (i.e. velocity at site BHAT). (d) Similar as described in (c) for site GUPT. (e) Topography along AA' (indicated as black dash line in Fig. 5.1b) generated from DEM of Cartosat Steropair. (f) Topography along BB' (indicated as irregular line in Fig.5.1b) estimated from RTK surveying. The two GPS sites with the dip of the bedrock are also shown.

The analysis of geodetic motion at BHTW and RATH is also complemented with InSAR (Interferometric Synthetic Aperture Radar) data. A high-resolution field survey using RTK (Real Time Kinematic) and detailed field investigations suggest that the bedrock dips eastward with spur slope of $\sim 19^\circ$ at sites RATH and BHTW (Fig.5.1e and f) and it dips north-eastward with spur slope of $\sim 14^\circ$ at site GUPT. This indicates that the residual motion at these sites is towards the dip of the bedrock. Also, towards the toe zone of Bhatwari village, the ground shows numerous arcuate fissures with subsidence that led to the destruction of several houses. Thus, a detailed analysis of abnormal motion at these sites indicates that the sites are situated on a slow-moving potential landslide zone. However, it is not obvious whether the measured movements in this region may lead to catastrophic landslides during an earthquake or monsoon (seasonal or extreme event) and thus detailed monitoring of the two identified regions is warranted to avoid potential secondary effects such as the damming of Bhagirathi and Mandakini River and subsequent floods.

5.2 Active Tectonics of Himalaya, Rift Basins in Central India and those Related to Crustal Deformation at Different Time Scales

(R Jayangondaperumal, R.L. Mishra, RS Priyanka, R.K. Yadav, DP Mohanty, A Pandey, I. Singh, A Anil, S Dash)

We summarize the research work based on geological (i.e. geomorphological, paleoseismological) and geodetic observations carried by the Indian authors from 2016-2019. Several geomorphological studies have been done in the Northwest and Northeast Himalaya to delineate and date the deformation signatures preserved in the tectonic units during past major seismic events (Joshi and Thakur, 2016; Devender Kumar et al., 2016; Mishra et al., 2016; Kothiyari et al., 2017; Sutar et al., 2017; Pandey et al., 2018). The major earthquake sequence from Hajipur to Ramnagar (Fig 5.2a) has been investigated through trenching of the exposed fault rupture and radiocarbon dating by Malik et al. (2017), Jayangondaperumal et al. (2017), and Rajendran et al. (2018). Their results provide three earthquake scenarios i.e. 1344 or 1400 AD earthquake, 1505 AD earthquake and 1803 AD earthquake from the ruptured segment of the HFT in Ramnagar. Rajendran et al., (2018) inferred a single medieval earthquake between 1266 to 1636 AD. Jayangondaperumal et al. (2017) mapped a fault scarp in the Mehandpur, i.e. the active backthrust in the northern margin of Janauri hill, of western Himalaya and mentioned that the last earthquake occurred after 1200 AD. They argued that the back thrust may develop either due to locking of forethrust or to accommodate large slip on the forethrust. Mishra et al., (2016) excavated a trench at Panijhora, West Bengal and found a major fault scarp indicating the faulting of surface during the 1255 AD earthquake. The paleoseismological studies at Pasighat, Arunachal Pradesh by Priyanka et al., (2017) revealed a ~ 3.1 m high fault scarp along the Brahmaputra river which was found to be developed during the AD 1950 earthquake (Mw 8.6) based on Multi-proxy radiometric dating.

A better constraint of the parameters important to objective analysis of seismic hazards, such as plate convergence rate and width of the locked portion of MHT, in the Northwest and Northeast Himalaya were reported utilizing Global Positioning System (GPS) measurements in the past five years (i.e. 2016-2019). Yadav et al. (2019) have provided

a robust estimate of plate convergence rate of 18 ± 1 mm/yr and depth of locking of MHT of 15 ± 2 km in the Kumaun Garhwal Himalaya. They reported strong interseismic coupling (>0.6) in the brittle part of MHT and indicate a large rate of slip deficit and the region has potential to produce at least one megathrust earthquake of $M_w \sim 8$ (Fig. 5.2b). Barman et al. (2017) have mentioned ~ 16 mm/yr of plate convergence and ~ 17 km of locking depth of MHT. They calculated 4.7 ± 1.3 mm/yr of dextral slip with a locking depth of 10.2 ± 1.4 km across the Kopili fault and ~ 16 mm/yr of oblique plate convergence in the Indo-Burmese fold and thrust belts. The plate interior surface deformations have been discussed by Jade et al. (2017) and Dumka et al. (2019). The characterization of source mechanism of the 2015 Gorkha earthquake and detection of asperity zones of strain accumulation in the Nepal Himalaya have been discussed (Sreejith et al., 2016; Yadav et al., 2017; Sunil et al., 2017; Sreejith et al., 2018). The non-tectonic deformations such as rapid depletion of groundwater (~ 1.3 m/yr) in the Gandhinagar (Choudhury et al., 2018), anomalous seasonal deformations ($H/V > 0.5$) at GPS sites situated in the transition zone of MHT (Panda et al., 2018) and role of loading/unloading of hydroelectric reservoirs (Gahalaut et al., 2018; Dumka et al., 2018) in perturbing the stresses on the tectonic features have been characterized.

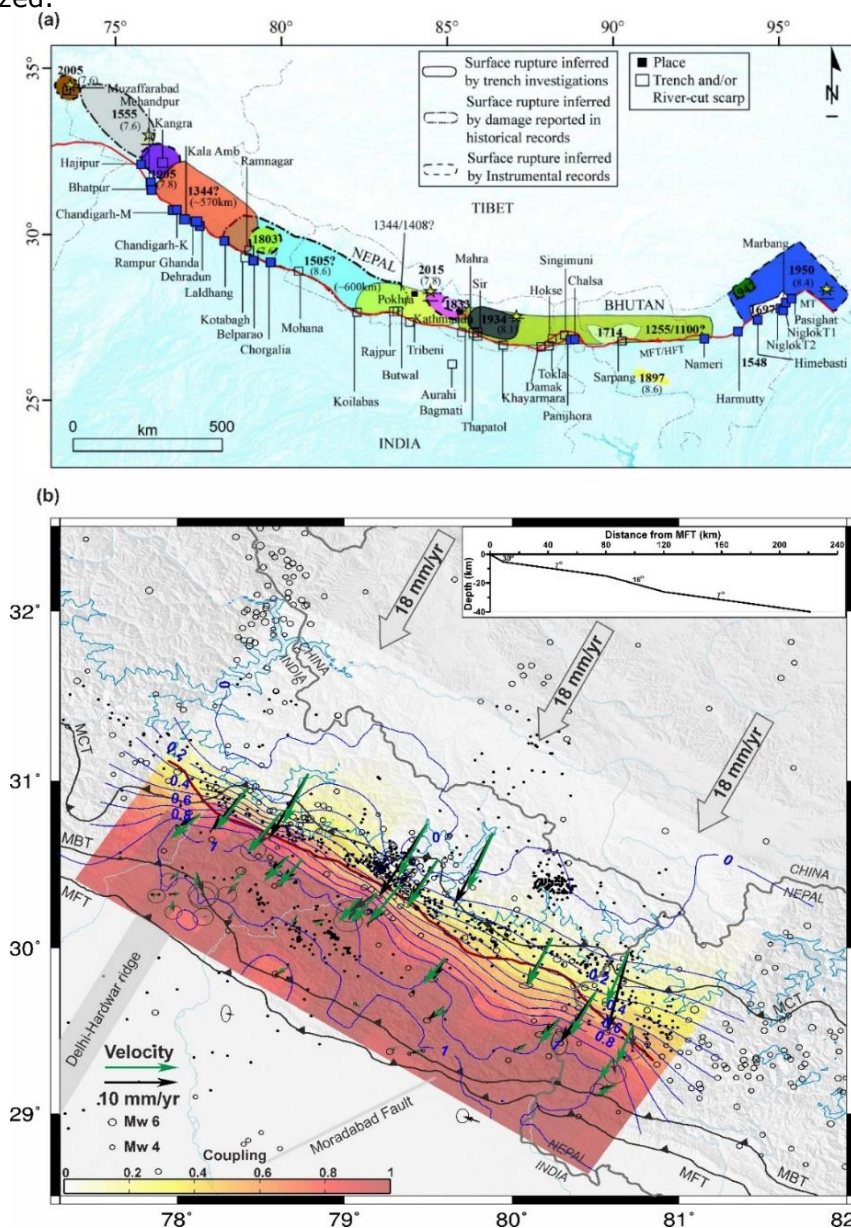


Fig. 5.2: (a) Simplified map showing the surface ruptures of great earthquakes along the Himalaya arc, and locations of paleoseismological trenches excavated along the Himalayan front by WIHG (solid blue squares). (source Jayangondaperumal et al., 2018). (b) Interseismic coupling map of

Garhwal-Kumaun Himalaya. The black and green colour vectors show the observed and calculated site velocity respectively. Black coloured open circles show seismicity from 1973 to 2015 (USGS earthquake catalogue) and solid circles represent the seismicity reported by Mahesh et al. (2013). The blue colour contour shows the interseismic coupling on detachment with an interval of 0.2. Brown curve represents the trace of PT2. Top inset shows the geometry of the MHT used in the analysis of interseismic coupling. (source Yadav et al., 2019)

5.3 Crustal deformation study of Gujarat

(Rakesh K Dumka, D. SuriBabu, P. Narain)

For the deformation analysis of Gujarat region, GPS data of all the permanent as well as campaign mode sites of ISR network are being processed using GAMIT-GLOBK software. For a better understanding of the deformation pattern of the region, velocities of all the sites were also calculated in the Indian Reference frame. Analysis indicates maximum amount of strain accumulation in Kachchh region and significant level of strain accumulation in Narmada region. Similarly, InSAR study along with the GPS study is being conducted in Kachchh and Narmada regions for pixel level deformation analysis of the region. Preliminary analysis of InSAR data along KMF highlights the importance of transverse features in the region.

5.4 Anomalous transients in GPS measurements due to induced changes in local site conditions

(Sandeep Gupta, Paresh Nath Singhroy, Rajeev Kumar Yadav, Joshi K Catherine, Roland Burgmann, Vineet Kumar Gahalaut)

We report distinct kind of transient deformation at two GPS sites. The site PTNA, situated in Patna, Bihar is located on the alluvium of the Indo-Gangetic plains and is about 6 km from the right bank of the Ganga river. A coseismic shift of ~ 7 mm towards north was recorded at site PTNA during the 2015 Gorkha earthquake. The nearby region has experienced moderate ground shaking. We observed an anomalous ground motion towards northwest which continued for 50-60 days after the 2015 Gorkha earthquake (Fig. 5.3a). The GPS sites situated at Ranchi, Dhanbad and Bhagalpur did not show such kind of transient behaviour. We found that the transient motion at PTNA was significantly larger than the expected maximum deformation from visco-elastic relaxation caused by the mainshock at the site location. The Geological Survey of India has reported evidence of soil liquefaction, ground fissure and sand boils from the Madhubani district while such phenomena in the neighbourhood of the site PTNA has not been reported, although both the regions, Patna and Madhubani, have experienced similar coseismic offsets due to the earthquake. We summarize that similar effect might have occurred close the PTNA site, though at a much lesser scale to be visible at the surface, but enough to be recorded at PTNA GPS site. We propose that the moderate shaking due to the 2015 Gorkha earthquake caused slow and permanent deformation in the water-saturated alluvial plains, which continued for nearly two months near PTNA.

Another GPS site, KUNR, located less than 1 km from Tehri reservoir shows anomalous seasonal variations in the displacement components. The reported secular motion at this site is consistent with the underlying locked main Himalayan thrust. We report that the transient deformation at this site is influenced by the reservoir filling and emptying cycles. We removed the influence of hydrological, atmospheric and non-tidal ocean loads from the GPS time series. The variations in the North and Up components of residual GPS time series show a good correspondence with the simulated displacement due to reservoir filling and emptying cycles (Fig. 5.3b). However, the East component exhibits some anomalous behaviour and shows biannual seasonal variations. We suggest that the reservoir impoundment may have locally altered the hydrological conditions leading to anomalous deformations that cause the biannual variations in the East component of the GPS measurements at KUNR.

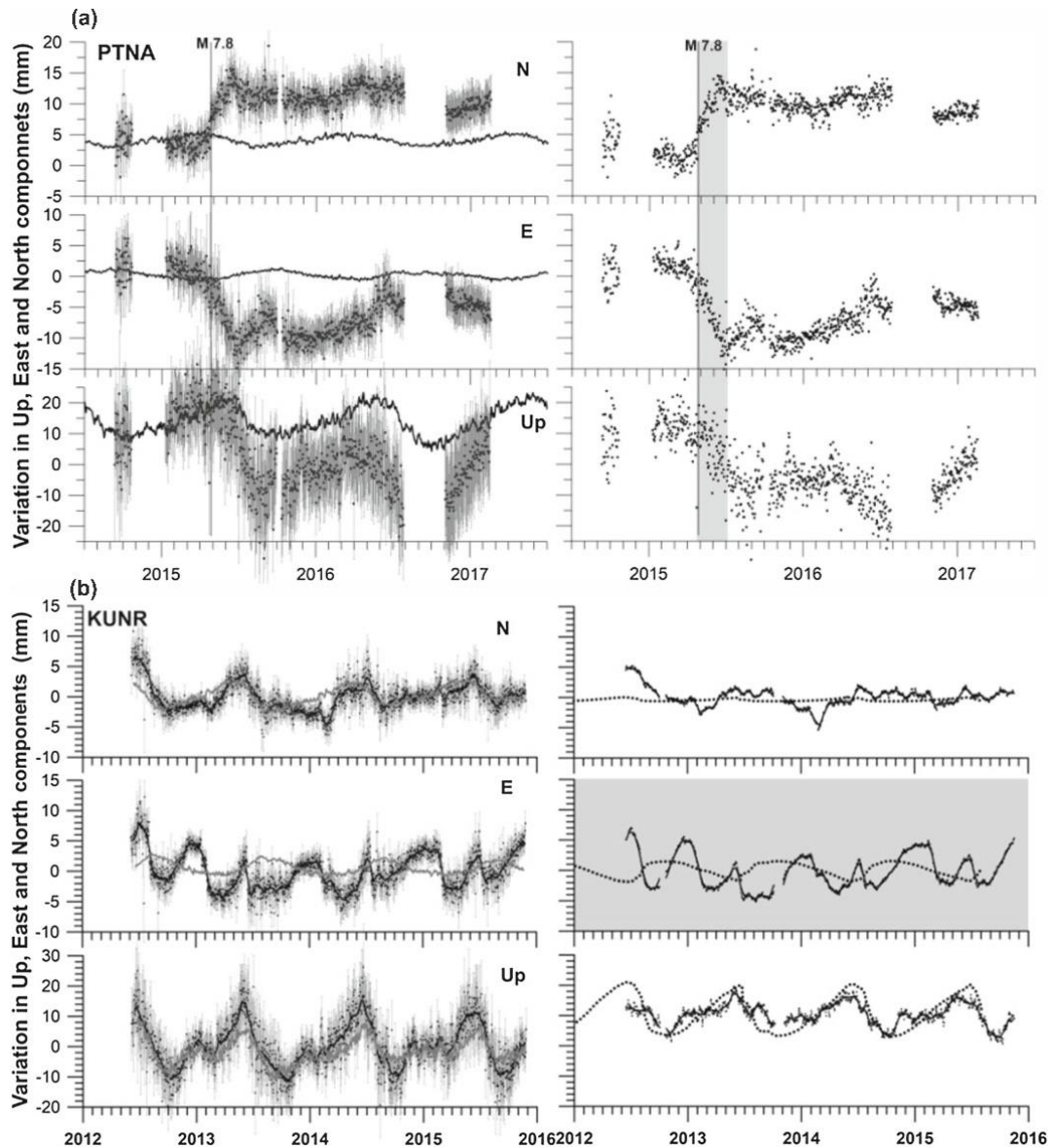


Fig. 5.3: (a) and (b) represent transient displacement at GPS sites, PTNA and KUNR. Left panel shows GPS time series (North, East and Vertical) in India reference frame along with the displacement components derived from the global hydrological model. Right panel shows residual time series after subtracting the contribution of the hydrological, atmospheric and non-tidal ocean load. The vertical line shows the time of occurrence of the 2015 Gorkha earthquake. The dotted curve shows the simulated displacement due to the Tehri reservoir filling and emptying cycles. Note the strong transient at PTNA after 2015 Gorkha earthquake and anomalous biannual seasonal variation in the East component at KUNR.

5.5 Reconstructing Late Quaternary Palaeo-environmental change from the dryland fluvial landscape of the Southern Kachchh Mainland, Western India: Insights from new OSL and sedimentological datasets

(Archana Das, Jaquelin Joseph, Tarun Solanki, Nisarg Makwana, Gaurav Chauhan, M. G. Thakkar)

The southern Kachchh Mainland (SKM) of western India, situated in a seismically active intraplate region with a considerable Quaternary landscape, provides an opportunity to reconstruct the roles of climate and tectonics. Employing geomorphology, detailed sedimentology supported by geochemistry and optical dating, we integrate the fluvial to fluvio-marine records to evaluate the potential of dryland environments in archiving the palaeo-events. The climate reconstructions suggest that the fluvial systems have responded to the variations in monsoonal strength through widespread aggradation during

57 ka until 41 ka, corresponding to the later part of MIS-3. Following this, a relative weakening of monsoon and onset of aridity is observed between 28 ka and 11 ka, with short spells of enhanced monsoon. The monsoonal conditions again strengthened during 11 ka to 6 ka, reaching their maximum during the Early Holocene optima, which triggered a sea-level rise during the Middle Holocene period, i.e. 6 ka to 3 ka. Following this, the sequences incised in response to the relative sea-level fall to the present level in post 3 ka. We have also employed these OSL ages to reconstruct the phases of aggradation and incision of valley fill sediments / estuarine tidal terraces from the SKM during the last 57 ka. The present study illustrates and contributes to the advancement in understanding of complex processes and their influence on climatic/tectonic signals in dryland landscape as well as their decoupling.

5.6 Did the seawater retreat play a key role in abandonment of the coastal Harappan settlement Lothal (Gujarat)?

(Archana Das, Chintan Vedpathak, Aashima Sodhi, S. P. Prizomwala, Rajesh Agnihorti, Nisarg Makwana, Binita Phartiyal, Jaquilin Joseph, Nikhil Patel, Sumer Chopra, M. Ravi Kumar)

The mighty Harappan civilization, well known for its town planning, maritime trade and organized living, flourished during the mature Harappan phase, along the Indus valley alluvial plains of the northwestern (undivided) India between ~ 2600 to ~1900 BCE. Decline of this ancient human civilization is intensely debated. The sudden decline also marks the beginning of a distinct sub-division of the Holocene being termed as the Meghalayan age (last ~4200 years). Whether this beginning marks holistic changes in hydro-climate together with regional sea level changes that collectively resulted in ending the mature phase of Indus civilization, is yet to be explored with suitable regional records. Lothal (an oldest Harappan dockyard), located ~23 km from the present day shoreline of western India could be holding the clue. We present here a detailed geochemical, stable isotopic, mineralogical, and sedimentological proxy based record revealing evidences for a marginally higher sea stand between (~5000 yr BP to ~2000 yr BP) indicating a higher sea stand pushing the estuarine zone close to the Lothal site, facilitating ship-movements. Thereafter, all proxy record, collectively hint at a sharp fall in the relative sea stand coinciding with the end of mature phase of Indus era. Several Indus archaeological sites already witnessed a drier (monsoonal aridity) phase at the same period. In light of these evidences we posit that these two aforesaid climatic manifestations possibly led to scarcity of water in the up as well as downstream Indus stretches, leading to a defunct dockyard for business and consequently a decline in trade.

5.7 Signatures of tectonic instability (?) along the North Cambay basin during the Late Holocene period, North Gujarat, India

(Archana Das, Tarun Solanki)

In the present study we investigate the Tectono-geomorphic attributes of the Northern part of the Cambay basin, Western India, which has recently witnessed a surge in seismic activity. We employ the anomalies in drainage network along with sedimentological character of the drainages along with OSL chronology to unravel the abrupt aggradation and incision processes during the Late Holocene period. The analysis reveals two major lineaments, i.e., NE-SW and NW-SE prevalent in the Northern Cambay Region. The NW-SE trend is exhibited in the first order streams which hints at the ongoing tectonic activity along the buried structural element/fault. The sedimentary architecture of the valley fill / channel fill sediments suggests one major phase of aggradation around 3.6 to 3.3 ka, which was attributed to stronger monsoonal conditions prevalent in the study region. These valley fill sediments were incised during the Late Holocene period i.e after 3 ka, which we ascribe to the tectonic activity along the buried structure/faults in the Tharad-Sanchor block of North Cambay basin. The present study for the first time has reported tectonic activity along the Tharad-Sanchor block of North Cambay basin.

5.8 Tectonic implications on controlled dimensions and fluid dynamics of Bedrock Gorge, Kachchh: Western India

(M G Thakkar, G C Kothiyari, Gaurav Chauhan, Abhishek Lakhote)

Formation of large scale deformations in the upperpart of crust during Quaternary resulted in opening of cracks on the rising/bulging landscape of the EW trending Kachchh basin. The present study pertains to an active crack (deep Khari gorge) development in the mainland region of Central Kachchh. The length of the crack (gorge) is 220 m and the maximum depth is 27.3 m, where the length and displacement/width vary from place to place. The estimated results show maximum dip dimension of 49.9 m and minimum 3.1m. The study shows that there is a regular and direct connection between the size (length) of crack openings and the rate of displacement. The controlling dimension of a crack is geometrically denoted by the strike and dip of a fracture. The volume of water flow (volumetric rate) on the horizontal bedrock surface and subsequent crack opening is directed by the fracture aperture. The opening of crack within the contact of two surfaces may have a variable aperture corresponding to the rate of volumetric fluid flow over the crack. The statistical parameter shows that the young's modulus of sandstone is 6 MPa., the Poisson's ratio is 0.2 and the tensile strength is 14 MPa in the fault zone.

5.9 Basin-wide aggradation-incision events and triggering processes: insights from the fluvial response of Shetrunji river (Western India) since the Last Glacial Maxima

(Tarun Solanki, S. P. Prizomwala, Nisarg Makwana, P M Solanki)

The present study is an attempt to infer the response of fluvial sequences to paleoenvironmental changes since the last glacial maximum (LGM) from the arid to semi-arid Saurashtra region, a Deccan Trap terrain, of Western India. We employed a conventional sedimentological analysis supported by sediment geochemistry, which was constrained by optical dating. Based on detailed field investigations, we identified five terrace sequences from the valley fill deposits in the Shetrunji River basin. Based on optical dating, we find that the Shetrunji river basin sequences have an exposed sedimentary record since 18 ka (i.e. Post LGM), in valley fill and terrace landforms. The sedimentary archives expose the deposition at discrete intervals in the form of three alternate phases of aggradation and incision. The study reveals that during the Late Pleistocene to Holocene period (18-9 ka), widespread valley aggradation occurred in response to the rising sea stand along the west coast of India gradually strengthening the monsoonal conditions. The Early Holocene climatic optima (9 to 7.5 ka) coupled with present but rising sea stand, triggered the intense erosion in the valleys of Shetrunji River, leading to erosion/lack of sediment preservation. This was followed by the Middle Holocene period (7.5 to 5 ka), which experienced valley aggradation. This was ended by the incision post 5.5 ka. The sea stand was similar to the present-day stand, as evidenced by the change from a fluvial to an estuarine environment in the top sequence of Site-SL, at 5.5 ka. The post-Middle Holocene relative sea stand lowering (at < 5.5 ka), led to an incision in the estuarine terrace of about 2m. The causal mechanism for triggering of this incision is most likely the relative fall in sea stand to the present-day level from its Middle Holocene high stand. The Late Holocene period (3 to 1 ka) shows aggradation in the upper reach in fluctuating hydrodynamic conditions with seasonality, followed by a relatively good monsoonal condition at < 1 ka, leading to the incision. These pulses of sedimentation could be recognized and explored as aided by basin-scale approach as shown in the present study. Site-specific studies do not enjoy such liberty.

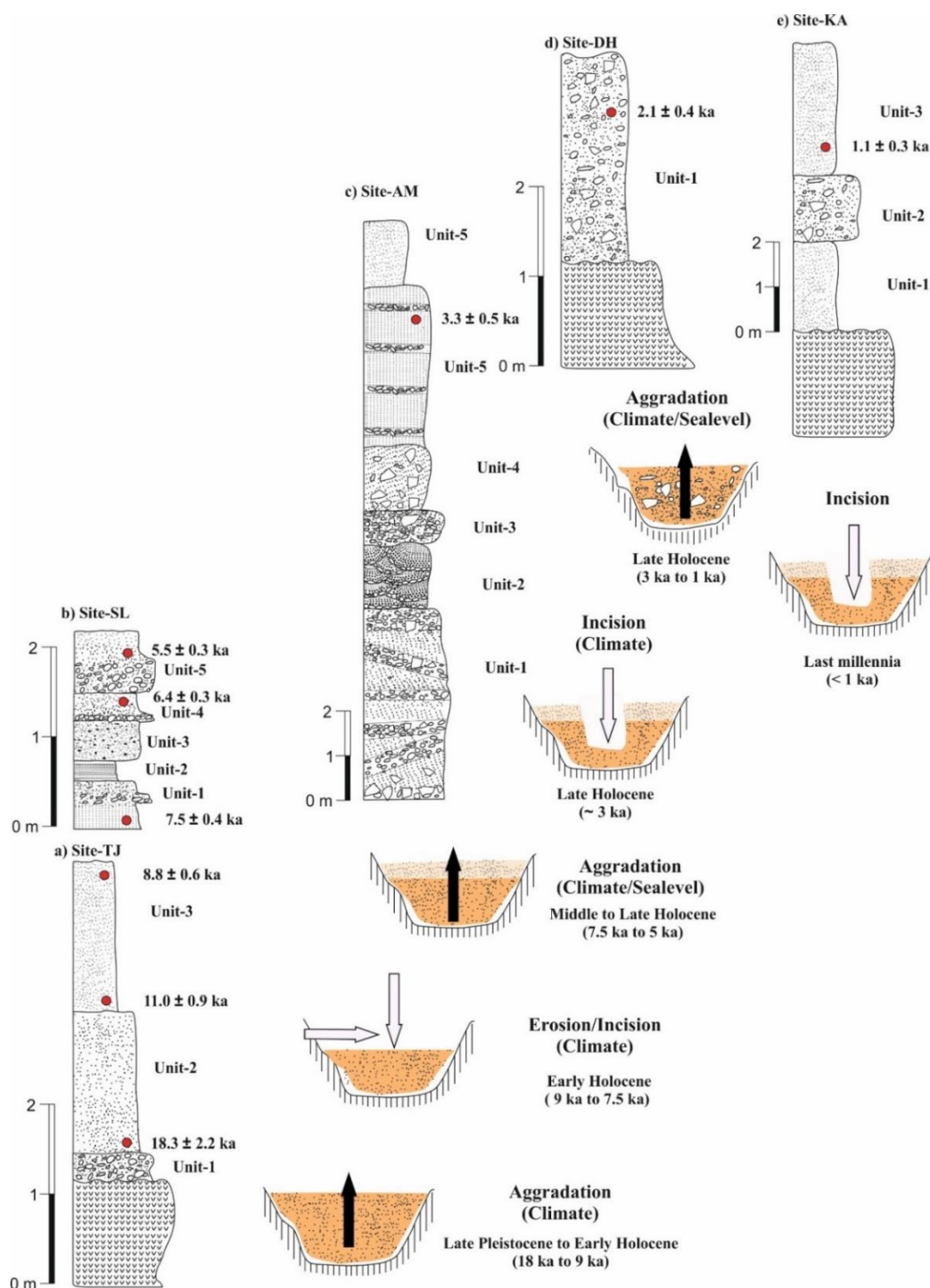


Fig. 5.4: Composite lithostratigraphy with aggradational and incisional events since the LGM

5.10 Geomorphic response to neotectonic instability in the Deccan volcanic province, Shetrunji River, Gujarat, Western India: Insights from quantitative geomorphology

(Tarun Solanki, P M Solanki, Nisarg Makwana, S. P. Prizomwala, G. C. Kothiyari)

Despite the occurrence of three moderate earthquakes, 2007 (M_w 5.0, M_w 4.9) and 2011 (M_w 5.1), the Saurashtra region lacks studies that document on-land information of active faults. In the present study, we investigated the geomorphology of the Shetrunji River basin located in the Deccan volcanic province, western India to identify the neotectonic signatures using detailed analyses of landforms and drainage patterns. The quantitative

geomorphic analysis and field investigations along with morphostructural analysis reveal the presence of drainage anomalies, such as offset in the channel, deflection in the stream, development of linear valleys and offset in ridge, in the river basin. We calculated the stream length gradient index (SL), drainage basin asymmetric factor (A_f) and basin shape index (B_s) to assess the landscape response to tectonic deformation. For the first time, we report the geomorphic evidence of two main faults 1) the Girnar Fault (GF), a left-lateral strike slip fault and 2) the Shetrunji Fault zone (SFz), that extends for 52 km in length and 2 km in width, showing a right-lateral strike slip motion as inferred from offset of the drainage pattern. However, the GF shows a linear zone of stream offset and faulted ridges. The findings are consistent with the geomorphic and structural setup of the region and coincide with the historical as well as current seismicity distribution. The study reveals prevalent neotectonic activity along the GF and the SFz in the south-eastern Saurashtra region dominated by Deccan basalts.

5.11 Testing the sensitivity of Relative Index of Active Tectonics from areas experiencing variable uplift: An example from the Himalayan Frontal Thrust in the NW and NE Himalayas

(Aashna Tandon, S. P. Prizomwala, Gunjan Yadav)

The geomorphic indices are important indicators for assessing the landform response to active tectonic processes and have been widely used as reconnaissance tools to differentiate zones / segments influenced by tectonic activity. Relative Index of Active Tectonics (RIAT) has been identified and employed successfully in a variety of terrains for assessing the relative degree of tectonic processes acting therein. In the present study, we attempt to assess the sensitivity of RIAT in identifying areas undergoing variable uplift, with an example from the Northwestern and Northeastern segments of the Himalayan Frontal Thrust (HFT). As the HFT is a thrust fault system, we employed the Mountain front sinuosity (S_{mf}), Valley floor width-height ratio (V_f) and Steepness index (K_{sn}) (i.e. uplift responsive parameters) as input parameters for estimating the RIAT. The resultant RIAT values were then classified into three classes, i.e., Class 1 (highly active) to Class 3 (least active). The westernmost part of NW segment, i.e., near Jammu sector shows Class 3, whereas the easternmost part of NW segment shows Class 2 of RIAT with moderate activity. Similarly in the northeastern segment of HFT, the westernmost rivers show Class 1, whereas three drainages from Tezpur to North Lakhimpur, show Class 2 of moderate activity. These results are in fine agreement with the long-term uplift / shortening rates and geodetic rates estimated using fault and GPS data. A close examination of variations in geomorphic parameters shows that the V_f and the K_{sn} index, in particular are more suitable to assess the most recent changes in valley morphology, whereas S_{mf} shows no spatial variations and functions as least sensitive to such study. The study illustrates that RIAT can be used as a reliable first hand tool to examine large fault segments, for assessing variability in relative degree of tectonic activity undergone by them.

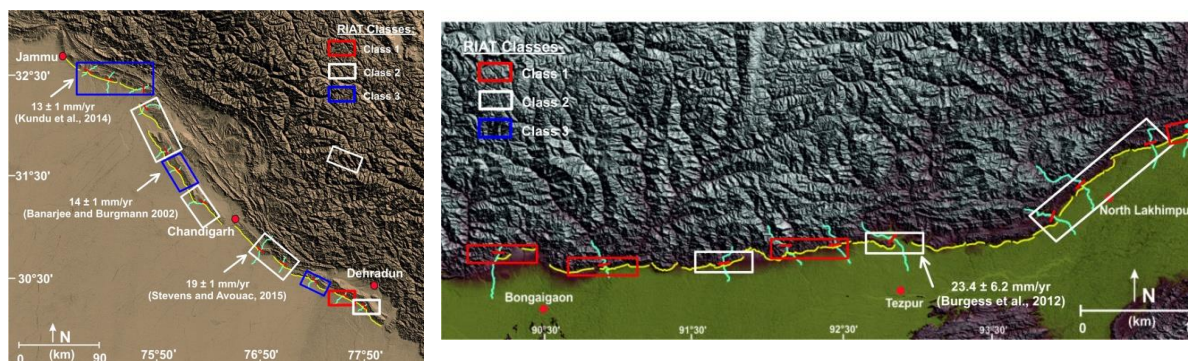


Fig. 5.5: Map showing variability in RIAT in the Northwest (left) and Northeast (right) segments of Himalayan Frontal Fault.

5.12 Morpho-structural approach in predicting the neotectonic attributes of Vigodi Fault, Kachchh, India

(Sneha Mishra, Girish Ch Kothyari, R. K. Dubey, Gaurav Chauhan, Raj Sunil Kandregula)

In present study, we analyzed geomorphic landform and drainage pattern within the NW-SE oriented Vigodi Fault (VF) to assess neotectonic deformation. The VF zone is located in the western part of Kachchh Basin, that shows a typical wrench geometry, where several compressional and extensional fault segments generating Vigodi-Gugriana-Khirasra fault complex, between the Katrol Hill Fault (KHF) and the Kachchh Mainland Fault (KMF). In this study, we present geomorphic evidences along the surface traces of neotectonically active VF zone. The fault zone is encompassed by several neotectonic landforms such as the development of strath terrace towards the upthrown block and, valley fill terrace in the downthrown block of the VF, youthful nature of fault scarps, warping in Quaternary sediments, the formation of slit canyon within Quaternary sediments, knick-points, slickensides, and river offset. Presence of strike and dip parallel slickensides indicates oblique slip motion within the VF zone. We used conventional geomorphic parameters of active tectonics such as stream length-gradient index (SL), steepness index (Ks) to determine neotectonic variability across the fault zone. Further, we tested a novel method called gradient length anomaly (GLA) to identify the surface deformation pattern within the VF zone. The observed negative and positive values of GLA correspond to the long-term uplift and subsidence associated with the VF. The results of geomorphic, geological and morphometric analyses together show that the area is neotectonically active. The combined observations made from the present investigation can be used to assess seismic hazard of the study area.

5.13 Structural Attributes and Paleostress Analysis of Vigodi Fault (VF) in Western Kachchh Region

(Sneha Mishra, R. K. Dubey, Girish Ch Kothyari, Gaurav Chauhan)

In this study we analyzed deformational and kinematic characteristics of the NW-SE trending Vigodi Fault (VF) in western Kachchh basin using Paleostress analysis. The Paleostress inversion of fault slip data was carried out within the VF using the available software, WinTensor, Fault-Kin, and T-Tecto, based on the attitudes of NW-SE, NE-SW faults and slickensided surfaces. In this work, we presented slip analysis and changes in stress reorientation of VF that displaced the Bhuj and Jhuran formations of Mesozoic age and a branch of VF that separates the boundary of Deccan Trap and Bhuj Formation. We adopted fault inversion technique using fault plane solutions to identify the principal stress axis (σ_1) position within the region. To obtain PTB axis, stress ratio, and principal (σ_1) axis, we used right Dihedron Method using the WinTensor and T-Tecto. The analysis indicates that the compressional stress dominates the area. In the rotation stress orientation, we identified N-S compression stress in the region.

5.14 Mudflats of little Rann of Kachchh: implication for palaeo climatic and palaeo environmental changes during Middle to Late Holocene period and understanding the role of such changes on the landscape and past human settlement

(Nisarg Makwana, Archana Das, Siddharth Prizomwala, Chinatan Vedpathak, Gaurav Chauhan)

The Little ran is a unique landscape in the southeastern part of the seismically active Kachchh basin that witnessed continuous shallow marine sedimentation from the beginning of the Holocene to 2 ka B.P. (Biswas 1974, Gupta 1975). The Little rann has not been studied so far for Holocene Palaeoclimatic and palaeoenvironmental changes (Maurya et al., 2009). The present study signifies the palaeoclimatic history of Middle to Late Holocene, Quantification of Middle to Late Holocene Sea stand, Evolution of little Rann of Kachchh, Provenance history of sediments into Little Rann of Kachchh, Role of palaeoclimate and past sea level changes onto past civilization and tectonic history in the region. We have initiated coring and sampling at every 1 to 1.5 cm and Grain size analysis of the upper 2m.

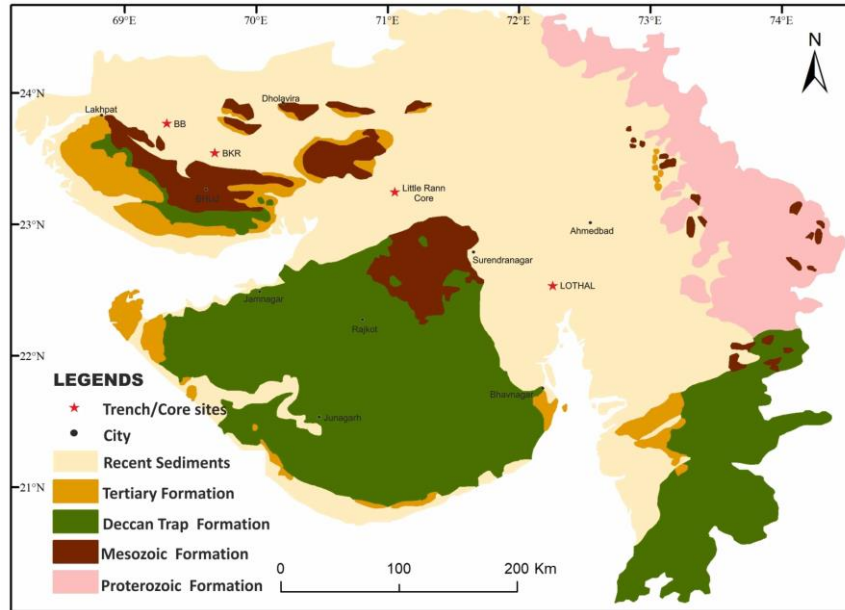


Fig. 5.6: Trench and core locations in the palae mudflats of Gujarat, Western India



Fig. 5.7: Sediment characteristics and sampling at every 1 cm.

The study will be carried out using methodology/proxies like Sediment Characteristics to understand the change in depositional environment with respect to time, Grain size analysis to have preliminary understanding of provenance, Sediment geochemistry to have understanding of elemental geochemistry of specific source, which will be helpful in bifurcating the major provenance over a specific time period, i.e., the source that dominantly brought sediments during a particular period. Some specific elements will be important tools to identify or distinguish major contributing source of sediments in a

domain where we have multiple sources. Also correlation between sediment geochemistry of present core and possible sediment sources into Little Rann of Kachchh will be key factor in identifying palaeoclimatic/palaeoenvironmental changes, Mineral Magnetics to understand nature of magnetic minerals in the study area, weathering history of the region as a supportive tool for palaeoclimatic reconstruction, Clay Mineralogy to understand source and provenance, and will be helpful in finding signature of Sea stand as supportive proxy, Carbon Isotopes to differentiate organic material of aquatic and terrestrial origin.

5.15 Palaeo climatic and paleo environmental reconstruction deduced from the higher Banni Plains, Kachchh (BKR trench site) during the last 5 Ka.

(N Makwana, A Das, S Prizomwala, G Chauhan, C Vedpathak, B Patriyal, M. G. Thakkar)

A shallow trench of 5.5 m was opened at BKR site, located on the Bhuj-Khavda road. The location of BKR site is at the margin of Banni plains in the proximity of Kachchh mainland, away from any human settlement assuring negligible to nil anthropological effect. A total of 55 samples were collected at every 10 cm depth for multi proxy analysis, viz, sediment geochemistry, Mineral magnetics and Carbon isotopes studies. Result suggests Major climatic fluctuations (two phases of wet climate and two phases of aridity) in the region during the last 5 Ka. The period ≥ 3.9 Ka BP has experienced an overall dry phase (aridity). Periods between 3.9 Ka and 3.2 Ka had experienced good monsoon indicating a wet phase and the period between 3.2Ka till present has experienced two alternate phases, i.e., dry and wet. A few more ages are required from the top and bottommost units in order to pick short abrupt events and signatures of marine influence in the Great Rann of Kachchh to understand role of tectonics and sea level change in the region.

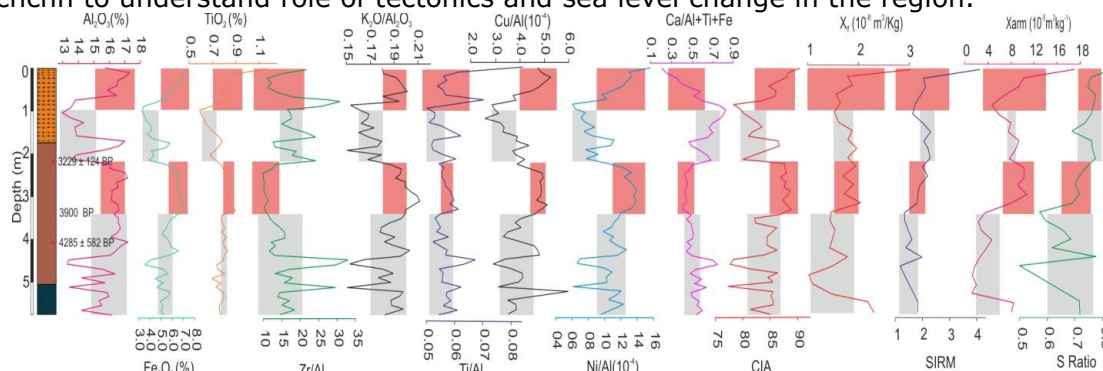


Fig. 5.8: Variation of major and trace elemental concentration and magnetic mineral parameters from the sediments of Banni plains, GRK. Grey shade indicates dry phase while light pink shade indicates wet phase.

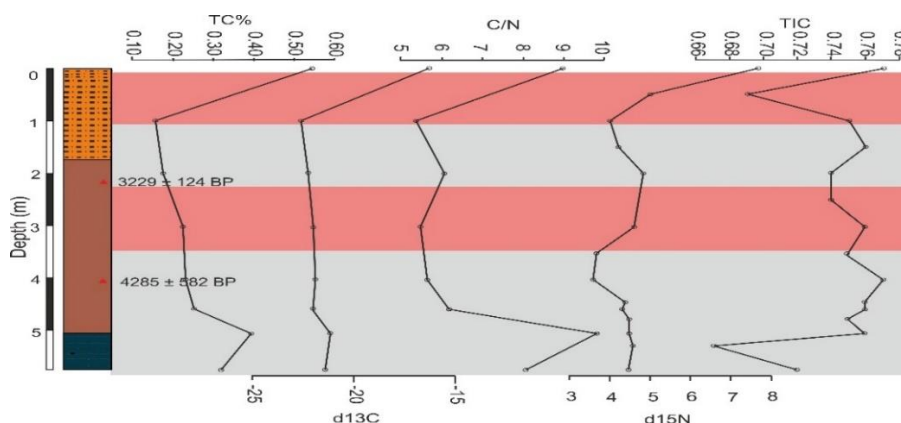


Fig. 5.9: Variation of carbon isotopes parameters from the sediments of Banni plains, GRK. Grey shade indicates dry phase while light pink shade indicates wet phase.

5.16 Response of Harappan coastal sites in Gujarat to middle-late Holocene Palaeo-environmental changes: a multiple proxy approach

(Chintan Vedpathak, Archana Das)

Lothal is situated on the bank of Bhogavo River, connected with the Gulf of Cambay. It was reported that Lothal was a dockyard in Middle to late Holocene period. We carried out field work in the southern part of Lothal in the Kamatalav village located near to the Gulf of Khambhat. It is a tidal regime in the Arabian Sea formed at the mouth of Sabarmati that forms estuaries along the west coast. The present KT trench site (22°19'N, 72°16'E) is located in the region influenced by the sea and part of a palaeomudflat regime. The trench site is about 14km from the archeological site of Lothal and at an elevation of 7m above the present high water line. At this site, we dug a 4.6 meter trench and collected 230 samples at 2cm intervals for a lab analysis and 5 samples for OSL dating to estimate the deposition age.

A 3.45m thick sediment profile has been trenched from the palaeomudflat of Kamatalav region. About 21 samples have been analyzed to determine the accurate depositional environment. Based on grain size analysis, the whole section is divided in to three litho units. The first unit (Unit-1), the upper most part from the top 2.2 meter, is dominated by clayey silt (98%) and lesser amount of sand (2%). The clayey silt is indicative of a lower energy level during the deposition time. Unit-2 represents sand with granule lesser amount of clay. The sand content (32% to 90%) is found to be increasing in Unit-3, indicating higher energy. It strongly suggests a shift in the depositional environment in the bottom most part of the trench in comparison with the top most part. The dominance of sand content may indicate that the deposition took place under a fluvial regime, whereas increase in silt and clay content suggests that the deposition has occurred under the influence of a mixed environment.

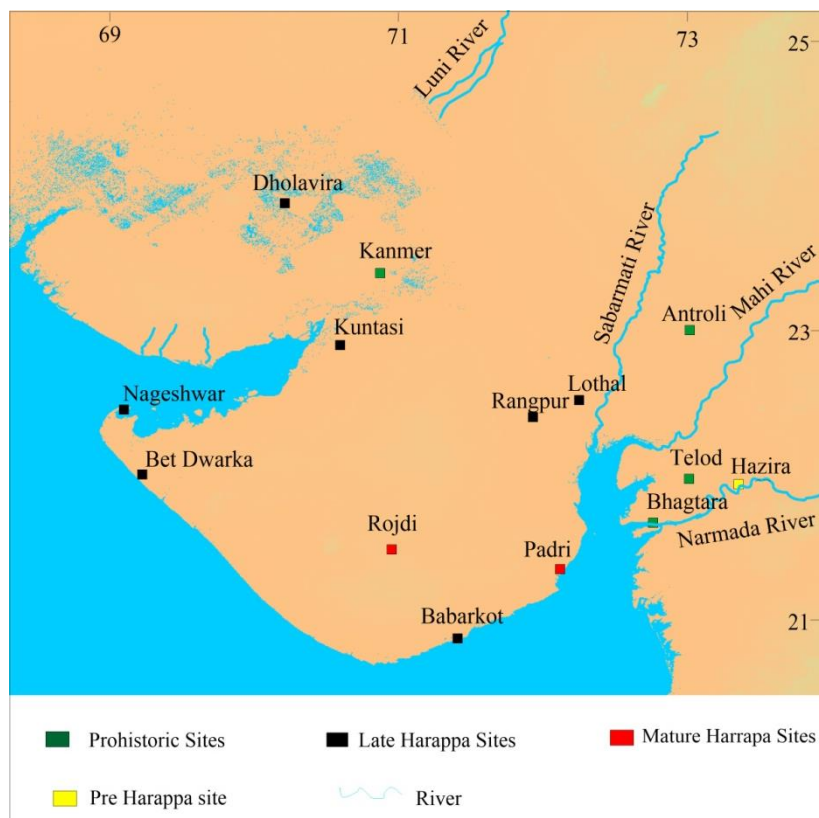


Fig. 5.10: Archeological sites of Gujarat

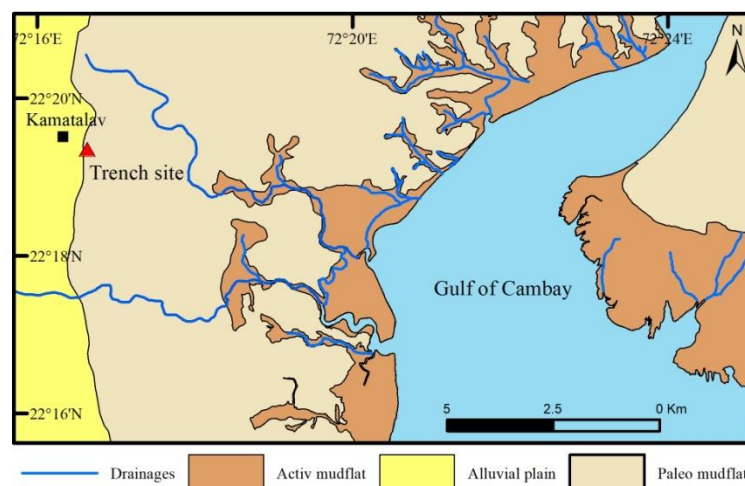


Fig. 5.11: Geomorphological Map of Kamatalav

We also performed a Micro-paleontological study on the foraminifera. We separated foraminifera from the sand fraction for AMS dating and identification. Because of their diversity, abundance and complex morphology, the assemblage foraminifera is useful for biostratigraphy and can accurately give relative ages. Foraminifera are found in the ancient sea they lived in. Thus, they are very useful in Paleo environmental analysis. The samples are analyzed in the lab by first drying them at 40°C, crushing and sieving them in <63-micron size for XRF analysis. The sieved samples were packed in cups using a thin propylene film, and analyzed in XRF machine to estimate the concentration of major and trace elements.

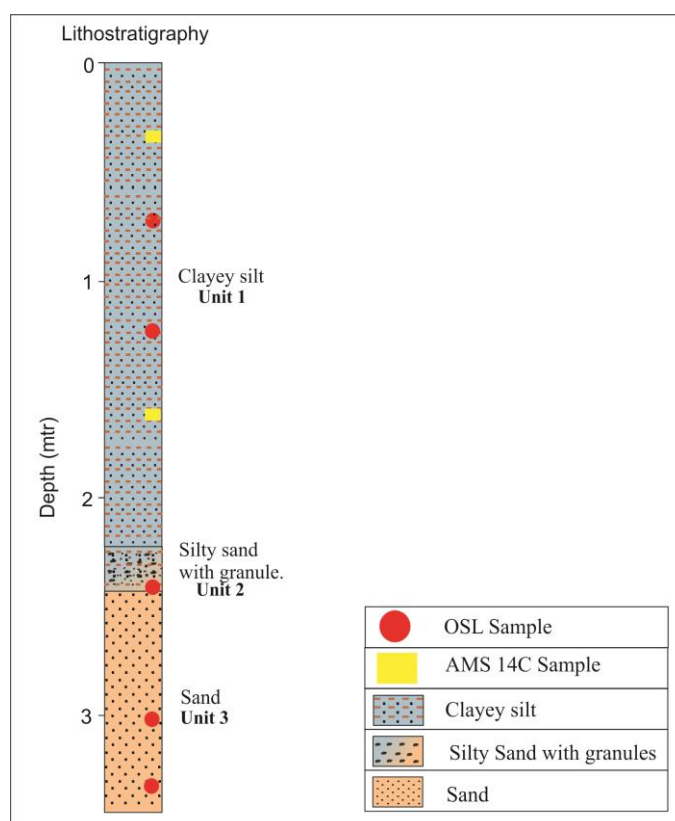


Fig. 5.12: Lithostratigraphy of Kamatalav site

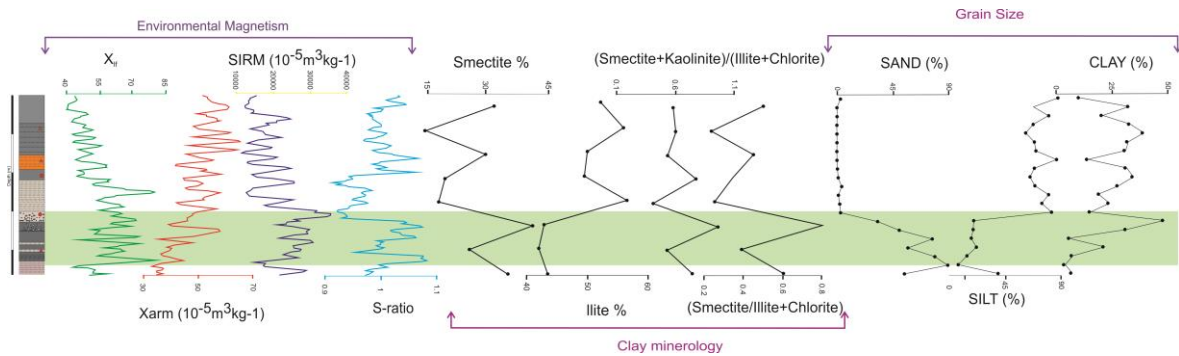


Fig. 5.13: Grain size analysis of Kamatalav site

Based on the grain size data, clay mineralogy and environmental magnetism analysis, we infer that the Kamatalav region has experienced two phases of strong and weak weathering conditions. The clay mineralogical data reveals dominance of Illite, ranging up to ~60%, indicating arid conditions, which could have been derived either from Precambrian feldspar rich metamorphic rocks or igneous rocks of the Aravallis and/or from the alluvial rivers, which have a catchment from the Aravallis. Similarly, the presence of Smectite indicates that the sediments were mainly derived from the Saurashtra peninsula and/or from adjacent Gujarat alluvial plains, with their primary source in the Aravalli's. The grain size data strongly suggests shifting in depositional environment in the bottom most part of the trench in comparison with the top most part. The dominance of sand content suggests that the deposition took place under a fluvial regime (?) whereas increase in silt and clay content suggests that the deposition has occurred under the influence of a mixed environment.

6 COMMERCIAL RESEARCH AND DEVELOPMENT

6.1 Time Domain Electromagnetic (TDEM) survey at Regional Science Museum, Patan

(Prutul Patel, Dilip Singh Kushwaha and Kapil Mohan)

The Gujarat Council on Science and Technology has requested ISR to conduct the TDEM survey at proposed Regional Science Museum at Patan. We have acquired 18 TDEM sites along two perpendicular profiles (Fig. 6.1) to locate fresh water zone with a target depth down to 700m. ISR deployed one equipment of TDEM survey for conducting such an investigation. The GDP 32-II data acquisition unit (Zonge, USA) together with a transmitter, generator-powered GGT-30 for larger loops system is used to conduct the TDEM field survey with 150 m square transmitter loop. The GDP 32-II was positioned at every 10-15m distance and ferrite-cored antenna was used to take the measurements. Most typical TDEM array is represented by a square loop, in which a trapezoidal (typically square) current waveform is driven. This current induces secondary (eddy) currents within the Earth, the rate of change of which produces an electromotive force (emf) that is picked up by a receiver coil normally located in the loop center. The amount of current injected in the transmitter loop is 9 Amps for all the TDEM sites. For each loop, the transmitter is operated for a sequence of data repetition frequencies of 16, 4 and 2 Hz. In the early and late times, the apparent resistivity is in general noisy and is removed for further inversion process, whenever necessary.



Fig. 6.1: The site location map

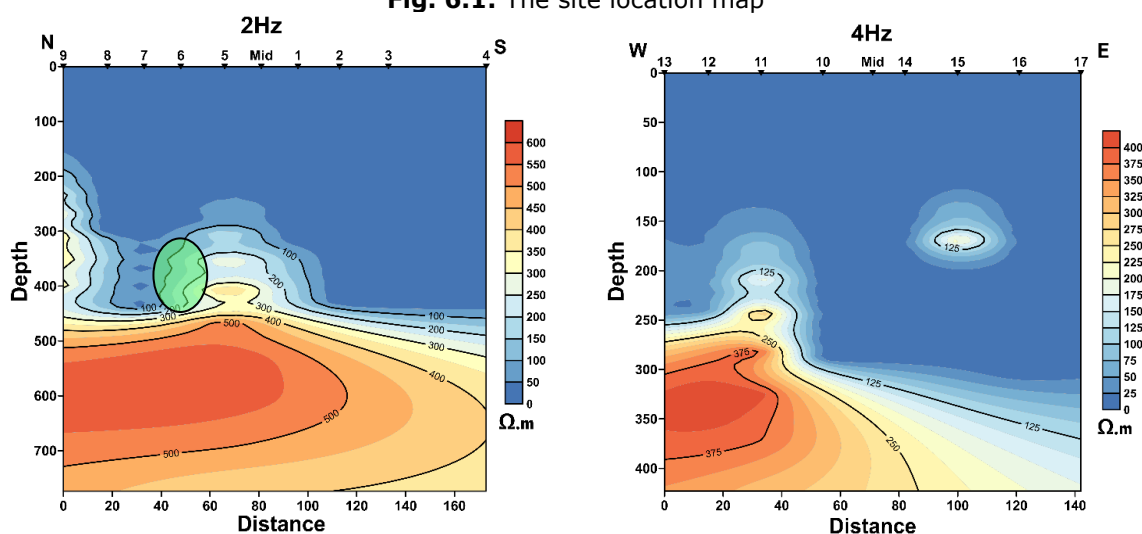


Fig. 6.2: 2D resistivity cross section of the subsurface derived using 1D inversions of the data acquired along the profiles.

Processing has been done and 1D inversion has been carried out for both the profiles. 1D cross section for both the profiles for 2 and 4 Hz have been shown in Fig. 6.2. The possibility of presence of fresh water is found at a depth of 300-400m (~50 Ohm.m to 100 Ohm.m) at site 7 in the NS profile (Fig. 6.2).

6.2 Magnetotelluric (MT) Investigation to locate geothermal source zone at Lasundra

(Kapil Mohan, Peush Chaudhary, Dilip Kushwaha, Naveen Kumar and Sumer Chopra)

Data from a total of 20 Magnetotellurics (MT) sites were acquired along two profiles (P1 and P2) in the NW-SE direction (Fig. 6.3) near and around Lasundra, for characterization of the hot spring sites. The data is recorded in the broadband frequency range (0.001-1000Hz) over a period of 2-3 days. The acquired data is processed with the help of Mapros processing software and the resistivity and phase curves are obtained for each site. The dimensionality and directionality analysis of the MT data is carried out by using the Phase Tensor approach of Caldwell et al. (2004) and Becken & Burkhardt (2004), respectively and shown in Fig. 6.4. A geo-electric strike direction of N17°W is obtained from the ellipticity criteria of Becken & Burkhardt (2004), that matches well with the geological setting of the area. The MT data is rotated in the direction of obtained geo-electric strike and decomposed into TE mode (electric field parallel to the strike) and TM mode (magnetic field parallel to the strike). After the decomposition of the data, 2D inversion is carried out with the help of WinGLink software and the final geoelectric depth sections along both the profiles (P1 and P2) are shown in Fig. 6.5 and Fig. 6.6.

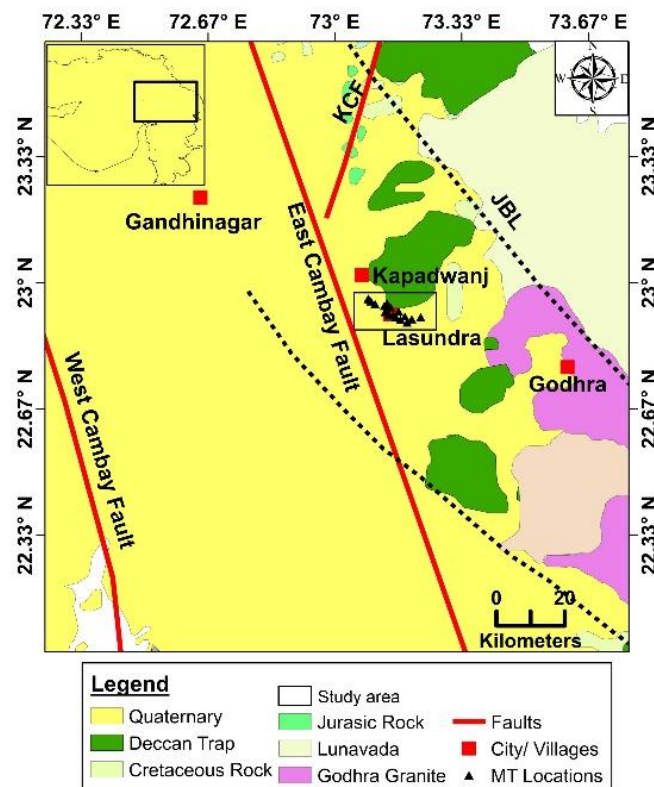


Fig. 6.3: Geological and Tectonic map of the area showing the acquired MT sites (black triangles)

The conductors C1 (at depth of 4-5km) and C2 (at depth of 2-3km) have been observed with resistivity of 10-15 ohm.m along the profile P1 (Fig. 6.5) and profile P2 (Fig. 6.6), respectively. These conductors might be the geothermal zones present at a depth of 2-5km. The water samples were also collected from the hot spring site and combined interpretation is in progress.

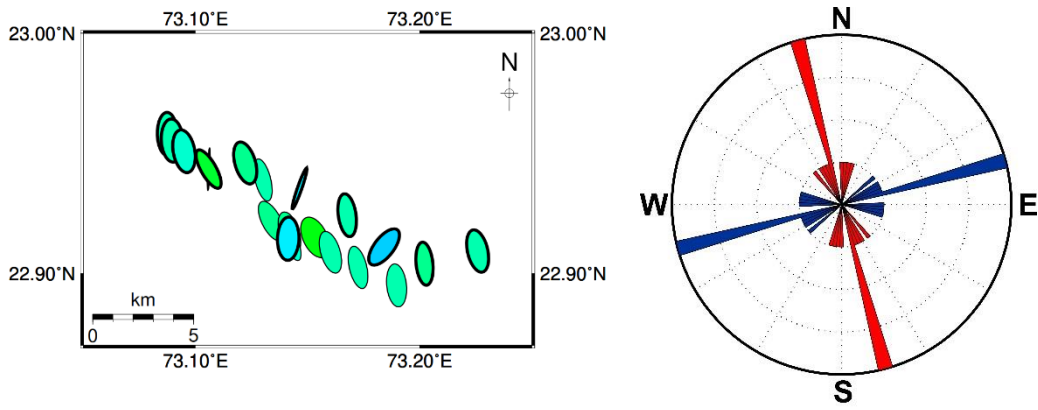


Fig. 6.4: Dimensionality (Left panel) and directionality (right panel). The red and blue wedge show two possible geo-electric strike directions.

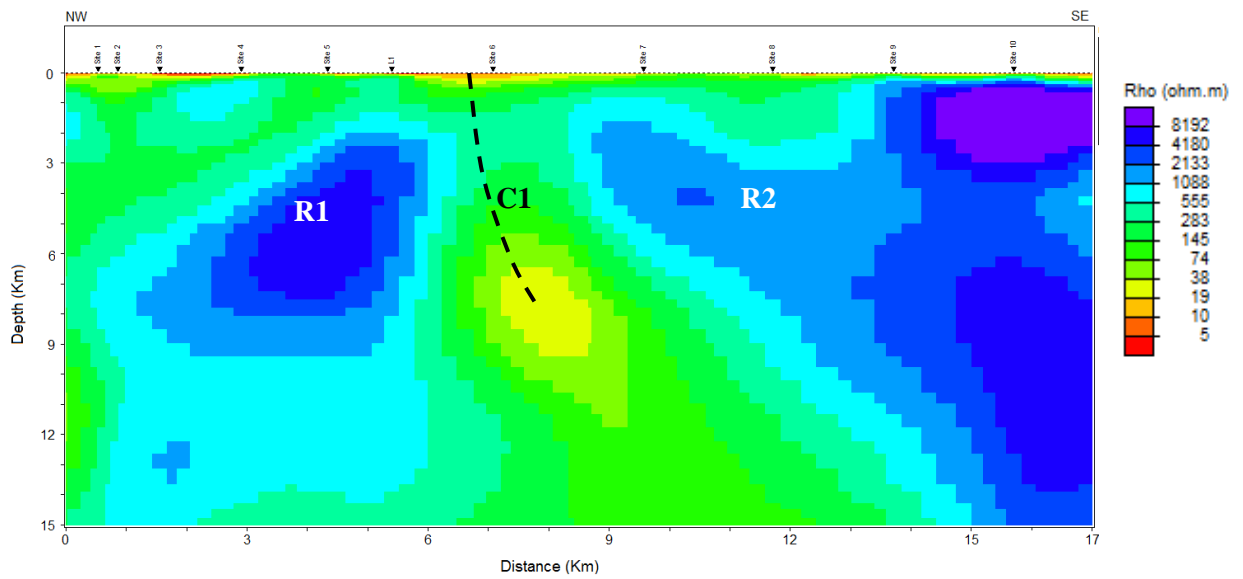


Fig. 6.5: Goelectric depth section (TE+TM mode) of the profile P1

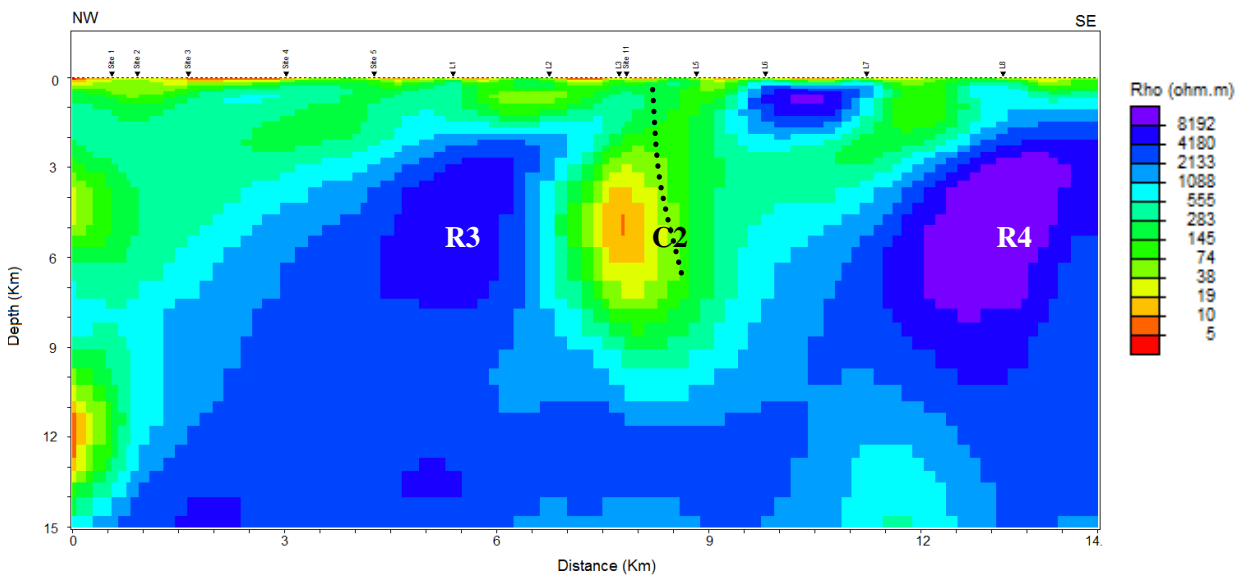


Fig. 6.6: The Goelectric depth section (TE+TM mode) of the profile P2

6.3 Phase-III, Delineation of Freshwater layer at selected sites in the Lakhpat, Nakhatrana, Bhuj (Banni area), Mandvi and Abdasa Talukas of Kachchh (Gujarat) using Time Domain Electromagnetic Survey

(Kapil Mohan, Prutul Patel, Dilip Singh Kushwaha, Naveen Kumar and Sumer Chopra)

The Gujarat Water Resources Development Corporation (GWRDC) invited ISR to conduct Time Domain Electromagnetic (TDEM) surveys to locate fresh water zones at some of the sites in the Great Rann of Kachchh and also in the Anjar and Bhachau talukas with a target depth down to 600m. ISR deployed two TDEM units for conducting such an investigation and carried out surveys at a total of 17 sites (Fig. 6.7) for mapping the fresh water aquifer layers and their thickness.

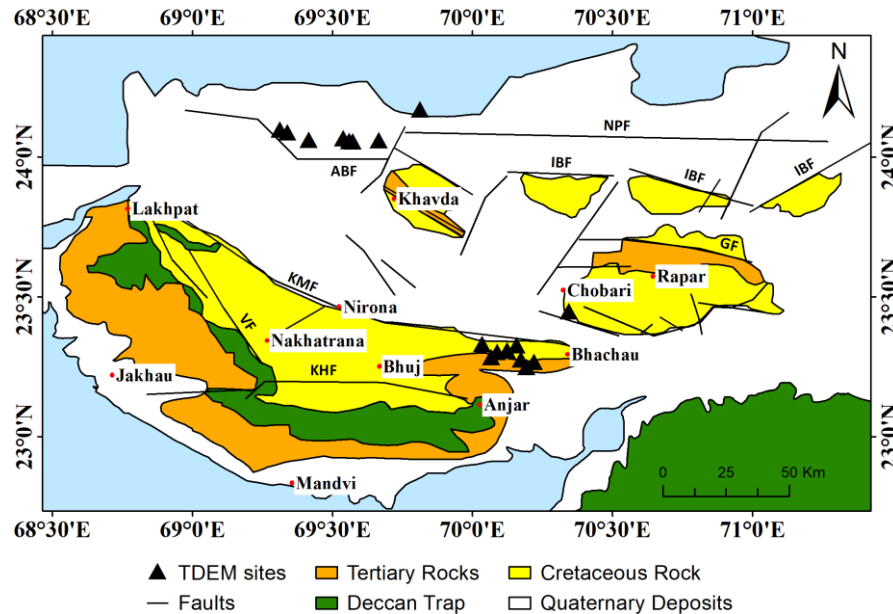


Fig. 6.7: Geological map of Kachchh Basin (after Biswas, 2005) and the TDEM survey points

The selected sites are located on different geological settings, namely, Quaternary sediments, Tertiary sediments and Cretaceous rocks. Data from eight sites, situated on Quaternary sediments, three sites on Tertiary formations and six sites on Cretaceous formations are acquired (Fig. 6.7).

The GDP 32-II data acquisition unit (Zonge, USA) together with a transmitter, generator-powered GGT-30 for larger loops system had been used to conduct the TDEM field survey with 200m and 100 square transmitter loop. The GDP 32-II was positioned at the center of each loop and ferrite-cored antenna was used to take the measurements. Most typical TDEM array is represented by a square loop, in which a trapezoidal (typically square) current waveform is driven. This current induces secondary (eddy) currents within the Earth, the rate of change of which produces an electromotive force (emf) that is picked up by a receiver coil normally located in the loop center. The amount of current injected in the transmitter loop is 9 Amps for all the TDEM sites. For each loop, the transmitter is operated for a sequence of data repetition frequencies ranging from 32 to 1 Hz. In the early and late times, the apparent resistivity is in general noisy and is removed for further inversion process, whenever necessary. The transient decay curves obtained by the survey are used to find out the depth and subsurface resistivity of the basin.

Using robust processing mode, data has been accepted or rejected according to the coherency and outlier limit tests. At most of the sites, good quality transient responses at late times (later recording windows of receiver) up to 100ms have also been obtained, which give considerably deeper information. The apparent resistivity has been computed

from the observed magnetic field (related to induced voltage in the receiver coil and the current injected in the loop).

ISR has used the data recorded at 8, 4, 2 and 1Hz transmitter frequency for one dimensional (1D) inversion based on quality and depth of penetration. The 1-D modelling of the TDEM soundings is performed using STEMINV (Zonge, USA) package which uses an iterating best-fit algorithm to minimize the RMS residuals between the observed and calculated apparent resistivity, to obtain layered-earth resistivity models. After generating the initial model, data points that are either anomalous or could not fit to any earth model due to large error bars are selectively discarded from the voltage vs. time decay curve. After removing the anomalous points, the inversion is re-executed to create the best possible model. The 1-D models of all 17 sites have been considered for the study.

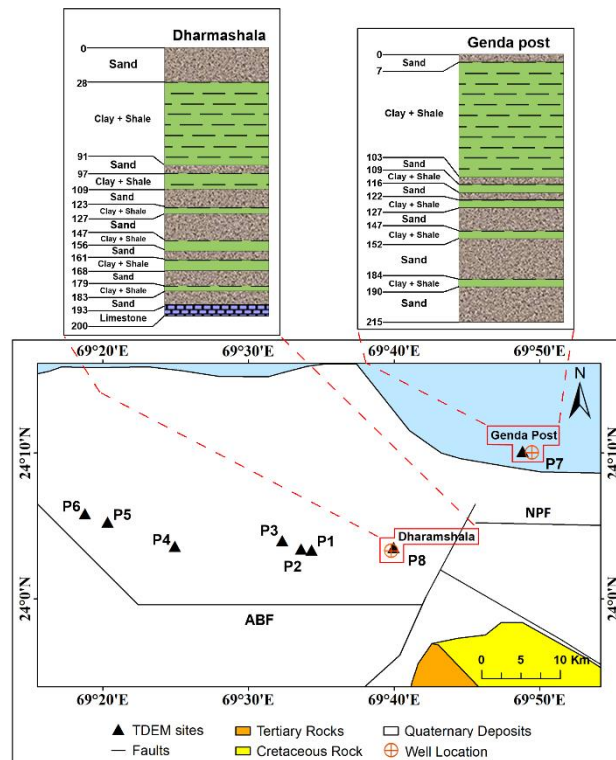


Fig. 6.8: The borehole locations (overlapped on geology of the region) and lithologies in the Great Rann of Kachchh.

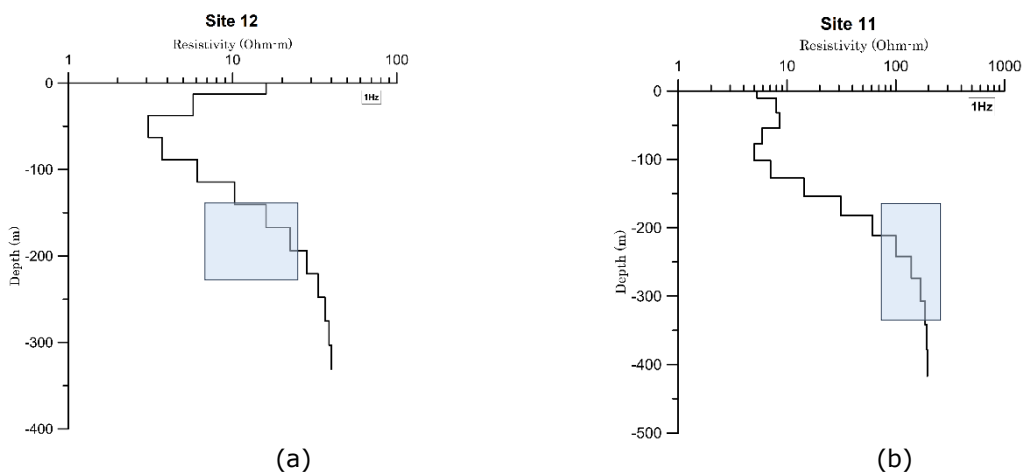


Fig. 6.9: 1D resistivity section generated from TDEM survey (a) at Sukhpar and (b) at Bhujpar village

The area of investigation is covered with Quaternary sediments and two different rock types, Tertiary and Cretaceous. The borehole data of about 200-300m depth is provided by GWRDC for validation purpose. The interpretation of the geophysical data below 200-300m depth is done purely on the basis of lithology suggested in the past literature and resistivity values obtained from the TDEM survey. From the 1D resistivity section generated through TDEM survey in the Great Rann of Kachchh, the Quaternary sediments have been observed down to 150-200m depth (Fig. 6.8) with resistivity of <1 Ohm.m. The high conductivity might be due to the presence of salinity.

In Anjar and Bhachau talukas, the TDEM sites have been sited on two different formations (Tertiary and Cretaceous). Three sites have been acquired on Tertiary formations and six sites on Cretaceous formations. The sites located on Tertiary formations have shown resistivity in the range of 0.01-5 Ohm.m down to a depth of ~450m. The resistivity range at all the three sites indicates presence of Clay/ Shale/ Sand (down to ~450m depth). Presence of fresh water has not been inferred at any site on the Tertiary formation.

The sites located on Cretaceous rocks have shown the first layer with resistivity of 1-10 Ohm.m till ~100m depth, suggesting the presence of Clay/Sand and Shale with Sandstone. At site 2, the first layer of resistivity 10-60 Ohm.m has been observed, inferring the presence of Sandstone followed by a layer of sandstone with saline water at depths >150m. Three sites have shown decreasing trend in resistivity from 1-0.01 Ohm.m below ~100 to 500m depth, indicating the presence of Sandstone with saline water (high conductivity might be due to the presence of salinity). At two sites, the second layer of sandstone with resistivity ~10-100 Ohm.m has been observed at depths >150m and >72m (Fig. 6.9). The presence of good quality ground water is observed at depths of 150-250m (at Sukhpar village) and 200-300m (at Bhujpar village) in Bhachau taluka.

In a nutshell, in the Great Rann of Kachchh area covered with Quaternary sediments, the saline water is found at a very shallow depth. In Anjar and Bhachau taluka, at the sites located on Cretaceous formations, Sandstone (of Cretaceous period) with freshwater has been inferred at a depth of 150-250m at Sukhpar village and 200-300m at Bhujpar village. The potential groundwater zone along with site location has also been given in Table 6.2.

Table 6.2: The potential groundwater zone along with site location

| Sr. No. | Location/ site no | Depth of investigation (in m) | Inferred fresh water/ good quality water zone depth (in m) |
|----------------|---------------------------|--------------------------------------|---|
| 1. | Site 11 (Sukhpar village) | 410 | 150-250 |
| 2. | Site 12 (Bhujpar village) | 340 | 200-300 |

PUBLICATIONS

Published

SCI

- ◆ Ali S. N., Dubey, J., Morthekai, P., Sharma A., Singh R, Prizomwala, S. P. (2019) Climate forcing and initiation of glacier advance during MIS 2 in the North Sikkim Himalaya, India, *Journal of Asian Earth Sciences*, 174, 381-388.
- ◆ Ali S. N., Morthekai, P., Bjpai, S., Phartiyal, B., Sharma A., Quamar MF., Prizomwala, S. P. (2020) Redefining the timing of Tongul glacial stage in the Suru valley, NW Himalaya, India: New insights from luminescence dating, *Journal of Earth System Science*, 129 (16), 1-11.
- ◆ Bulusu, J., Simha, C.P., Arora, K., Rao, K.M. (2019) Statistical Characterisitcs of low latitude Pc4s: Insights from solar wind and IMF parameters, *Advances in Space Research*, doi: 10/1016/j.asr.2020.01.001.
- ◆ Choudhury P., Chopra S., Kamra C., Das A. (2019) New insight into recent earthquake activity in North Cambay basin, western India: Seismological and Geodetic perspectives, *Bulletin of Seismological Society of America* , doi: 10.1785/0120190126.
- ◆ Chouhan, A. K., Choudhury, P. & Pal, S. K. (2020) New evidence for a thin crust and magmatic underplating beneath the Cambay rift basin, Western India through modelling of EIGEN-6C4 gravity data, *Journal of Earth System Science*, 129:64. <https://doi.org/10.1007/s12040-019-1335-y>
- ◆ Chouhan, A. K., Singh, D., Pal, S. K. & Choudhury, P. (2020) Delineation of lineaments in the Cambay rift and surrounding regions of NW India utilizing satellite derived EIGEN6C4 gravity data, *Geocarto International*, doi:10.1080/10106049.2020.1716395.
- ◆ Danda, N., Rao, C. K., Kumar, A., Rao, P. R, & Rao, P. B. V. S. (2020) Implications for the lithospheric structure of Cambay rift zone, western India: Inferences from a magnetotelluric study, *Geoscience Frontiers*, doi: 10.1016/j.gsf.2020.01.014.
- ◆ Das, A., Joseph J., Solanki T., Makwana N. M., Chauhan G., Thakkar M. G. (2020) Climate-tectonic interplay from the dry land fluvial landscape of the Southern Kachchh Mainland, Western India: Insights from new OSL and Sedimentological datasets, *Geological journal* (accepted).
- ◆ Das A., Prizomwala S. P., Solanki T., Chauhan G., Thakkar M. G., Bhatt N. (2019) Relative Assessment of Tectonic Activity along the seismically active Katrol Hill Fault, Kachchh, Western India, *Journal of Geological Society of India*, doi: 10.1007/s12594-019-1287-5.
- ◆ Dwivedi, V. K., Dubey R K., Pancholi, V., Rout, M. M., Singh P., Sairam, B., Chopra, S., Rastogi, B. K. (2019) Multi criteria study for Seismic Hazard Assessment of UNESCO world heritage Ahmedabad city, Gujarat, Western India, *Bulletin of Engineering Geology & Environment*, doi:10.1007/s10064-019-01644-6.
- ◆ Gahalaut V. K., Gahalaut K., Dumka R. K., Choudhury P., Yadav R. K. (2019) Geodetic Evidence of High Compression Across Seismically Active Kachchh Paleorift, India, *Tectonics*, doi: 10.1029/2019TC005496.
- ◆ Gupta, S., Singhroy, P.N., Yadav, R.K., Catherine, J.K., Burgmann, R., Gahalaut, V.K., (2019) Anomalous transients in GPS measurements due to induced changes in local site conditions. *Journal of Earth System Science*, 128:186.
- ◆ Joshi, V. (2019) Crustal velocity models retrieved from surface wave dispersion data for Gujarat region, Western Peninsular India, *Earth Sci. Res. J.*, 23(2), 147-155.
- ◆ Joshi, V., Chopra, S. and Kumar, S. (2020) A local magnitude scale ML for Saurashtra horst; An active intraplate region, Gujarat, India, *Journal of Earth System Science*, 129 114, 1-9.

- ◆ Kandregula, R.S., Kothyari, G.C., Swamy, K.V. and Rawat S. (2019) Quantitative assessment of tectonic activity in Northern Saurashtra, Western India, the journal of India Geophysical Union, 23 (6), 542-558.
- ◆ Kumar N., Mohan K., Dumka R. K., Chopra S. (2020) Soft sediment deformation structures in Quaternary sediments from Dadra and Nagar Haveli, Western India, Journal of the Geological Society of India (accepted).
- ◆ Modi R., Mohan K. (2019) Rapid Visual Screening of RC frame buildings in 2001 Bhuj earthquake affected Rambaug area of Ahmedabad, Gujarat, Jour of Ind Geoph Union, 23(2), 143-151.
- ◆ Mahesh, P., Sateesh, A. Kamra, C., Kumar, S., Chopra, S., Kumar, M.R. (2020) Earthquake swarms in Palghar district, Maharashtra, Deccan Volcanic Province in Current Science, 118 (5), 701-704.
- ◆ Panda, D., Kundu, B., Gahalaut, V.K., Burgmann, R., Jha, B., Asaithambi, R., Yadav, R.K., Vissa, N.K., and Bansal, A.K. (2020) Reply to "A warning against over-interpretation of seasonal signals measured by Global Navigation Satellite System". Nature Communications, 11:1376.
- ◆ Patel, P., Mohan, K., Chaudhary, P. (2020) Estimation of sediment thickness (including Mesozoic) in the western central part of Kachchh Basin, Gujarat (India) using Magnetotellurics. Journal of Applied Geophysics, 103943.
- ◆ Roy S., K., Takeuchi N., Srinagesh D., Kumar M. R., Kawakatsu, H. (2019) Topography of the western Pacific LLSVP constrained by S-wave multipathing, Geophysical Journal International, 218(1), 190-199.
- ◆ Sahoo S. K., Rao K. M., Barman C., Udaya Laxmi G. (2020) Identification of Earthquake precursors in soil radon-222 data monitored at Badargadh, Kutch, Gujarat, India using Empirical Mode Decomposition based Hilbert Huang Transform, Journal of Environmental Radioactivity (accepted).
- ◆ Saikia D., Kumar M. R., Singh A. (2020) Palaeoslab and plume signatures in the mantle transition zone beneath Eastern Himalaya and adjoining regions Geophysical Journal International, 221(1), 468-477.
- ◆ Saikia S., Baruah S., Chopra S., Gogoi B., Singh U. K., Bharali B. (2019) An appraisal of crustal structure of Indo-Burmese subduction zone, Journal of Geodynamics, 127, 16-30.
- ◆ Sairam B., Singh A.P., Patel V., Chopra S., Kumar M.R. (2019) VS30 mapping and site characterization in the seismically active intraplate region of Western India- implications for risk mitigation, Near Surface Geophysics, 17(5), 533-546.
- ◆ Sateesh, A., Mahesh, P., Singh, A.P., Kumar, S., Chopra, S., Kumar, M.R. (2019) Are Earthquake Swarms in South Gujarat, Northwest Deccan Volcanic Province of India Monsoon induced? *Environmental earth sciences*, DOI: 10.1007/s12665-019-8382-1.
- ◆ Shreyasvi C., Venkataramana K., Chopra S. (2019) Local site-effect incorporation in probabilistic seismic hazard analysis- A case study from southern peninsula, an intraplate region, Soil Dynamics and Earthquake Engineering, 123, 381-398.
- ◆ Simha C. P., Natarajan, V., Rao K. M., (2019) Pre-earthquake Atmospheric and Ionospheric anomalies before Taiwan earthquake (M 6.4) on 6th February 2018, Geomagnetism and Aeronomy (accepted).
- ◆ Singh A.P., Kumar M. R., Pandey A., Roy K. S. (2019) Investigation of spatial and temporal variability of site response in the Arunachal Himalaya using ambient seismic noise and earthquake waveforms, *Near Surface Geophysics*, DOI: 10.1002/nsg.12053.
- ◆ Singh C., Biswas R., Jaiswal N., Kumar M. R. (2019) Spatial variations of coda wave attenuation in Andaman-Nicobar subduction zone, Geophysical Journal International, 217(3), 1515-1523.
- ◆ Solanki, A., Mohan, K. (2019) The scenario based seismic risk assessment in Gandhinagar city (Gujarat), India, accepted in J. Ind. Geophys. Union, 23 (3), 223-237.
- ◆ Talukdar R., Kothyari G. C., Pant C. C. (2019) Evaluation of neotectonic variability along major Himalayan thrusts within the Kali River basin using geomorphic

markers, Central Kumaun Himalaya, India, Geological Journal, doi: 10.1002/gj.3452.

- ◆ V. Sharma, M. Wadhawan, N. Rana, K. M. Sreejith, R. Agrawal, C. Kamra, K. S. Hosalikar, K. V. Narkhede, G. Suresh, V. K. Gahalaut (2020) A long duration non-volcanic earthquake sequence in the stable continental region of India: The Palghar swarm, *Tectonophysics* 779, 228376.
- ◆ Yadav, R.K., Gahalaut, V. K., Gautam, P., Jayangondaperumal, R., Sreejith, K.M., Sati, S.P., Bansal, A.K., Agrawal, R., Singh, I., Vivek, J., (2020) Geodetic monitoring of a slow-moving landslide in the Garhwal Himalaya. *Himalayan Geology*, 41(1), 126-138.

Non-SCI

- ◆ Jayangondaperumal, R., Mishra, R.L., Priyanka, R.S., Yadav, R.K., Mohanty, D.P., Pandey, A., Singh, I., Anil, A., and Dash, S. (2020). Active Tectonic of Himalaya, Rift Basins in Central India and those Related to Crustal Deformation at Different Time Scales. *Proceedings of the Indian National Science Academy*, 86(1), pp-445-458.
- ◆ Joshi S., Rao K. K. (2019) Influence of Solar wind parameters on equatorial magnetic observatories during intense Geomagnetic storms of the year 2015, *Journal of Scientific Research*.
- ◆ Sahoo S. K., Rao K. M. (2019) Soil Radon Emanation and its dependence on Meteorological Parameters in Kachchh Region, Gujarat, India, *Journal of Xi'an University of Architecture & Technology*, ISSN NO: 1006-7930.
- ◆ Srijayanthi, G. and Kumar, M. R. (2019). Seismicity, lithospheric structure and mantle deformation in the Andaman Nicobar Subduction Zone. In: Ray J., Radhakrishna M. (eds) *The Andaman Islands and Adjoining Offshore: Geology, Tectonics and Palaeoclimate*, Society of Earth Scientists Series. 107-136, Springer, Cham. https://doi.org/10.1007/978-3-030-39843-9_6.
- ◆ Srijayanthi, G., Kumar, M. R. and Gahalaut, V. K. (2020). A review of seismological research in India during the past five years (2015-2019), *Proc Indian Natn Sci Acad*, 86(1), 531-552.

Under review/ communicated

- ◆ Chouhan A.K. (2019) Structural fabric over the seismically active Kachchh rift basin, India: Insight from world gravity model 2012, *Environmental Earth Science*.
- ◆ Chouhan, A.K., Singh, D. & Chopra, S. (2019) Structural interpretation over the epicentre zone of 1819 Allah-Bund earthquake, North-western India in an intraplate setup using gravity data, *Journal of Earth System Science*.
- ◆ Das A., Joseph J., Solanki T., Makwana N. M., Chauhan G., Thakkar M. G. (2019) Climate-tectonic interplay from the dry land fluvial landscape of the Southern Kachchh Mainland, Western India: Insights from new OSL and Sedimentological datasets, *Geological journal*.
- ◆ Das A., Vedpathak C., Sodhi A., Makwana N., Phartiyal B., Agnihotri R., Joseph J., Prizomwala S. P., Kumar M. R., Chopra S. (2019) Did the Meghalayan sea stand fluctuations play a role in deurbanization of the coastal Harappan settlers? *Nature Scientific Reports*.
- ◆ Kumar, V., Chopra, S., Choudhury, P. and Kumar, D., (2019) Estimation of near surface attenuation parameter Kappa (κ) in Northwest and Northeast Himalaya region, *Soil Dynamics and Earthquake Engineering*.
- ◆ Kundreja R. S, Kothyari, G. C., Pancholi, V., Swami, K. V., Chauhan G. (2019) Assessment of seismic hazard by employing river gradient length and geomorphic anomaly technique: A case study from the intraplate Kachchh region, Western India, *Geomorphology*.

- ◆ Mohan, K., Dugar, S., Pancholi, V., Dwivedi, V., Chopra, S., Sairam, B., Micro-seismic hazard assessment of Ahmedabad City, Gujarat (Western India) through near-surface characterization/soil modelling, *Bulletin of Earthquake Engineering*.
- ◆ Nagar, M., Gayatri, P. K., Nikam, R., Chouhan, A. K., Perugu, M., Chopra, S. (2019) Magnetotellurics evidence of trapped fluids beneath the seismogenic zone of Anjar earthquake (M_w 6.0), Kachchh intraplate region, northwest India, *Tectonics*.
- ◆ Pancholi, V., Bhatt, N.Y., Chopra, S. and Singh P. (2019) Multi-criteria approach using GIS for macro-level seismic hazard assessment of Kachchh intraplate region, Gujarat, Western India– First step towards earthquake disaster mitigation, *Journal of Earth System Science*.
- ◆ Pancholi, V., Bhatt, N.Y., Dwivedi, V. K., Choudhury P. Chopra, S. (2019) Estimation of the Liquefaction potential index for the capital city of Gujarat state, Western India, *Geotechnical and Geological Engineering*.
- ◆ Prizomwala, S.P., Makwana, N. and Gandhi, D. (2020) From remote sensing to coastal processes: Odds of finding a palaeotsunami deposit (Gulf of Kachchh, Western India), *Geo Marine Letters*.
- ◆ Singh, A.P., Sairam, B., Pancholi, V., Chopra, S., Kumar, M.R. (2019) Delineation of thickness of intrabasaltic rocks beneath the Deccan Volcanic province of western India through Microtremor analysis, *Bulletin of Earthquake Engineering*.
- ◆ Tandon, A., Prizomwala, S.P. and Yadav, G. (2019) Testing the sensitivity of Relative Index of Active Tectonics from areas experiencing variable uplift: An example from the Himalayan Frontal Thrust in the NW and NE Himalayas, *Geomorphology*.
- ◆ Tandon, A., Prizomwala, S.P., Yadav, G. (2020) Assessing the along strike variability in tectonic activity along the northwest and northeast segments of the Himalayan Frontal Thrust (India) using the Relative Index of Active Tectonics, *Geological Journal*.
- ◆ Thakkar, M.G., Kothiyari, G.C., Chauhan, G. and Lakhote, A. (2019) Tectonic implications on controlled dimensions and fluid dynamics of Bedrock Gorge, Kachchh: Western India, *Current Science*.

Technical Reports

- ◆ Final Report "Site Specific Seismic study to develop Site Specific Response Spectrum at Khavda windmill site, Kachchh (Gujarat)", Project PI: Kapil Mohan, Project Coordinator: Sumer Chopra, Co-PI: Naveen Kumara, Project Coordinator: Madan Mohan Raut and Shruti Dugar, ISR Technical Report No. 131, Submitted to M/s. Adani Green (Gujarat) Pvt. Ltd. in April 2019.
- ◆ Final Report "Geophysical survey for the Groundwater evaluation at the proposed Centers of Excellence for different horticultural crops at Majivana village, District Porbandar (Gujarat)" by Kapil Mohan, Pruthul Patel, Akash Solanki, Naveen Kumar and Sumer Chopra, April-May 2019, ISR Technical Report No. 132 submitted to Gujarat Horticulture Mission.
- ◆ Report on "Phase-II, Delineation of Freshwater layer at the selected sites in the Lakhpat, Nakhatrana, Bhuj (Banni area), Mandvi and Abdasa Talukas of Kachchh (Gujarat) using Time Domain Electromagnetic Survey" by Kapil Mohan, Pruthul Patel, Mehul Nagar, Akash Solanki, Dilip Kumar, Naveen Kumar and Sumer Chopra, ISR Technical Report no. 133, submitted to Gujarat Water Resource Development Corporation (GWRDC) in May 2019.
- ◆ Final Report "Operational definition of seismic risk and intervention techniques for strategic buildings: an integrated system on HPC platform" by Kapil Mohan, Neha Tanwar and Sumer Chopra, ISR Technical Report No.134, submitted to OGS – National Institute of Oceanography and Experimental Geophysics, Seismological Research Centre, Udine, Italy in May 2019.
- ◆ A.P. Singh, ISR Technical Report No.135, A Report on Feasibility Study of Low Frequency Passive Seismic (LFPS) Survey in and Around Dholka Village, Ahmedabad.

- ◆ A.P.Singh, Harsh Limbachiya, Madan Mohan Rout, Ketan Singha Roy, Sateesh Alla (2019) A Preliminary Report on Feasibility Study of Low Frequency Passive Seismic (LFPS) Survey in and Around Digas Village, Bharuch, PP 35, ISR Technical Report No. 136, submitted to GSPC, Gandhinagar
- ◆ Tarun Solanki, S.P. Prizomwala and Sumer Chopra (2019) A technical report on replenishment study for Avidha ordinary sand mining project, ISR Technical Report No. 137 submitted to Shri Dhirubhai Manjibhai Hirapara.
- ◆ Pruthul Patel, Dilip Singh Kushwaha, Naveen Kumar, Kapil Mohan and Sumer Chopra, Time Domain Electromagnetic (TDEM) survey to delineate freshwater zone at Regional Science Museum, Patan, ISR Technical Report no. 138. Submitted to GUJCOST, Gandhinagar in August 2019.
- ◆ P. Mahesh, Santosh Kumar, A.P. Singh, M. Ravi Kumar & Sumer Chopra (2019) A report on Earthquake data processing and interpretation of MEQ data collected during Jan. to Dec. 2018 for study of Seismogenic sources around the Subansiri lower H.E. project, NHPC Ltd., ISR Technical Report No. 139, submitted to NHPC Ltd.
- ◆ Kapil Mohan, Pruthul Patel, Dilip Singh Kushwaha, Naveen Kumar and Sumer Chopra, Phase-III, Delineation of Freshwater layer at the selected sites in the Great Rann of Kachchh, Anjar and Bhachau Talukas of Kachchh (Gujarat) using Time Domain Electromagnetic Survey”, ISR Technical Report no. 140. Submitted to Gujarat Water Resources Development Corporation (GWRDC) in September 2019.
- ◆ Dr. A.P. Singh, Mr. Gaurav Dave, Mr. Ketan Singha Roy, Dr. Madan Mohan Rout, Mr. Yash Vyas, Mr. Jay Pandit, Mr. Harsh Limbachiya, Dr. Santosh Kumar, Dr. Sumer Chopra and Dr. M. Ravi Kumar, “A Report on Low Frequency Passive Seismic [LFPS] Surveys in Mansa, Jotana and Linch, Cambay Basin, Gujarat State” [SAP Nos. 9010029833], ISR Technical Report no. 141. Submitted to Oil and Natural Gas Corporation, Baroda.
- ◆ Dr. A.P. Singh, Mr. Harsh Limbachiya, Mr. Sateesh Alla, Mr. Ketan Singha Roy, Dr. Madan Mohan Rout, Dr. Sumer Chopra and Dr. M. Ravi Kumar, “A Report on Low Frequency Passive Seismic Survey in Dholka (Ahmedabad) and Digas (Bharuch)”, ISR Technical Report no. 142. Submitted to Gujarat State Petroleum Corporation, Gandhinagar.
- ◆ Srijayanthi, G., Chopra, S., Santosh Kumar, Harsh Limbachiya and Kumar, M. R. (2019). Report on recent seismic activity in Jamnagar district, Gujarat. ISR Technical Report No. 143, Institute of Seismological Research, Department of Science and Technology.
- ◆ G. Srijayanthi, P. Mahesh, Santosh Kumar, Kunjal Parmar and Sumer Chopra (2019). Earthquake Data Processing and Interpretation of MEQ Data Collected During January to June 2019 for the Study of Seismogenic Sources Around the Subansiri Lower Hydro Electric Project, NHPC Ltd. Technical Report No. 144, Institute of Seismological Research. December 2019.
- ◆ 2nd Annual progress report of the ISR-ISRO collaborative project titled “Study of Geothermal processes in Gujarat using Remote Sensing and Geophysical techniques: A potential to Martian analogue” has been submitted in April 2019 (PI: Dr. Sumer Chopra and Co-PI: Dr. Kapil Mohan).

NOTABLE EVENTS

Awards/Recognition

- ◆ Dr. Nisarg Bhatt received his Ph.D degree (Geology) on September 29, 2019 from M G Science Institute, Gujarat University.
- ◆ Dr. Peush Chaudhary received his Ph.D degree (Geophysics) on November 13, 2019 from Kurukshetra University.
- ◆ Dr. Tarun Solanki received his Ph.D degree (Geology) on November 21, 2019 from Gujarat University.
- ◆ The study "GPS measurements of deformation caused by seasonal filling and emptying cycles of four hydroelectric reservoirs in India (Dumka et al., 2018, BSSA)" appeared in the science snapshot of UNAVCO.

Thesis submission

- ◆ Mr. A. Sateesh submitted his Ph.D. thesis entitled "Nature of Seismicity and its relation to velocity structure in diverse tectonic environments of North-West Deccan Volcanic province" to Osmania University, Hyderabad. Joint supervisor: Dr. P Mahesh.
- ◆ Ms. Jyoti Sharma submitted her PhD thesis entitled "Imprints of Plume-Lithosphere Interaction Beneath the Northwestern Deccan Volcanic Province from Rayleigh and Love Wave Tomography" at Department of Applied Geophysics, Indian Institute of Technology (Indian School of Mines), Dhanbad, Jharkhand. Joint supervisor: Dr. M. Ravi Kumar.

Mou's signed

- ◆ An MoU for scientific collaboration was signed between ISR, Gandhinagar and RK University, Rajkot on September 18, 2019
- ◆ An MoU between ISR and SSNNL was signed in February 2020 for five years (2020-24) to carry out the seismological studies in and around the Sardar Sarovar Project, at a cost of Rs. 1509.14 lakhs.

Visits Abroad

- ◆ Dr. G. Srijayanthi attended the IUGG conference at Montreal from July 8 to 18, 2019.
- ◆ Jyoti Sharma attended the advanced workshop on Earthquake Fault Mechanics: Theory, Simulation and Observations, held at the International Centre for Theoretical Physics (ICTP), Trieste, Italy during September 2-14, 2019 and presented her research work "Radially Anisotropic Shear Wave Velocity Structure Beneath the Northwestern Deccan Volcanic Province".
- ◆ Dr. Sumer Chopra attended the Expert Meeting for Establishment of a Regional Working Group and Working Process between North West Indian Ocean Countries on Risk Knowledge during September 3-6, 2019 at Muscat, Oman as a Tsunami expert from western India.

Meetings/ conferences attended/ papers presented

- ◆ Mr. Ketan S. Roy delivered a talk on "The processing steps of LFPS software" at a workshop titled "Low Frequency Passive Seismic Survey", held at ONGC, Vadodara.
- ◆ Dr. Kapil Mohan has attended a meeting with the representative of M/s Adani Greens Ltd., on seismic hazard assessment of Khavda windmill site on April 18, 2019.

- ◆ Dr. Rajeev Yadav attended the International Workshop on “Extreme events and climate change in the Himalaya” at Indian Institute of Technology Mandi, Himachal Pradesh during April 18-20, 2019 and presented a paper on “Strain budget of Northwest Himalaya from GPS measurements”.
- ◆ Dr. Rajeev Yadav attended a special course work on “Microwave Remote Sensing Applications in Geosciences with Emphasis on Surface Deformation Studies” at Indian Institute of Remote Sensing, Dehradun, during April 22-26, 2019.
- ◆ Rakesh K Dumka, D. SuriBabu and P. Narain, attended a special course on “Microwave Remote Sensing Applications in Geosciences with Emphasis on surface Deformation studies” during 22-27 April 2019 at IIRS Dehradun.
- ◆ Dr. A. P. Singh delivered a lecture on H/V ratio measurements tests: Codal Provisions and current state of practice in the Workshop (TC102) on “Ground Property Characterization from In-Situ Tests on April 26, 2019 at Indian Institute of Science (IISc), Bangalore.
- ◆ Mr. Naveen Kumar has attended the project progress meeting of the project titled “Seismic Hazard Assessment and salinity ingression monitoring for the proposed Barrage across River Narmada near Bhadbhut, Distt. Bharuch” on May 28, 2019.
- ◆ Dr. A.P.Singh delivered a lecture in a Workshop on “Low Frequency Passive Seismic (LFPS) for petroleum exploration” on June 3, 2019 at ONGC, Vadodara.
- ◆ Dr. Kapil Mohan has presented proposal for the Seismic Hazard assessment of Windmill Park at Khavda on June 13, 2019 at the office of M/s Adani Green (Gujarat) Pvt. Ltd. at Adani Shantigram, Ahmedabad.
- ◆ Dr. P. Mahesh, attend the Indo-Norway project meeting during June 14-15, 2019 and delivered a talk on “The Gujarat Seismic Network, Seismicity and Seismogenesis”.
- ◆ Dr. Kapil Mohan has attended National field workshop on Bicentenary commemoration of 1819 Intra-plate Allah Band earthquake of Kachchh Basin: Post Chronicle and future opportunities during June 15-16, 2019, organized by KSKV Kachchh University and ISR Gandhinagar.
- ◆ Dr. Sumer Chopra delivered a keynote address on “Geophysical investigations in Allah-Bund region” in National field workshop on Bicentenary commemoration of 1819 Intra-plate Allah Band earthquake of Kachchh Basin: Post Chronicle and future opportunities during June 15-16, 2019, organized by KSKV Kachchh University and ISR Gandhinagar.
- ◆ Tarun Solanki attended national field workshop on “Bicentenary Commemoration of 1819 Intra-Plate Allah Band Earthquake of Kachchh Basin: Past Chronicle and Future Opportunities” organized by K.S.K.V. Kachchh University, Bhuj, Kachchh, during June 15-16, 2019.
- ◆ Dr. Girish Kothiyari attended two days field workshop on Allah Bund earthquake, during June 15-16, 2019, jointly organised by KSKV Kachchh University and ISR Gandhinagar.
- ◆ Dr. Sumer Chopra was invited by NDRF for attending a kickoff meeting on delivering lecture in National Security Strategy meeting conducted by Ministry of Home Affairs, Govt. of India on June 20, 2019.
- ◆ Dr. Kapil Mohan has delivered an expert lecture on “Seismic Microzonation of Gujarat” in a training programme on DRM inclusion in WASH and Health Institutions (Structural/Non-structural Safety) on June 27, 2019 at GIDM, Gandhinagar.
- ◆ Dr. Sumer Chopra was invited by Ministry of Home Affairs, Govt. of India for attending and delivering lecture in National Security Strategy meeting at Vigyan Bhawan during June 27-28, 2019.
- ◆ Dr. Sumer Chopra was invited as an external examiner for PhD viva of a student of IIT, Roorkee on July 8, 2019.
- ◆ Dr. G. Srijayanthi attended the IUGG conference at Montreal from July 8 to 18, 2019.
- ◆ Dr. A. P. Singh delivered a lecture on Low frequency Passive Seismic Attributes in Hydrocarbon Reservoirs Detection and Characterization and trained the ONGC personnel during a workshop on Low Frequency Passive Seismic (LFPS) for

petroleum exploration on July 26, 2019 at Oil Natural Gas Corporation (ONGC), Jorhat, Assam.

- ◆ Sh. Ketan Singha Roy delivered a talk on Processing of LFPS data in the workshop on "Low Frequency Passive Seismic Survey" at ONGC, Jorhat, Assam.
- ◆ Peush Chaudhary presented a paper titled "Characterisation of Narmada North Fault in the western part of Narmada Basin using Magnetotellurics" in the 24th International Conference of International Academy of Physical Sciences (CONIAPS XXIV) held at CCS University, Meerut (U.P.) during August 9-11, 2019.
- ◆ Dr. Sumer Chopra attended the RDC meeting of Gujarat University on August 13, 2019.
- ◆ Jyoti Sharma attended the advanced workshop on Earthquake Fault Mechanics: Theory, Simulation and Observations, held at the International Centre for Theoretical Physics (ICTP), Trieste, Italy during September 2-14, 2019 and presented her research work "Radially Anisotropic Shear Wave Velocity Structure Beneath the Northwestern Deccan Volcanic Province" as a Poster.
- ◆ Dr. A. P. Singh delivered a lecture and training on microtremor measurements and its application to seismic risk assessment at Department of Geophysics, Banaras Hindu University, Varanasi on September 13, 2019
- ◆ Dr. Kapil Mohan has attended a meeting with C.E.(K-1) & A.S on September 13, 2019 at Kalpasar Department regarding establishing a network of eight seismological observatories around the Kalpasar Project and delivered a presentation on Geophysical Surveys for Dams to newly appointed engineers of the Kalpasar department.
- ◆ Mr. Peush Chaudhary and Mr. Pruthul Patel have attended a training course titled "Near Surface Shallow Seismic Techniques-Applications", conducted by National Geophysical Research Institute (NGRI) Hyderabad, during September 16-25, 2019.
- ◆ Rakesh K Dumka attended a conference "Climate, water and Environment" organised by Humbolt House Uttarakhand and Humbolt Foundation Germany and presented a paper "GPS and InSAR derived Crustal deformation Study of Kachchh, western India" during September 25-28, 2019, at Nainital.
- ◆ D. Suri Babu attended a conference "Climate, water and Environment" organised by Humbolt House Uttarakhand and Humbolt Foundation Germany and presented a poster "GPS derived TEC anomaly towards western part of India" during September 25-28, 2019, at Nainital.
- ◆ Dr. Kapil Mohan has attended the 3rd Doctoral Committee review meeting of a research scholar (Ms. Mehta Payal), Deptt. of Civil Engineering, Pandit Deen Dayal Petroleum University on September 30, 2019.
- ◆ Dr. Sumer Chopra was invited as member of committee to select specialists at SAARC IU, GIDM, Gandhinagar.
- ◆ Dr. Santosh Kumar inspected two large dams of the state namely Ukai, and Shetrunji as a member of Dam Safety Review Panel under DRIP program of GoI. The recommendations on seismic instrumentation, site specific seismic hazard assessment, and geophysical investigations have been submitted.
- ◆ C.P.Simha has given a poster presentation on "Local Trend Analysis of Irregular pulsations (Pi2:6-25 mHz) at low latitude Station of Desalpar, Kachchh. Gujarat", Federation of Indian Geosciences Associations 2nd Triennial Congress on Geosciences for Sustainable Development Goals during 13-16 October 2019 at Hyderabad
- ◆ Shivam Joshi has given a poster presentation on "Pre-seismic ULF electromagnetic emissions for a moderate earthquake on 19th June 2012 (M 5.1) in Bhuj epicentral region, Gujarat, India", Federation of Indian Geosciences Associations 2nd Triennial Congress on Geosciences for Sustainable Development Goals during 13-16 October 2019 at Hyderabad
- ◆ Dr. Santosh Kumar visited Kadana dam from 15th -18th Oct 2019 as a member of Dam Safety Review Panel (DSRP) under Dam Rehabilitation and Improvement (DRIP) Programme. A report regarding the seismic instrumentation, and

reassessment of the site specific seismic hazard needed for the dam has been submitted to the project authorities.

- ◆ Sushanta Ku Sahoo has given an oral presentation on "Influence of Meteorological Parameters on the Soil radon (Rn^{222}) emanation in Kutch, Gujarat, India", National conference on "Solid State Nuclear Track Detectors and their Applications (SSNTD-2019)" during 18th-20th October, 2019 at Khalsa College, Amritsar, Punjab
- ◆ Sushanta Sahoo has given a poster presentation on "Empirical Mode Decomposition based Hilbert Huang Transform on soil-radon (Rn^{222}) data of Badargarh, Kutch, Gujarat, India: Identification of Earthquake Precursors", National conference on "Solid State Nuclear Track Detectors and their Applications (SSNTD-2019)" during 18th-20th October, 2019 at Khalsa College, Amritsar, Punjab
- ◆ Dr. Santosh Kumar visited Dharoi dam from 13th to 16th Nov 2019 as a member of Dam Safety Review Panel under Dam Rehabilitation and Improvement (DRIP) Programme. A report regarding the Seismic instrumentation, reassessment of the site specific seismic hazard, and geophysical investigations required for the dam has been submitted to the project authorities.
- ◆ Dr. Rakesh Dumka attended the PAMC meeting on AFM and presented progress of the project entitled "Crustal deformation analysis along Katrol Hill Fault (KHF) in the central part of mainland Kachchh" held at ISR, Gandhinagar on 16 November 2019.
- ◆ Ms. Aashima Sodhi visited IUAC during 25 Nov- 1 Dec 2019. The objective of the visit was to be acquainted with the AMS technique, which is often used as one of the chronological techniques. The Foraminifer and shells were picked from the respective samples (total 5 samples) at ISR, and the AMS dating of the same was further carried out at IUAC.
- ◆ Peush Chaudhary and Prothul Patel attended the training workshop on Fundamentals of Ground Based Transient Electro-Magnetic (TEM) Data Processing and Inversion, held at Delhi on November 27, 2019. This training workshop was jointly organized by the Aqua Foundation (AF) Academy and the European Association of Geoscientists & Engineers (EAGE) and mainly focused on the application of TEM data by using the software packages SPIA and Aarhus Workbench.
- ◆ Dr. Santosh Kumar visited Panam dam from 6th to 9th Dec 2019 as a member of DRIP-DSRP. A report on the seismic instrumentation in and around dam, reassessment of the site specific seismic hazard and geophysical investigations required for the dam has been submitted to the project authorities.
- ◆ Mr. Tarun Solanki attended the workshop on Luminescence Dating: Methodology and Applications, during 7-11 December 2019, held in NGRI, Hyderabad.
- ◆ Vinay Kumar Dwivedi and Pawan Kumar Singh attended an International workshop on Advance Seismology, Seismic Hazards & Earthquake Engineering: Theory, Simulation and observation, during December 12-17, 2019 at Department of Civil Engineering, National Institute of Technology, Agartala, Tripura.
- ◆ Dr. Pallabee Choudhury delivered a talk on "Assessment of seismic hazard: few case studies" in a one day workshop organized for the civil engineers with focus on dams and civil structures, at ISR on 13 December 2019.
- ◆ Peush Chaudhary attended the one day workshop held at ISR on 13 December 2019 and presented the preliminary results of Electrical resistivity Tomography (ERT) conducted at Ukai Dam site.
- ◆ Mr. D. Suri Babu presented a poster during the 8th SAC meeting of ISR, held on 19 December 2019.
- ◆ Chaitnya Kumar presented a poster titled "Discrimination between earthquakes and blasts" in the 8th meeting of the Scientific Advisory Committee of the ISR, held on 19 December 2019.
- ◆ Peush Chaudhary presented a poster titled "Magnetotelluric Investigation of the western part of Narmada Son Lineament zone, central western India" in the 8th meeting of the Scientific Advisory Committee of the ISR, held on 19 December 2019.

- ◆ Dr. Santosh Kumar visited Hiran-1 and Machchundri dams of Junagarh district, as a member of the DSRP under DRIP from 19th – 22th Dec 2019. A report on Seismic instrumentation reassessment of the site specific seismic hazard and Geophysical investigations was submitted to the project authorities.
- ◆ Ms. Charu Kamra visited CSIR –NGRI, Hyderabad for a training on “Local, Regional and Teleseismic earthquake data processing and interpretation” during 3-5 Feb 2020.
- ◆ Dr. Pallabee Choudhury delivered two Invited Lectures in a National Seminar on "Earthquake Hazards: Education, Preparedness, Mitigation and Management", organized by Environmental Watch and Management institute during 6-8 February 2020, held at North-Eastern Hill University (NEHU), Shillong.
- ◆ Ms. Aashima Sodhi attended a 10 days workshop on “Advanced Training Program on Analytical Geochemistry”, held at NGRI, Hyderabad, during 10-19 February 2020.
- ◆ Mr. Sushanta Ku Sahoo has given an oral presentation on “Assessment of Soil gas radon (Rn222) emission and transportation in Kachchh, Gujarat, India: Its dependence on Meteorological parameters”, National Seminar on “Advances in Earth Sciences for Exploration and management of Natural Resources” during 27th & 28th February 2020 at Department of Geophysics, Osmania University, Hyderabad.
- ◆ Dr. Santosh Kumar visited Navagam dam, Kevadia Colony from 16 to 18 March 2020 as a member of 2nd Dam Safety Review Panel (DSRP), SSNNL.

Distiguated Visitors

- ◆ Shri B.K. Mishra, Senior Advisor (Technical), Bihar State Disaster Management Authority (BSDMA) visited ISR on April 11, 2019.
- ◆ Dr. V.M. Tiwari (Director, NGRI), Dr. Vineet Gahalaut (Director, NCS), Prof. D.C. Srivastava (Head, Earth Science Dept., IIT Roorkee) and Dr P. K. Khan (Professor, ISM- Dhanbad) visited ISR to participate in 8th Scientific Advisory Committee (SAC) meeting of ISR on 16.11.2019
- ◆ Dr. Biswajit Mandal, Sr. Scientist, NGRI presented the progress report of the project "Sub-surface imaging of the Kutch region using DSS data" on 22.11.2019

Visit of Student Groups

- ◆ A group of 18 students of 8th Semester B.E. Civil Engineering department with two faculty members from SPCE Engineering College, Bakrol, Vallabh Vidhyanagar, Gujarat visited ISR on April 3, 2019.
- ◆ A group of 60 students of 5th and 7th Sem B.E. Civil Engineering department with their three faculty members from R.K. University, Rajkot- Bhavnagar Highway, Rajkot, Gujarat visited ISR on July 29, 2019
- ◆ A group of 54 students of 9th standard with their two faculty members from Jamnabai Narsee School, GIFT City, Gandhinagar visited ISR on August 8, 2019
- ◆ A group of 30 students of faculty of Technology, CEPT University, Ahmedabad with their two faculty members visited ISR on August 14, 2019
- ◆ A group of 27 students of 1st and 3rd Sem. M.Tech. Civil Engineering Department along with two faculty members from Ganpat University, Mehsana visited ISR on August 30, 2019.
- ◆ A group of 50 students of 7th Sem. B.Tech. Civil Engineering Department along with two faculty members from Ganpat University, Mehsana visited ISR on August 31, 2019.
- ◆ A group of 35 students of Civil Engineering Department along with two faculty members from Marwadi University, Rajkot visited ISR on September 05, 2019.

- ◆ A group of 54 students of B.E. Civil Engineering Department along with their 02 faculty member from G.H. Patel College of Engg. and Tech., Vallabh Vidhyanagar visited ISR on 04/10/2019.
- ◆ A group of 29 students of 1st and 3rd Sem. M.Tech. Civil Engineering Department along with their 02 faculty member from V.V.P. Engineering College, Rajkot visited ISR on 27/01/2020
- ◆ A group of 17 students of 4th Sem. M.E. Civil Engineering Department along with their 02 faculty member from SAL Institute of Technology and Engineering Research, Ahmedabad visited ISR on 19/02/2020.
- ◆ A group of 47 students of 8th Sem. B.E. Electronics and Communication (E.C.) Engineering Department along with their 03 faculty member from SVIT, Vasad visited ISR on 26/02/2020.

Staff members joined /resigned

- ◆ Dr. Himangshu Paul, NPDF, resigned ISR on June 27, 2019 and joined as a Scientist at CSIR - National Geophysical Research Institute (NGRI), Hyderabad.
- ◆ Ms. Riyanka Talukdar (project Fellow) resigned ISR.
- ◆ Mr. Himanshu Chaube, Project Assistant resigned ISR on July 31, 2019.
- ◆ Ms. Nitu Yadav, Geophysicist resigned on September 2, 2019 and joined as a Project Assistant at CSIR-National Geophysical Research Institute, Hyderabad.
- ◆ Mr. Dinesh Singh, Project Assistant, resigned ISR on September 28, 2019, and joined Larsen and Toubro, Ahmedabad.
- ◆ Dr. P Mahesh, Scientist-C, resigned on 24 October 2019 and joined as a Scientist at CSIR - National Institute of Oceanography (NIO), GOA.
- ◆ Dr. Kapil Mohan, Scientist-D, resigned on 26 December 2019 and joined as a Scientist in Ministry of Earth Sciences (MoES), New Delhi.
- ◆ Dr. A.P. Singh, Scientist-C, resigned on 15 January 2020 and joined as a Scientist in Ministry of Earth Sciences(MoES), New Delhi.

SOCEITAL OUTREACH

Training/supervision of students

- ◆ Dr. P. Mahesh supervised Mr. K. Venkata Ramana, a second year student of M. Sc. in Geophysics, Adikavi Nannaya University, Rajahmundry, for his Master's dissertation on "Seismicity pattern of Kachchh" during January-April 2019.
- ◆ Dr. B Sairam supervised the dissertation work of Ms. V. Muthulakshimim, a final year student of M.Sc. Applied Geophysics, the Center for Geotechnology, Manonmaniam Sundaranar University, Tirunelveli, Tamilnadu, on "Two-Dimensional Reflection Land Seismic Data Processing and Interpretation", during January-April 2019.
- ◆ Dr. B Sairam supervised dissertation work of Mr. P. Balachandar, Final student of M.Sc. Applied Geophysics, the Center for Geotechnology, Manonmaniam Sundaranar University, Tirunelveli, Tamilnadu, on "Processing of Two-Dimensional Reflection Land Seismic Data of Alaska Oil field data using Seismic Unix", during January-April 2019.
- ◆ Ms. Vishwa Joshi guided Ms. Uppada Naga Vijaya, a third year M.Sc. student of Department of Geophysics, Andhra University, Visakhapatnam, on "Study of Epicentral Location of Kachchh Earthquakes" during 9 May - 28 June 2019.
- ◆ Dr. P. Mahesh guided Mr. Debadutta Priyadarshi Swain a student of integrated M.Sc. Exploration Geophysics, Department of Geology and Geophysics, IIT Kharagpur for his summer training on "Estimation of earthquake hypocentral parameters" under my guidance and supervision at Institute of Seismological Research, Gandhinagar during 11 May- 5 June 2019.
- ◆ Pallabee Choudhury guided Mr. Rushikesh Chopade, a 2nd year UG student of Department of Geology and Geophysics, Indian Institute of Technology, Kharagpur for the summer internship programme, during 13 May- 19 June 2019.
- ◆ Pallabee Choudhury guided Mr. Jitendra Gangwar, a 2nd year student of Department of Earth Sciences, Indian Institute of Technology, Bombay for the summer internship programme, during 13 May- 2 July 2019.
- ◆ Dr. A.P. Singh supervised Mr. Harshit Jangde, a student of integrated M.Sc. Exploration Geophysics from the Department of Geology and Geophysics, Indian Institute of Technology, Kharagpur for summer internship during the period from 13 May to 25 June 2019.
- ◆ Dr. Rajeev Yadav supervised two summer training students of the Department of Geology and Geophysics, Indian Institute of Technology Kharagpur, during 13 May -15 June 2019.
- ◆ Dr. P. Mahesh guided Ms. Niharika Jain and Ms. Cherry Jain, second year students of integrated M. Tech in Geophysical Technology, Department of Earth Sciences, IIT, Roorkee for their summer training on "Developing MATLAB codes for earthquake catalogue analysis" during 14 May-12 June 2019.
- ◆ Dr. Santosh Kumar guided Mr. Neelanchal Joshi, a student of M.Sc (Physics), B.E (Electrical and Electronics), BITS Pilani, on "Seismic Signal Processing to estimate the Source Parameters from 21 May to 12 July 2019.
- ◆ Dr. A.P. Singh guided Ms. Shweta Rai, Mr. Satyam Agrawal and Mr. Vijay Kumar Yadav, students of M.Sc. (Tech.) semester-II from Department of Geophysics, Banaras Hindu University, Varanasi, for their summer internships during 25 May-15 July 2019.
- ◆ Mr. Ketan S Roy supervised two students, Mr. Vihar Shah and Miss. Khushboo Kumari of BITS, Pilani on "A web-based seismological data requesting tool". This tool is dependent on Python, PHP and html.
- ◆ Vasu Pancholi guided two students from BITS, Pilani for the summer internship program, during May-June 2019.
- ◆ Dr. Rakesh Dumka supervised two students from Andhra University for their M. Sc. dissertation work.

- ◆ Mrs. Jyoti Sharma has provided training to four students, Ms. Vishwa Vora, Ms. Falguni Patel, Ms. Riya Thakore and Ms. Vishruti Kakkad of Pandit Deendayal Petroleum University (PDPU), Gandhinagar, Gujarat on the topic "Python based GUI for pre-processing of Seismological data" during June- July 2019.
- ◆ Ms. Rama Pandey, M.Sc. Tech. Geophysics (1st year) has completed her internship entitled "Seismic Hazard assessment of Bharuch, Gujarat from June 4 to July 15 2019 under the guidance of Dr. Kapil Mohan.
- ◆ Two students, Poorna Jagadeeshwari and Naga Lakshmi from Adi Kavi Nannaya University and Andhra University did their MSc dissertation work on "Analysis of Seismic Anisotropy in Gujarat Region Using Core Refracted SK(K)S Waves" under the guidance of Dr. G. Srijayanthi.
- ◆ Four students, Charli Gandhi, Shyamali Toluchuri, Varun Pandya and Sumeet Sachdev from PDPU did their summer internship on "Platform independent, GUI based 3D earthquake plotting tool" under the guidance of Dr. G. Srijayanthi.
- ◆ Mr. Kaushal Kapadia, a B. Tech student from PDPU did his summer internship on "Automation of core refracted shear wave splitting determination using Python platform" under the guidance of Dr. G. Srijayanthi.
- ◆ Two students from Andhra University did their M. Sc. dissertation work under the supervision of Dr. Rakesh Dumka.
- ◆ Pallabee Choudhury is supervising a student for MTech dissertation work on Analysis of SMA data. The duration of the training is 6 Dec 2019-28 Feb 2020.
- ◆ 100 students from different colleges along with their faculty members visited the Geotechnical Lab of ISR
- ◆ M.Sc. dissertation by two students, namely A. Krishna Sai and M. Manikanta Siddantham, "Analysis of seismological waveform data for local earthquakes in Gujarat, North-western India" under the guidance of Dr. G. Srijayanthi, Scientist-B, ISR.
- ◆ Ms. Dhanya Krishnan, M.Sc. Marine Geophysics student from Cochin University of Science and Technology (CUSAT), Kochi, Kerala, is carrying out her dissertation work "Source characterization of the Northwestern Deccan Volcanic Province" under the guidance of Ms. Jyoti Sharma, Scientist-C, ISR.
- ◆ Mr. Avinash Chouhan supervised three M.Sc. Geology student Ms. Riyal Chaudhari, Ms. Jaimini Prajapati and Ms. Avani Patel of Hemachandra North Gujarat University (HNGU), Patan during 01 Dec.- 29 Feb. 2020
- ◆ Dr. B. Sairam supervised M.Sc. dissertation work of Ms. Pinal G. Patel and Ms. Ragi R. Patel, final year students of Hemchandracharya North Gujarat University, Patan, Gujarat on Determining P-wave velocity using refraction method. The duration is 1 Dec 2019-28 Feb 2020.
- ◆ Dr. Nagarjuna Danda supervised two M.Sc. Geology student Ms. Nikita Patel and Ms. Vaishali Ravat of Hemachandra North Gujarat University (HNGU), Patan during 01 Dec.- 29 Feb. 2020
- ◆ Dr. Jyoti Sharma supervised one M.Sc. Geology student Ms. Dhanya Krishnan of Cochin University of Science and Technology (CUSAT), Kochi, Kerala during 04 Dec.- 29 Feb. 2020
- ◆ Dr. Pallabee Choudhury supervised Anju K S, a student of Kochin University of Science and Technology for her MTech dissertation work on Analysis of SMA data. The duration of the training is 6 Dec 2019-28 Feb 2020.
- ◆ Dr. R.K. Yadav supervised one M.Sc. Geology student Mr. K. Saish Shekhar of Osmania University during 6 Feb-7 Mar 2020.

List of Projects received

| SI no | Title | Funding agency |
|-------|--|---|
| 1. | Geo Physical Survey at Bhaxi Village, Ta. Rajula, Dist. Amreli | Commissioner of Geology & Mining, Gujarat |
| 2. | Intra plate seismicity in India and Norway: Distribution, properties and causes - (IPSIN) | Ministry of Earth Sciences, Govt. of India |
| 3. | Low Frequency Passive Seismic (LFPS) Survey in Mansa, Jotana and linch, Cambay Basin, Gujarat State | ONGC Limited |
| 4. | Investigation of site properties for seismic hazard analysis in and around Gorakhpur city, Uttar Pradesh (india) using microtremor measurements | Ministry of Earth Sciences, Govt. of India |
| 5. | Phase-III, Delineation of Freshwater layer at the selected sites in the Great Rann of Kachchh, Anjar and Bhachau Talukas of Kachchh (Gujarat) using Teme Domain Electromagnetic Survey | Salinity Control Divison Bhuj |
| 6. | Sand mining replenishment studies in and around Bharuch District of Gujarat for total 49,000 m2 | Hirpara Dhirubhai Manjibhai |
| 7. | Development of site specific response spectrum at Khavda Wind mill site Kutch, Gujarat | Adani Green Energy Ltd. |
| 8. | Source-to-Sink spatio-temporal variability in sediment fluxes and their control on coastal sediment dispersal systems in Gujarat | Ministry of Earth Sciences, Govt. of India |
| 9. | Low Frequency Passive Seismic (LFPS) Survey in Dholka, Ahmedabad & Digas, Ankleshwar | Gujarat State Petroleum Corporation Limited |
| 10. | OSL Dating | The Maharaja Sayajirao University of Baroda |
| 11. | Preparing Land use map for the core zone and buffer zone of the Ghogha Surka Lignite Mine, Dist. Bhavnagar | P.C. Patel Mahalaxmi Infra LLP |
| 12. | Gravity Survey in Dubarpeth Karanji Copper Block in Chandrapur District (Maharashtra) | Vedanta Limited, Mumbai |
| 13. | Geophysical, Geological investigation for construction of the additional spillway and Seismological investigation for Shetrunji Dam | Bhavnagar Irrigation Project Circle (BIPC), NWRWSKD |
| 14. | Geophysical/ Geological investigations at Machhundri Dam site, Dist. Gir Somnath | Junagadh Irrigation Divison, Junagadh |
| 15. | Geophysical/ Geological investigations at Hiran-1 Dam site, Dist. Gir Somnath | Junagadh Irrigation Divison, Junagadh |
| 16. | Seismological Investigation for Kadana Dam | DIRP-DSRP, NWRWSKD |
| 17. | Site Specific Hazard Investigation for Panam Dam | DIRP-DSRP, NWRWSKD |
| 18. | Seismological Studies in and around SSNNL Dam | Sardar Sarovar Narmada Nigam Ltd |
| 19. | Geophysical Investigation (Electrical survey) for pinpoint location at 2512 Dug wells to be constructed under PMKSY-HKGP-GW Irrigation-district Dangs, Gujarat | Gujarat Water Resources Development Corporation (GWRDC) |